

University of Ferrara

Department of Physics and Earth Science

Ph.D. in Physics

**Probing the neutrino sector through Cosmic
Microwave Background observations**

Co-Advisor:

Massimiliano Lattanzi

Student

Advisor:

Paolo Natoli

Francesco Forastieri

2014-2017 – XXX course
Coord. Prof. Vincenzo Guidi – FIS/02



University of Ferrara

Department of Physics and Earth Science

Ph.D. in Physics

**Probing the neutrino sector through Cosmic
Microwave Background observations**

Co-Advisor:

Massimiliano Lattanzi

Advisor:

Paolo Natoli

Student

Francesco Forastieri

2014-2017 – XXX course
Coord. Prof. Vincenzo Guidi – FIS/02

*To the woman who, piece by piece, without ever complaining,
has built my foundation,
so that I could be able to build my own life.*

Contents

Abstract	2
Sommario	4
Introduction	6
1 The standard cosmological model	10
1.1 All you need is a principle (cosmological principle and mathematical framework)	11
1.1.1 Dynamics of homogeneous and isotropic Universe	13
1.1.2 Cosmological parameters	16
1.1.3 Many distances	18
1.2 Thermodynamics of the early Universe	19
1.2.1 Relativistic and nonrelativistic limits	21
1.2.2 Entropy conservation	22
1.2.3 Boltzmann equation	23
1.3 Thermal history of the early Universe	25
1.3.1 Early age	25
1.3.2 Neutrino decoupling	28
1.3.3 Electron-positron annihilation	29
1.3.4 Big bang nucleosynthesis	31
1.3.5 Recombination, photon decoupling and last scattering	33
1.4 Inhomogeneous Universe	35
1.4.1 Perturbation theory	36
1.5 Inflation	44
1.5.1 Flatness and horizon problems	45
1.5.2 Basics of Inflation	47
1.5.3 Primordial scalar power spectrum	49

1.5.4	Tensor perturbations	51
1.6	Observational cornerstones	51
2	Cosmic Microwave Background radiation	53
2.1	Gravitational potential and inhomogeneities	55
2.1.1	Large scales	58
2.1.2	Small Scales	59
2.2	CMB temperature anisotropies	62
2.2.1	Temperature perturbation	64
2.2.2	Primary anisotropies:	70
2.2.3	Secondary anisotropies:	74
2.3	CMB polarization anisotropies	76
2.3.1	E modes	79
2.3.2	B modes	79
2.4	Observing the CMB	81
2.4.1	Cosmic variance and instrumental error	82
2.4.2	Foregrounds	82
3	Neutrinos	87
3.1	State of the art	87
3.2	The Standard Model	89
3.2.1	Mass generation mechanism	92
3.2.2	Effective low-energy theory	93
3.2.3	Dirac mass and mixing	94
3.2.4	Majorana mass and mixing	96
3.2.5	Dirac-Majorana neutrinos	98
3.2.6	Flavour oscillations in vacuum	99
3.2.7	Flavour oscillations in matter	100
3.3	Neutrino experiments	103
3.3.1	Oscillation experiments	103
3.3.2	Neutrino mass experiments	107
3.4	Neutrino Cosmology	109
3.4.1	Massless neutrinos effects	110
3.4.2	Effects of massive neutrinos	113
3.4.3	Massive sterile neutrinos	117
4	(Pseudo)scalar interacting neutrinos	120
4.1	(Pseudo)scalar formalism	121
4.1.1	State of the art	123
4.1.2	Our method	125
4.2	Massless neutrinos	126

4.2.1	Perturbation evolution and APS	127
4.3	Constraints from Planck 2013 data	137
4.4	Constraints from Planck 2015 data	141
5	Fermi-like interacting neutrinos	149
5.1	Fermi-like formalism	149
5.2	Massive sterile neutrinos	151
5.2.1	Sterile neutrino production in the primordial Universe	153
5.2.2	Sterile massive interacting neutrinos	155
5.2.3	Effects on the cosmological perturbations	158
5.3	Cosmological analysis	161
5.3.1	Method and data	162
5.4	Constraints from Planck 2105 data	164
	Conclusions and Outlook	170
	Appendices	174
A	Tools and data	176
1.1	Tools and data	176
B	Bayesian inference	181
	References	187

Abstract

Neutrino interactions beyond the standard model of particle physics are an open field both from theoretical and experimental point of view. In this thesis we present how non-standard neutrino properties can be constrained using cosmological observations and in particular cosmic microwave background data like those of the Planck satellites. We will consider the possibility that neutrinos possess secret scalar or pseudoscalar interactions mediated by the Nambu-Goldstone boson of a still unknown spontaneously broken global $U(1)$ symmetry, as in, e.g., Majoron models or that secret contact interactions among eV sterile neutrinos, mediated by a massive gauge boson X (with $M_X \ll M_W$) exist. We will present constraints on the interaction strength and on the neutrino mass allowed by cosmological data alone or in combination with astrophysical observations and we will discuss the feasibility of the considered models.

Sommario

Le interazioni tra neutrini oltre il modello standard della fisica delle particelle sono un campo aperto sia dal punto di vista teorico che sperimentale. In questa tesi presentiamo come le proprietà non standard dei neutrini possano essere vincolate usando le osservazioni cosmologiche e in particolare i dati della radiazione di fondo cosmica, come i dati di Planck. Considereremo la possibilità che i neutrini posseggano interazioni segrete scalari o pseudoscalari mediate da un bosone Nambu-Goldstone di una simmetria globale spontaneamente rotta $U(1)$ ancora sconosciuta, come ad esempio i modelli che includono i Majoroni oppure quelle interazioni segrete di contatto tra neutrini sterili leggeri (~ 1 eV), mediati da un bosone di gauge massivo X (con $M_X \ll M_W$). Presenteremo vincoli sulla forza di interazione e sulla massa di neutrini consentita dai dati cosmologici o in combinazione con osservazioni astrofisiche, infine discuteremo la fattibilità dei modelli considerati.

Introduction

The observation of the Cosmic Microwave Background (CMB) radiation dramatically changed how humanity perceived the Universe. The hot big bang theory proposed by G.Gamow in the late 40's was confirmed when in 1964 two American physicists, Arno Penzias and Robert Wilson, observed an omnidirectional, homogeneous and isotropic noise in the microwave bands, whose power was consistent with a black body at $T = 3$ K. This discovery, that as several other discoveries in the scientific history was a fortunate chance, was the evidence that long time ago the Universe was hotter and denser, hence, it does behaves like an expanding thermodynamic system.

After the first observation, a sequence of spatial and atmospheric missions like COBE (1989-1992), WMAP (2001-2008) and Planck (2009-today) and more than a dozen other suborbital experiments, have revealed and are still revealing the existence of a pattern of tiny anisotropies in the CMB temperature and polarization. This pattern encodes a wealth of information about the Universe, for example its energy and matter content, the expansion rate, the primordial spectrum of perturbations, and more. The rapid series of experiments that has been performed transformed cosmology into a precision science, moreover the new generation of ground based experiments, (Keck Array, ACTpol, Simons Observatory), the balloon experiments (Spider, LSPE, Piper) and the future space missions (COre, LiteBird, Pixie) will increase the precision of the observations, in particular for the polarized anisotropies.

Therefore, actual cosmological data, in particular the latest release of Planck data, allow to study of the Universe evolution and constrain the cosmological parameters below the percent level. Thanks to this precision we can use the primordial Universe as a laboratory to test fundamental physics in particular in the neutrino sector. In fact neutrinos are the most elusive particles in the standard model (SM) of particle physics. We know that they are massive since we have observed the phenomenon of flavour oscillations, however, their mass is so small that it has not yet been measured. The smallness of their masses is itself a puzzle in the context of the SM and the mass generation mechanism could be related to new physics beyond the SM. Purpose of this

thesis is to investigate neutrino properties using cosmological data, in particular testing some extension of the standard model including “secret” interactions in the neutrino sector.

This thesis is organized as follows:

- 1) In the first chapter, Ch.(1), we provide an overview of the standard cosmological model (SCM). We start from the Cosmological Principle and General Relativity in order to describe the background evolution of the Universe before introducing the main aspects of the perturbation theory. We present the full set of Boltzmann equations for the evolution of cosmological perturbations. Finally we provide a brief introduction of the theory of inflation.
- 2) In the second chapter, Ch.(2), we move our attention on the CMB, which is the main observable used in this thesis. The processes giving rise to the CMB are outlined, we show how gravitational potential is connected to matter perturbations and how their mutual influence changes the properties of the photon-baryon fluid. In addition we derived the expression for the CMB temperature anisotropies power spectrum (APS), describing in details the features and the physics encoded within. After that we describe the polarization aspects of the CMB, i.e. how polarization is originated and its treatment. At the end of this chapter we briefly discuss the principal foreground contaminations.
- 3) Ch.(3) focuses on the neutrino figure. The role of this particle inside the standard model of particle physics is reviewed in the beginning of the chapter. We also present a quick review of the current observations regarding both the flavour oscillations and mass constraints coming from laboratory experiments. Finally we present the effects on the cosmological observables and the current cosmological constraints on the neutrino properties.
- 4) In Ch.(4) we start to present the original work of this thesis. This part begins with the introduction of non-standard interaction in the neutrino sector. We present the formalism for a (pseudo)scalar-type interaction, its implication in the cosmological framework and the expected signature in the CMB APS. After a brief overview of the state of the art, we discuss the constraints for non-standard interaction among massless neutrinos obtained using the the 2013 and 2015 Planck data releases and some additional astrophysical dataset like geometrical information from baryon acoustic oscillations or direct measurements of the Hubble constant.
- 5) In the last chapter we extend the analysis performed in the massless neutrino framework to the massive one. This time we consider a Fermi-like interaction between active and sterile neutrinos instead of a (pseudo)scalar interaction, in particular we follow the model described in Ref. [158] and successively in Ref. [135]. Secret contact interactions among eV sterile neutrinos, mediated by a massive

gauge boson X (with $M_X \ll M_W$), and characterized by a gauge coupling g_X , have been proposed as a mean to reconcile cosmological observations and short-baseline laboratory anomalies. We proceed constraining this scenario using the latest Planck 2015 data and some additional data coming from baryon acoustic oscillations measurements. In analogy to what we have done in Ch. 4 we study the effects of the interaction on the perturbation evolution. This time we follow explicitly all the neutrino mass eigenstates in order to fully understand the impact of the interaction on the anisotropies power spectra. After that we present the constraints on both the $\sum m_\nu$ and the interaction strength G_X for the considered models. Finally we compare our constraints with the results presented in literature.

1

The standard cosmological model

Non importa in quale parte di esso tu stai; sempre in qualunque luogo stia qualunque persona, da ogni lato si lascia sempre un tutto infinito. Inoltre, se si considera tutto lo spazio come finito, e qualcuno arrivasse alle ultime sponde di esso, e di là scagliasse una freccia, pensi che essa, tirata a tutta forza, arrivi là dove è stata mandata e voli a lungo più oltre, oppure che qualcosa possa frapporsi e impedirle il volo? È necessario assumere una di queste due opinioni, ma entrambe chiudono ogni via di scampo e obbligano a riconoscere che l'universo si estende senza confine.

Lucrezio, "De Rerum Natura I", vv. 965-976

The formulation of a solid cosmological model is based on two ingredients: one principle and a solid mathematical formalism. The cosmological principle is the natural extension of the Copernican principle and assumes that the Universe is invariant under translation and rotation; this leads to two important consequences: there are no privileged observers and physics is the same everywhere. Every model that pretends to be a suitable cosmological model cannot violate this principle. The mathematical formalism used to describe the gravitational framework of the Universe is the theory of General Relativity (GR) which has been formulated more than a century ago by Albert Einstein. It succeeds in merging concepts such as Newtonian gravitation inside a curved space without breaking the Lorentz invariance, basically it describes the space-time as a Lorentzian manifold or a pseudo-Riemann manifold where every tangent space can be considered as a flat Minkowski space. Nowadays there is no better theory able to describe and explain the cosmological evolution and the gravitational behaviour of the astrophysical objects.

In this chapter we will start focusing on the main aspects of these two ingredients

and finally we will provide a consistent description of the background evolution of the Universe, as well as the linear evolution of cosmological perturbations.

1.1 *All you need is a principle (cosmological principle and mathematical framework)*

The cosmological principle says that, on large scales, for any observer, the Universe appears to be isotropic and homogeneous [41, 82, 117, 138, 173]. This is not obvious looking at our galaxy and the nearby Universe, but observations on scales larger than ~ 100 Mpc (where $1 \text{ Mpc} = 3.086 \times 10^{22} \text{ m}$) such as Cosmic Microwave Background, Large Scale Structure (LSS), etc... all show isotropy and homogeneity. While isotropy means a simple concept: no preferred directions for any observer, homogeneity introduces a stronger concept, it assumes that in every patch of the Universe we can find the same physical properties (energy density, temperature, etc...). We can explain these observations claiming that the Earth occupies a privileged position in the center of the cosmos or assuming that there are no special observers at all. The second one is the explanation proposed and universally accepted by the scientific community as the Cosmological principle.

Paying more attention to the definitions, it is clear that isotropy does not imply homogeneity and the other way around, i.e. assuming isotropy from a single point of observation does not ensure homogeneity and measuring physical quantities in different areas of the universe does not guarantee isotropy. Probing isotropy, at least, about two different observables would be a confirmation of the cosmological principle, however, observationally speaking, we are limited in space and time.

It is interesting to see how imposing the cosmological principle leads to a series of implications: homogeneous and isotropic means that the the spacetime can be exfoliated in a a series of 3D hyper-surfaces all characterized by a time coordinate; thus a comoving observer sees the universe only in function of “t”. Starting from the most general metric:

$$ds^2 = g_{\mu\nu} dx^\mu dx^\nu, \tag{1.1a}$$

$$= g_{00}(dx^0)^2 + 2g_{0i}dx^0 dx^i + g_{ij}dx^i dx^j, \tag{1.1b}$$

where $g_{\mu\nu}$ is the metric tensor. The most convenient choice of coordinates is considered $g_{00} = -1$, thus an universal time, while the third term of Eq.(1.1), hypothesizing an expanding Universe where $a \equiv a(t)$ is the scale factor of the expansion (giving the current value of a as $a(t_0) = 1$), takes the following form:

$$g_{ij} = a^2 \gamma_{ij}(r), \tag{1.2}$$

All you need is a principle (cosmological principle and mathematical framework)

where $\gamma_{ij}(r)$ is the spatial part of the metric which, in light of isotropy assumption, is function only of the radial coordinate r . Putting together the infinite foliations the results is a metric for a 4D spacetime:

$$ds^2 = -dt^2 + a^2 \gamma_{ij} dx^i dx^j, \quad (1.3)$$

Notice that having a Universe which respect the cosmological principle is necessary and sufficient in order to obtain the metric shown in Eq.(1.3). If we consider simply connected spaces i.e. a space where, staying within the boundaries, every path between two points can be continuously transformed into any other path, we can write a simpler version of Eq.(1.3). This is known as Friedmann–Robertson–Walker (FRW) metric and in 3D spaces of constant curvature takes the form :

$$ds^2 = -dt^2 + a^2 \frac{dr^2}{1 - \kappa r^2} + r^2 d\Omega^2, \quad (1.4)$$

here κ is the curvature of the spacetime and $d\Omega^2 = d\theta^2 + \sin^2\theta d\phi^2$. One again the crucial point is the assumption of homogeneity and isotropy, considering the spacetime as a series of layers or foliations independent on time makes sure that all we need to know about its geometry is contained within $a(t)$, κ and r . Moreover, constant curvature means that κ is a dimensionless number which can take on only three discrete values: $\kappa = 0$ in case of flat Universe, $\kappa = -1$ if the Universe has negative curvature, and $\kappa = 1$ for a positively curved Universe.

General Relativity is the second ingredient of the model. As said before, the theory has to be Lorentz covariant, this basically means passing from $\nabla^2 \phi_N \rightarrow \square \phi_N$ (\square is the d'Alembert operator) when the speeds under considerations are of the same order of the speed of light (c). Thus, it could be thought of as a simple generalization of the Newtonian gravity, i.e. a description of the gravitational potential which satisfies the Poisson equation:

$$\nabla^2 \phi_N = 4\pi G \rho_m, \quad (1.5)$$

where ϕ_N is the Newtonian potential and ρ_m represents the mass density, inside the special relativity picture. In addition to Lorentz invariance, theory has to be always attractive and must obey the *principle of equivalence* (PE), whose most powerful definition says: “*In any sufficiently local region of spacetime, the effect of gravity can be transformed away*”. Here "local" means that the observer must be in the same reference system of the experiment and that the latter must be small with respect to the variations of the gravitational potential. Roughly speaking PE suggests that gravity is only a matter of geometry: an observer able to measure a portion of space to be flat is exactly in the same condition of another observer, elsewhere in the Universe, who is measuring an equivalent flat space. The metric derived from the cosmological principle, Eq.(1.4) is exactly what is needed in order to built the theory. Thus, considering GR as

a classical field theory allows to a self-consistent derivation of the equations of motion:

$$G_{\mu\nu} = 8\pi G T_{\mu\nu}, \quad (1.6)$$

where G and $T_{\mu\nu}$ are the universal constant of gravitation and the energy momentum tensor respectively and $G_{\mu\nu} = R_{\mu\nu} - \frac{1}{2}\mathcal{R}g_{\mu\nu}$ is the Einstein tensor in which appear the Ricci tensor $R_{\mu\nu}$ and the correspondent scalar \mathcal{R} . Here $c = \hbar = 1$. The left hand of Eq.(1.6) contains the information about the variation of metric and curvature and rises from the vacuum part of the Einstein Hilbert action, while in the right-hand side we find the source of the curvature due to matter and energy. Einstein's field equation is a second order differential equation for the metric tensor, since we deal with a symmetric rank-2 tensor, there are 10 independent equations, however imposing some reasonable properties would reduce the numbers of degrees of freedom. Imposing a statement of energy conservation:

$$\mathcal{D}_\mu T^{\mu\nu} = 0, \quad (1.7)$$

which leaves us with only 6 truly independent equations.

1.1.1 Dynamics of homogeneous and isotropic Universe

The first step to study the dynamics of an homogeneous and isotropic Universe is to define the matter content in terms of its energy momentum tensor $T_{\mu\nu}$. For the main components it is appropriate to approximate the energetic content as energy density and pressure [41, 82, 117, 138, 173]. It is correct to assume the perfect fluid notation:

$$T_{\mu\nu} = (\rho + P)V_\mu V_\nu - P g_{\mu\nu}, \quad (1.8)$$

where ρ is the energy density, P is the pressure and V_μ is the 4-velocity. In order to have a simplified description, from now on we are going to consider a flat Universe with constant curvature $\kappa = 0$. Solving the 6 equations, one for every degree of freedom of the theory, leads to the derivation of a famous set of equations named Friedmann equations, the first one comes from the time-time component $G_{00} = k/3 T_{00}$:

$$H^2 \equiv \left(\frac{\dot{a}}{a}\right)^2 = \frac{8\pi\rho G}{3}, \quad (1.9)$$

here H is the Hubble parameter. The latter parameter, measured today, is called Hubble constant H_0 and it is used as the unit of measurement to describe the expansion of the Universe. It appears inside the empirical law which relates the distance of an object with its recession velocity, known as Hubble law:

$$v = H_0 d. \quad (1.10)$$

All you need is a principle (cosmological principle and mathematical framework)

If, as observations have showed, every object in the sky is moving away from us following the Hubble law, the only possible explanation is that the Universe itself is expanding. Eq.(1.9) says us that the Hubble parameter (or the expansion rate) depends on the energy content of the Universe and, thus, it is not constant during the its evolution. On the other hand, the Hubble parameter, and consequently the Hubble law, are local quantities that can be measured only in the local Universe. Considering the first Friedmann equation and the space-space component i.e. $G_{ij} = k/3 T_{ij}$, it comes:

$$\frac{\ddot{a}}{a} = -\frac{4\pi G}{3} (3P + \rho) , \quad (1.11)$$

that is called acceleration equation. A feature of Eq.(1.11) is that also pressure contributes to gravitation, moreover if $\rho + 3P < 0$ the cosmic expansion would be accelerated. Basically theory allows the possibility of an anti-gravitational fluid on cosmological scales. Putting together Eqs.(1.9 and 1.11) a third one rises:

$$\dot{\rho} + 3 \frac{\dot{a}}{a} (P + \rho) = 0 , \quad (1.12)$$

which is a continuity equation or fluid equation, it simply expresses the conservation of energy momentum tensor, Eq.(1.7). Since the last equation is not independent a fourth equation describing properties of matter is needed in order to solve the system, the choice falls on an equation of state $P = P(\rho)$ in its simple linear form:

$$P = w\rho , \quad (1.13)$$

where w is a constant determining the properties of the matter. Thus the continuity equation can be rewritten in function of the parameter w in the following way:

$$\dot{\rho} + 3H\rho(1+w) = 0 \quad (1.14a)$$

$$\rightarrow \rho = \rho_0 a^{-3(1+w)} , \quad (1.14b)$$

where a subscript 0 means that the quantity is evaluated today. Having this set of equations we can analyse one by one the contributions of the different constituents of the Universe. It is reasonable, in light of the observations done in the latest 60 years, to classify the different energy densities into three main families: non relativistic matter having $w = 0$ (baryon, dark matter), relativistic matter with $w = \frac{1}{3}$ (radiation, light neutrinos) and fluids having negative pressure with $w = -1$ (dark energy).

It is possible to solve Friedmann's equations in all the three cases. The energy

density of the different matter contents scales in the following way:

$$\rho \propto \begin{cases} a^{-4} & \text{if } w = \frac{1}{3} \\ a^{-3} & \text{if } w = 0 \\ \text{const} & \text{if } w = -1 \end{cases} \quad (1.15)$$

If the case of relativistic and nonrelativistic matter are well known, on the contrary dark energy results more unusual. Historically it was proposed by Einstein in order to have a static description of the Universe, he introduced a constant source Λ term in Eq.(1.6), that does not violate the covariance derivative of the Einstein tensor:

$$R_{\mu\nu} - \frac{1}{2}\mathcal{R}g_{\mu\nu} + \Lambda g_{\mu\nu} = 8\pi G T_{\mu\nu} . \quad (1.16)$$

Accordingly, the cosmological constant appears inside the first two Friedmann's equations:

$$H^2 = \frac{8\pi\rho G}{3} - \frac{\kappa}{a^2} + \frac{\Lambda}{3} , \quad (1.17a)$$

$$\frac{\ddot{a}}{a} = -\frac{4\pi G}{3} (3P + \rho) + \frac{\Lambda}{3} . \quad (1.17b)$$

It is a curious fact that what was originally introduced to erase the acceleration of the Universe, today is used to describe the observed accelerated expansion of the same. From a theoretical and mathematical point of view there is no need for such an addition inside the framework described till now, except for the fact that observations suggest it. Indeed, in 1998 two independent projects, the Supernova Cosmology Project and the High-Z Supernova Search Team, discovered the accelerated expansion of the Universe using distant type Ia supernovae as standard candles [145, 151]. The cosmological constant plays exactly this role: for a flat, Λ dominated Universe, the Friedmann equation, Eq.(1.17b), takes the form:

$$\dot{a}^2 = \frac{8\pi G\rho_\Lambda}{3} a^2 , \quad (1.18)$$

since ρ_Λ is constant in time the latter equation can be rewritten as:

$$H_0 = \left(\frac{8\pi G\rho_\Lambda}{3} \right)^{\frac{1}{2}} . \quad (1.19)$$

The solution for such an equation is an exponentially expanding scale factor,

$$a(t) = e^{H_0(t-t_0)} . \quad (1.20)$$

Finally let us remember that the fact that the Universe is expanding leads to a

All you need is a principle (cosmological principle and mathematical framework)

phenomenon that is known as redshift z . The wavelength of the light emitted by a distance object which is receding from us results "shifted" towards lower energies, i.e. "redshifted"; the other way around, objects that are moving towards us will be "blueshifted".

$$1 + z \equiv \frac{\lambda_{\text{obs}}}{\lambda_{\text{em}}} = \frac{1}{a}, \quad (1.21)$$

This is a convenient definition that provides a simple way to measure distances, time and the stretching factor of the Universe. It is relatively easy to measure the light spectrum of a distant galaxy, hence, it is pretty easy to get its recession speed (e.g. for low redshifts the standard Doppler $z \simeq v/c$ is valid). Knowing how fast an object is receding from us translates into a distance information thanks to the Hubble law, Eq.(1.10), and, since the velocity of recession is related to the expansion rate, we are measuring also the stretching factor $a(t)$ of the Universe. It is possible to see the same effect considering the momentum of a photon moving along a geodesics, if p is the momentum of the particle emitted at t_{em} in a flat space we can write:

$$\dot{p} = -Hp. \quad (1.22)$$

Eq.(1.22) has an immediate solution in $p \propto 1/a(t_{em})$ which translates into the redshift of the momentum of the considered particle in a FRW background.

1.1.2 Cosmological parameters

As we have seen, the expansion rate of the Universe is described by the Hubble parameter H which depends on the energy density through Eq.(1.9). From Eq.(1.9), considering a spatially flat Universe, is evident that exists a critical energy density:

$$\rho_c = \frac{3H_0^2}{8\pi G}, \quad (1.23)$$

thus the contribution that every species i gives can be parametrized in a dimensionless parameter:

$$\Omega_i = \rho_i / \rho_c. \quad (1.24)$$

Under this formalism, the Friedmann equation, Eq.(1.9), takes the following form:

$$H = H_0 \sqrt{\sum_i \Omega_{i0} a^{-3(1+w)}}. \quad (1.25)$$

This set of parameters are the standard way to obtain an "identikit" of what the Universe is composed of. For a spatially flat Universe the sum of all contribution must be $\Omega_{tot} = 1$. Since the densities of various species scale as different powers of a (see

Eqs.(1.15)) the Friedmann equation can be rewritten as a sum of contribution,

$$H = H_0 \sqrt{\Omega_{m0} a^{-3} + \Omega_{r0} a^{-4} + \Omega_\Lambda}. \quad (1.26)$$

Here Ω_{m0} , Ω_{r0} and Ω_Λ are the density parameters for nonrelativistic, relativistic matter and dark energy respectively. Looking at the time dependencies inside Eq.(1.26) is evident that different species dominates different ages: radiation or relativistic matter is more important at early times, when the scale factor is small, but at a certain time nonrelativistic matter starts to be the dominant part in terms of energy contribution. Finally when the expansion has diluted matter and radiation components, the age of cosmological constant domain starts. Basically the scale factor changes following the Friedmann's equations:

$$a(t) \propto \begin{cases} t^{\frac{1}{2}} & \text{if } w = \frac{1}{3} \\ t^{\frac{2}{3}} & \text{if } w = 0 \\ e^{Ht} & \text{if } w = -1. \end{cases} \quad (1.27)$$

The exact time of transition between two regimes depends on the amount of the constituents, in Fig.(1.1) we show the different expansion regimes in the case of a three component toy model (matter + radiation + cosmological constant). [153]. In

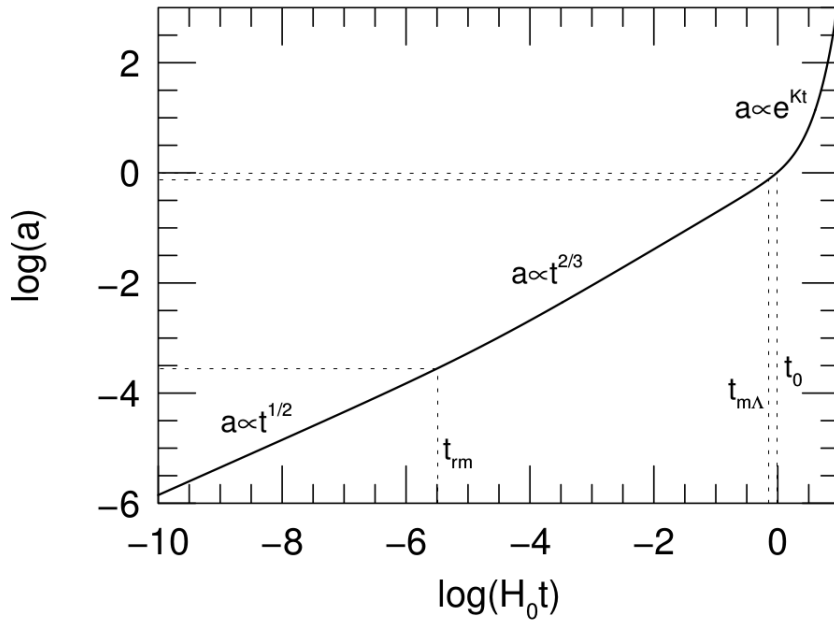


Figure 1.1: The scale factor a in function of the time t measured in units of Hubble constant H_0 . The parameter used are $\Omega_{m0} \sim 0.3$, $\Omega_{r0} \sim 10^{-5}$, $\Omega_\Lambda \sim 0.7$ and $\Omega_\kappa = 0$. [153]

All you need is a principle (cosmological principle and mathematical framework)

this model radiation gives way to matter at a scale factor $a_{\text{eq}} = \Omega_{r0}/\Omega_{m0} \simeq 3 \times 10^{-4}$ corresponding to a time $t_{\text{eq}} \simeq 5 \times 10^4$ Yr. The cosmological constant, instead, starts to dominate at $a_{m\Lambda} = (\Omega_{m0}/\Omega_{\Lambda})^{1/3} \simeq 0.75$, corresponding to $t_{m\Lambda} \simeq 9.8$ GYr. The age of such a Universe is $t_0 \simeq 13.5$ GYr. Although it is a first, simple and not refined model, the one described so far provides a good description of the most significant moments of its history.

1.1.3 Many distances

The topic of measuring distances is not trivial in a multicomponent expanding Universe where the metric changes under the effect of different matter and energy species contributions. One can measure different distances using different methodologies.

- 1 Proper distance d_p between us and a cosmological object is measured imagining to stop the expansion of the Universe and directly measure the distance. For the multicomponent Universe shown in Sec.(1.1.2) the proper distance is:

$$d_p = \int_1^{1+z} \frac{c dz'}{z' H(z')}, \quad (1.28a)$$

$$= \frac{c}{H_0} \int_1^{1+z} \frac{dz}{\sqrt{\Omega_{m0} z'^3 + \Omega_{r0} z'^4 + \Omega_{\Lambda}}}. \quad (1.28b)$$

- 2 Luminosity distance d_L measured using the flux emitted by a known source, e.g. type Ia supernovae, considering the space as Euclidean. The observed flux from a source is by definition:

$$F = \frac{N h \nu_{em}}{\Delta t_{em}}, \quad (1.29)$$

where N is the number of photons, h is the Planck constant and ν_{em} is the frequency of emitted photons. The luminosity of the source is:

$$L = \frac{N h \nu_{ob}}{A \Delta t_{ob}}, \quad (1.30)$$

where ob means observed and $A = 4\pi d_p^2$ is the surface and the isotropic spherical emission. Since frequency and time intervals are redshifted, (i.e. $\nu_{ob} = \nu_{em}(1+z)$ and $\Delta t_{ob} = \Delta t_{em}(1+z)$) the flux in terms of luminosity takes the form:

$$F = \frac{L}{4\pi d_p^2 (1+z)^2}. \quad (1.31)$$

This implies that the luminosity distance is:

$$d_L = d_p (1+z). \quad (1.32)$$

3 Angular diameter distance d_A of an object of known size l (standard ruler) in an Euclidean space. The subtended angle between the observer and the emitter is $\delta\theta = l/d_A$, considering that the size of the ruler is increasing due to expansion, the angular diameter distance becomes:

$$d_A = \frac{d_p}{1+z} \tag{1.33a}$$

$$= \frac{d_L}{(1+z)^2}. \tag{1.33b}$$

Every definition of distance depends on the metric (here we have assumed a flat geometry) and on the abundances of the species that contribute to the energy budget.

1.2 *Thermodynamics of the early Universe*

Before proceeding further let us introduce briefly the natural system units i.e. $\hbar = c = k_B = 1$, where the latter is the Boltzmann constant. All dimensional quantities now have dimension of length, time or mass (energy), for example $G \equiv 1/m_{Pl}^2$ and $m_{Pl} = 1.221 \times 10^{19} \text{GeV}$ is the Planck mass.

Till now, starting only from the cosmological principle and the strong principle of equivalence, we have built a simple but reasonable cosmological model. However in order to yield a detailed description of dynamics and evolution of the Universe, we need to know very well the properties of the species introduced in the previous section. One of the main feature that rises in the picture described so far, and that we have not yet discussed, is that because the Universe has a finite age and because it is expanding, in the past it must have been smaller, hotter and denser. Thus we need to study the thermodynamics properties of the species that populate the Universe today and in the past [30]. We have good observational evidence (see chapter CMB) that the early Universe was a system in local thermal equilibrium. If the expansion is slow enough, particles have enough time to settle close to local equilibrium and since the Universe is homogeneous, the local values of thermodynamics quantities are also global values. In quantum mechanics, due to Uncertainty principle

$$\Delta p \Delta x \geq \hbar/2, \tag{1.34}$$

the momentum of a particle can be described only considering a finite volume V . Solving the Schroedinger equation inside this box gives us energy and momentum eigenstates. Moving to phase space the state density of a particle having g internal degrees of

freedom is:

$$\text{density of states} = \frac{g}{h} = \frac{g}{(2\pi)^3}, \quad (1.35)$$

All the information about how particles are distributed among momentum eigenstates is contained in the probability distribution function $f(\vec{p})$. The number density of particles is by definition:

$$n = \frac{g}{(2\pi)^3} \int d^3p f(\vec{p}), \quad (1.36)$$

while to obtain the energy density we have to weight each momentum by its energy,

$$\rho = \frac{g}{(2\pi)^3} \int d^3p f(\vec{p}) E(\vec{p}). \quad (1.37)$$

For pressure we have to consider the exchange of momentum as follows:

$$P = \frac{g}{(2\pi)^3} \int d^3p f(\vec{p}) \frac{p^2}{3E}. \quad (1.38)$$

Moreover, particles are classified into two classes, fermions and bosons, depending on the behaviours manifested when observed; in thermodynamic equilibrium fermions follow the *Fermi-Dirac* distribution, while bosons follow the *Bose-Einstein* distribution.

$$f(\vec{p}) = \frac{1}{e^{(E-\mu)/T} \pm 1}, \quad (1.39)$$

where $+$ is for fermions and $-$ is for bosons. The distribution function in equilibrium depends on two parameters: temperature (T) and chemical potential (μ). Chemical potential is the quantity that maps the response of the system to a change in particle number, e.g. the entropy of a system can be written as:

$$dS = \frac{dU + PdV - \mu dN}{T}, \quad (1.40)$$

thus, in binary processes, it implies that particles flow to the side of the reaction with the lower chemical potential. In a $1 + 2 \leftrightarrow 3 + 4$ scenario the system reach the chemical equilibrium when $\mu_1 + \mu_2 = \mu_3 + \mu_4$. Thermal equilibrium is, instead, that condition in which there is a common temperature among the species. In cosmology the expansion of the Universe is slow enough to guarantee, instant by instant, the thermal equilibrium of the fluid of particle. Given the distribution function the next step consists in carrying out the integral on the momentum. The solutions are well known [111] and we just review the relativistic and nonrelativistic limits.

1.2.1 Relativistic and nonrelativistic limits

If the temperature is much greater than the mass of the particles an average energy can be approximated as $E = \sqrt{m^2 + p^2} \simeq p$. Considering the equilibrium described above and assuming the chemical potential $\mu = 0$, number, energy density and pressure take the following form:

$$n = \frac{g}{(2\pi)^3} \int_0^\infty \frac{4\pi p^2 dp}{e^{p/T} \pm 1} = \begin{cases} \frac{3}{4\pi^2} g \zeta(3) T^3 & \text{fermions} \\ \frac{1}{\pi^2} g \zeta(3) T^3 & \text{bosons} \end{cases}, \quad (1.41)$$

$$\rho = \frac{g}{(2\pi)^3} \int_0^\infty \frac{4\pi p^3 dp}{e^{p/T} \pm 1} = \begin{cases} \frac{7}{8} \frac{\pi^2}{30} g T^4 & \text{fermions} \\ \frac{\pi^2}{30} g T^4 & \text{bosons} \end{cases}, \quad (1.42)$$

$$P = \frac{g}{(2\pi)^3} \int_0^\infty \frac{\frac{4}{3}\pi p^3 dp}{e^{p/T} \pm 1} = \frac{\rho}{3}. \quad (1.43)$$

The average energy per particle is:

$$\langle E \rangle = \begin{cases} \frac{7\pi^4}{180\zeta(3)} T \simeq 3.15 T & \text{fermions} \\ \frac{\pi^4}{30\zeta(3)} T \simeq 2.70 T & \text{bosons} \end{cases}, \quad (1.44)$$

where $\zeta(3)$ is the Riemann zeta function. In the early Universe temperature was high enough to allow the existence of a zoology of particles which have been relativistic for a relative long time (it depends on their masses). The total radiation density is the sum of all the contributions is:

$$\rho_r = \sum_i \rho_i = \frac{\pi^2}{30} g_*(T) T^4, \quad (1.45)$$

where i runs on the relativistic species present in the plasma and g_* is the effective number of relativistic degrees of freedom. The general formulation takes into account the boson and fermion contribution in the following way:

$$g_*(T) = \sum_{i=b} g_i \left(\frac{T_i}{T}\right)^4 + \frac{7}{8} \sum_{j=f} g_j \left(\frac{T_j}{T}\right)^4, \quad (1.46)$$

where the b index stays for bosons while f for fermions. In case of thermal equilibrium the temperature of the single component is the same of the fluid T and the dependence vanishes.

In case of $T \ll m$ Eq.(1.39) reduces to the Boltzmann distribution function $f \simeq \exp[p/T]$, bosons and fermions cannot be distinguished and the statistical quantities

becomes:

$$n = g \left(\frac{mT}{2\pi} \right)^{\frac{3}{2}} e^{-\frac{m}{T}}, \quad (1.47)$$

$$\rho = n \left(m + \frac{3T}{2} \right), \quad (1.48)$$

$$P = nT \ll \rho, \quad (1.49)$$

$$\langle E \rangle = m + \frac{3T}{2}. \quad (1.50)$$

Number density, energy density and pressure of a species drop down exponentially once the temperature of the fluid becomes smaller than the its mass. The physical interpretation of this behaviour is a massive particle-antiparticle annihilation, the same processes happened also at higher temperatures (in the relativistic regime), but in this case annihilations have been balanced by pair productions.

1.2.2 Entropy conservation

In order to describe in a proper way the thermal history of the Universe we need to define a conserved quantity; energy and number of particles are not the correct choices, as we have seen, however it can be shown that entropy is the right one (it is enough to carry out the time derivative of Eq.(1.40)). In agreement with Eq.(1.40) the entropy density \mathcal{S} of a collection of different particles can be written as:

$$\mathcal{S} = \sum_i \frac{\rho_i + P_i}{T_i} \equiv \frac{2\pi^2}{45} g_{*\mathcal{S}} T^3, \quad (1.51)$$

where $g_{*\mathcal{S}}$ is the effective number of degrees of freedom in entropy,

$$g_{*\mathcal{S}} = \sum_{i=b} g_i \left(\frac{T_i}{T} \right)^3 + \frac{7}{8} \sum_{j=f} g_j \left(\frac{T_j}{T} \right)^3, \quad (1.52)$$

If all the relativistic species are in thermal equilibrium, $g_* = g_{*\mathcal{S}}$. Entropy conservation leads to important consequences:

- 1 the number density in a comoving volume is constant and proportional to the number $N_i \equiv n_i/\mathcal{S}$,
- 2 the entropy per comoving volume is conserved, $S \propto g_{*\mathcal{S}} T_0^3 a^3 = \text{const}$, thus as long as the effective number of degrees of freedom is constant, the temperature of the fluid is proportional to the inverse of the scale factor.

1.2.3 Boltzmann equation

Now we have a model for the description of the spacetime dynamics and a set of thermodynamic quantities that ensure a complete description of both relativistic and nonrelativistic energetic content of the Universe. The first approximation in order to have a rough indication of these dynamics is considering a $2 \leftrightarrow 2$ reaction and the associated ratio between the scattering rate Γ of the species and the Hubble rate of expansion H ,

$$\Gamma > H \quad \text{coupled}, \quad (1.53)$$

$$\Gamma < H \quad \text{decoupled}. \quad (1.54)$$

The left-hand side of the latter equation can be written as:

$$\Gamma = n \langle \sigma v \rangle, \quad (1.55)$$

where σ is the interaction cross section and v is the average velocity of the particles, while the Hubble rate H is derived from the Friedmann equation, Eq.(1.9). This rule is surprisingly accurate but the correct way in order to reconstruct the phase-space evolution of the distribution function is to provide an equation able to merge the behaviour of the thermodynamic quantities introduced in the previous section with the metric evolution. The Boltzmann transfer equation is the correct tool:

$$\hat{L} [f(E, t)] = \hat{C} [f(E, t)], \quad (1.56)$$

where \hat{L} is the Liouville operator and \hat{C} is the collisional term. The covariant relativistic generalization of the Liouville operator is:

$$\hat{L} = p^\mu \frac{\partial}{\partial x^\mu} - \Gamma^\mu_{\nu\gamma} p^\nu p^\gamma \frac{\partial}{\partial x^\mu}. \quad (1.57)$$

In a FRW metric the left-hand side of Eq.(1.56) takes the following form:

$$\hat{L} [f(E, t)] = E \frac{\partial f}{\partial t} - H |\vec{p}|^2 \frac{\partial f}{\partial E}. \quad (1.58)$$

Multiplying by $g/2\pi$ and integrating over the momentum we get the evolution of the number density of a species:

$$\frac{dn_i}{dt} + 3H n_i = \frac{g_i}{2\pi^3} \int C [E_i, t] \frac{d^3 p_i}{E_i}. \quad (1.59)$$

The equation above is describing a change in number density due to the Hubble rate of expansion ($3H n_i$) and to the interaction (the collisional term). The collisional term

of the Boltzmann equation is a complicated object in this case, i.e a binary process $1 + 2 \leftrightarrow 3 + 4$, under some approximations (CP invariance and absence of Bose-Einstein condensation or Fermi degeneracies [111]) it can be written in the following way:

$$\begin{aligned} \frac{dn_i}{dt} + 3H n_i = & - \int d\Pi_1 d\Pi_2 d\Pi_3 d\Pi_4 (2\pi)^4 |\mathcal{M}|^2 \\ & \times \delta^4(p_3 + p_4 - p_2 - p_1) [f_1 f_2 - f_3 f_4], \end{aligned} \quad (1.60)$$

where the integral is carried on the momentum space $d\Pi_i = (g_i/2\pi^3) (d^3p_i/E_i)$ and $|\mathcal{M}|^2$ is the matrix containing the scattering amplitudes. At this point, while the Universe is expanding two main processes may happen:

- 1 the interaction rate of the binary scattering processes becomes smaller than the Hubble rate of expansion preventing the $2 \leftrightarrow 2$ interactions,
- 2 the temperature T of the fluid becomes of the order of the mass of the species x ($T < m_x$) and the relativistic to nonrelativistic transition occurs.

If a massive particle remained in thermal equilibrium until the present day its abundance would be suppressed following Eq.(1.47), while, if the interaction rate becomes smaller than the Hubble rate, Eq.(1.53), that species can have a significant relic abundance today. In this case the Boltzmann equation can be rewritten as [30, 111]:

$$\frac{1}{a^3} \frac{d(n_1 a^3)}{dt} = -\langle \sigma v \rangle \left[n_1 n_2 - \left(\frac{n_1 n_2}{n_3 n_4} \right)_{\text{eq}} n_3 n_4 \right]. \quad (1.61)$$

Here n_{eq} means the number density calculated at the equilibrium. Writing the latter in terms of comoving density N_i (see Sec.(1.2.2) for details) we get:

$$\frac{d \ln N_1}{d \ln a} = -\frac{\Gamma_1}{H} \left[1 - \left(\frac{N_1 N_2}{N_3 N_4} \right)_{\text{eq}} \frac{N_3 N_4}{N_1 N_2} \right], \quad (1.62)$$

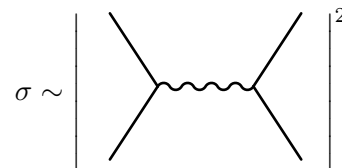
where $\Gamma_1 \equiv n_2 \langle \sigma v \rangle$ and the right-hand side of the equation describes the interaction efficiency. When $\Gamma \gg H$ the system evolves in function of the comoving number density: if $N_1 \gg N_1^{eq}$ the interaction efficiency results negative and particles of type 1 are destroyed during the scattering/annihilation process and the other way around. On the contrary if $\Gamma \ll H$ the right-hand side of Eq.(1.62) gets suppressed and N_1 goes asymptotically to a constant value.

1.3 Thermal history of the early Universe

Living in an expanding and adiabatically cooling Universe means that, at early times, it must have been denser and hotter. If we push this concept to the extreme, at a certain time, the macroscopic quantities described so far and the theory developed by Einstein diverge and the physical description that we are carrying out here is no longer valid. This condition or singularity of the theory is called Big bang (BB). It is known that the term "big bang" was coined by F.Hoyle for describing the initial stage of hot and dense Universe in a contempt sense: initially he did not believe in the model of expanding Universe. Today we refer to the big bang as the primordial singularity or the extrapolation of the expansion, back in time, of the universe which yields an infinite temperature and density at a finite time in the past. Physicists suggest that after the BB the Universe has experienced an epoch of exponential expansion called inflation. The existence of this era is needed by several discrepancies between theory and observations that are brilliantly fixed by inflation, Sec.(1.5). This is the earliest time in the Universe history that we are sure existed and nowadays there are several models of inflation [109, 123], however every one has to end with a suitable mechanism for generating particles, otherwise the Universe would have been diluted by the expansion (See Sec.(1.5) for more details). Nevertheless, at a certain point of the evolution, the Universe was a hot and dense phase, in this primordial fluid, composed by all the species described in the standard model of particles, we can make a safe approximation assuming local thermal equilibrium. Once we made this assumption we are going to consider the primordial fluid as a system in which particles interact each other mainly through binary processes, i.e. $1 + 2 \leftrightarrow 3 + 4$.

1.3.1 Early age

Start at sufficiently early times ($T > 100\text{GeV}$), all the known species were ultrarelativistic; the temperature of the soup was larger enough to consider the masses negligible and the cross section for the processes that took place in this era has the following form:

$$\sigma \sim \left| \begin{array}{c} \diagup \\ \diagdown \\ \diagdown \\ \diagup \end{array} \right|^2 \sim \frac{\alpha^2}{T^2}, \quad (1.63)$$


where α is the generalized coupling constant for such an interaction mediated by a gauge boson. From Eq.(1.41) the number density for ultrarelativistic particles is proportional to T^3 , as a result the reaction rate, Eq.(1.55) becomes:

$$\Gamma \sim \alpha^2 T. \quad (1.64)$$

The Hubble rate, considering Eq.(1.25), in the radiation dominated era the energy density scales proportionally to T^4 , thus:

$$H \sim \frac{T^2}{m_{\text{Pl}}} . \quad (1.65)$$

The ratio between the scattering rate and Hubble rate thus scales as $\Gamma/H \sim \alpha^2 m_{\text{Pl}}/T \propto 1/T$ that ensures an efficient mechanism for maximizing the entropy of the system. This is exactly the situation of thermodynamic and chemical equilibrium in which the distribution function of fermions and bosons are the Fermi-Dirac or Bose-Einstein distribution respectively.

As soon as the temperature falls below the mass of a particle $T \ll m$, that species becomes nonrelativistic and the number density is exponentially suppressed. In Fig.(1.2) we show the evolution of the comoving number density in function of the mass-temperature ratio m/T for a species that encounters both the relativistic to nonrelativistic transition and the decoupling.

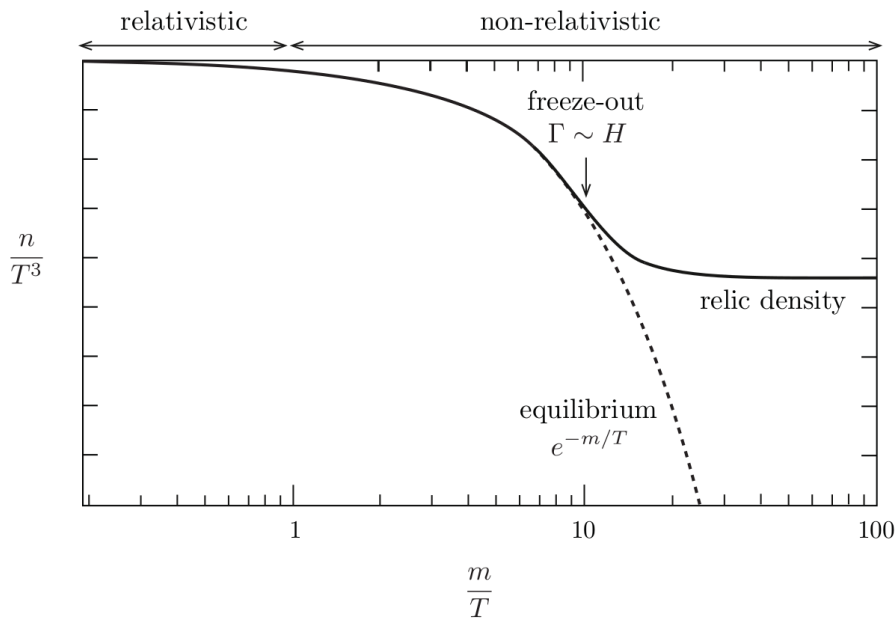


Figure 1.2: Simple evolution of the number density of a species in function of the m/T ratio; at high temperature ($m/T \ll 1$) it is relativistic and follows the equilibrium distribution function, then when the $m/T \sim 1$ it starts to be exponentially suppressed until the scattering ratio becomes of the order of the Hubble expansion rate. This inhibits the scattering processes and originates a relic density [30].

This process happened for every component of the primordial soup that is kept in equilibrium by scattering processes. In agreement with the prediction of SM and with

the results obtained in laboratory experiments [144], the evolution of the number of relativistic degrees of freedom can be summarized in Fig.(1.3), in particular it shows how the annihilations processes impact on g_* . During the early stages of the evolution of the

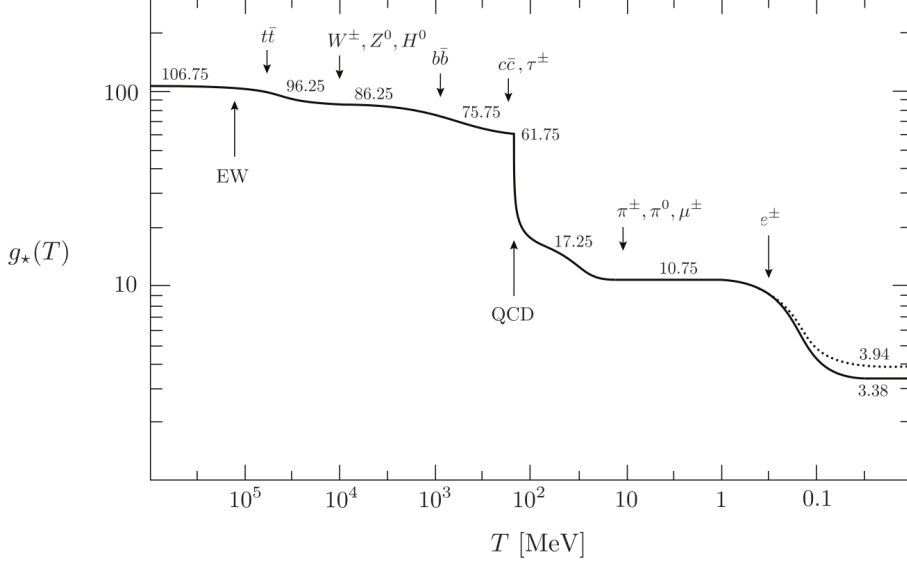


Figure 1.3: Evolution of the number of relativistic degrees of freedom assuming the species zoology provided by the SM. The top is the heaviest particle and annihilates at $T \sim 1/6m_t = 30\text{GeV}$ and so on following the mass hierarchy. The dotted line represent g_{*S} [30].

Universe the matter was in a hot plasma state, during the expansion and the associated cooling, the state of the primordial plasma encounters two phase transitions the first one is the Electroweak (EW), at $T \sim 300\text{ GeV}$. In this transition the SM provides an elegant and precise mechanism to generate the mass of the particles: the Higgs mechanism [99]. At this point quarks and leptons populate the plasma, the coupling constant for strong interactions g_s is small enough such that quarks behave like free particles. Usually this state is called quark-gluon plasma (QGP). From now, every time a fermion becomes nonrelativistic, due to annihilations or decays, g_* decreases of a factor $7/8 \times g_f$, while for a boson, for the same reasons, the reduction of g_* is by a factor g_b . The first species that encounters this fate is the heaviest lepton: the *top* (t). The Universe cools further more, bottom b , charm c and tau τ^- annihilate following the mass hierarchy, until temperatures reach scales $\sim 300 - 100\text{ MeV}$. At this point we can no longer assume g_s negligible, a new phase transition is predicted there: the Quantum chromo dynamics (QCD) phase transition. With the increase of the strong coupling constant the QGP gets replaced with the hadronic phase in which quarks are confined inside (neutrally coloured) baryons and mesons. After the QCD phase transition the quarks that survived to the annihilations processes are bound mainly in protons, neutrons (qqq) and mesons ($q\bar{q}$). Protons and neutrons can be

considered very stable particles (neutrons have a mean lifetime of $\tau_n \sim 890$ s that is larger than the Universe life-time at that epoch, protons are considered stable particles), while mesons like π^+ , π^- and π^0 and muons μ^\pm annihilate when $T \lesssim m_\mu \sim 100$ MeV. At this point the only relativistic particles left in the primordial soup are photons, neutrinos and electrons, the processes involving these species are very important and have consequences on the entropy conservation (dotted line in Fig.(1.3)), hence, we will see them in details later. In table, Tab.(1.1) we show a brief summary.

$T \sim 200$ GeV	All species	
$T < 170$ GeV	t annihilation	Start when t acquires mass
$T \sim 100$ GeV	Electroweak transition	Mass generation
$T < 80$ GeV	W^\pm, Z^0 annihilation	
$T < 1$ GeV	b, c, τ^- annihilation	
$T < 150$ MeV	QCD phase transition	hadron phase
$T < 100$ MeV	π^+, π^-, π^0 annihilation	e^\pm, γ, ν left

Table 1.1: In this table we show a summary of the main steps that occur in the hot ($T > 100$ MeV) primordial Universe. Notice that the temperature values are suggested values, annihilations and phase transitions are not instantaneous processes.

1.3.2 Neutrino decoupling

It is clear that, if the equilibrium had lasted and if every particle was annihilated, today Universe would have been composed mostly by photons, indeed, there is a mechanism that ensure the persistence of certain species. Deviations from equilibrium guarantee processes like decoupling and freeze-out of both massless and massive particles. When the $T \leq 100$ GeV, under the scale of electroweak symmetry breaking, the weak interaction mediators acquire mass $m_{Z^0} \sim m_{W^\pm}$, and the cross section for weak processes becomes:

$$\sigma \sim \left| \begin{array}{c} \diagdown \\ \diagup \end{array} \right|^2 \sim G_F^2 T^2, \quad (1.66)$$

where

$$G_F = \frac{\sqrt{2}}{8} \frac{\mathbf{g}^2}{m_W^2} = 1.1664 \times 10^{-5} \text{ GeV}^{-2}, \quad (1.67)$$

is the Fermi weak coupling constant and \mathbf{g} is the associated dimensionless coupling constant. For the ratio Γ/H :

$$\frac{\Gamma}{H} \sim \left(\frac{T}{1 \text{ MeV}} \right)^3, \quad (1.68)$$

hence, the weak interaction goes out of equilibrium very quickly (with the power to the temperature cube) once the mean temperature of the primordial fluid is less than 1 MeV. This process is called *decoupling* and leads to a conservation of the number density called *freeze-out*. The temperature $T \sim 1 \text{ MeV}$ is a crucial point in the history of the Universe: till that time a series of annihilations have depleted the variety of species (as shown in the previous section), leaving a few relativistic particles such as electrons, neutrinos and photons. In this scenario neutrinos, that have been in equilibrium due to weak interactions:

$$\nu_e + \bar{\nu}_e \leftrightarrow e^+ + e^-, \quad (1.69a)$$

$$e^- + \bar{\nu}_i \leftrightarrow e^- + \bar{\nu}_i, \quad (1.69b)$$

decoupled from the rest of the components, that means reactions, Eq.(1.69) no longer occur. Since we know that neutrinos have tiny masses (${}^3\text{H}$ decay Troitsk and Mainz experiments) at $T \sim 1 \text{ MeV}$ they were ultrarelativistic at the decoupling time and their distribution function was a pure Fermi-Dirac; thus when they decouple from the rest of the plasma they preserve their distribution. In order to see such a feature it is a good choice defining a time independent quantity that is unaffected by the expansion, Eq.(1.22) implies that $p \propto a^{-1}$ and thus the choice falls on the time-independent momentum $q \equiv ap$. Rewriting the Fermi-Dirac distribution in function of q as:

$$f_D = \frac{1}{e^{q/aT} + 1}, \quad (1.70)$$

implies that the neutrino distribution at later times is therefore again a Fermi-Dirac function.

1.3.3 Electron-positron annihilation

Other processes together with Eqs.(1.69) were in the primordial Universe, in particular one of the most important is the electron-positron annihilation and the associated pair creation:

$$e^+ + e^- \leftrightarrow \gamma + \gamma, \quad (1.71)$$

since the electron mass is $m_e = 0.511 \text{ MeV}$, the energy needed in order to make couple creation happen is exactly of the MeV order, this implies that, in a realistic case in which neutrino decoupling is not an instantaneous process, the time window in which couple creation starts to be inefficient partially overlap with the neutrino decoupling process. From Eq.(1.51) it is easy to see that entropy of the Universe is conserved in

agreement with the second law of thermodynamics (at least until we are considering it as a close adiabatically expanding thermodynamic system), however an injection of photons in the primordial plasma slightly change the evolution of relativistic degrees of freedom g_{*S} (see the dotted line in Fig.(1.3)). Photons are thus heated with respect neutrinos, i.e.

$$g_{*S} = \begin{cases} 2 + \frac{7}{8} \times 4 = \frac{11}{2} & T \geq m_e \\ 2 & T \leq m_e \end{cases}, \quad (1.72)$$

after electron annihilation the injection of energy leads to an increase of the entropy and consequently it would be redistributed in the temperature of the photon fluid T_γ that increases of a factor $(11/4)^{1/3}$ while T_ν remains the same. Taking the photon temperature as the reference temperature, we get:

$$T_\nu = \left(\frac{4}{11}\right)^{1/3} T_\gamma. \quad (1.73)$$

When the electron-positron annihilation finished at $T \ll m_e$ it is useful to separate the weight of the relativistic species into the count of the degrees of freedom,

$$g_* \equiv 2 + \frac{7}{8} \times 2 \times 3 \left(\frac{4}{11}\right)^{4/3}, \quad (1.74)$$

where the factor 3 is the number of neutrino families in the standard model of particles. This is what we would expect if neutrino decoupling was an instantaneous process. However, as we have said previously, it took some time for weak interactions to go out of equilibrium and the result is that these processes (neutrino decoupling and electron-positron annihilation) have been overlapping for a while. Part of the entropy released in the $e^+ e^-$ annihilation process was transferred to the neutrino sector. This leads to an extra contribution which has been parametrised using an effective number of neutrino families N_{eff} ,

$$g_* \equiv 2 + \frac{7}{8} \times 2 \times N_{\text{eff}} \left(\frac{4}{11}\right)^{4/3}. \quad (1.75)$$

Taking this into account these considerations the standard value is $N_{\text{eff}} = 3.046$ (3.045 as calculated more precisely by [55]). Using this parametrisation it is also possible to take into account other species that could contribute to the relativistic energy density in the early Universe or any other deviation from the standard prediction for this quantity (e.g. chemical potential for the neutrinos or low-reheating scenarios). In that case N_{eff} is a free parameter of the model.

1.3.4 Big bang nucleosynthesis

At temperature $T > 1$ MeV that corresponds to $t < 1$ second after the big bang, protons and neutrons are no longer relativistic and their number densities follow the Maxwell Boltzmann distribution, Eq.(1.47). Neutrons have larger masses with respect to protons $Q_n = m_n - m_p = 1.29$ MeV and they are unstable $\tau_n \sim 890$ s and decay through weak interactions in:

$$n \rightarrow p^+ + e^- + \bar{\nu}_e, \quad (1.76)$$

However, until weak interactions are in equilibrium, i.e. $t < 1$ s neutron decay is a negligible process, instead we have to consider the following:

$$n + \nu_e \leftrightarrow p^+ + e^-, \quad (1.77)$$

$$n + e^+ \leftrightarrow p^+ + \bar{\nu}_e. \quad (1.78)$$

After neutrino decoupling Eqs.(1.78) do not affect the neutrino distribution since the number density of neutrons and protons is small. The neutron to proton (n-p) ratio remains almost constant except neutrons decay, Eq.(1.76). The neutron to proton ratio, using Eq.(1.47), is:

$$\left(\frac{n_n}{n_p}\right)_{\text{eq}} = \left(\frac{m_n}{m_p}\right)^{3/2} e^{-Q_n/T}, \quad (1.79)$$

that basically show us the exponential drop of the n-p ratio once the mean temperature of the fluid is $T \ll Q_n$. In a more detailed way, using the Boltzmann equation, Eq.(1.61) with $1 = \text{neutrons}$, $2, 4 = \text{leptons}$ and $3 = \text{protons}$ we find:

$$\frac{1}{a^3} \frac{d(n_n a^3)}{dt} = -n_\ell \langle \sigma v \rangle \left[n_n - \left(\frac{n_n}{n_p}\right)_{\text{eq}} n_p \right] \quad (1.80)$$

Defining $X_n = n_n/(n_n + n_p)$ as the neutron fraction it is possible to find (see [30, 62] for more details) its value when the reaction becomes slow:

$$X_n^\infty \equiv X_n(Q/T \rightarrow \infty) = 0.15. \quad (1.81)$$

In this way the neutron decay can be calculated by multiplying the latter by an exponential decay factor:

$$X_n(t) = X_n^\infty e^{-\frac{t}{\tau_n}}. \quad (1.82)$$

The processes which take into account neutrons described so far are fundamental, they set the initial condition for the nucleosynthesis of the light elements in the primordial Universe. Indeed we have to consider that other reactions are in equilibrium in the

primordial plasma:

$$p^+ + p^+ \leftrightarrow D + e^+ + \bar{\nu}_e, \quad (1.83)$$

$$n + n \leftrightarrow D + e^- + \nu_e, \quad (1.84)$$

$$n + p^+ \leftrightarrow D + \gamma, \quad (1.85)$$

the first two processes are suppressed with respect to the third one because of the Columbian repulsive potential between two equally charged particles and the weakness of the weak interaction respectively. While the third one is the so called Deuterium nucleosynthesis. The binding energy of deuterium is $m_n + m_p - m_D = 2.22 \text{ MeV}$, applying the same procedure used in Eq.(1.79) we write down an equation for the deuterium-to-proton ratio:

$$\left(\frac{n_D}{n_p}\right)_{\text{eq}} \simeq \eta \left(\frac{T}{m_p}\right) e^{\frac{Q_D}{T}}, \quad (1.86)$$

where η is the baryon-to-photon ratio [144]:

$$\eta = n_b/n_\gamma \sim (5.1 - 6.5)^{-10} (95\% \text{ CL}). \quad (1.87)$$

It is useful to express the deuterium-to-proton ratio in terms of η , this is telling us that the production of D is inhibited until the temperature drops well beneath the binding energy Q_D . Notice the huge amount of photons with respect baryons that comes from the series of annihilation precesses described so far.

When the mean temperature of the primordial fluid drops below $T \sim 0.2 \text{ MeV}$ ($t \sim 100 \text{ s}$), helium cannot form directly, the density is too low and there is not enough time, this leads to a obliged path whose steps are:

$$D + p^+ \leftrightarrow {}^3\text{He} + \gamma, \quad (1.88)$$

$$D + {}^3\text{He} \leftrightarrow {}^4\text{He} + p^+. \quad (1.89)$$

$$(1.90)$$

In Fig.(1.4) one can see the fractional abundance evolution as a function of the temperature. Since the binding energy of helium is larger than the deuterium one (in Tab.(1.2) we show the main Q_i for the lightest nuclei), the Boltzmann equation favours the production of helium. It is possible to calculate the helium-to-proton ratio in the following way:

$$\frac{n_{\text{He}}}{n_p} = \frac{1}{2} X_n(t_{\text{nuc}}) \sim \frac{1}{16}, \quad (1.91)$$

where $t_{\text{nuc}} \sim 250 \text{ s}$ is the temperature at which BBN light elements production ends. Other elements have been produced in relatively low abundance during BBN such as lithium ${}^7\text{Li}$, and beryllium ${}^7\text{Be}$, but the synthesis of heavier elements is hampered by

A_Z	Q_i [MeV]
2H	2.22
3H	8.48
3He	7.72
4He	28.3

Table 1.2: Binding energies for the lightest nuclei produced during the BBN, A is the mass number and Z is the atomic number of the element.

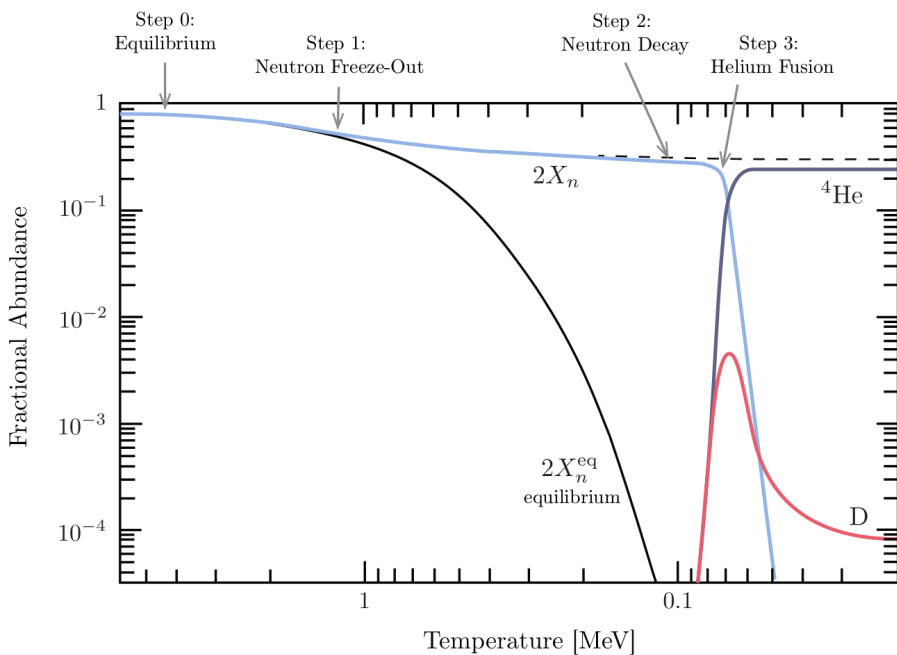


Figure 1.4: Fractional abundance of the lightest elements produced during BBN in function of temperature [30].

the absence of stable nuclei with $A = 8$.

1.3.5 Recombination, photon decoupling and last scattering

We continue to follow the expansion of the Universe, the next fundamental step encountered is the formation of neutral matter, i.e. atoms. At $T \geq 1$ eV the primordial soup is made of e^- (survived to electron-positron annihilation due to matter-antimatter asymmetry), γ , p^+ and the light nuclei produced during BBN; neutrinos are free-streaming and do not influence directly the dynamics that we are going to describe. In

this situation electromagnetic interaction guarantee the process:

$$p^+ + e^- \leftrightarrow H + \gamma, \quad (1.92)$$

which, however, does not provide the formation of neutral matter because of the great efficiency of the photo-dissociation process (remember the huge amount of photons with respect baryons Eq.(1.87)). Photons were tightly coupled to electrons via Compton scattering while Coulomb force kept tied protons with electrons. The equilibrium abundance ratio among hydrogen atoms, protons and electrons is given by the following formula:

$$\left(\frac{n_H}{n_e n_p} \right)_{eq} = \frac{g_H}{g_e g_p} \left(\frac{m_h}{m_e m_p} \frac{2\pi}{T} \right)^{3/2} e^{\frac{Q_H}{T}}, \quad (1.93)$$

where $Q_H = m_p + m_e - m_H = 13.6 \text{ eV}$ is the binding energy of the hydrogen atom. Assuming $n_p = n_e$ and following exactly what we have done in the previous section for deuterium and protons, Eq.(1.86), we can define a free electron fraction:

$$X_e = \frac{n_e}{n_b}, \quad (1.94)$$

and finally write the Saha equation:

$$\left(\frac{1 - X_e}{X_e^2} \right)_{eq} = \frac{2\zeta(3)}{\pi^2} \eta \left(\frac{2\pi T}{m_e} \right)^{3/2} e^{\frac{Q_H}{T}}. \quad (1.95)$$

When 90% of electrons are bound with protons the mean temperature is $T_{\text{rec}} \sim 0.3 \text{ eV}$ which correspond to $z_{\text{rec}} \sim 1300$, notice that it is almost two orders of magnitude lower than the hydrogen binding energy, but once again it is due to the η ratio: the great number of photons increases the statistical weight of the tail of photon distribution, that is, when the mean temperature is of the order of Q_H , there are still many photons with $T \gg 13.6 \text{ eV}$ that prevent recombination. When hydrogen recombines the free electron density drops down quickly, photons inside the plasma, that were kept tied by Compton scattering, no longer interact and therefore are free to stream in a neutral Universe. This process takes the name of *photon decoupling*, the physics under the process cannot be explained only using the Saha equation, see Fig.(1.5), we need a complete discussion through the Boltzmann equation, however in order to estimate the temperature and time of photon decoupling we can compare $\Gamma_\gamma(T) = n_b X_e(T) \sigma_{\text{Th}}$ and $H(T) = H_0 \sqrt{\Omega_m} (T/T_0)^{3/2}$ (here T_0 is the temperature of photons today). We find that decoupling happened at

$$T_{\text{dec}} \sim 0.27 \text{ eV}, \quad (1.96)$$

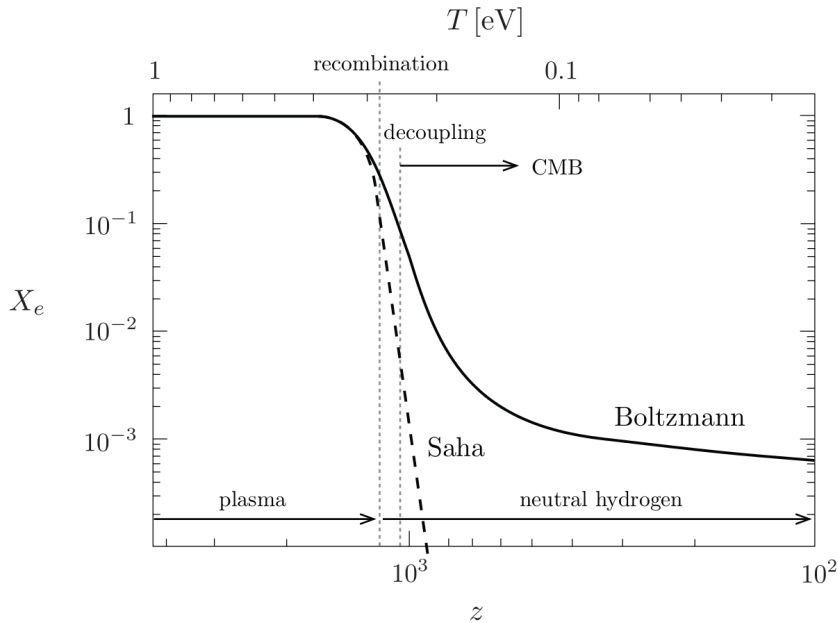


Figure 1.5: Free electron fraction in function of the redshift z or temperature T , hydrogen recombination is well described by the Saha equation that starts to fail when the photon decoupling happens [30].

which corresponds to

$$z_{\text{dec}} \sim 1100, \tag{1.97}$$

$$t_{\text{dec}} \sim 380\,000 \text{ Yr}. \tag{1.98}$$

These processes originate a last scattering layer that, compared with the Universe time scale, can be considered a *Last Scattering Surface*, this is the last moment when photons interact with the primordial plasma. From now on they are free to travel in the Universe that is, now, transparent to electromagnetic radiation. These photons carry on information of the pre-last-scattering Universe, this relic radiation is known as Cosmic Microwave Background (CMB) radiation and it is one of the most important discoveries of mankind.

1.4 Inhomogeneous Universe

So far, following the cosmological principle, we have considered and treated the Universe as a homogeneous system, however the complete description of the evolution of particle

densities during the thermal history of the Universe and the observations such as the CMB anisotropies [9], and the formation of large-scale structures, requires to introduce a perturbation theory able to describe the evolution of the different species i.e. baryons, dark matter, photons, neutrinos and dark energy inside the proper theoretical framework. In this section we will provide a description of the relativistic perturbation theory and of the associated Einstein and Boltzmann equations for the perturbed Universe. We will follow the approach described in [127], taking as time variable the conformal time $d\tau = dt/a$ and going to the Fourier space in order to simplify the problem facing of differential equation problem instead of partial differential equations.

1.4.1 Perturbation theory

Considering small perturbations $\delta g_{\mu\nu}$ of the FRW metric $\bar{g}_{\mu\nu}$ ¹, the perturbed metric takes the form:

$$g_{\mu\nu} = \bar{g}_{\mu\nu} + \delta g_{\mu\nu}, \quad (1.99)$$

with $|\delta g_{\mu\nu}| \ll |\bar{g}_{\mu\nu}|$. As we said before we are going to consider two gauges in which it is possible to write down the equations, in the *Newtonian* gauge the perturbations are characterized by two scalar potentials ψ and ϕ :

$$ds^2 = a^2(\tau) \left[-(1 + 2\psi) d\tau^2 + (1 - 2\phi) dx^i dx_i \right], \quad (1.100)$$

the advantages of this gauge choice is that the metric tensor $g_{\mu\nu}$ is diagonal, however as it appears it is valid only for scalar modes of the metric. Making the choice of the *synchronous* gauge the perturbed metric, Eq.(1.3) becomes:

$$ds^2 = a^2(\tau) \left[-d\tau^2 + (\delta_{ij} + h_{ij}) dx^i dx^j \right], \quad (1.101)$$

where the perturbation to the spatial part of the metric can be decomposed in

$$h_{ij} = h(\vec{x}, \tau) \delta_{ij} / 3 + h_{ij}^{\parallel}(\vec{x}, \tau) + h_{ij}^{\perp}(\vec{x}, \tau) + h_{ij}^T(\vec{x}, \tau). \quad (1.102)$$

The terms in the right hand side are, in order of appearance: the trace part $h = h_{ii}$, the longitudinal and transverse traceless parts where $h\delta_{ij}/3 + h_{ij}^{\parallel}$ represent the scalar modes, h_{ij}^{\perp} corresponds to the vector modes and finally h_{ij}^T is the tensor mode source. In the Fourier space we introduce two fields $h(\vec{k}, \tau)$ and $\eta(\vec{k}, \tau)$, which are related to $h(\vec{x}, \tau)$ and $h_{ij}^{\parallel}(\vec{x}, \tau)$:

$$h_{ij}(\vec{x}, \tau) = \int d^3k e^{i\vec{k}\cdot\vec{x}} \left[\hat{k}_i \hat{k}_j h(\vec{k}, \tau) + \left(\hat{k}_i \hat{k}_j - \frac{1}{3} \delta_{ij} \right) 6 \eta(\vec{k}, \tau) \right]. \quad (1.103)$$

¹In this section the unperturbed terms will be defined with an overbar.

Considering only the scalar modes, in the k-space it is possible to connect the synchronous and Newtonian gauge potentials through the following relations:

$$\psi(\vec{k}, \tau) = \frac{1}{2k^2} \left[\ddot{h}(\vec{k}, \tau) + 6\ddot{\eta}(\vec{k}, \tau) + \frac{\dot{a}}{a} \left[\dot{h}(\vec{k}, \tau) + 6\dot{\eta}(\vec{k}, \tau) \right] \right], \quad (1.104)$$

$$\phi(\vec{k}, \tau) = \eta(\vec{k}, \tau) - \frac{1}{2k^2} \frac{\dot{a}}{a} \left[\dot{h}(\vec{k}, \tau) + 6\dot{\eta}(\vec{k}, \tau) \right]. \quad (1.105)$$

Let us describe only the synchronous gauge case. Once established the potential in both gauges the following step consist in writing a set of linear Einstein equations, in analogy to what we have done in the unperturbed case, the starting point is the energy momentum tensor, Eq.(1.8), the perturbed form of $T^\mu_\nu = \bar{T}^\mu_\nu + \delta T^\mu_\nu$ is given by:

$$T^0_0 = -(\bar{\rho} + \delta\rho), \quad (1.106a)$$

$$T^0_i = -T^i_0 = -(\bar{\rho} + \bar{P})V_i, \quad (1.106b)$$

$$T^i_j = (\bar{P} + \delta P)\delta^i_j + \Sigma^i_j, \quad (1.106c)$$

where $\Sigma^i_j = T^i_j - \delta^i_j T^k_k/3$ is the anisotropic shear and $\delta\rho$, δP are the density and pressure perturbations respectively. In the Synchronous gauge, in light of the perturbed energy momentum tensor, the Einstein equations take the form:

$$k^2\eta - \frac{1}{2} \frac{\dot{a}}{a} \dot{h} = 4\pi G a^2 \delta T^0_0, \quad (1.107a)$$

$$k^2\dot{\eta} = 4\pi G a^2 (\bar{\rho} + \bar{P})\theta, \quad (1.107b)$$

$$\ddot{h} + 2\frac{\dot{a}}{a} \dot{h} - 2k^2\eta = -8\pi G a^2 \delta T^i_j, \quad (1.107c)$$

$$\ddot{h} + 6\ddot{\eta} + 2\frac{\dot{a}}{a} (\dot{h} + 6\dot{\eta}) - 2k^2\eta = -24\pi G a^2 (\bar{\rho} + \bar{P})\sigma. \quad (1.107d)$$

with $(\bar{\rho} + \bar{P})\theta = ik^j \delta T^0_j$ and $(\bar{\rho} + \bar{P})\sigma = -(\hat{k}_i \cdot \hat{k}_j - \frac{1}{3}\delta_{ij})\Sigma^i_j$, the divergence of the velocity of the fluid is $\theta = ik^j V_j$ and σ is the anisotropic stress. We report also the Newtonian gauge version of the latter system of equations:

$$k^2\phi + 2\frac{\dot{a}}{a} \left(\dot{\phi} + \frac{\dot{a}}{a} \psi \right) = 4\pi G a^2 \delta T^0_0,$$

$$k^2 \left(\dot{\phi} + \frac{\dot{a}}{a} \psi \right) = 4\pi G (\bar{\rho} + \bar{P}) \theta, \quad (1.108)$$

$$\ddot{\phi} + \frac{\dot{a}}{a} (\dot{\psi} + 2\dot{\phi}) + \left(2\frac{\ddot{a}}{a} - \frac{\dot{a}^2}{a^2} \right) \psi + \frac{k^2}{3} (\phi - \psi) = \frac{4\pi}{3} G a^2 \delta T^i_i,$$

$$k(\phi - \psi) = 12\pi G a^2 (\bar{\rho} + \bar{P}) \sigma.$$

Now, defining

$$\delta \equiv \frac{\delta\rho}{\bar{\rho}}, \quad (1.109)$$

and considering the conservation of the energy momentum tensor, or the second Bianchi identity in k-space we get:

$$\dot{\delta} = -(1+w) \left(\theta + \frac{\dot{h}}{2} \right) - 3 \left(\frac{\delta P}{\delta \rho} - w \right) \delta, \quad (1.110a)$$

$$\dot{\theta} = -\frac{\dot{a}}{a}(1-3w)\theta - \frac{\dot{w}}{1+w}\theta + \frac{\delta P/\delta \rho}{1+w}k^2\delta - k^2\sigma. \quad (1.110b)$$

These are the relativistic generalization of the continuity and Euler equations, they are valid for the total matter and velocity components of a single uncoupled fluid, thus they need to be modified in order to take into account the effect of interactions, for example, in case of baryons which interacts with photon fluid through Thomson scattering.

The proper description of the fluids in the early Universe, as we have seen in Sec.(1.2.3), requires the use of the Boltzmann equation, Eq.(1.56). Working in the phase-space we have to deal with the conformal time τ plus six variables: three positions x^i and the corresponding conjugate momenta $P_j = a(\delta_{ij} + h_{ij}/2)p^j$ (in Sync. gauge), where p^j is the proper momentum. In analogy to the real space, the phase-space distribution $f(x^i, P_j, \tau)$ gives us information about the microscopical properties of a species in a differential volume $dx^1 dx^2 dx^3 dP_1 dP_2 dP_3$, i.e. the number of particles is:

$$dN = f(x^i, P_j, \tau) dx^1 dx^2 dx^3 dP_1 dP_2 dP_3. \quad (1.111)$$

It is important to notice that also in the perturbative theory x^i and P_j remain canonical variables [90] allowing the carrying out of the Hamilton's equation [34], however for this purpose it is convenient to change the coordinate system passing from (x^i, P_j, τ) to (x^i, q, n_j, τ) with

$$q_j \equiv ap_j = qn_j, \quad (1.112)$$

defined as comoving three momentum. Even if this is not a canonical transformation, the coordinate change is still valid once the same transformation has been applied to the Hamilton's equation. In this case the phase-space distribution can be factorized into two contributions, the unperturbed one f_0 and a pure perturbative part Ψ :

$$f(x^i, q, n_j, \tau) = f_0(q) [1 + \Psi(x^i, q, n_j, \tau)], \quad (1.113)$$

and the linearized energy momentum tensor becomes:

$$T_0^0 = -a^{-4} \int q^2 dq d\Omega \sqrt{q^2 + m^2 a^2} f_0(q) (1 + \Psi), \quad (1.114a)$$

$$T_i^0 = a^{-4} \int q^2 dq d\Omega q n_i f_0(q) \Psi, \quad (1.114b)$$

$$T_j^i = a^{-4} \int q^2 dq d\Omega f_0(q) \frac{q^2 n_i n_j}{\sqrt{q^2 + m^2 a^2}} (1 + \Psi). \quad (1.114c)$$

Moreover, also the Liouville operator can be expressed in a different way:

$$\hat{L} = \frac{\partial}{\partial \tau} + \frac{dx^i}{d\tau} \frac{\partial}{\partial x^i} + \frac{dq}{d\tau} \frac{\partial}{\partial q} + \frac{dn_j}{d\tau} \frac{\partial}{\partial n_j}, \quad (1.115)$$

leading to the phase-space Boltzmann equation:

$$\frac{Df}{d\tau} = \frac{\partial f}{\partial \tau} + \frac{dx^i}{d\tau} \frac{\partial f}{\partial x^i} + \frac{dq}{d\tau} \frac{\partial f}{\partial q} + \frac{dn_j}{d\tau} \frac{\partial f}{\partial n_j} = \left(\frac{\partial f}{\partial \tau} \right)_C, \quad (1.116)$$

where the left hand side is the collisional term. It is possible to simplify the Boltzmann equation using the geodesics equation for deriving the time derivative of the momentum,

$$dq/d\tau = -\frac{1}{2} q \dot{h}_{ij} n_i n_j, \quad (1.117)$$

and considering the time derivative of the direction $dn_j/d\tau$ constant, at least at the zero order. Thus in the Synchronous gauge the k-space Boltzmann equation can be written as follows.

$$\frac{\partial \Psi}{\partial \tau} + i \frac{q}{\epsilon} (\vec{k} \cdot \hat{n}) \Psi + \frac{d \ln f_0}{d \ln q} \left[\dot{\eta} - \frac{\dot{h} + 6\dot{\eta}}{2} (\hat{k} \cdot \hat{n})^2 \right] = \frac{1}{f_0} \left(\frac{\partial f}{\partial \tau} \right)_C, \quad (1.118)$$

where $\epsilon \equiv (q^2 + a^2 m^2)^{1/2}$ is the proper energy measured by a comoving observer. In the Newtonian gauge, instead, the phase-space Boltzmann equation is,

$$\frac{\partial \Psi}{\partial \tau} + i \frac{q}{\epsilon} (\vec{k} \cdot \hat{n}) \Psi + \frac{d \ln f_0}{d \ln q} \left[\dot{\phi} - i \frac{\epsilon}{q} (\vec{k} \cdot \hat{n}) \psi \right] = \frac{1}{f_0} \left(\frac{\partial f}{\partial \tau} \right)_C. \quad (1.119)$$

It is possible to carry out a set of equations for every species: cold dark matter, neutrinos, baryons and photons. We are going to present these equation in the Synchronous gauge only remanding to [127] for further details.

Cold dark matter

Observations of CMB radiation, structure formation and galaxy dynamics seems to point towards the existence of a cold, i.e. non relativistic, pressureless fluid which interacts only via gravity. In the Synchronous gauge the evolution of CDM density perturbation is governed by:

$$\dot{\delta}_c = -\frac{1}{2} \dot{h}, \quad (\text{Syn}) \quad (1.120)$$

while all higher moments vanish.

Massless neutrinos

Massless neutrinos can be treated as a relativistic collisionless fluid ($\rho_\nu = 3P_\nu = -T^0_0 = T^i_i$), from Eqs.(1.114) it is possible to write the unperturbed energy density as:

$$\bar{\rho}_\nu = 3\bar{P}_\nu = a^{-4} \int q^2 dq d\Omega q f_0(q) \Psi. \quad (1.121)$$

One of the advantages of considering neutrinos as massless is that it is possible to evolve the distribution function integrating out the momentum q :

$$F_\nu(\vec{k}, \hat{n}, \tau) \equiv \frac{\int q^2 dq q f_0(q) \Psi}{\int q^2 dq q f_0(q)} \quad (1.122)$$

where F_ν is the perturbation to the distribution function. Performing a Legendre polynomial expansion Eq.(1.122) can be rewritten in the following way:

$$F_\nu \equiv \sum_0^\infty (-i)^\ell (2\ell + 1) F_{\nu\ell} P_\ell(\hat{k} \cdot \hat{n}). \quad (1.123)$$

In this framework the perturbations δ_ν , θ_ν and σ_ν become,

$$\delta_\nu = \frac{1}{4\pi} \int d\Omega F_\nu(\vec{k}, \hat{n}, \tau) = F_{\nu 0}, \quad (1.124a)$$

$$\theta_\nu = \frac{3i}{16\pi} \int d\Omega (\vec{k} \cdot \hat{n}) F_\nu(\vec{k}, \hat{n}, \tau) = \frac{3}{4} k F_{\nu 1}, \quad (1.124b)$$

$$\sigma_\nu = \frac{3}{16\pi} \int d\Omega \left[(\vec{k} \cdot \hat{n})^2 - \frac{1}{3} \right] F_\nu(\vec{k}, \hat{n}, \tau) = \frac{1}{2} F_{\nu 2}. \quad (1.124c)$$

and the Boltzmann equation takes the general form:

$$\frac{\partial F_\nu}{\partial \tau} + ik\mu F_\nu = -\frac{2}{3}\dot{h} - \frac{4}{3}(\dot{h} + 6\dot{\eta}) P_2(\mu) \quad (\text{Syn}), \quad (1.125)$$

Carrying out the integration over μ of two or more Legendre polynomials we obtain the ℓ moment is affected only by the previous $\ell - 1$ and the following $\ell + 1$ moments, this allows us to write,

$$\dot{\delta}_\nu = -\frac{4}{3}\dot{\theta}_\nu - \frac{2}{3}\dot{h}, \quad (1.126a)$$

$$\dot{\theta}_\nu = k^2 \left(\frac{1}{4}\dot{\delta}_\nu - \dot{\sigma}_\nu \right) \quad (1.126b)$$

$$\dot{\sigma}_\nu = \frac{4}{15}\dot{\theta}_\nu - \frac{3}{10}kF_{\nu 3} + \frac{2}{15}\dot{h} + \frac{4}{5}\dot{\eta}, \quad (1.126c)$$

$$\dot{F}_{\nu\ell} = \frac{k}{2\ell + 1} [\ell F_{\nu(\ell-1)} - (\ell + 1) F_{\nu(\ell+1)}]. \quad (\ell \geq 3) \quad (1.126d)$$

This infinite hierarchy can only be solved numerically, and thus needs to be truncated at some point; a rough truncation imposing $F_{\nu\ell} = 0$ for $\ell > \ell_{\max}$, in light of what was previously said about ℓ dependence, generates a propagation of errors from the higher multipoles towards the lowers. In order to avoid this behaviour a more sophisticated method was provided in [127], this consists in extrapolating the behaviour of $F_{\nu(\ell_{\max}+1)}$. Looking at the last equation of Eq.(1.126) it is evident that the form of $F_{\nu\ell}$ is similar to a spherical Bessel function $1/k j_\ell = 1/(2\ell + 1) [\ell j_{\ell-1} - (\ell + 1)j_{\ell+1}]$, thus it is possible to approximate the last moment of the hierarchy is such a way:

$$F_{\nu(\ell_{\max}+1)} \simeq \frac{2\ell_{\max} + 1}{k \tau} F_{\nu(\ell_{\max})} - F_{\nu(\ell_{\max}-1)}. \quad (1.127)$$

Massive neutrinos

Considering neutrinos as massless particles is a good approximation for the study of their properties in the early Universe. However, it is well known, see Ch.(3), that they have a mass and this, if large enough, may impact on the primordial inhomogeneities and anisotropies, thus we need to describe also the massive case with an appropriate Boltzmann formalism. Dealing with massive neutrinos prevents, by definition, the approximation of massless particles ($\epsilon = q$) and the possibility of simplify the form of the Boltzmann equation by integrating out the comoving momentum. From Eq.(1.118), expanding the perturbation directly inside the Boltzmann equation, it is possible to write the following,

$$\frac{\partial \Psi}{\partial \tau} + i \frac{q}{\epsilon} k \mu \Psi - \frac{d \ln f_0}{d \ln q} \left[\frac{1}{6} \dot{h} + \frac{1}{3} (\dot{h} + 6\dot{\eta}) P_2(\mu) \right] = 0. \quad (1.128)$$

This, as done for the massless case, leads to a hierarchy of equations and to a similar truncation method:

$$\dot{\Psi}_{\nu,0} = -\frac{qk}{\epsilon} \Psi_{\nu,1} + \frac{1}{6} \dot{h} \frac{d \ln f_0}{d \ln q}, \quad (1.129a)$$

$$\dot{\Psi}_{\nu,1} = \frac{qk}{3\epsilon} (\Psi_{\nu,0} - 2\Psi_{\nu,2}), \quad (1.129b)$$

$$\dot{\Psi}_{\nu,2} = \frac{qk}{5\epsilon} (2\Psi_{\nu,1} - 3\Psi_{\nu,3}) - \left(\frac{1}{15} \dot{h} + \frac{2}{5} \dot{\eta} \right) \frac{d \ln f_0}{d \ln q}, \quad (1.129c)$$

$$\dot{\Psi}_{\nu,\ell} = \frac{qk}{(2\ell + 1)\epsilon} \left[\ell \Psi_{\nu,(\ell-1)} - (\ell + 1) \Psi_{\nu,(\ell+1)} \right], \quad (\ell \geq 3), \quad (1.129d)$$

and the corresponding truncation,

$$\Psi_{\nu(\ell_{\max}+1)} \simeq \frac{(2\ell_{\max} + 1) \epsilon}{q k \tau} \Psi_{\nu(\ell_{\max})} - \Psi_{\nu(\ell_{\max}-1)}. \quad (1.130)$$

Notice that the q dependence requires the existence of a different hierarchy for every comoving moment. This leads to a more complicated set of equation that have to be integrated.

Photons

One of the advantages of the Boltzmann formalism is that the geometrical information and the effects on the metric, and thus on the potential, are encoded exclusively in the left-hand part of Eq.(1.118), e.g. every massless species share the same left-hand part. Since photons are massless particles, they can be described exactly as we done for massless neutrinos, however, as mediators of electromagnetic interactions, photons are deeply involved, through the Thomson scattering, in the processes before hydrogen recombination. This behaviour introduces two collisional terms in the right-hand side of Eq.(1.118):

$$\left(\frac{\partial F_\gamma}{\partial \tau}\right)_C = an_e \sigma_T \left[-F_\gamma + F_{\gamma 0} + 4\hat{n} \cdot \vec{v}_e - \frac{1}{2} (F_{\gamma 2} + G_{\gamma 0} + G_{\gamma 2}) P_2 \right], \quad (1.131)$$

$$\left(\frac{\partial G_\gamma}{\partial \tau}\right)_C = an_e \sigma_T \left[G_\gamma + \frac{1}{2} (F_{\gamma 2} + G_{\gamma 0} + G_{\gamma 2}) (1 - P_2) \right]. \quad (1.132)$$

The quantities F_γ and G_γ are respectively the total intensity perturbation and the difference between the polarization states and σ_T is the Thomson scattering cross section. In presence of multipoles of order greater then 2 in the scattering term, photons can undergo a process of polarization during the interaction. Basically, considering an unpolarized wave propagating along the direction \hat{z} and scattered by an electron to the direction \hat{x} , the resulting direction of the electric field would be \hat{y} , with a depletion of the \hat{x} component. From a more realistic point of view, incoming directions of photons, outgoing scattering angles are randomly distributed and thus the final polarization results as an integration over all the possible directions. Carrying out the same multipole expansion we have seen for massless neutrinos, the photon Boltzmann hierarchy, in

Synchronous gauge, takes the following form:

$$\dot{\delta}_\gamma = -\frac{4}{3}\theta_\gamma - \frac{2}{3}\dot{h}, \quad (1.133a)$$

$$\dot{\theta}_\gamma = k^2 \left(\frac{1}{4}\delta_\gamma - \sigma_\gamma \right) + a n_e \sigma_T (\theta_b - \theta_\gamma) \quad (1.133b)$$

$$\dot{\sigma}_\gamma = \frac{4}{15}\theta_\gamma - \frac{3}{10}kF_{\gamma 3} + \frac{2}{15}\dot{h} + \frac{4}{5}\dot{\eta} - \frac{9}{10}a n_e \sigma_T \sigma_\gamma + \frac{1}{20}a n_e \sigma_T (G_{\gamma 0} + G_{\gamma 2}), \quad (1.133c)$$

$$\dot{F}_{\gamma \ell} = \frac{k}{2\ell + 1} [\ell F_{\gamma(\ell-1)} - (\ell + 1) F_{\gamma(\ell+1)}] - a n_e \sigma_T F_{\gamma \ell}. \quad (\ell \geq 3) \quad (1.133d)$$

$$\begin{aligned} \dot{G}_{\gamma \ell} = & \frac{k}{2\ell + 1} [\ell G_{\gamma(\ell-1)} - (\ell + 1) G_{\gamma(\ell+1)}] \\ & + a n_e \sigma_T \left[-G_{\gamma \ell} + \frac{1}{2} (F_{\gamma 2} + G_{\gamma 0} + G_{\gamma 2}) \left(\delta_{\ell 0} + \frac{\delta_{\ell 2}}{5} \right) \right]. \end{aligned} \quad (1.133e)$$

In this set of equations the subscript b is referred to the baryon part of the fluid which takes part to the scattering processes and $\theta_b \equiv \frac{3k}{4}v_b$, as it is possible to see from Eq.(1.124). The Thomson opacity has to be taken into account also in the truncation of the hierarchy, i.e.

$$\dot{F}_{\ell_{\max}} = kF_{(\ell_{\max}-1)} - \frac{(\ell + 1)}{\tau} F_{\ell_{\max}} - a n_e \sigma_T F_{\ell_{\max}}, \quad (1.134a)$$

$$\dot{G}_{\ell_{\max}} = kG_{(\ell_{\max}-1)} - \frac{(\ell + 1)}{\tau} G_{\ell_{\max}} - a n_e \sigma_T G_{\ell_{\max}}. \quad (1.134b)$$

Baryons

During the process described so far, at least after neutrino decoupling, baryons can be considered as non relativistic. In analogy to what we have done for photons, whose left-hand side part of the Boltzmann equation is identical to the neutrino one, the left-hand side part of the Boltzmann equation for baryons has common elements with the dark matter one (in this case the average velocity term that did not appear in the dark matter case). The collisional part, instead, comes from interactions with photons, and it is present only in the velocity perturbation equation:

$$\dot{\delta}_b = -\theta_b - \frac{1}{2}\dot{h}, \quad (1.135a)$$

$$\dot{\theta}_b = -H\theta_b + c_s^2 k^2 \delta_b + \frac{4\bar{\rho}_\gamma}{3\bar{\rho}_b} a n_e \sigma_T (\theta_\gamma - \theta_b), \quad (1.135b)$$

where c_s^2 is the squared sound speed of baryons and it is defined as:

$$c_s^2 \equiv \frac{\dot{P}_b}{\dot{\rho}_b}. \quad (1.136)$$

All the higher terms of the hierarchy are suppressed.

Tight coupling regime

The scattering rate among photons and baryons that appears in the Boltzmann hierarchies of both species becomes larger when the scale factor is smaller, this means that, at a certain point, the Thomson opacity will be so large that the collisional term would dominate the dynamics. This is not only an interesting regime, but, also from a numerical point of view, it requires an extra effort for having a stable set of equations. When the scattering rate $\Gamma = \tau_c^{-1}$ is much larger than the Hubble rate $H = \tau^{-1}$ the number of multipole equations that are required for a complete description reduces to $\ell = 2$ and can be obtained combining the velocity equations for the baryon, Eq.(1.135) and photon, Eq.(1.133) fluid. Defining

$$R = \frac{4\bar{\rho}_\gamma}{3\bar{\rho}_b} \quad (1.137)$$

one can write a joint formula:

$$\theta_b - \theta_\gamma = \frac{\tau_c}{(1+R)} \left[-H\theta_b + c_s^2 k^2 \delta_b - k^2 \left(\frac{1}{4} \delta_\gamma - \sigma_\gamma \right) + \dot{\theta}_\gamma - \dot{\theta}_b \right]. \quad (1.138)$$

and the corresponding shear

$$\sigma_\gamma = \frac{\tau_c}{9} \left(\frac{8}{3} \theta_\gamma + \frac{4}{3} \dot{h} + 8\dot{\eta} - 10\dot{\sigma}_\gamma - 3kF_{\gamma 3} \right). \quad (1.139)$$

All the higher moments in the photon distribution are smaller and thus we can neglect in the Boltzmann hierarchy. Playing more with the equations presented so far (see [127] for details) it is possible to write an equation for $\dot{\theta}_\gamma$:

$$\dot{\theta}_\gamma = -R^{-1} \left(\dot{\theta}_b + H\theta_b - c_s^2 k^2 \delta_b \right) + k^2 \left(\frac{1}{4} \delta_\gamma - \sigma_\gamma \right). \quad (1.140)$$

1.5 Inflation

In order to complete the overview of the standard cosmological model we need a suitable set of initial conditions, valid when the inhomogeneity size (wavelength λ_k) is larger than the horizon distance τ . Moreover the picture described so far needs a mechanism able to solve some *problems* that naturally rises. Inflation is a period of exponential accelerated expansion where the scale factor evolves in the following way

$$a(t) \sim e^{Ht}, \quad (1.141)$$

the accelerated expansion is due to spontaneous symmetry breaking of a scalar field ϕ coupled with the primordial plasma. This mechanism solves three problems of the Standard Cosmological model such as flatness, causality and monopole abundance, moreover it provides an elegant explanation to the homogeneity and isotropy of the Universe introducing a channel for the creation of primordial fluctuations. In 1980 D. Kazanas [108] argued that an exponential regime could solve the observed homogeneity and isotropy, a few month later Guth [92] in the famous paper “Inflationary Universe” published the solution to the horizon and causality problem. However these first works on Inflation do not provide a good description of the Universe, the first reliable model was suggested by A.Linde [124] and Albrecht and Steinhardt [18] in 1983. The scientific production of papers on Inflationary models is one of the most rich and variegated and we have no time to present everyone, in the next sections we will present the simplest model.

1.5.1 Flatness and horizon problems

If we do not include Inflation inside the SCM a couple of problems arise:

- 1 The entire CMB sky is homogeneous and isotropic up to one part in 100000 although photons come from regions that were causally disconnected at the time of emission.
- 2 Our Universe appears to be flat, Planck [10] measures the curvature parameter $\Omega_\kappa \sim -0.005 \pm 0.016$

Let us start from the first problem, taking a light-like metric $ds^2 = -dt^2 + a dx^2 = 0$, the horizon distance or the distance travelled by a photon at the Last-Scattering time is

$$d_{\text{hor}}^\gamma \sim \frac{2}{H(t_{\text{LS}})} \sim 0.4 \text{ Mpc}, \quad (1.142)$$

if we calculate the angle subtended by this horizon, Eq.(1.33), we obtain:

$$\theta_{\text{hor}} = \frac{d_{\text{hor}}^\gamma}{d_A} \sim 1.6 \text{ deg}. \quad (1.143)$$

This is the angular size of a causally connected region on the Last-Scattering surface, that is in contrast with the apparently homogeneous emission of the CMB sky. Inflation provides a solution basically making H^{-1} constant during the entire process of expansion, in Fig.(1.6) we show how a perturbation mode, during cosmological inflation, grows larger than the horizon and then comes back inside the horizon, which grows slower during radiation domination.

The flatness problem or Dicke coincidence arises from the Friedmann equation,

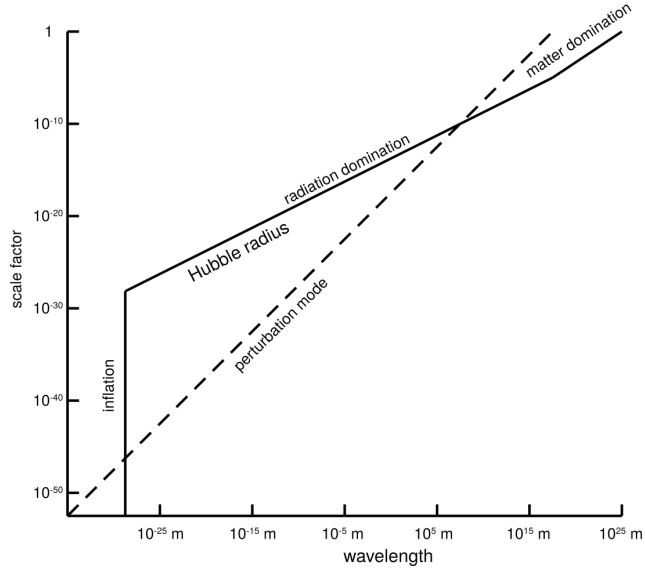


Figure 1.6: Scale factor in function of the wavelength, here we can see the Hubble radius (solid line) and the horizon distance of a perturbation mode (dashed line).

Eq.(1.26), which, considering $a = a_0 = 1$, can be rewritten in the following way:

$$\Omega_{\text{tot}-1} = \frac{H_0^2}{H^2(a)} \frac{\Omega_\kappa}{a^2} \quad (1.144a)$$

$$= \frac{\kappa}{H^2(a) a^2}, \quad (1.144b)$$

This is an object that looking back in time becomes smaller and smaller, in order to quantify the magnitude we can compare the total densities parameters, in the radiation epoch:

$$\frac{\Omega_{\text{tot}} - 1|_{t=t_{\text{early}}}}{\Omega_{\text{tot}} - 1|_{t=t_{\text{late}}}} = \left(\frac{a_0}{a_{\text{early}}} \right)^2 \quad (1.145a)$$

$$= \left(\frac{T_0}{T_{\text{Planck}}} \right)^2 \quad (1.145b)$$

$$\simeq 10^{-64}. \quad (1.145c)$$

This is a fine-tuning problem of 64 orders of magnitude which is difficult to reconcile, on the other hand Inflation provides a suitable solution by considering the exponential evolution of the density parameter during the expansion phase which stretches the initial curvature up to the present value.

1.5.2 Basics of Inflation

The basic idea under Inflation is the Spontaneous Symmetry Breaking mechanism: there is a certain energy scale above which a symmetry existed, i.e. an invariance of the theory. In its simplest form, we introduce a scalar field ϕ called Inflaton, thus we can write the action,

$$\mathcal{A} = \int d^4x \sqrt{-g} \mathcal{L}(\phi, \partial\phi) \quad (1.146a)$$

$$= \int d^4x \sqrt{-g} \left[\frac{1}{2} \partial^\mu \phi \partial_\mu \phi + V(\phi) \right], \quad (1.146b)$$

as usually in classic field theory, solving the Euler-Lagrange equation leads to the equation of motion:

$$\ddot{\phi} + 3H\dot{\phi} + \frac{dV(\phi)}{d\phi} = 0. \quad (1.147)$$

Notice that the second term of the left-hand side is a velocity term weighted by the Hubble parameter, it behaves like a Hubble friction. During the period dominated by the scalar field component we can rewrite the Friedmann equation as:

$$H = \sqrt{\frac{8\pi G \left(\frac{1}{2} \dot{\phi}^2 + V(\phi) \right)}{3}}, \quad (1.148)$$

putting together the latter equation and Eq.(1.147) it is possible to write a useful formula,

$$2H\dot{H} = \frac{8\pi G}{3} \left(\dot{\phi} \ddot{\phi} + V'(\phi) \dot{\phi} \right) = -8\pi G H \dot{\phi}^2, \quad (1.149)$$

thus,

$$\dot{H} = -4\pi G \dot{\phi}^2. \quad (1.150)$$

With Eqs.(1.150 and 1.148) and assuming that the fractional change between \dot{H} and H during the expansion time must be negligible, we get:

$$\ddot{\phi} \ll |V(\phi)|. \quad (1.151)$$

Moreover this implies also that $P = -\rho$ and, finally

$$H \simeq \sqrt{\frac{8\pi G V(\phi)}{3}}. \quad (1.152)$$

In the slow roll model it is also assumed that the ratio between $\ddot{\phi}$ and $\dot{\phi}$ must be much less than the unity,

$$\ddot{\phi} \ll H\dot{\phi}, \quad (1.153)$$

in such a way it is possible to drop the inertial term in Eq.(1.147) and thus obtain that:

$$\dot{\phi} = -\frac{V'(\phi)}{3}. \quad (1.154)$$

Putting together all these considerations it is possible to write the “flatness” conditions for the potential in order to allow a slow roll motion of the inflaton field. Eqs.(1.151 and 1.153) lead, respectively, to

$$\frac{V'(\phi)}{V(\phi)} \ll H = \sqrt{24\pi G}, \quad (1.155a)$$

$$\frac{V''(\phi)}{V(\phi^2)} \ll H^2 = 24\pi G. \quad (1.155b)$$

Depending on the potential shape, the latter equations (flatness conditions) can provide conditions on the initial value of the scalar field or on the parameters of the potential itself. In the slow roll model we suppose that the potential $\phi(t)$ underwent a shift in a finite time from an initial value ϕ_1 to a final one ϕ_2 with $0 < V(\phi_2) < V(\phi_1)$. This implies an increase in the scale factor of the metric by a factor:

$$\frac{a(t_2)}{a(t_1)} = \exp \left[\int_{t_1}^{t_2} H dt \right] = \exp \left[\int_{\phi_1}^{\phi_2} \frac{H}{\dot{\phi}} d\phi \right]. \quad (1.156)$$

The decreasing of the inflaton field translates into an exponential increase of the scale factor. Eq.(1.156) corresponds to the number of e-folds of accelerated expansion.

Finally we will only address the reheating in a qualitative manner. During the inflation the largest part of the energy density was contained into the Inflaton potential. When Inflation ends the energy of the potential had been transformed in kinetic energy and, thus, transferred to the particles of the Standard Model through a process called **reheating**. The field ϕ oscillates in the bottom of the potential and its equation of motion can be written as:

$$\ddot{\phi} + 3H\dot{\phi} = -m^2\phi, \quad (1.157)$$

where m is the mass associated to the minimum of $V(\phi) = \frac{1}{2}m^2\phi^2$. In this condition the amplitude of ϕ must be considered small. When the expansion rate becomes larger than the oscillation period $H^{-1} \gg m^{-1}$ the friction term can be neglected and the oscillatory pattern becomes dominant,

$$\dot{\rho}_\phi + 3H\rho_\phi = -3HP_\phi = -\frac{3}{2}H \left(m^2\phi^2 - \dot{\phi}^2 \right). \quad (1.158)$$

In order to not leave an empty Universe the energy stored in the Inflation field must be transferred to the Standard Model sector through a decay process. The equation that

describe the decay of the Inflaton field into ordinary particles is the following,

$$\dot{\rho}_\phi + 3H\rho_\phi = -\Gamma_\phi\rho_\phi. \quad (1.159)$$

At this point the particles created underwent scattering processes that will thermalize the primordial plasma. The reheating temperature depends on the energy density ρ_{rh} at the end of the reheating epoch.

1.5.3 Primordial scalar power spectrum

Finally, one of the main aspects of Inflation is that it naturally originates fluctuations; considering the uncertainty principle, Eq.(1.34), every quantum-mechanical quantities have some variance, that in the Inflaton case is,

$$\delta\phi(\vec{x}, t) = \phi(\vec{x}, t) - \bar{\phi}(t), \quad (1.160)$$

these local differences in time implies different inflation durations and consequently different end times, thus quantum fluctuations in time translates into local classical spatial fluctuations, see [30] for a full treatment. In the Fourier space the whole set of perturbations can be factorized in single k -modes allowing to write a distribution having zero mean and non-zero variance:

$$\langle \delta\phi(k) \delta^*\phi(k) \rangle = (2\pi)^3 \mathcal{P}_\phi(k) \delta^3(k - k'), \quad (1.161)$$

where $\mathcal{P}_\phi(k)$ is the *Power Spectrum* of the scalar perturbations. Considering the conservation of the energy momentum tensor (see [62]) in the Fourier space:

$$(\ddot{\delta\phi}) + 2a\dot{H}(\delta\phi) + k^2\delta\phi = 0. \quad (1.162)$$

it is possible to write the *scale invariant* power spectrum of the fluctuations as:

$$\mathcal{P}_\phi = \frac{8\pi}{9k^3} \frac{H^2}{m_{\text{Pl}}^2}, \quad (1.163)$$

this means that, considering $k^3\mathcal{P}_\phi$, all the perturbation have the same initial amplitude independently from the k . This is the reason for which the primordial scalar power spectrum is also called scale-invariant power spectrum. It means that all the perturbations have the same amplitude after the horizon crossing. After the horizon crossing, perturbations are super-horizon and, thus, their evolution is driven uniquely by the quantum fluctuations that, due to the accelerated expansion, now are metric perturbations.

Although the perturbations are originated by the Inflaton fields they end up as a linear combination of ϕ and $\delta\phi$ more generally as a linear combination of ψ and

perturbations to the energy-momentum tensor. It is convenient to define a constant quantity:

$$\zeta \equiv -\frac{ik_i \delta T^0_i H}{k^2(\rho + P)} - \psi, \quad (1.164)$$

that can connect the metric perturbation and the energy density. For sub-horizon modes and for those modes that have just left the horizon the potential ψ is negligible and the latter equation can be rewritten in the following way:

$$\zeta = -\frac{aH\delta\phi}{\dot{\phi}^0}, \quad (1.165)$$

where $\dot{\phi}^0$ is the conformal derivative of the primordial field. The latter equation, well after the end of inflation, assumes the well known form,

$$\zeta = -\frac{3aH\Theta_1}{k} - \psi = -\frac{3}{2}\phi. \quad (1.166)$$

In this way, the power spectrum of ψ is related to the horizon-crossing spectrum of $\delta\phi$ in the following way:

$$\mathcal{P}_\psi(k) = \frac{4}{9} \left(\frac{aH}{\dot{\phi}^0} \right)^2 \mathcal{P}_\phi(k)|_{aH=k}, \quad (1.167)$$

or in function of the constant primordial parameter ζ ,

$$\mathcal{P}_\zeta(k) = \left(\frac{aH}{\dot{\phi}^0} \right)^2 \mathcal{P}_\phi(k). \quad (1.168)$$

The normalized version of this power spectrum has the following form:

$$\Delta_\zeta^2 = \frac{k^3}{2\pi^2} \mathcal{P}_\zeta(k). \quad (1.169)$$

As we have shown, there are several ways to parametrize the power spectrum, however one of the most used is in function of the initial scalar tilt parameter n_s :

$$\mathcal{P}_\phi = \frac{50\pi^2}{9k^3} \left(\frac{k}{H_0} \right)^{n_s-1} \delta_H \left(\frac{\Omega_m}{D(a=1)} \right)^2, \quad (1.170)$$

with δ_H scalar amplitude at horizon crossing. A scale-free scalar spectrum will have $n_s = 1$, observations by Planck [10] measure $n_s \simeq 0.96$. Thus, at the end, we can write a useful equation that relates the primordial power spectrum, Eq.(1.169), with n_s :

$$\Delta_\zeta^2(k) = A_s(k_0) \left(\frac{k}{k_0} \right)^{n_s-1}, \quad (1.171)$$

where k_0 is a reference scale (pivot).

1.5.4 Tensor perturbations

Inflation provides also the generation of primordial tensor perturbations. There is no need to have a complete treatment of this aspect inside this thesis, however, following Ref. [62] we can give a flavour of its importance. Tensor perturbation modes h_+ and h_\times can be decomposed, as usually done for the quantum harmonic oscillator, in terms of ladder operators. This harmonic behaviour leaves an imprint during the accelerated expansion generated by the Inflaton field. Hence we can write, in analogy to what done for the scalar sector, a tensor perturbation power spectrum:

$$\langle h^\dagger(\vec{k}, \tau) h(\vec{k}', \tau) \rangle = \frac{16\pi G}{a^2} |v(\vec{k}, \tau)|^2 (2\pi)^3 \delta^3(\vec{k} - \vec{k}') \equiv (2\pi)^3 \mathcal{P}_h(k) \delta^3(\vec{k} - \vec{k}'). \quad (1.172)$$

The total tensor PS is the sum of the two polarization states and it is possible to write the normalized power spectrum:

$$\Delta_t^2(k) = A_t(k_0) \left(\frac{k}{k_0} \right)^{n_t} \quad (1.173)$$

1.6 Observational cornerstones

Physics is an experimental science and, thus, great claims require great evidence. As a branch of physics, cosmology can not stand out to provide evidence. There are several observations that confirm and sustain the picture described so far, actually birth and drafting of the cosmological model was done in synergy with observations.

- 1 The existence of an isotropic and homogeneous relic sea of photons, the CMB, that permeates the Universe,
- 2 the observed abundance of light elements that is in extremely good agreement with theoretical expectations,
- 3 the direct observation of the Universe expansion,
- 4 the formation of galaxies and large-scale structure.

CMB is the relic sea of photons that free-stream from the Last Scattering Surface soon after the process called decoupling. These photons have been in thermal equilibrium with the rest of the primordial fluid since the very beginning and bring information about the conditions of the early Universe: their energy distribution and their statistical properties are powerful tools for studying the properties, the composition. the geometry of the primordial Universe. Moreover, since the CMB map observed by Planck [9] is basically a picture of the first light emitted and the source of information farther in time

and space, it represents the largest and more ancient observable to test fundamental physics.

Another probe of the big bang model is the abundance of light elements, the description of the BBN given in Sec.(1.3.4) is a toy model, that provides good predictions, but can be widely refined e.g. [27, 52, 71, 156]. Theoretical predictions are in really good agreement with observations and can be summarized in Fig.(1.7), here mass fraction of ^4He and the abundances, relative to hydrogen, of deuterium, ^3He and lithium are expressed in function of the photon-to baryon ratio η . Observed data are shown as grey bands, WMAP is the dark-gray vertical band and the light-grey horizontal band represents other astrophysical data, while coloured lines correspond to theoretical predictions. The expansion of the Universe is known since the early 1900s, Georges

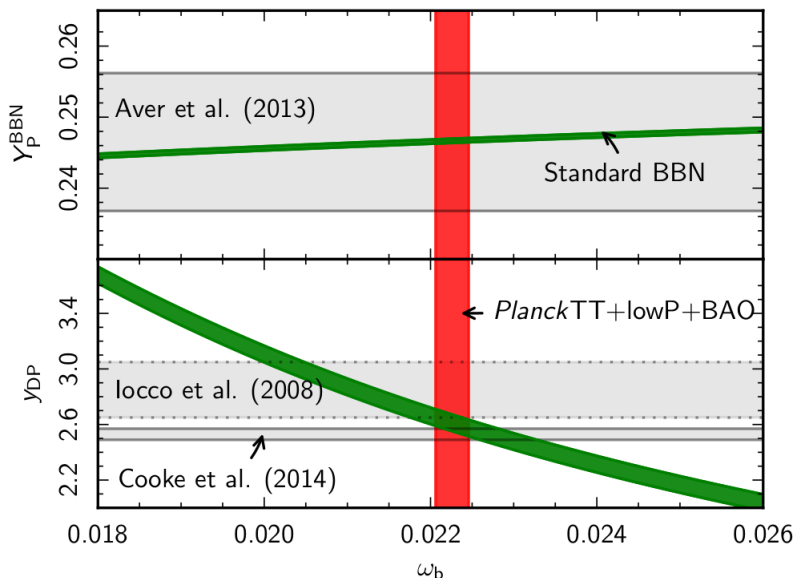


Figure 1.7: Helium (^4He) and deuterium (D) primordial abundances (relative to hydrogen) in function of the baryon density $\omega_b \equiv \Omega_b h^2$. Green lines are the theoretical expectations from nuclear reactions rates on the neutron lifetime, the horizontal gray bands show direct observations on primordial element abundances, while the red band corresponds to Planck bounds on ω_b (the width corresponds to the 68% CL.)

Lemaitre in 1927 and Edwin Hubble in 1929 formulated the famous law, Eq.(1.10), which as been proven e.g. [105, 110] and it is still under investigation [10, 152].

2

Cosmic Microwave Background radiation

In ogni secolo gli esseri umani hanno pensato di aver capito definitivamente l'universo e, in ogni secolo, si è capito che avevano sbagliato. Da ciò segue che l'unica cosa certa che possiamo dire oggi sulle nostre attuali conoscenze è che sono sbagliate.

Isaac Asimov, Grande come l'universo, 1988

The main observable used in this thesis to constrain neutrino properties is the cosmic microwave background (CMB) radiation. It has been introduced in Sec.(1.6), however in this chapter we will give a more complete description of its properties. The existence of a relic photon background, homogeneous and isotropic up to one part in 10^5 , is one of the most important scientific discoveries of the last century. It is the evidence that we do not live in a steady endless universe, indeed, while it is hard to obtain a CMB like source in a Steady State model, in a Big Bang universe it rises naturally.

CMB was discovered in 1965 when two researchers of the Bell Industries, Arno Penzias e Robert Woodrow Wilson, accidentally encountered an isotropic radiation in the radio-microwave region of the electromagnetic spectrum [60]. They were working with a Dicke radiometer built for satellite communication experiments. On 20 May 1964 they made the first measurement which clearly showed the presence of the microwave background, the instrument have measured an excess of 4.2 K. The times were however ripe, simultaneously a group in Princeton (30 km far from the Bell's laboratory) was looking for the same radiation, theorized a few years earlier (1946) by R.Alpher and G.Gamov as a probe of the Hot Big Bang (HBB) model [19, 78]. Penzias and Wilson received the 1978 Nobel Prize in Physics. After this discovery, the CMB spectrum was

measured by the spacecraft COBE (COsmic Background Explorer) in 1989 [72, 73, 163]. The science mission was conducted by the three instruments: DIRBE, a multiwavelength infrared detector used to map dust emission, FIRAS a spectrophotometer used to measure the spectrum of the CMB and the DMR a microwave instrument that would map anisotropies in the CMB. The scientific goals reached were: a full sky map of the CMB radiation and a almost (up to 10^{-4}) perfect measurement of the black body spectrum,

$$B_\nu(\nu, T) = \frac{2\nu^3}{c^2} \left(e^{h\nu/T} - 1 \right)^{-1}, \quad (2.1)$$

the associated black-body temperature $T = 2.72548 \pm 0.00057$ K and the presence of small temperature fluctuations of the order of:

$$\frac{\delta T}{T} \sim 10^{-5}. \quad (2.2)$$

After COBE-DMR, the CMB anisotropies have been observed by many ground-based and balloon-borne experiments, as well as by two other satellites, WMAP [102] and Planck [9], launched in 2001 and 2009 respectively. The data obtained are much better

	Frequency [GHz]	Sensitivity ($\frac{\Delta T}{T}$)	Angular resolution
COBE	31.5, 53, 90	$\sim 10^{-5}$	7°
WMAP	23, 33, 41, 61, 94	$\sim \text{few} \times 10^{-6}$	$15'$
Planck	30, 44, 70, 100, 143, 217, 353, 545, 853	$\sim 2 \times 10^{-6}$	$5'$

Table 2.1: Frequency channels, sensitivity and angular resolution of COBE, WMAP and Planck satellites. The sensitivity and angular resolution actually depend on the frequency band; the values shown in the table are the reference values.

in terms of sensitivity and angular resolution (as we can see in Tab.(2.1)). Moreover, WMAP and especially Planck have observed the sky with a wider frequency coverage, allowing a better foreground cleaning. In Fig.(2.1) we show a comparison of the CMB as seen by Penzias and Wilson antenna, COBE, WMAP and Planck. The first thing that jumps to the eyes is that, increasing the sensitivity and resolution of the observations, the universe does not appear homogeneous and isotropic. However since the temperature fluctuations that fill the CMB sky are of order of one part in 10^5 , the cosmological principle is still valid. Before we go in details of anisotropies, let us see how the CMB can originate from the inhomogeneities.

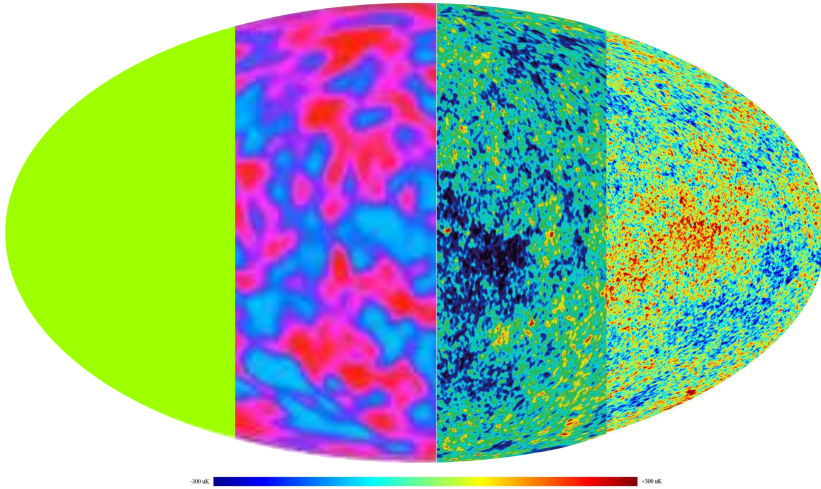


Figure 2.1: CMB as seen in 1965 by Penzias and Wilson (if they were able to observe the full sky realization), COBE, WMAP and Planck, from left to right.

2.1 Gravitational potential and inhomogeneities

In the previous chapter we provided a quite complete overview of the equations that govern the evolution of cosmological perturbations. It is possible to numerically solve these equations, but it is, also, extremely useful try to understand the physics through analytical solution valid in certain specific regimes (see [62] for details). The basic idea is the following: there are three main physical quantities that are bound in the evolution of the Universe, the gravitational potential, the matter inhomogeneities and the temperature anisotropies. Let us start looking at how gravitational instability and the evolution of the potential drive the matter inhomogeneities. In this section we will follow Ref. [62] in the description of the dark matter perturbations. Dark matter, by definition, is not affected directly by radiation and, thus, its evolution is coupled only with the metric perturbations. At early time, we will see, the potential is determined by the radiation, but it is relatively simple since it depends, at most, on the radiation monopole and dipole. While at “late” times matter dominates the evolution and the expansion history and these potentials are independent by radiation. The starting point of this discussion is the concept of gravitational instability: if there is an initial local overdense region, dark matter will fall into the overdensity increasing the potential and attracting more matter. This means that nearby an overdense region, mass is attracted by gravity and repulsed by pressure, if the attractive potential is larger than the pressure, then the overdensity will grew with time, otherwise it will bounce until it

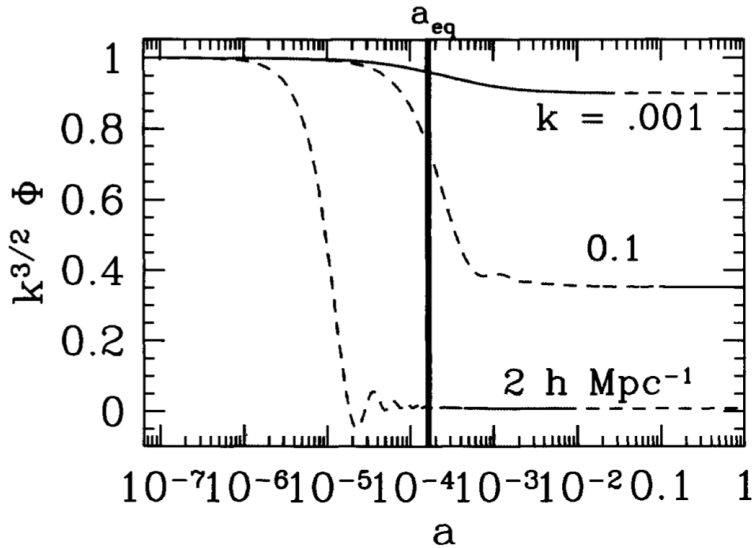


Figure 2.2: Linear potential evolution for three different modes.

reaches the balance. The physics of this phenomenon is the harmonic oscillator:

$$\ddot{\delta} + [\text{Pressure} - \text{Gravity}] \delta = 0. \quad (2.3)$$

At this point, we can follow the evolution of a single overdensity that pass through all the evolution steps: from being larger than the horizon size, i.e. *super-horizon* ($k\tau \ll 1$), to the moment in which its size become of the order of the horizon size *horizon-crossing* ($k\tau \sim 1$), until the *sub-horizon* ($k\tau \gg 1$) stage. The horizon (τ) depends on the expansion history of the Universe and, thus, on the matter and energy content, while the size of the overdensities (in the phase-space it is the mode k) is strictly related to the initial conditions of the considered overdensity. Let us emphasize that following the evolution of a single overdensity is identical to look at overdensities of different size at the same moment, i.e. studying the evolution of one k mode is equivalent to take a picture of all the k modes at a given time.

In order to follow the potential evolution is extremely important to take into account that the horizon-crossing process which can happen before, during or after the matter-radiation equality. This behaviour strictly depends on the initial size of the perturbation. In Fig.(2.2) we show the linear evolution of the gravitational potential ϕ in function of the scale factor: smaller the size of the mode (larger the k wave number) earlier the potential decay. If the mode enter the horizon before the matter-radiation equality its potential will enter in an oscillatory regime. Since it is not easy to measure the potential, moreover we are able to infer it by the matter distribution only at relatively late times, we can express ϕ depending on a primordial potential ϕ^0 , set during inflation,

times a growing function and a transfer function:

$$\phi(\vec{k}, a) = \frac{9}{10} \phi^0(\vec{k}) T(k) \frac{D(a)}{a}, \quad (2.4)$$

where

$$\frac{D(a)}{a} = \frac{\phi(a)}{\phi(a_{\text{late-times}})}, \quad (2.5)$$

is the growth function and

$$T(\vec{k}) = \frac{\phi(k)}{\phi_{\text{Large-scale}}(k)}, \quad (2.6)$$

is the transfer function. The transfer function provides a description of perturbations through the horizon-crossing process, while the growth function $D(a)$ describes the evolution of the matter perturbations at late times. It is possible to express the power spectrum of the matter distribution, during the matter era, using the Poisson equation Eq.(1.5), which can be rewritten in the following way:

$$\phi = \frac{4\pi G \rho_m a^2 \delta_c}{k^2}, \quad (2.7)$$

this is the simplest expression to relate the matter overdensity to the gravitational potential:

$$\delta_c(\vec{k}, a) = \frac{2k^2 a}{3\Omega_m H_0^2} \phi(\vec{k}, a) = \frac{3}{5} \frac{k^2}{\Omega_m H_0^2} \phi^0(\vec{k}, a) D(a) T(k), \quad (2.8)$$

where we used the background matter density

$$\rho_m = \frac{\Omega_m (3/2) H_0^2}{a^3 (4\pi G)}. \quad (2.9)$$

Finally we need a reduced set of equations in order. Starting from the full set of Boltzmann equation presented in Sec.(1.4.1) we can reduce it to a simpler version considering that, at early times, the photon distribution can be characterized by the lower moments Θ_0 and Θ_1 ¹. This leads to the following set of equations:

$$\dot{\Theta}_{r0} + k\Theta_{r1} = -\phi, \quad (2.10)$$

$$\dot{\Theta}_{r1} - \frac{k}{3}\Theta_{r0} = -\frac{k}{3}\phi, \quad (2.11)$$

$$\dot{\delta}_c + ik\theta_c = -3\dot{\phi}, \quad (2.12)$$

$$\dot{\theta}_c + H\theta_c = ik\phi. \quad (2.13)$$

In Eq.(2.13) the subscript r means that we are enclosing the contribution of neutrinos in the relativistic perturbations. This approximation is acceptable until we are in a

¹We have used the notation of [62].

non tight-coupling photon regime, since photons and neutrinos have the same initial conditions and impact on the gravitational potential. In addition, in absence of quadrupole terms, we have used the relation $\psi \rightarrow \phi$. Moreover, we can rewrite the time-time component of Eq.(1.108) in order to have a set of 5 equations:

$$k^2\phi + 3H(\dot{\phi} + H\phi) = 4\pi G a^2 [\rho_c \delta_c + 4\rho_r \Theta_{r0}] . \quad (2.14)$$

At this point, in order to have a better comprehension of the potential behaviour we will report the analytical solution dividing the problem into two different regimes: large and small scales with respect the horizon size.

2.1.1 Large scales

For the scales which are super-horizon for very long times (up until matter-domination or decoupling) $k/k_{\text{eq}} \ll 1$. At this point, we can distinguish into two regimes, scales that are super-horizon and scales which cross the horizon during the matter-dominated era.

Super-horizon In the first case it is possible to assume $k\tau \ll 1$ and thus we can neglect k from the set of Eqs.(2.13 and 2.14), this leads to the following set:

$$\dot{\Theta}_{r0} = -\dot{\phi} , \quad (2.15)$$

$$\dot{\delta}_c = -3\dot{\phi} , \quad (2.16)$$

$$3H(\dot{\phi} + H\phi) = 4\pi G [\rho_c \delta_c + 4\rho_r \Theta_{r0}] . \quad (2.17)$$

Rewriting the time variable as

$$y = \frac{a}{a_{\text{eq}}} , \quad (2.18)$$

the analytical solution for the potential (see [62] for the detailed calculation) is:

$$\phi = \frac{\phi^0}{10y^3} \left[16\sqrt{1+y} + 9y^3 + 2y^2 - 8y - 16 \right] . \quad (2.19)$$

This potential goes to $\phi(0)$ at early times when y is small and at large y when the universe is matter dominated $\phi \rightarrow 9/10 \phi(0)$.

Crossing-horizon While in the second case we can assume ϕ constant, because these modes enter the horizon at very late times (well after recombination), when the universe is matter dominated. The potential depends only by the matter content of the universe,

thus we can neglect the radiation equations in Eq.(2.13 and 2.14),

$$\dot{\delta}_c + ik\theta_c = 0, \quad (2.20a)$$

$$\dot{\theta}_c + aH\theta_c = ik\phi, \quad (2.20b)$$

$$k^2\phi = \frac{3}{2}a^2H^2 \left[\delta_c + \frac{3aHi\theta_c}{k} \right]. \quad (2.20c)$$

Moreover, as we said before, the initial conditions is that the potential is constant, thus $\dot{\phi} = 0$. These set of equations leads, after some algebra and some considerations about the matter-dominated regime (see [62]).

$$\begin{aligned} & \left[\frac{i\theta_c}{k} + \frac{\phi}{3} \right] \left(\frac{9a^2H^2}{2} + k^2 \right) + \left[\frac{i\theta_c}{k} + \frac{2\phi}{3Ha} \right] \frac{d}{d\tau} \frac{9a^2H^2}{2} \\ & = - \left[\frac{iaH\theta_c}{k} + \frac{2\phi}{3} \right] (9a^2H^2 + k^2). \end{aligned} \quad (2.21)$$

Potential remains constant as long as the matter domains the dynamics, that is up to $a \simeq 1/10$, when dark energy starts to dominate.

2.1.2 Small Scales

These are scales which cross the horizon before or during the matter-radiation equality epoch $k/k_{\text{eq}} \gg 1$. Also in this case we can distinguish into scales that undergo the horizon crossing and modes that are basically always sub-horizon.

Crossing-horizon The scales that cross the horizon during the radiation dominated epoch falls the potential from presence of photons. Indeed, in this regime, the potential is coupled with the radiation, hence we have to consider only the Θ_{r0} , Θ_{r1} contributions of Eq.(2.13). In analogy, the potential equation, Eq.(2.14), which can be rewritten in the following way:

$$\phi = \frac{6a^2H^2}{k^2} \left[\Theta_{r0} + \frac{3aH}{k} \Theta_{r1} \right], \quad (2.22)$$

Using this latter equation in the first two Eq.(2.13) we can eliminate the contribution of the monopole and rewrite the first two equations of Eq.(2.13):

$$-\frac{3}{k\tau} \dot{\Theta}_{r1} + k\Theta_{r1} \left[1 + \frac{3}{k^2\tau^2} \right] = -\dot{\phi} \left[1 + \frac{k^2\tau^2}{6} \right] - \phi \frac{k^2\tau}{3}. \quad (2.23)$$

$$\dot{\Theta}_{r1} + \frac{1}{\tau} \theta_{r1} = -\frac{k}{3} \phi \left[1 - \frac{k^2\tau^2}{6} \right]. \quad (2.24)$$

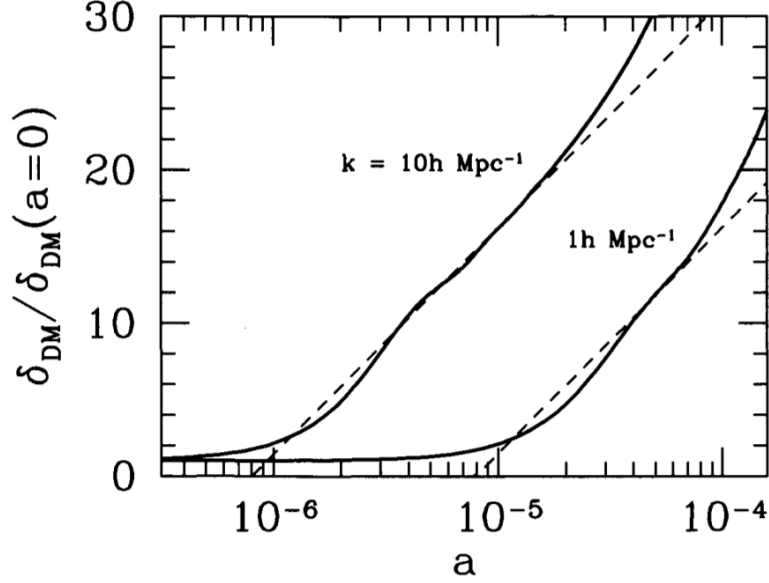


Figure 2.3: Dark matter perturbation evolution for two different modes. Dashed lines correspond to approximate solution, while solid lines represent the exact solutions.

It is possible to turn these two first-order equations into a second-order equation for ϕ . Hence, the equation that governs the potential evolution is the following:

$$\ddot{\phi} + \frac{4}{\tau}\dot{\phi} + \frac{k^2}{3}\phi = 0, \quad (2.25)$$

that is a spherical Bessel of order 1 whose solution is,

$$\phi = 3\phi(0) \left[\frac{\sin(k\tau\sqrt{3}) - (k\tau\sqrt{3})\cos(k\tau\sqrt{3})}{(k\tau\sqrt{3})^3} \right]. \quad (2.26)$$

This means that as soon as the mode enters the horizon, the potential drops down and then starts to oscillate.

Once we know the behaviour of the potential it is possible to find the associated equation for the dark matter component. The matter perturbations are affected by the potential, which we have seen is driven by radiation, the equation that describes its behaviour has the following form,

$$\ddot{\delta}_c + \frac{1}{\tau}\dot{\delta}_c = -3\ddot{\phi} + k^2\phi - \frac{3}{\tau}\dot{\phi}, \quad (2.27)$$

where the right-hand part of the equation represents the source term for the dark matter perturbations. In Fig.(2.3) we show the analytical and numerical solutions for

the evolution of matter perturbation in the radiation dominated era. It is evident that Eq.(2.27) has two solutions $\delta = 0$ and $\delta = \ln(a)$, which leads to a logarithmic growth of the dark matter perturbations. In general it is possible to build a general solution using the source term weighted by a Green's function [62], however results are comparable to the approximate solution and show that matter perturbations grow also in the radiation dominated epoch, but the growth is smaller than in the matter-dominated era due to the presence of the radiation pressure.

Sub-horizon Since we know from Eq.(2.27) that radiation pressure induces the decay of gravitational potential. However it could happen that $\rho_c \delta_c$ becomes larger than $\rho_r \Theta_r$, even if the radiation dominates the energetic content of the Universe. This is exactly what happened in the sub-horizon modes, in this case we can neglect the radiation contribution and rewrite our equation taking into account only the dark matter density contribution:

$$\delta'_c + \frac{ikv}{aHy} = -3\phi', \quad (2.28)$$

$$\theta'_c \frac{\theta_c}{y} = \frac{ik\phi}{aHy}, \quad (2.29)$$

$$k^2 \phi = \frac{3y}{2(y+1)} a^2 H^2 \delta_c. \quad (2.30)$$

where the time derivatives has been replaced by the derivative on y . In analogy to what we have done in the crossing-horizon case, we can write a second order equation from Eq.(2.30):

$$\delta''_c - \frac{ik(2+3y)\theta_c}{2aHy^2(1+y)} = -3\phi'' + \frac{k^2\phi}{a^2H^2y^2}. \quad (2.31)$$

Replacing the velocity in the latter using the first equation of (2.30) it is possible to find the following second-order equation for the dark matter component:

$$\delta''_c + \frac{2+3y}{2y(y+1)} \delta'_c - \frac{3}{2y(y+1)} \delta_c = 0, \quad (2.32)$$

this is a quite important equation called "Meszaros equation" which governs the evolution of sub-horizon dark matter perturbations. The solutions of this equation are rather complicated and we will illustrate only the final result; the general solution is:

$$\delta_c = C_1 D(y) + C_2 D_2(y), \quad (2.33)$$

where the first and second contributions are,

$$D = y + \frac{2}{3}, \quad (2.34)$$

$$D_2 = D \ln \left[\frac{\sqrt{1+y} + 1}{\sqrt{1+y} - 1} \right] - 2\sqrt{1+y}. \quad (2.35)$$

At late times ($y \gg 1$) the solution scales like y while in the radiation dominated case ($y \ll 1$) the solution is proportional to the $\ln y$. This is basically saying to us that, at early times, the dominant energy of radiation drives the universe to expand so fast that the matter has no time to follow it. The consequence is that δ_c is fixed to a constant value. While at late times, when radiation becomes negligible, the dark matter perturbations grow $\delta_c \propto a$. When matter perturbations enter the horizon having $\dot{\delta}_c > 0$, the dark matter perturbation is not frozen and continues to grow giving a total boost factor of $\ln y$.

2.2 CMB temperature anisotropies

Until now we have provided a description of the mathematical tools and of the physical model that allows us to describe the formation of inhomogeneities in the primordial universe. We have seen that, when hydrogen recombines, photons start to free stream in a neutral Universe, carrying on the information imprinted in their energy and angular distribution by years of thermalisation. On the average temperature of the CMB there are temperature fluctuations defined in the following way:

$$\frac{\delta T}{T}(\theta, \phi) = \frac{T(\theta, \phi) - \langle T \rangle}{\langle T \rangle}. \quad (2.36)$$

It has no meaning to study every fluctuation one by one, the most important information is, by far, the statistical distribution of the anisotropies and the analysis of the corresponding momenta and momenta direction. For most purposes, the anisotropies are better studied in harmonic space, so we operate an angular decomposition,

$$\frac{\delta T}{T}(\theta, \phi) = \sum_{\ell=0}^{\infty} \sum_{m=-\ell}^{\ell} a_{\ell m} Y_{\ell m}(\theta, \phi), \quad (2.37)$$

As we have seen in the previous chapter, the potential fluctuations as well as the matter inhomogeneities, the temperature anisotropies and all the structure on large scales originated from primordial quantum fluctuations. However, the theory is only able to give predictions about the stochastic properties of the primordial perturbations. Thus we are only interested in the statistical properties of the temperature anisotropies. Inflation predicts that the initial perturbations are, to a high degree, Gaussian distributed, and, if the evolution is linear, the Gaussianity is conserved in time. As we have seen in chapter, Ch.(1), the perturbations evolution, that originates the anisotropies before the recombination, follows a linear regime and thus the deviations

from a Gaussian distribution is negligible. Under this assumption the $a_{\ell m}$ s follow the Normal distribution with zero mean and non-zero variance. In this case, all the statistical information about the anisotropy field is encoded in the two-point correlation function:

$$C(\theta) = \left\langle \frac{\delta T}{T}(\hat{n}) \frac{\delta T}{T}(\hat{n}') \right\rangle, \quad (2.38)$$

where $\theta = \hat{n} \cdot \hat{n}'$. This quantity, in the harmonic space, has the form:

$$C(\theta) = \sum_{\ell=0}^{\infty} \frac{2\ell+1}{4\pi} C_{\ell} P_{\ell}(\theta), \quad (2.39)$$

with $P_{\ell}(\theta)$ Legendre polynomials. The C_{ℓ} coefficients related to the variance of the $a_{\ell m}$'s:

$$\begin{aligned} C_{\ell} &= \langle a_{\ell m} a_{\ell m}^* \rangle = \frac{1}{2\ell+1} \sum_{m=-\ell}^{\ell} |a_{\ell m}|^2, \\ &= \frac{1}{4\pi} \int d\Omega d\Omega' P_{\ell}(\hat{n} \cdot \hat{n}') \left\langle \frac{\delta T}{T}(\hat{n}) \frac{\delta T}{T}(\hat{n}') \right\rangle. \end{aligned} \quad (2.40)$$

In order to calculate the latter quantity we have to figure out the dependences, basically it requires the knowledge of two different things: initial conditions of perturbations (Gaussian from inflation) and evolution of initial perturbations. The field $\Theta \equiv \delta T/T$ can be rewritten in function of the primordial curvature perturbation ζ , this leads to the following form:

$$C_{\ell} = \frac{2}{\pi} \int_0^{\infty} k^2 P_{\zeta}(k) \left| \frac{\Theta_{\ell}(k)}{\zeta(k)} \right|^2 dk \quad (2.41)$$

which involve the curvature power spectrum $P_{\zeta}(k)$, see Eq.(1.168). Each of the C_{ℓ} 's measures the variance in fluctuations at an angular scale:

$$\theta \sim \frac{\pi}{\ell}. \quad (2.42)$$

The C_{ℓ} 's coefficients are thus the power spectrum of temperature fluctuations. The angular power spectrum is usually plotted using the combination:

$$\mathcal{D}_{\ell} = \frac{\ell(\ell+1)}{2\pi} C_{\ell}, \quad (2.43)$$

which we show in Fig.(2.4). The unique shape of the angular power spectrum is the main source of information and it is common procedure to divide the analysis in two sectors: primary and secondary anisotropies.

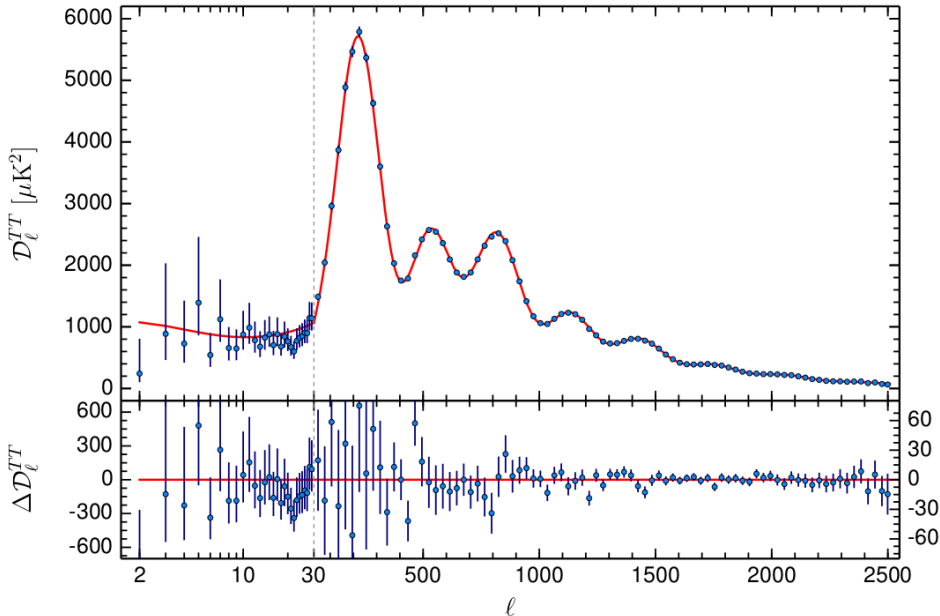


Figure 2.4: Temperature angular power spectrum of the CMB temperature anisotropies measured by the Planck satellite. In the upper panel the red line corresponds to the best fit of theoretical model described in Ch.(1) and based on the six basic parameter, while the blue points are the binned \mathcal{D}_ℓ extracted from Planck 2015 data. In the lower panel we show the residuals. [10]

2.2.1 Temperature perturbation

Before to see in details the sources and fingerprints of primary and secondary anisotropies, we need to derive analytical solutions for determined regimes. In Sec.(2.1) we have shown that it is possible to find analytical solutions for the gravitational potential and for the dark matter distribution in some limiting regimes. The aim of this section is to present how the perturbations in the gravitational potential are coupled with the temperature anisotropies. In order to do this we will refer to the temperature field as its Fourier decomposition:

$$\Theta(x) = \int \frac{d^3k}{(2\pi)^3} e^{ik \cdot x} \Theta(k), \tag{2.44}$$

thus, as we have done for the gravitational potential, we are moving to analyse the problem from different points of view, first of all considering the free-streaming case.

Free streaming

After hydrogen recombination, photons decouple from matter and start to free stream in the Universe. When photons decoupled the Universe is dominated by the matter component and the amount of energy density carried out by the relativistic species can be considered negligible. In this case we can consider $\psi = -\phi$, in the Eqs.(1.108) and the Boltzmann equation takes the following form:

$$\dot{\Theta} + (ik\mu - \dot{\tau}_c) \Theta = e^{-ik\mu\tau + \tau_c} \frac{d}{d\tau} \left(\Theta e^{ik\mu\tau - \tau_c} \right) = S, \quad (2.45)$$

$$S \equiv -\dot{\phi} - ik\mu\psi - \dot{\tau}_c \left[\Theta_0 + \mu v_b + \frac{1}{2} P_2(\mu) (\Theta_2 + 1/4(G_{\gamma 0} + G_{\gamma 2})) \right]. \quad (2.46)$$

In the latter the quantity S is the source term for the temperature field anisotropy and τ_c is the optical depth for the photon Compton scattering. We are going to neglect in this section the contribution of the polarization fields $G_{\gamma 0}$ and $G_{\gamma 2}$. In order to obtain the temperature field we integrate over the comoving time τ and approximate the medium as optically thick $\tau_c \gg 1$:

$$\Theta(k, \mu, \tau_0) = \Theta(\tau_i) e^{ik\mu(\tau_i - \tau_0) - \tau_{c_i}} + \int S(k, \mu, \tau) e^{ik\mu(\tau - \tau_0) - \tau_c(\tau)} d\tau, \quad (2.47)$$

$$= \int_0^{\tau_0} d\tau S(k, \mu, \tau) e^{ik\mu(\tau - \tau_0) - \tau_c(\tau)}, \quad (2.48)$$

where in the second equivalence we have considered that any contribution to the integral from $\tau < \tau_i$ is completely negligible. In this case we use the usual formalism of the Bessel function j_ℓ in order to describe the oscillatory behavior of the wave propagation. In this way it is easy to see that the temperature field that we observe today is only the propagation through an optically thick medium of the source term S . Notice that the S term still depends on the angle μ , if there is no μ dependence it will be possible to rewrite immediately the latter equation into the ℓ hierarchy which we were accustomed. The solution proposed in Ref. [62] is to replace μ with the time derivative $\mu = \frac{1}{k\tau} \frac{d}{d\tau}$, this leads to the following expression:

$$\Theta_\ell(k, \tau_0) = (-1)^\ell \int_0^{\tau_0} S(k, \tau) e^{-\tau_c(\tau)} j_\ell[k(\tau - \tau_0)] d\tau, \quad (2.49)$$

where the source function S now is defined as:

$$S(k, \tau) \equiv e^{-\tau_c} \left[-\dot{\phi} - \dot{\tau}_c \left(\Theta_0 + \frac{1}{4} (\Theta_2 + 1/4(G_{\gamma 0} + G_{\gamma 2})) \right) \right] + \frac{d}{d\tau} \left[e^{-\tau_c} \left(\psi - \frac{iv_b \dot{\tau}_c}{k} \right) \right] - \frac{3}{4k^2} \frac{d^2}{d\tau^2} \left(e^{-\tau_c} \dot{\tau}_c (\Theta_2 + 1/4(G_{\gamma 0} + G_{\gamma 2})) \right). \quad (2.50)$$

At this point a useful trick is to consider a visibility function,

$$g(\tau) = -\tau_c e^{-\tau_c}, \quad (2.51)$$

The visibility function is, basically, the probability that a photon last scattered at a given τ . It is peaked at recombination time and rapidly declines after that (see Fig.(2.5)). We can rewrite Eq.(2.50) in the following way:

$$S \simeq g(\tau) [\Theta_0(k, \tau) + \psi(k, \tau)] + \frac{d}{d\tau} \left(\frac{iv_b(k, \tau)g(\tau)}{k} \right) - e^{-\tau_c} [\dot{\psi}(k, \tau) - \dot{\phi}(k, \tau)]. \quad (2.52)$$

Replacing it into Eq.(2.46) we obtain the formula that describes the evolution of the temperature field up to today,

$$\begin{aligned} \Theta_\ell(k, \tau_0) = & \int_0^{\tau_0} d\tau g(\tau) [\Theta_0(k, \tau) + \psi(k, \tau)] \times j_\ell[k(\tau_0 - \tau)] \\ & - \int_0^{\tau_0} g(\tau) \frac{iv_b(k, \tau)}{k} \frac{d}{d\tau} \times j_\ell[k(\tau_0 - \tau)] \\ & + \int_0^{\tau_0} d\tau e^{-\tau_c} [\dot{\psi}(k, \tau) - \dot{\phi}(k, \tau)] \times j_\ell[k(\tau_0 - \tau)]. \end{aligned} \quad (2.53)$$

There are two types of term in the latter equation, the former are weighted by $e^{-\tau_c}$ and these contribute as long as $\tau_c \leq 1$, i.e. after the recombination. These are basically contributions on the integrated path that photons cover from the last scattering surface up to now. The last row of Eq.(2.53) it is called the Integrated Sachs Wolfe (ISW) effect and it basically encodes the information about the gravitational potential that lays between us and the last scattering surface. The second terms are the one weighted by the visibility function $g(\tau)$. Since this is peaked at recombination time, see Fig.(2.5), we can rewrite Eq.(2.53) considering the first two terms as calculated at the recombination:

$$\begin{aligned} \Theta_\ell(k, \tau_0) = & [\Theta_0(k, \tau_{\text{rec}}) + \psi(k, \tau_{\text{rec}})] \times j_\ell[k(\tau_0 - \tau_{\text{rec}})] \\ & + 3\Theta_1(k, \tau_{\text{rec}}) \left(j_{(\ell-1)}[k(\tau_0 - \tau_{\text{rec}})] - \frac{(\ell+1)j_\ell[k(\tau_0 - \tau_{\text{rec}})]}{k(\tau_0 - \tau_{\text{rec}})} \right) \\ & + \int_0^{\tau_0} d\tau e^{-\tau_c} [\dot{\psi}(k, \tau) - \dot{\phi}(k, \tau)] \times j_\ell[k(\tau_0 - \tau)]. \end{aligned} \quad (2.54)$$

The latter equation is the basis for the semianalytic calculation of the APS. In order to do that we have to know temperature monopole and dipole and gravitational potential at the recombination time, moreover it takes into account also the contributions of time-dependent potentials inside the ISW terms. In addition, given a certain mode k this contributes to the angular scales of the order $\ell \sim k\tau_0$, it is possible to see that

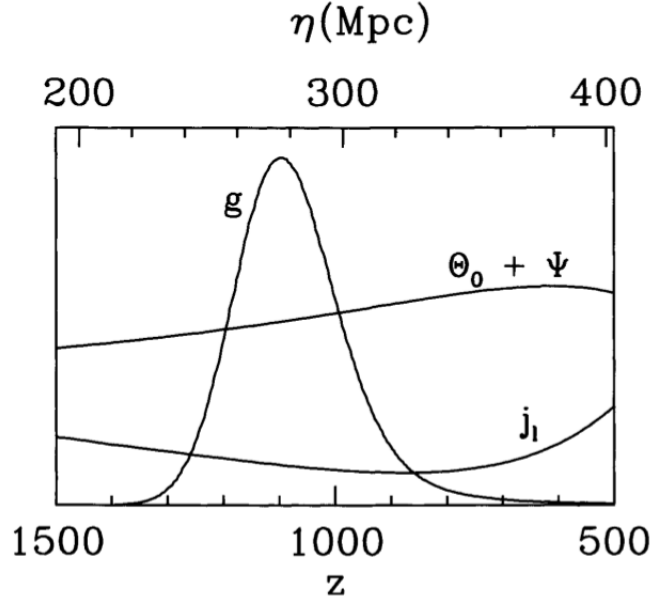


Figure 2.5: Visibility function g , monopole term $\Theta_0 + \psi$ and Bessel function j_ℓ contributions in function of the scale factor [62].

considering the form of the Bessel function in the high- ℓ limit case:

$$\lim_{\ell \rightarrow \infty} j_\ell(x) = \frac{1}{\ell} \left(\frac{x}{\ell} \right)^{\ell-1/2}. \quad (2.55)$$

That is, $j_\ell(x)$ is small when ℓ is large, leading to a zero value for the associated temperature anisotropy. Finally it is evident from Eq.(2.54) that the contribution to the anisotropy temperature today is not only a function of Θ_0 , but of $\Theta_0 + \phi$, which means that photons have to pass through potential wells in order to reach us, as we will see in the next sections.

Large scales

Scales that are super-horizon at recombination are basically driven by the metric where $\psi = -\phi$. In this regime we have already found the right set of equations (see Eq.(2.13) for details). The initial conditions are such that at recombination the photon perturbations satisfy:

$$\Theta_0(k, \tau_{\text{rec}}) = -\phi(k, \tau_{\text{rec}}) + \frac{3}{2}\phi^0 = \frac{2}{3}\phi(k, \tau_{\text{rec}}). \quad (2.56)$$

Hence, the observed anisotropy results:

$$(\Theta_0 + \psi)(k, \tau_{\text{rec}}) = \frac{1}{3}\psi(k, \tau_{\text{rec}}), \quad (2.57)$$

since we can consider as approximation $\psi \simeq -\phi$. The latter equations leads to a relation between the anisotropy observed today and the dark matter density at the recombination era:

$$(\Theta_0 + \psi)(k, \tau_{\text{rec}}) = -\frac{1}{6}\delta_c(\tau_{\text{rec}}). \quad (2.58)$$

This implies that potential wells contained hotter photons at the recombination, but these photons have to move out of the potential well in order to reach us and this translates into a lose of energy that is larger that the initial inhomogeneity. Moreover, what we see at large scales as a temperature fluctuation of $\frac{\delta T}{T} \sim 10^{-5}$ K corresponds to a $\frac{\delta \rho}{\rho} \sim 6 \times 10^{-5}$.

Generally speaking we can write the anisotropies power spectrum starting from the Einstein and the Boltzmann equations, Eq.(1.108), that can be reduced to a simpler version and give us the following equation:

$$\Theta_\ell(\tau_0) = -\frac{3}{10}\phi(0)j_\ell(k\tau_0) = \frac{1}{5}\zeta j_\ell(k\tau_0), \quad (2.59)$$

where we remember that $\Theta_0(k, \tau_{\text{rec}}) = \frac{3}{5}\phi(0)$ and $\phi = \frac{2}{3}\zeta$ is constant. The latter equation predicts a rescaling of the power at large scales of a factor of 5, which is clearly visible comparing the plateau and the first peak amplitude in Fig.(2.4). This reflects into the form of the C_ℓ definition that becomes:

$$C_\ell = \frac{4\pi}{25} \int \mathcal{P}(k) |j_\ell(k\tau_0)|^2 d \ln k. \quad (2.60)$$

Using the definition of the primordial power spectrum, Eq.(1.171) the latter equation becomes,

$$C_\ell = \frac{2\pi}{\ell(\ell+1)} \frac{A_s}{25}. \quad (2.61)$$

This solution is valid only for the low frequency part of the spectrum, i.e. $\ell < 50$, where the potential is constant ($k \ll aH$).

Intermediate scales

In the central region of the spectrum we have to deal with perturbations that enter the horizon, or are already sub-horizon, before the recombination. We are in a condition of ionized plasma where all the electrons are unbound. The photon mean free path is much smaller that the horizon size and Compton scattering keep photons and baryons tightly coupled. When the medium is optically thick, the moments, inside the Boltzmann hierarchy, of order higher than $\ell = 1$ are exponentially suppressed by the collisional

term. This allows us to consider the ℓ -th moment as:

$$\Theta_\ell \sim \frac{k\tau}{2\tau_c} \Theta_{(\ell-1)}. \quad (2.62)$$

Thus we can modify the Eq.(2.13) introducing the collisional term:

$$\dot{\Theta}_0 + k\theta_1 = -\dot{\phi}, \quad (2.63)$$

$$\dot{\Theta}_1 - \frac{k\Theta_0}{3} = -\frac{k}{3}\phi + \dot{\tau}_c \left[\Theta_1 + \frac{i\theta_b}{3} \right]. \quad (2.64)$$

Replacing the baryon velocity term,

$$\theta_b = -3i\Theta_1 + \frac{R}{\dot{\tau}_c} \left[\dot{\theta}_b + H\theta_b + ik\psi \right], \quad (2.65)$$

in Eq.(2.64) we get a second-order equation for the monopole that describes the oscillations of the primordial fluid:

$$\ddot{\Theta}_0 + H \frac{R}{1+R} \dot{\Theta}_0 + k^2 c_s^2 \Theta_0 = \frac{k}{3} \phi - H \frac{R}{1+R} \dot{\phi} - \ddot{\phi}, \quad (2.66)$$

where $R \equiv \frac{4}{3} \frac{\rho_\gamma}{\rho_b}$ is the baryon to photon ratio. The sound speed depend on the baryon density. The latter equation describes how the primordial fluid oscillates driven by the potential in both space and time with a period that depends on the sound speed:

$$c_s = \sqrt{\frac{1}{3(1+R)}}. \quad (2.67)$$

In this case the shape of the spectrum cannot be approximated as a Bessel function, that is the solution cannot be considered a pure cosine function. We have to take into account also the dipole term in the photon Boltzmann equation that is in opposite phase with respect the monopole. The CMB APS can be written as a superposition of sine and cosine functions in the following way:

$$C_\ell = 4\pi \int \mathcal{P}(k) \left| \frac{\Theta_0}{\zeta}(k) j_\ell(h\Delta\tau) + \frac{\Theta_1}{\zeta}(k) j'_\ell(h\Delta\tau) \right|^2 d \ln k, \quad (2.68)$$

where immediately appears that we have two out of phases contributions coming from the monopole and dipole respectively. Looking more carefully to the latter equation it is evident that there is also a cross correlated term that vanishes due to the phase shift described so far.

Small scales

Finally for the smaller scales, where small means comparable with the photon mean free path:

$$\lambda_D \simeq \lambda_{\text{MFP}} \times (N \text{ scattering})^{1/2} = \frac{1}{\sqrt{n_e \sigma_T H}}, \quad (2.69)$$

we can no longer neglect the quadrupole in the Boltzmann hierarchy. The reason is that, at these scales the viscosity of the fluid plays a fundamental rule. We have to add the quadrupole contribution to Eq.(2.64):

$$\dot{\Theta}_0 + k\theta_1 = -\dot{\phi}, \quad (2.70)$$

$$\dot{\Theta}_1 - \frac{k\Theta_0}{3} = -\frac{k}{3}\dot{\phi} + \dot{\tau}_c \left[\Theta_1 + \frac{i\theta_b}{3} \right], \quad (2.71)$$

$$\dot{\Theta}_2 - \frac{2k}{5}\Theta_1 = \frac{9}{10}\dot{\tau}_c\Theta_2. \quad (2.72)$$

In addition we need also an equation for the baryon speed θ_b , we chose Eq.(2.65) neglecting the potential since the dynamics is dominated by photons. In order to solve this set of equations it is possible to write the baryon speed as:

$$\theta_b \propto e^{i \int \omega d\tau}, \quad (2.73)$$

where $\omega = kc_s$. After some algebra (see [62] for details) we end up with the following equation, which is the zero-th order:

$$\omega(1 + R) - \frac{k^2}{3} + \frac{i\omega}{\dot{\tau}_c} \left(\omega^2 R^2 + \frac{8k^2}{27} \right) = 0. \quad (2.74)$$

The damping correction, which is due to the second order approximation, can be written as,

$$\delta\omega = -\frac{ik^2}{2(1+R)\dot{\tau}_c} \left(c_s^2 R^2 + \frac{8}{27} \right). \quad (2.75)$$

The final form of the monopole and dipole moments in the Boltzmann hierarchy are:

$$\Theta_\ell \propto e^{ik \int c_s d\tau} e^{-(k/k_D)^2}, \quad (2.76)$$

where k_D is the wave number associated to the damping length of photons.

2.2.2 Primary anisotropies:

In this section we will present the fingerprints that the physics described so far has on the CMB APS. We have presented how gravitational potential, dark matter inhomogeneities and temperature fluctuation are bound and, thus in this Section we will provide a more qualitative description. Summarizing what we have presented so far, we can distinguish

three sources:

- The field perturbations $\frac{\Delta\phi}{\phi}$ are the initial perturbations, probably originated by primordial quantum fluctuations stretched by inflationary process.
- The density perturbations $\frac{\Delta\rho}{\rho}$ are wells/hills of potentials where the photon-baryon fluid falls/slips. In general the denser the fluid the higher the temperature.
- The velocity perturbations $\frac{\Delta v}{v}$ are photons that have a greater momentum and smaller mean free path and the other way around.

Looking at the anisotropies power spectrum in Fig.(2.4) we start our considerations from the low multipoles, ($2 \leq \ell \leq 50$), after that we will move to the central region, from $\ell = 50$ to $\ell = 1500$, where the APS exhibits an oscillatory pattern with a major peak at $\ell \sim 220$, finally we will focus on the series of smaller peaks that are characterized by the Silk damping.

Super-horizon scales: In the first multipoles the APS is characterized by a long plateau that goes from $\ell = 2$ to $\ell \simeq 50$, these scales are always super-horizon scales and are independent on the physics of the fluid component, that is the oscillations of the baryon-photon fluid are completely irrelevant. At these scales fluctuations basically reflects the distribution of dark matter and thus the gravitational potential, see Sec.(2.2.1) for details. The effect that photons undergo is called *Sachs-Wolfe effect* from the names of Rainer Sachs and Arthur Wolfe that introduced it in 1967. Having a dark matter density which presents spatial fluctuations generates a fluctuating gravitational potential, which translates into a temperature fluctuation, Eq.(2.57):

$$\left(\frac{\delta T}{T}\right)_{\text{s-w}} = \frac{1}{3}\delta\psi. \quad (2.77)$$

There are two contribution to this result: photons that pass through large-scale gravitational wells(hills) experience a gravitational redshift losing(increasing) their energy. GR teaches that the gravitational echo is $\delta\nu/\nu = \psi$, thus in order to maintain the black-body spectrum unchanged the temperature fluctuations follows

$$\delta T/T = \psi. \quad (2.78)$$

In addition there is a time effect, due to the fact that photons from denser regions were scattered at earlier times, that induces a further $\delta T/T$, in particular:

$$\frac{\delta T}{T} = -\frac{2}{3}\frac{\delta t}{t} = -\frac{2}{3}\psi. \quad (2.79)$$

Surprisingly, Eq.(2.77) shows that large-scales regions of higher density will appear as colder in the CMB map and the other way around.

The first peak Recalling some of the arguments presented in the previous sections, the APS is the statistical point of view of the anisotropies on the last scattering surface, at that epoch the universe was mainly composed by hydrogen, helium, photons, neutrinos and dark matter. Baryons and photons have been tightly coupled until the decoupling and they have experienced the behaviours described in Sec.(2.2.1) depending on their size: inhomogeneities feel their own gravity and collapse if they enter the horizon the radiation pressure dominates the equation and they start to oscillate. Therefore, it is natural that the first peak have exact correspondence with the sound horizon at the recombination time

$$d_{\text{hor}}(z_{\text{rec}}) \simeq \frac{2}{\sqrt{3}H_0} \Omega_{m0}^{-1/2} (1 + z_{\text{rec}})^{-3/2}, \quad (2.80)$$

notice that the previous equations differs from the causality horizon of photons (Eq.1.142) because this time we are considering the sound horizon, which means that we cannot consider photons travelling at the speed of light, but sound waves travelling at $c_s = 1/\sqrt{3}c = 1/\sqrt{3}$. We know that it is always possible to calculate the angular distance of an object in the sky (see Sec.(1.1.3)), thus we can write an expression for the observed angle,

$$\theta_{\text{hor}}(z_{\text{rec}}) \simeq \frac{1}{\sqrt{3}} \left(\frac{(1 - \Omega_{k0})}{z_{\text{rec}}} \right)^{1/2} \sim 1^\circ. \quad (2.81)$$

We can say that the theoretical value of $\theta_{\text{hor}}(z_{\text{rec}})$ shown in Eq.(2.81) and perfectly coincident with the value observed in the Planck APS, Fig.(2.4), is obtained postulating a flat universe or, more accurately, that observed data are in excellent agreement with the theoretical prediction of a flat universe. We show in Fig.(2.6) that positive value of Ω_κ moves the first peak of the APS towards higher multipoles and the other way around. This is a very sensitive feature that allows the Planck collaboration to constrain the curvature of the Universe with an astonishing precision level:

$$\Omega_\kappa = -0.004 \pm 0.015. \quad (2.82)$$

Higher order peaks Fluctuations larger than the first peak are super horizon, while fluctuations on smaller scales are sub-horizon, thus they follow the oscillatory behaviour driven by gravity and pressure. The series of peaks and troughs that we observe in the temperature power spectrum is the result of these oscillatory processes: modes that were frozen by the recombination at the maximum of compression or rarefaction are mapped into the peaks, while those that are exactly in phase with the background are mapped into the troughs. Hence the first peak represents a mode that has completed just one compression, the second peak, which has half the wavelength, has completed one compression and one rarefaction and so on. In this framework we can consider for the first time the contribution of the baryon masses. If we consider an inertial mass contribution the effect on the oscillation is easily predictable: the peaks that

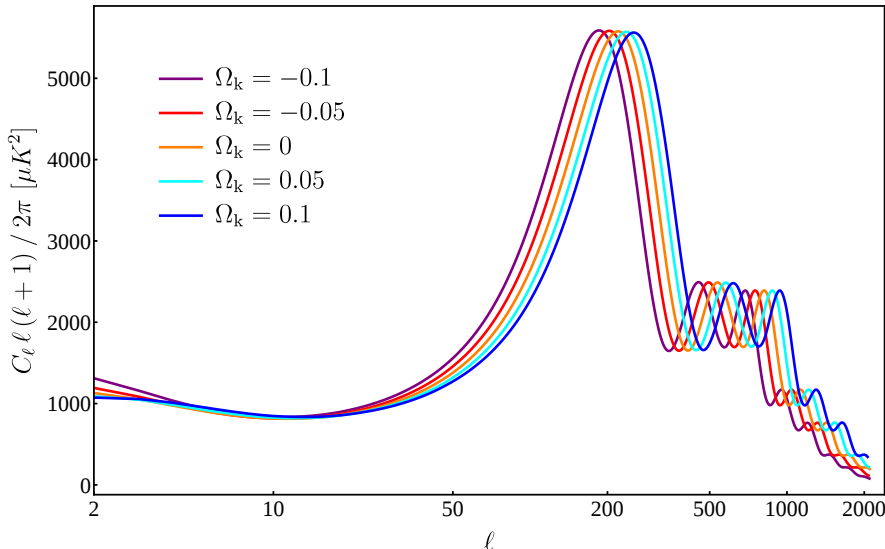


Figure 2.6: Temperature anisotropies power spectrum for 5 different values of the curvature density, here it is possible to appreciate how much the position of the first peak is sensitive to changes of Ω_κ .

corresponds to compression (the odd ones) would be enhanced and the other way around for the even peaks, see Fig.(2.7). This behaviour is known as *baryon loading* and it is extremely useful for constraining of the amount of baryon matter (Ω_{b0}). Another important impact that the baryon loading has on the APS is that it decrease the frequency of the oscillations, as one can expect increasing the inertia of the fluid, this should translate into a shift of the peaks towards higher multipoles. Given the APS in Fig.(2.4) the amount of baryons is well determined by Planck [10]:

$$\Omega_{b0} = (4.884 \pm 0.035) \times 10^{-2}, \quad \Omega_{b0} h^2 = (2.226 \pm 0.016) \times 10^{-2}, \quad (2.83)$$

where $h = H_0/100$ is another way to write the Hubble constant and here it is set to $h = 0.675$ Km/s/Mpc.

The damping tail As said before from $\ell > 1200/1500$ the APS starts to be the dominated by the *damping effect*, see Sec.(2.2.1) for details. In this region of the spetrum we are dealing with scales that are very small and thus are well inside the sound horizon; vhin this framework we have to consider inside the equations the mean-free path of photons. In a few works, if we think the last scattering as a non instantaneous process (i.e. we consider a *last-scattering layer* instead of a last-scattering surface), all the temperature fluctuations on scales that are smaller than the thickness of the layer (which depends on the mean-free path of photons) will be exponentially

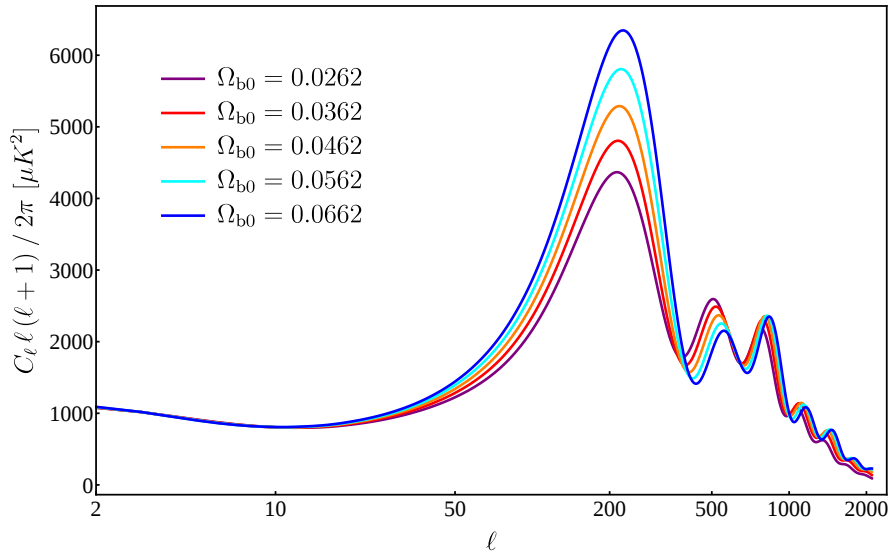


Figure 2.7: Temperature anisotropies power spectrum for 5 different values of the baryon density, in this case the behaviour described in Par.(2.2.2) is clearly visible, the baryon loading effect moves the power from even to odd peaks. The amount of baryon has been changed keeping constant the matter density Ω_{m0} and the cosmological constant contribution Ω_{Λ} .

damped. The characteristic distance covered by a photon during a Hubble time is described in Eq.(2.69), hence, increasing the baryon density (Ω_b) translated into a more tightly coupled photon-baryon at recombination, the mean free path of the photons becomes shorter, and finally the damping tail shifts to smaller angular scales. Another parameter that affects the damping process is the total matter density (Ω_m): a different amount of matter moves the recombination redshift back and forth in time changing the dimension of the angular diameter distance. This reflects into more damping, at a fixed multipole, increasing the total matter density.

2.2.3 Secondary anisotropies:

These anisotropies are not directly connected to the primary, their existence is due to effects that happens well after the Last Scattering. We can summarize the most important:

- The reionization optical depth: well after the decoupling, CMB photons encounter again a distribution of free electrons, probably reionized by UV photons produced by the first stars. Inside the standard cosmological model this effect is parametrized as a *reionization layer* that reduces, see Fig.(2.8) the fluctuation amplitude on all scales by a factor $e^{-\tau_{\text{rei}}}$, where τ_{rei} is the *reionization optical depth*. It is possible

to infer the reionization redshift z_{rei} once measured the optical depth, the latest constraints obtained by Planck temperature and low- ℓ polarization data [10] are:

$$\tau_{\text{rei}} = 0.066 \pm 0.016, \quad z_{\text{rei}} = 8.8^{+1.7}_{-1.4}. \quad (2.84)$$

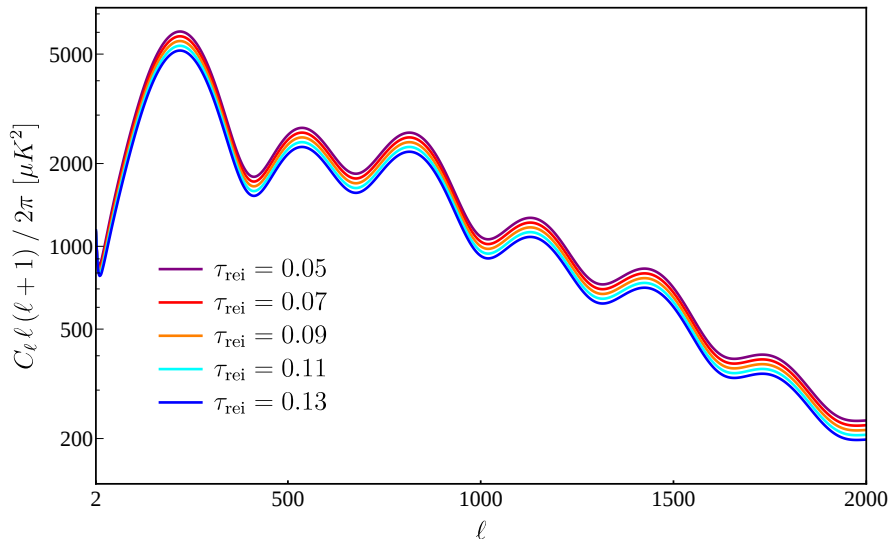


Figure 2.8: Temperature anisotropies power spectrum for 5 different values of τ_{rei} , the larger the value of the reionization optical depth, the greater the suppression over all the multipoles.

- The cosmic shear: weak gravitational lensing produced by potential distortions due to non uniform distribution of mass (galaxies, cluster of galaxies) leads to change in photon direction. This impacts mainly on small angular scales that are slightly distorted. The propagation of a photon in the universe is deflected by the mass distribution along its path,
- The integrated Sachs-Wolfe effect (ISW): during the journey from the last scattering surface to the detectors, photons travel in gravitational potentials that are not constant in time (See Sec.(2.2.1) and in particular Eq.(2.53) for details). This is an important effect for potentials on large scale: these potentials change over cosmological time-scales because the expansion of the universe impacts on the density composition, for example when the Hubble expansion becomes exponential, under the effect of the cosmological constant. The wells(peaks) decay over the time it takes a photon to travel through them, thus, the blueshift(redshift) experienced by photons falling(rising) the potential is not balanced by the redshift(blueshift) as they come out.

- The Sunyaev-Zeldovich (S-Z): CMB photons are scattered by high energy photons in intracluster gas. This is a typical effect that happens in galaxy clusters, in these formations most of baryons are in hot intracluster ionized gas and have very high temperature $\sim 10^8$ K. Electrons transfer energy to CMB photons through inverse Compton processes and simultaneously change their direction of propagation. However, on average, the statistical information remains unchanged. This effect impacts on the blackbody distribution, which results distorted in the high frequency part, basically it move photons from the Rayleigh-Jeans part of the CMB spectrum in the Wien region. It is possible to calculate the change of intensity, which, of course, depends on the physical properties of the cluster,

$$\frac{\Delta I_\nu^{\text{RJ}}}{I_\nu^{\text{RJ}}} = -2 \int \frac{kT}{m_e} \sigma_T n_e dl, \quad (2.85)$$

where $\int dl$ is the path length of the cluster. The latter equation shows that the change in intensity is independent on the redshift of the observed cluster, thus the SZ effect assumes great importance also for the identification of high redshift clusters.

2.3 CMB polarization anisotropies

Till now we have described only the temperature fluctuation of the CMB, moreover Thomson scattering provides also a mild polarization of the radiation. Consider the page as a Cartesian system with $\pm\hat{y}$ vertical direction and $\pm\hat{x}$ horizontal direction, then consider the scattering of a photon propagating in the $+\hat{x}$ direction to the observer ($+\hat{z}$), which is perpendicular to the page. If the incoming photon is linearly polarized in the $(\pm\hat{z})$ direction, then the electron will oscillate in the same direction no dipole radiation is emitted toward the observer. Otherwise if the incident electric field oscillates in the $\pm\hat{y}$, the observer will see a $\pm\hat{y}$ linearly polarized emission. In the most realistic case, if the incident radiation is unpolarized, only the $\pm\hat{y}$ component of the electric field would be scattered toward the observer. In the primordial universe, before the decoupling, Thomson scattering acts exactly in this way, having an electric field of this type,

$$E_x = a_x \cos(\omega t - \xi_x), \quad E_y = a_y \cos(\omega t - \xi_y), \quad (2.86)$$

it is useful write down the Stokes parameters for intensity (I) and linear polarization (Q and U):

$$I = a_x^2 + a_y^2, \quad Q = a_x^2 - a_y^2, \quad U = 2a_x a_y \cos(\xi_x - \xi_y), \quad (2.87)$$

and circular polarization (V):

$$V = 2a_x a_y \sin(\xi_x - \xi_y). \quad (2.88)$$

Thomson scattering does not produce circular polarization, while the Q component correspond to the polarization in the $\hat{x} - \hat{y}$ direction and U rotated of 45 degrees. The usually approach followed in CMB analysis is to consider two combinations for the polarization components $Q \pm iU$, thus, if the temperature component is:

$$T(\hat{n}) = \sum_{\ell=0}^{\infty} \sum_{m=-\ell}^{\ell} a_{\ell m} Y_{\ell m}(\hat{n}), \quad (2.89)$$

as we have seen in Sec.(2.2), linear combination of Q and U can be expanded in analogy with Eq.(2.37),

$$Q(\hat{n}) - iU(\hat{n}) = \sum_{\ell=0}^{\infty} \sum_{m=-\ell}^{\ell} a_{2,\ell m} {}_2Y_{\ell m}(\hat{n}), \quad (2.90a)$$

$$Q(\hat{n}) + iU(\hat{n}) = \sum_{\ell=0}^{\infty} \sum_{m=-\ell}^{\ell} a_{-2,\ell m} {}_{-2}Y_{\ell m}(\hat{n}). \quad (2.90b)$$

In the latter set of equations $a_{\pm 2,\ell m}$ are the expansion coefficients of the spin-2 ${}_{\pm 2}Y_{\ell m}$. Using some properties of spin-2 harmonics coefficients, as done in [177], it is possible to write the polarization field in the most common representation used in cosmology:

$$a_{E,\ell m} = -\frac{a_{2,\ell m} + a_{-2,\ell m}}{2}, \quad (2.91a)$$

$$a_{B,\ell m} = i\frac{a_{2,\ell m} - a_{-2,\ell m}}{2}, \quad (2.91b)$$

where $E(\hat{n})$ and $B(\hat{n})$ are the gradient and curl fields. The main characteristic of this set $T(\hat{n})$, $E(\hat{n})$ and $B(\hat{n})$ of fields is that they are invariant under rotations, moreover they are also invariant under parity transformation. In analogy to what we have done in Eq.(2.40) we can write down all the combination of $T(\hat{n})$, $E(\hat{n})$ and $B(\hat{n})$ spectra:

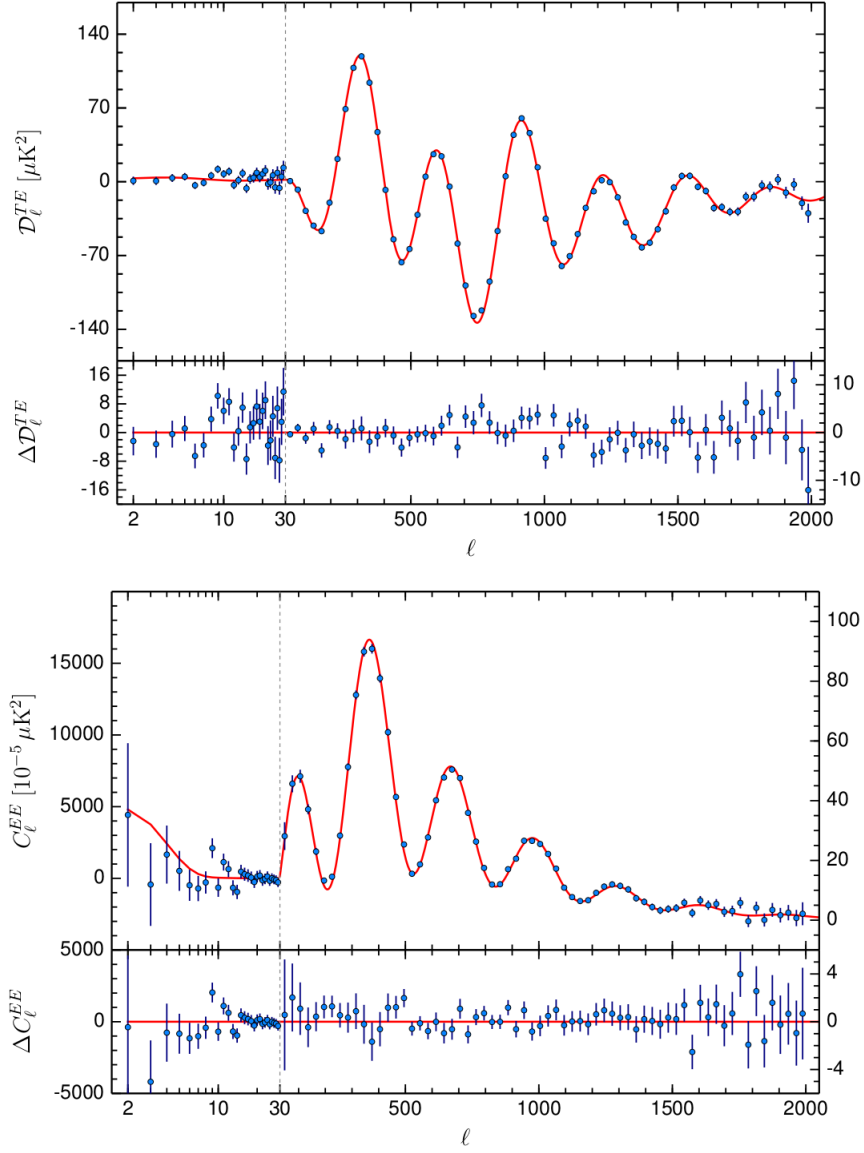


Figure 2.9: TE (upper figure) and EE (lower figure) angular power spectra of the CMB temperature anisotropies measured by the Planck satellite. In both the pictures red lines correspond to the best fit of theoretical model described in Ch.(1) and based on the six standard parameters, while the blue points are the binned value of \mathcal{D}_ℓ and C_ℓ with the corresponding error bars. In the lower panels of each figure there are the residuals. [51]

$$C_\ell^{TT} = \frac{1}{2\ell + 1} \sum_{m=-\ell}^{\ell} (a_{\ell m}^* a_{\ell m}) , \quad (2.92a)$$

$$C_\ell^{EE} = \frac{1}{2\ell + 1} \sum_{m=-\ell}^{\ell} (a_{E,\ell m}^* a_{E,\ell m}) , \quad (2.92b)$$

$$C_\ell^{BB} = \frac{1}{2\ell + 1} \sum_{m=-\ell}^{\ell} (a_{B,\ell m}^* a_{B,\ell m}) , \quad (2.92c)$$

$$C_\ell^{TE} = \frac{1}{2\ell + 1} \sum_{m=-\ell}^{\ell} (a_{\ell m}^* a_{E,\ell m}) , \quad (2.92d)$$

$$C_\ell^{EB} = C_\ell^{TB} = 0 , \quad (2.92e)$$

where the last equation above is valid only if there are no parity violation mechanisms. In Fig.(2.9) we show the public TE and EE power spectra made by the Planck collaboration [51], as noticed for the TT power spectrum in the previous section, the observed data (blue dots) are in very good agreement with the theoretical prediction of the standard cosmological model (red line).

2.3.1 *E modes*

One of the most important signature in the CMB polarization spectra comes from the reionization era, free electrons are subject to large-scale CMB quadrupole, this, in principle, originates a polarization signal at low multipoles in the TE, EE and BB power spectrum. The signal amplitude goes like τ_{rei} and, thus, the power scales as τ_{rei}^2 . This imprint is known as the *reionization bump* and such a feature in the spectrum has no degeneracies with other parameters, this translates into a unique and powerful tool for the study of the universe after the recombination. In Fig.(2.10) it is possible to see the "bump" due to the different vales of τ_{rei} . Notice that, although at $\ell \leq 50$ the EE power spectrum shows more power increasing the optical depth of reionization, at smaller scale we find the same suppression seen in the TT spectrum, see Fig.(2.8). The reason is quite simple to explain: the presence of an additional layer of free electrons that scatters with CMB photons reduces the power in the APS because it is basically an optically thick medium. However, at large scales, it increases the polarization effect that we have described so far, giving more power to the polarized signal in particular between $\ell = 2$ and $\ell = 10$.

2.3.2 *B modes*

In addition to scalar perturbations, another source of polarization can be identified in gravitational wave emission. GWs distort the space-time in directions perpendicular to

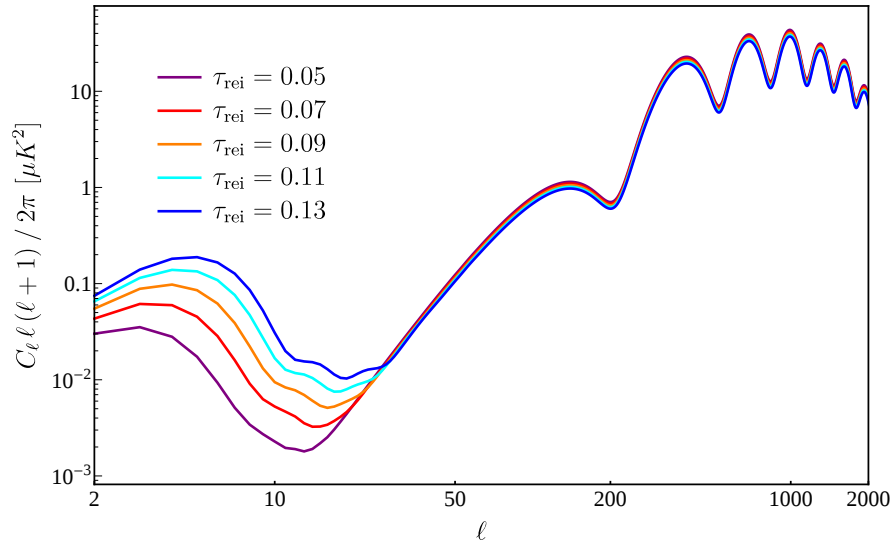


Figure 2.10: *EE power spectrum for 5 different value of τ_{rei}*

their propagation, this effect aligns quadrupole to the plane perpendicular to the wave vector leading to a loss in the axial symmetry that originates E and B polarization modes. In order to produce primordial E and B modes these GWs have to be originated in the primordial universe, Inflation is proposed as the source of both scalar, density perturbations, and tensor gravity wave perturbations. Notice that there are no other known mechanism able to produce a signal in the B modes, primordial GW's are the only channel. As said before, scalar perturbations correspond to quantum fluctuations in the Inflaton field, while it is common belief that two independent polarization states of the gravitational field may experience quantum fluctuations in the vacuum state, originating tensor perturbation i.e GWs. The detection of B-modes on an angular scale corresponding to 1° (the sound horizon at decoupling) would be a smoking gun for the Inflation theory, however there is now no measure of this signal yet. To complicate the picture B-modes can be generated also by gravitational lensing well after the decoupling and the last-scattering of CMB photons. Gravitational lensing masks the primordial source of B-mode with a foreground signal that cannot be removed using information of the electromagnetic spectrum, however, it is possible to extract and remove the lensing signal by studying the higher order spectra (three-point correlation function or bispectrum) which are induced by the lensing [141]. Thus it is possible to separate the contribution of B-modes due to lensing with respect to the contribution due to primordial GWs. The effect of tensor perturbations is parametrized inside the standard cosmological model as a tensor-to-scalar ratio $r \equiv \mathcal{P}_t/\mathcal{P}_s|_k$ that is the ratio between the tensor and scalar power spectra measured at the same k . The values of this parameter depends on the intensity of primordial tensor perturbations that is, of course, model

dependent. In Fig.(2.11) we show the effect of increasing the tensor contribution from $r = 0$ up to $r = 0.12$. Actually there is not a theoretical prediction for the r parameter,

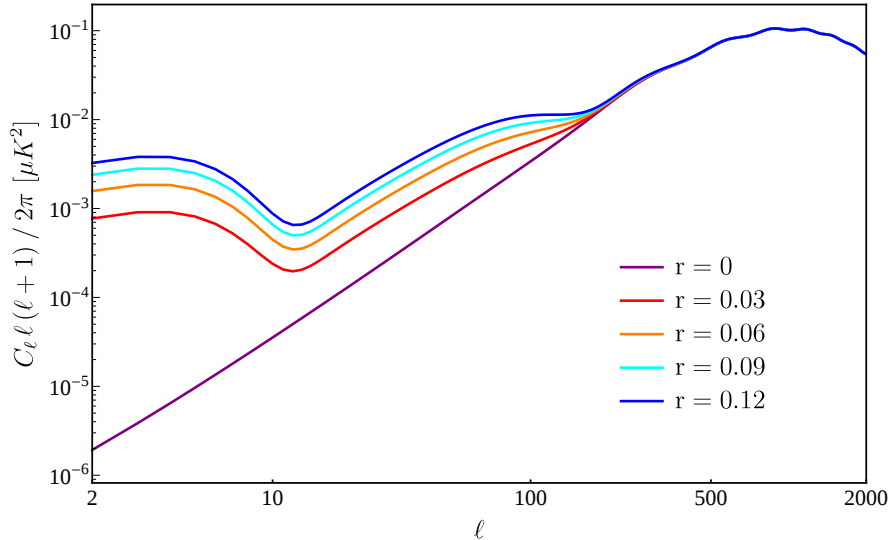


Figure 2.11: *BB power spectrum for 5 different value of r . For $r = 0$ the contribution to the B-mode power spectrum is due only to lensing effects, increasing the value of r we appreciate an increase in power at large angular scales.*

i.e. there are too many inflationary models that can originate a great variety of tensor-to-scalar ratio values (basically values lower that $r < 0.1$ (fixed by Planck [10]) allow a impressive number of models), this means that, in principle, it is always possible to consider the observation not sensitive enough. However, as said before, the detection of primordial B-modes is the only channel for studying fundamental physics in the Inflation field, in analogy to what has been done for the astrophysical gravitational waves detection in the last century.

2.4 Observing the CMB

All the theoretical spectra presented so far have been done considering a perfect sky where the only observable source of CMB. Instead the data in Fig.(2.9 and 2.4) are result of a cleaning process made by the Planck collaboration and well described in [6]. The real picture, however, is much more complicated and in this section we are going to present very briefly the major sources of contaminations that a CMB study must take into account.

2.4.1 Cosmic variance and instrumental error

There is an unavoidable uncertainty called *cosmic variance* related to the fact that we are observing only one CMB sky: as we observe large scales the number of points that are correlated decreases (it is a pure geometrical effect), the smaller the number of points available the greater the statistical uncertainty which we have to deal with. Mathematically speaking, we have seen that in every multipole the quantity of information is encoded in the amount of $m \in [-\ell, \ell]$ i.e. $(2\ell + 1)$ moments. Basically we measure an observed variance C_ℓ^{obs} in the sky and then compare the latter with the expected value. This leads to an intrinsic uncertainty that has the following form:

$$\left\langle \left(\frac{C_\ell^{\text{obs}} - C_\ell}{C_\ell} \right)^2 \right\rangle = \frac{1}{(2\ell + 1)^2 C_\ell^2} \sum_{m=-\ell}^{\ell} \sum_{m'=-\ell}^{\ell'} \langle a_{\ell m} a_{\ell m}^* a_{\ell' m'} a_{\ell' m'}^* \rangle - 1 \quad (2.93a)$$

$$= \sqrt{\frac{2}{2\ell + 1}}. \quad (2.93b)$$

Eq.(2.93b) is valid considering a perfect observation of the entire sky, however, as we will see in Sec.(2.4.2) there are a long series of foregrounds that cover the CMB information in different areas of the celestial sphere, thus we are forced to mask part of the sky. Masking the sky means losing information also at large scales and thus further increasing the cosmic variance uncertainty, basically using a fraction of the sky f_{sky} increases the cosmic variance of a factor $1/f_{\text{sky}}$. In order to reduce this uncertainty, in principle, one should be able to observe the CMB from different frames, but this is clearly impossible, thus we have to deal with such an issue during the analysis rather than in the interpretation of data.

During the analysis we have to deal also with instrumental uncertainties. The origin of these errors have many different sources: the detector intrinsic precision, pointing issues, calibrations, data analysis, noise removal and so on and do forth (see [11, 12, 167] for some references). In order to summarize this information effectively, in Fig.(2.12) we show the theoretical temperature power spectrum (red) and the corresponding cosmic variance (green) obtained using the Planck $f_{\text{sky}} = 0.57$, in addition we overplot the \mathcal{D}_ℓ extracted from the Planck 2015 data both for low- ℓ and high- ℓ . The latter contains the cosmic variance information and the uncertainties related to the instrument. Looking the green area, it is evident that the cosmic variance contributes at large scales and it is sub-dominant for $\ell > 1000$, while the instrumental errors dramatically increase for the small-scale anisotropies.

2.4.2 Foregrounds

Since the CMB is, by definition, a background emission, other sources that are between the last-scattering surface and us are called *foregrounds*. The presence of these astrophysical sources, which is of great interest for other physics branches, represents an

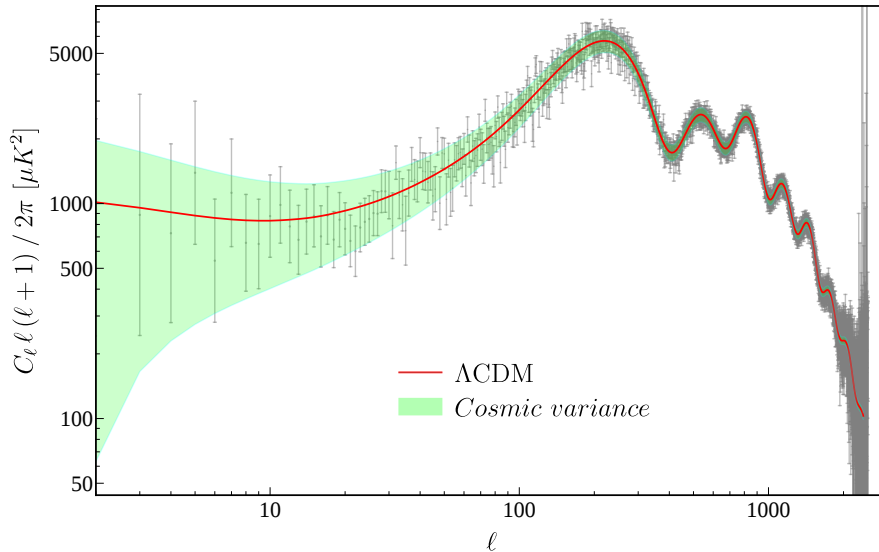


Figure 2.12: Theoretical temperature anisotropies power spectrum (red line), corresponding cosmic variance (green region) obtained using $f_{\text{sky}} = 0.57$ and \mathcal{D}_ℓ extracted from Planck 2015 data (grey dots). We chose to plot in logarithmic scale both axes in order to compare the uncertainty due to cosmic variance, that are dominant until $\ell \sim 800$ and the error coming from instrumental uncertainties which, on the other hand becomes relevant at high multipoles $\ell > 2000$.

obstacle for a CMB study, in order to remove these emissions and clean the maps, it is necessary to know what type of processes we are dealing with and how to parametrize them.

Synchrotron: diffuse emission due to spiraling electrons in the galactic magnetic fields. This radiation may be highly polarized, up to a 75%. The spectrum of synchrotron emission is basically flat at frequencies $\nu \leq 20\text{GHz}$ and then, for higher frequencies, follows an exponential law with a negative index $\beta_s \sim -3$. We show the frequency spectra used by the Planck collaboration in Fig.(2.14), the top-left panel corresponds to synchrotron emission. Synchrotron radiation is present in both temperature and polarization maps.

Free-free: bremsstrahlung emission coming from electron-ion collision, its spectrum is close to a power law for frequencies greater than 1 GHz and presents a visible break at lower frequencies. This happens because the medium becomes optically thick, in addition the brightness temperature becomes equal to the electron temperature. Free-free spectrum is similar to the synchrotron one at low frequencies, but can be

distinguished because its power-law index is flatter than the synchrotron one. We show the free-free spectrum in the top-right panel of Fig.(2.14).

Spinning dust: dust grain having non-zero dipole moment that rotates and emits in the microwave region of the e-m spectrum. The frequency spectrum shows a peak between 25 and 30 GHz and then it follows a power law in analogy with the synchrotron and free-free case. Spinning dust is shown in middle-left panel of Fig.(2.14).

CO lines: three of the nine frequency bands of the Planck experiment (100, 217, 353 GHz) strongly detected emission lines of carbon monoxide (CO). It is possible to separate these lines from the other diffuse components and to describe parametrically in terms of an amplitude $a(p)$ inside the corresponding detector map.

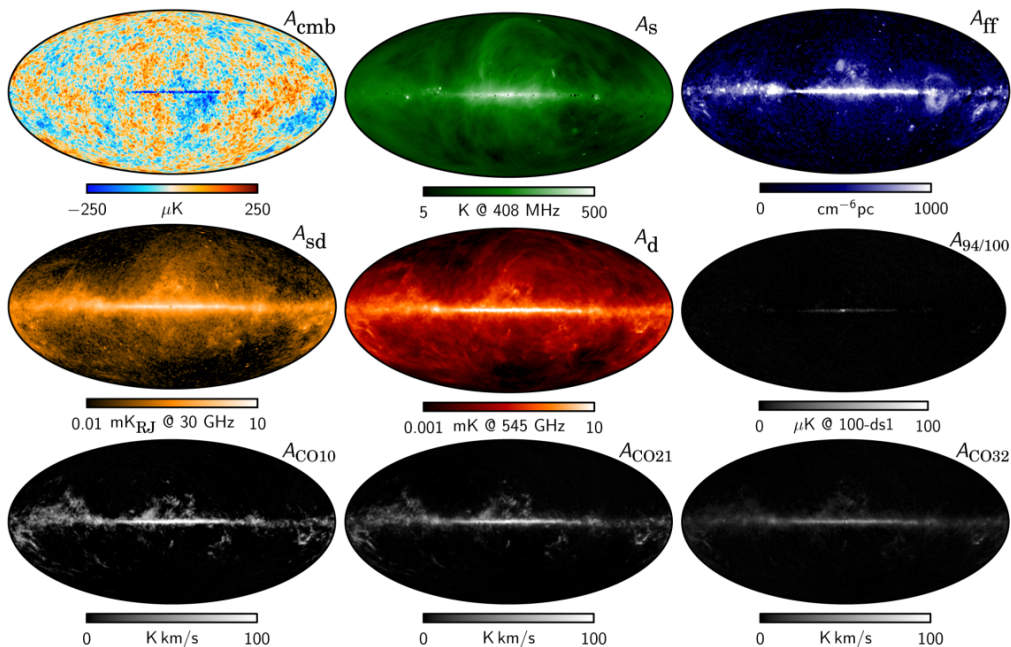


Figure 2.13: Foreground maps delivered by the Planck collaboration, for the top-left to the bottom-right we show CMB, synchrotron, free-free, spinning dust, thermal dust, and four CO amplitude maps. [6]

Thermal dust: this is the dominant component at frequencies $\nu > 100$ GHz, the characteristic spectrum is basically a modified black body with a free emissivity index β_d and a characteristic temperature T_d . Thermal dust gives its contribution also in polarization, because aspherical dust grains tend to distribute along the local magnetic

field lines. This behaviour translates into a polarized emission in the microwave band with the same thermal-dust spectrum. We show the spectrum in the lower-left panel of Fig.(2.14).

Thermal SZ: in the right-bottom panel of Fig.(2.14) we show the spectrum of the Sunyaev-Zeldovich effect. The deviation from the black body spectrum of photons which undergo inverse compton scattering leaves an imprint increasing the brightness on high frequencies.

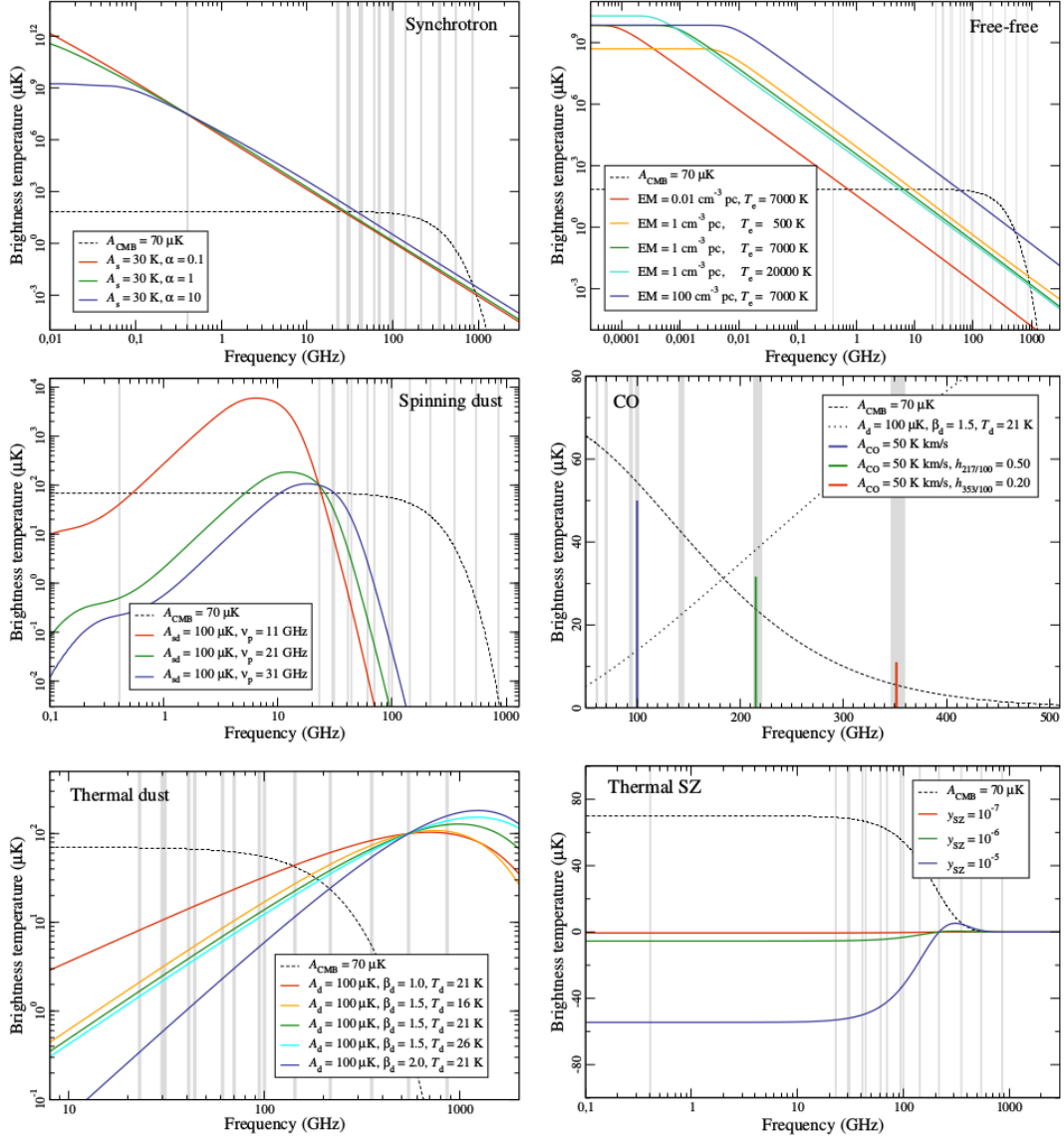


Figure 2.14: Brightness temperatures in function of the frequency for the main foregrounds: synchrotron, free-free, spinning dust, CO, thermal dust and SZ. For every spectrum there are shown several parameter combinations in order to show the behaviours of the spectra. The black-dashed line is representative of the CMB brightness temperature corresponding to a $T = 70\mu\text{K}$, while the gray vertical lines show the central value of the Planck frequency bands. [6]

3

Neutrinos

This thesis focuses on the neutrino figure, this multifaceted particle plays different roles in the cosmological history: it is neutral and weakly interacting, i.e. there is no way to understand its properties by direct observations of the electromagnetic spectrum. However neutrinos feel the gravitational interaction and contribute to Einstein equations as additional relativistic degrees of freedom and took part to electroweak interactions with the other components of the primordial fluid until their decoupling at $T \sim 1$ MeV. This translates in an indirect channel for the study of neutrinos, indeed, these behaviours leave clear imprints on the temperature and polarization anisotropies of the cosmic microwave background radiation. CMB measurements have become extremely precise, Planck measures the CMB APS below the % level, hence, cosmology has become a parallel and complementary tool, with respect to laboratory experiments, to constrain fundamental properties of the neutrino background. In this chapter we are going to see the main cosmological aspects of primordial neutrinos, however, in order to understand their properties we need a very brief introduction of the theoretical framework within which they are described: the standard model of particles.

3.1 *State of the art*

Neutrinos are one of the most studied particles in physics both from the theoretical and experimental point of view; the reason of this interest resides in the amount of reactions that see them participating and in the fact that they represent one of the most interesting channels for extending of the actually known model of particle physics. The history of this particle starts in 1930 when Wolfgang Pauli, in order to explain the observation made by Chadwick (1914) and Ellis (1927) of the continuous energy distribution of the electron in the β -spectrum, wrote to his friend Walter Baade: *I have done a terrible thing today, something which no theoretical physicist should ever do. I*

have suggested something that can never be verified experimentally. One year later Pauli proposed, in an open letter to a physics conference at Tübingen on 4 December 1930, the existence of a neutral weakly interacting particle called *neutron*. However, after the discovery of the “real” neutron by Chadwick in 1932, E. Fermi and Pauli renamed this particle *neutrino*. In 1934 Fermi proposed the theory of weak interactions [69] in analogy with quantum electrodynamics; however, theoretical particle physics was a relative new sector, P. Dirac introduced his equation only few years before in 1928 [61], and the understanding of the picture that now we call standard model of particle physics was incomplete. Change of one unit of the nuclear spin that often happens in β -decays, that represent a CP violation, induced G. Gamow to extend the theory introducing new axial-vector currents, parity was a fundamental symmetry at that time and its violation was impossible. The universality of the weak interaction was postulated by B. Pontecorvo after the observation of the muon decay (1947) [147] and simultaneously began to circulate the notion of neutrino “families”. The succession of discoveries was really impressive: in 1956 Reines and Cowan had the first detection in a reactor-neutrino experiment, the same year the validity of parity conservation was questioned thanks to observations of the K meson decay [118]. This opened the way to a new theory called vector-axial theory ($V - A$). Formulated in 1958 by R.P. Feynman and M. Gell-Mann [70] it provides a description using massless neutrinos as proposed by L. Landau [116] and A. Salam [155]; left-handed and right-handed neutrinos rise spontaneously from the theory. The concept of lepton numbers introduced in 1953 was briefly replaced by the strongest lepton-family number (processes like $\mu \rightarrow e + \gamma$ do not take place). In 1967 the weak interaction theory became part of a more complete picture, the Glashow-Weinberg-Salam Model or Standard Model [89]. Based on a solid mathematical framework such as the group theory it is based on a $SU(2) \otimes U(1)$ gauge model. It predicts with success the existence of vector bosons W^\pm and Z^0 , provides an explanation for the existence of a massless boson γ and incorporates the Higgs mechanism (1964) [100] that allows the original massless gauge bosons to acquire longitudinal degrees of freedom (mass) through the interaction with a scalar field. The successes of the SM are astonishing and confirm the extreme power of prediction of the theory; the number of generations was fixed at three in 1989 by the measurements by LEP experiments at CERN of the width of the Z^0 boson [2, 16, 57].

There are no clear deviations from the SM except for the neutrino oscillations experiments. The concept of oscillation was proposed by Pontecorvo in 1957 [148] in analogy with the $K^0 \leftrightarrow \bar{K}^0$ observed by Gell-Mann in 1955 [83], in this first case the oscillation was introduced between $\nu \leftrightarrow \bar{\nu}$ considering Majorana neutrinos, but few years later a more realistic case of $\nu_e \leftrightarrow \nu_\mu$ oscillation became dominant in the community. In 1975 the theory of oscillation was finally published in [37].

In recent years an ever-increasing effort has been put into the study and observation of these particles: KamLAND [67], Kamiokande [166], GALLEX/GNO [94], GERDA [14], SAGE [4], Super-Kamiokande [75], SNO SNO+ [114], MiniBooNE [168],

IceCube [165], Juno [20], OPERA [5] are only some of the main experiments that have investigated, and are investigating, neutrino properties. Observations of solar and atmospheric neutrinos provided evidence of the oscillation framework of three-neutrino mixing, i.e. three flavours are the unitary linear combination of three massive eigenstates. As this work is writing, the mass differences (Δm_{21}^2 , Δm_{31}^2 , Δm_{32}^2) and the mixing angles (θ_{12} , θ_{13} , θ_{23}) have been measured; the unknown quantities left are the mass hierarchy (the sign of Δm_{31}^2), the CP phase δ [133] and the absolute scale of the masses. As said before, another open question is the nature of neutrinos, if they are Dirac or Majorana particles, the smoking gun experiment to shed light on this is the neutrinoless double beta decay ($0\nu\beta\beta$) [50, 58] which can take place only inside the Majorana picture, violating the lepton number conservation, see the *black box theorem* in Ref. [161].

3.2 The Standard Model

Before showing details about neutrino physics we need to briefly describe the picture where they live, that is the standard model of particles. The SM is the result of the theories developed in the previous decades and centuries: classical mechanics [90, 169], quantum mechanics and quantum field theory [45, 131, 146, 154], group theory [26, 86], are the pillars of modern physics. It is based on the notion of gauge theory which describes the fundamental interactions through a relativistic quantum field theory, based on the gauge symmetry principle for the group $SU(3)_C \otimes SU(2)_L \otimes U(1)_Y$, where C, L and Y denote colour, left-handed chirality and weak hypercharge. The part associated to the strong sector $SU(3)_C$ is an exact symmetry and it remains unbroken at any energy level, the part associated to electroweak interactions, i.e. $SU(2)_L \otimes U(1)_Y$, through the Higgs mechanism, undergoes to a spontaneous symmetry breaking $SU(2)_L \otimes U(1)_Y \rightarrow U(1)_Q$ and the relative formation of the massive bosons W^\pm and Z^0 . Using this elegant picture we know of the existence of fundamental particles which are divided into quarks and leptons; and the respective anti-particles, see Tab.(3.1). The defining property of quarks is that they carry color charge, and thus, interact via the strong interaction, as we know, there are three colors and the associated anti-colors. Moreover quarks carry electric charge and weak isospin, hence they interact with other fermions both electromagnetically and via weak interaction.

Since the main topic of this thesis are neutrinos, let us concentrate on the electroweak part of the theory, the $SU(2)_L$ group is called weak isospin I and the subscript L means that the natural components are the ones with left-handed chirality. The weak isospin is the charge associated to a non-abelian group which implies that for every representation of the group the generators are fixed, in particular $I_\alpha = \sigma_\alpha/2$ that are the Pauli matrices. The symmetry group $U(1)_Y$ is called hypercharge, isospin and to each

The Standard Model

	1 st generation	2 nd generation	3 rd generation
quarks:	u (up)	c (charm)	t (top)
	d (down)	s (strange)	b (bottom)
leptons:	ν_e (electron ν)	ν_μ (muon ν)	ν_τ (tau ν)
	e (electron)	μ (muon)	τ (tau)

Table 3.1: *In this table we show the three generations of fermions: quarks and leptons. These 12 particles are the fundamental building blocks of the standard model of particles. The SM does not provide any explanation for the number of generations, it is just an experimental evidence.*

generator corresponds a boson field, i.e. for the 3 component isospin the vector gauge field A_α^μ and for the hypercharge one vector gauge field B^μ . The covariant derivative that is needed by the theory is defined as:

$$\mathcal{D}_\mu \equiv \partial_\mu + ig \underline{A}_\mu \cdot \underline{I} + ig' B^\mu \frac{Y}{2} \quad (3.1)$$

where the underline means we are considering vectors and g and g' are the couplings of the bosons fields. The best and most economical way to summarize this knowledge is to write down the Lagrangian of the EW theory:

$$\begin{aligned} \mathcal{L} = & i\bar{L}_L \not{D} L_L + i\bar{Q}_L \not{D} Q_L + \sum_{f=e,u,d} i\bar{f}_R \not{D} f_R \\ & - \frac{1}{4} \underline{A}_{\mu\nu} \underline{A}^{\mu\nu} - \frac{1}{4} B_{\mu\nu} B^{\mu\nu} \\ & + (\mathcal{D}_\mu \phi)^\dagger (\mathcal{D}^\mu \phi) - \mu^2 \phi^\dagger \phi - \lambda (\phi^\dagger \phi)^2 \\ & - y^e (\bar{L}_L \phi e_R + \bar{e}_R \phi^\dagger L_L) \\ & - y^d (\bar{Q}_L \phi d_R + \bar{d}_R \phi^\dagger Q_L) - y^u (\bar{Q}_L \tilde{\phi} u_R + \bar{u}_R \tilde{\phi}^\dagger Q_L), \end{aligned} \quad (3.2)$$

where the first line contains the left-handed chiral components of the fermion fields grouped into weak isospin doublets:

$$L_L \equiv \begin{pmatrix} \nu_{eL} \\ e_L \end{pmatrix}, \quad Q_L \equiv \begin{pmatrix} u_L \\ d_L \end{pmatrix}, \quad (3.3)$$

their covariant derivatives in the Dirac formalism ($\not{D} = \gamma_\mu \mathcal{D}_\mu$) and the symbol \dagger means the hermitian adjoint. The second line contains the kinetic terms and the self-couplings of the gauge bosons, the third row is the Higgs field (ϕ) Lagrangian and the last

two lines contain the Higgs-fermion Yukawa couplings (y^x), responsible of the mass generation in the fermion sector (for further details see [45, 49, 131, 146]). In the SM neutrino fields have only left-handed components, since right-handed neutrinos have never been observed, this is a consequence of the first two-component theory of neutrinos developed by Landau and Salam i.e. right-handed fields are singlets under weak isospin group, i.e. they have isospin $I = I_3 = 0$. It is possible to expand the terms in the first line of Eq.(3.2) obtaining the interaction Lagrangian that describes the coupling between fermions and gauge bosons, following the steps in [88], the interacting part can be divided into two contributions the first due to charged currents and the second generated by neutral currents:

$$\mathcal{L}_{int}^{CC} = -\frac{g}{2} [\bar{\nu}_{eL} (A_1 - iA_2) e_L + \bar{e}_L (A_1 + iA_2) \nu_{eL}] , \quad (3.4)$$

$$\mathcal{L}_{int}^{NC} = -\frac{1}{2} [\bar{\nu}_{eL} (gA_3 - g'\not{B}) \nu_{eL} - \bar{e}_L (gA_3 - g'\not{B}) e_L - 2g'\bar{e}_R \not{B} e_R] , \quad (3.5)$$

In the charged current we can define a field that corresponds to the charged boson W^\pm in such a way:

$$W^\mu = \frac{A_1^\mu - iA_2^\mu}{\sqrt{2}} , \quad (3.6)$$

that leads to a Lagrangian density:

$$\mathcal{L}_{int}^{CC} = -\frac{g}{2\sqrt{2}} j_{W,L}^\mu W_\mu + h.c. , \quad (3.7)$$

where

$$j_{W,L}^\mu = \bar{\nu}_L \gamma^\mu (1 - \gamma^5) e , \quad (3.8)$$

is the leptonic charged current. Carrying out a similar calculation for the neutral current we obtain:

$$\mathcal{L}_{int}^{NC} = \mathcal{L}_I^Z + \mathcal{L}_I^\gamma \quad (3.9a)$$

$$= -\frac{g}{2 \cos \theta_W} j_{Z,L}^\mu Z_\mu - e j_{\gamma,L}^\mu A_\mu , \quad (3.9b)$$

where A^μ and Z^μ are the electromagnetic and the neutral vector boson fields expressed as linear combination of the A_3^μ and B^μ fields rotated with the Weinberg angle θ_W :

$$A^\mu = \sin \theta_W A_3^\mu + \cos \theta_W B^\mu \quad (3.10a)$$

$$Z^\mu = \cos \theta_W A_3^\mu - \sin \theta_W B^\mu . \quad (3.10b)$$

In this case $j_{\gamma,L}^\mu$ and $j_{Z,L}^\mu$ are the electromagnetic current and the neutral charged current respectively. The Noether currents that we have written in Eqs.(3.8 and 3.9) are conserved quantities that describes the trilinear couplings in the Feynman diagrams.

3.2.1 Mass generation mechanism

In the SM there is a mechanism responsible for the generation of the masses of fermions and bosons: the Higgs mechanism. Let us start introducing the Higgs doublet:

$$\phi(x) = \begin{pmatrix} \phi^+(x) \\ \phi^0(x) \end{pmatrix}. \quad (3.11)$$

We define the third line of Eq.(3.2) and impose:

$$v \equiv \sqrt{-\frac{\mu^2}{\lambda}}, \quad (3.12)$$

where the squared mass-like coefficient μ^2 is assumed to be negative to realize the spontaneous symmetry breaking $SU(2)_L \otimes U(1)_Y \rightarrow U(1)_Q$ and λ is the coefficient of the quadratic self-coupling; this leads to a potential of the form:

$$V(\phi) = \lambda \left(\phi^\dagger \phi - \frac{v^2}{2} \right)^2, \quad (3.13)$$

the minimum of this potential is the vacuum or the lowest energy state, all the quantized excitations of the fields corresponds to particle states. While charged fields and those which have non-zero spin must have a zero value in the vacuum, neutral scalar fields have non-zero value in vacuum called *vacuum expectation value* (VEV). In particular, for the Higgs field, the ϕ^0 is the source of this VEV. In the so called *unitary gauge* [26, 88, 131] it is possible to write the Higgs doublet making clear the physical states:

$$\phi(x) = \frac{1}{\sqrt{2}} \begin{pmatrix} 0 \\ v + H(x) \end{pmatrix}, \quad (3.14)$$

Expanding the Higgs part in the Eq.(3.2) with Eq.(3.14) the mass terms of the bosons appear:

$$\begin{aligned} \mathcal{L}_{\text{Higgs}} = & \frac{1}{2} (\partial H)^2 - \lambda v^2 H^2 - \lambda v H^3 - \lambda H^4 + \frac{g^2 v^2}{4} W_\mu^\dagger W^\mu \\ & + \frac{g^2 v^2}{8 \cos^2 \theta_W} Z_\mu Z^\mu + \frac{g^2 v}{2} W_\mu^\dagger W^\mu H + \frac{g^2 v}{4 \cos^2 \theta_W} Z_\mu Z^\mu H \\ & + \frac{g^2}{4} W_\mu^\dagger W^\mu H^2 + \frac{g^2}{8 \cos^2 \theta_W} Z_\mu Z^\mu H^2. \end{aligned} \quad (3.15)$$

Reading the Lagrangian in Eq.(3.15), the first term is the kinetic term for the Higgs boson, then the Higgs mass term appears ($m_H = \sqrt{2\lambda v^2}$), third and fourth terms are trilinear and quadrilinear self-coupling of the Higgs field. The W^\pm and Z^0 masses are

described in the fifth and sixth terms in particular:

$$m_W = \frac{gv}{2}, \quad m_Z = \frac{gv}{2 \cos \theta_W}, \quad (3.16)$$

the last four terms in the Higgs Lagrangian are the trilinear and quadrilinear couplings between vector bosons and the Higgs field.

Fermions acquire mass as a result of the Higgs mechanism through the presence of the Yukawa couplings (fourth and fifth row of Eq.(3.2)). As done before, in the unitary gauge, the Higgs-lepton Yukawa Lagrangian can be written in a more convenient form, however the Yukawa coupling, that are complex 3×3 matrix, are not diagonal, we need to diagonalize ¹ changing the lepton basis to the new $|\ell_L, \ell_R\rangle = |(e_L, \mu_L, \tau_L)^T, (e_R, \mu_R, \tau_R)^T\rangle$ (for further details see [88]), after this procedure the Lagrangian takes the form:

$$\mathcal{L}_{H,L} = - \left(\frac{v+H}{\sqrt{2}} \right) \bar{\ell}_L Y^\ell \ell_R + h.c., \quad (3.17)$$

$$= - \sum_{\alpha=e,\mu,\tau} \frac{y_\alpha^\ell v}{\sqrt{2}} \bar{\ell}_\alpha \ell_\alpha - \sum_{\alpha=e,\mu,\tau} \frac{y_\alpha^\ell}{\sqrt{2}} \bar{\ell}_\alpha \ell_\alpha H, \quad (3.18)$$

where the part with the Yukawa matrix elements (y_α^ℓ) and the Higgs VEV represents the mass term for the lepton:

$$m_\alpha = \frac{y_\alpha^\ell v}{\sqrt{2}}, \quad \text{with } \alpha = e, \mu, \tau. \quad (3.19)$$

Here $\ell_\alpha = \ell_{\alpha L} + \ell_{\alpha R}$ and α corresponds to the family lepton indices. Every lepton has a Yukawa coupling proportional to its mass, which is a free parameter of the model, i.e. there is a need to perform a measurement, at least one time, of the mass in order to provide a value of the y_α^ℓ .

3.2.2 Effective low-energy theory

As we have seen in Ch.(1) standard cosmology is able to provide a description of the universe up to high temperatures ($T \geq 100 \text{ GeV}$), however the processes involving neutrinos start to be interesting at relatively low temperatures $T \lesssim 10 \text{ MeV}$ i.e. temperatures much lower than the mass scale of the vector bosons W^\pm and Z^0 . In this regime it is useful to approximate the standard interacting picture in using a low energy Lagrangian both for charged and neutral currents. In this approximation the gauge boson propagators in the momentum space can be rewritten in a simpler form:

$$G_{\mu\nu}^W(p) \rightarrow i \frac{g}{m_W^2}, \quad G_{\mu\nu}^Z(p) \rightarrow i \frac{g}{m_Z^2}, \quad (3.20)$$

¹A general complex matrix A' can be diagonalized through a unitary transformation $V_L^\dagger A' V_R = A$, where V_L and V_R are unitary matrices.

and the effective Lagrangian take the following form:

$$\mathcal{L}_{\text{eff}} = \mathcal{L}_{\text{eff}}^{CC} + \mathcal{L}_{\text{eff}}^{NC} \quad (3.21)$$

$$- \frac{G_F}{\sqrt{2}} j_{\mu(W)}^\dagger j_{\mu(W)}^\mu - \frac{G_F}{\sqrt{2}} j_{\mu(Z)}^\mu j_{\mu(Z)} \cdot \quad (3.22)$$

where G_F is the universal weak interaction constant or Fermi constant that can be written as:

$$G_F = \frac{\sqrt{2}}{8} \frac{g^2}{m_W^2} = \frac{\sqrt{2}}{8} \frac{g^2}{\cos^2 \theta_W m_Z^2}. \quad (3.23)$$

Basically the mass of the mediator bosons is large enough to collapse the two vertices of the $2 \leftrightarrow 2$ process into a unique four-point interaction as it is possible to see in Fig.(3.1).

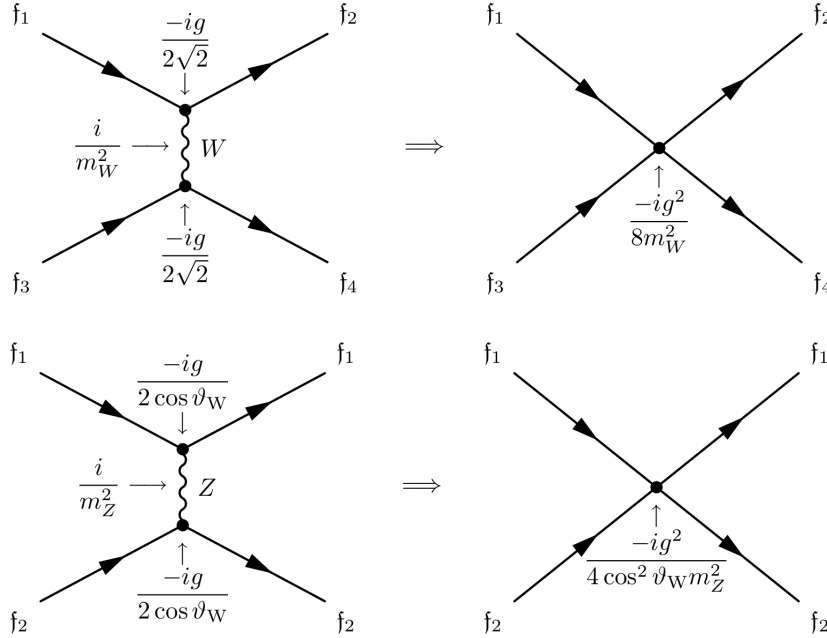


Figure 3.1: Contraction of the W^\pm (top panel) and Z^0 (bottom panel) in the effective low-energy theory of weak interactions.

3.2.3 Dirac mass and mixing

As said in the previous sections, neutrinos are well described inside the SM, moreover the understanding of the weak interactions is one of the cornerstones of the model. Nevertheless they represents the first hint of non-standard physics. Basically there are two ways to consider massive neutrinos in the SM: the first is to treat them as Dirac

particles, as we have done for leptons, the second is to adopt the Majorana formalism. The nature and the origin of their tiny masses is still unknown and thus it is one of the most interesting and studied features, in this section we will briefly present the most important properties of both theories.

It is clear from Eqs.(3.2 and 3.18) that inside the standard picture, in order to generate a mass term in the lepton sector, we need the presence of both left and right-handed components of the corresponding field. This is the reason why neutrinos, in the SM, naturally have to be massless particles; however, the existence of oscillations among flavour eigenstates is unmistakable proof of the existence of massive eigenstates. Thus, if we want to explain this situation inside the SM, we have to modify the theory introducing a right-handed component in the neutrino sector. The neutrino term in the Lagrangian is similar to the lepton one, Eq.(3.18), here we show the diagonalized form, parallel to what was done for the lepton case, in the new basis $|n_L, n_R\rangle$, with the Yukawa Y^ν :

$$\mathcal{L}_{H,\nu} = - \left(\frac{v + H}{\sqrt{2}} \right) \bar{n}_L Y^\nu n_R + h.c. \quad (3.24)$$

$$= - \sum_{k=1}^3 \frac{y_k^\nu v}{\sqrt{2}} \bar{\nu}_k \nu_k - \sum_{k=1}^3 \frac{y_k^\nu}{\sqrt{2}} \bar{\nu}_k \nu_k H, \quad (3.25)$$

where the $\nu_k = \nu_{kL} + \nu_{kR}$ and k is the number of massive eigenstates. The basis $|n_L, n_R\rangle$ is a new representation of the arrays contained the left-handed and right-handed components of the neutrino fields. In particular $n_L = V_L^{\nu\dagger} \nu'_L \equiv (\nu_{1L}, \nu_{2L}, \nu_{3L})^T$ and $n_R = V_R^{\nu\dagger} \nu'_R \equiv (\nu_{1R}, \nu_{2R}, \nu_{3R})^T$.

Once again the mass term is given by the part with the VEV and the Yukawa:

$$m_\kappa = \frac{y_k^\nu v}{\sqrt{2}}, \quad (3.26)$$

Notice that the neutrino mass term is proportional to the same Higgs VEV used in the lepton case, thus, in order to explain the tiny mass suggested by laboratory experiments and cosmological observation, we need to consider very small values for the eigenvalues of the Higgs-neutrino Yukawa matrix y_k^ν . Define an unitary matrix in the following way:

$$U^D = V_L^{\ell\dagger} V_L^\nu, \quad (3.27)$$

it is possible to write down the charged current in both the flavour $\nu_{\alpha L}$ and mass ν_{kL} eigenstates:

$$j_{W,L}^\mu = 2\bar{\nu}_{\alpha L} \gamma^\mu \ell_L^\alpha, \quad (3.28)$$

$$j_{W,L}^\mu = 2\bar{\nu}_L^k \gamma^\mu U_{k\beta}^\dagger \ell_L^\beta. \quad (3.29)$$

The U matrix is the *Pontecorvo-Maki-Nakagawa-Sakata* matrix and it is the neutrino

analogous of the mixing matrix in the lepton sector [88]. The family lepton number is not conserved, instead of the total lepton number which is a global symmetry, it is clear looking at the neutrino part of the Lagrangian, Eq.(3.25) where there are no transformations on the right-handed part that leave the Lagrangian unchanged. The mixing matrix U^D is defined as follows:

$$U^D = \begin{pmatrix} c_{12}c_{13} & s_{12}s_{13} & s_{13}e^{-i\delta} \\ -s_{12}c_{23} - c_{12}s_{23}s_{13}e^{i\delta} & c_{12}c_{23} - s_{12}s_{23}s_{13}e^{i\delta} & s_{23}c_{13} \\ s_{12}s_{23} - c_{12}c_{23}s_{13}e^{i\delta} & -c_{12}s_{23} - s_{12}c_{23}s_{13}e^{i\delta} & c_{23}c_{13} \end{pmatrix}, \quad (3.30)$$

where $s_{ij} = \sin \theta_{ij}$, $c_{ij} = \cos \theta_{ij}$ with $0 < \theta_{ij} < \pi/2$ and δ is the phase related to the CP violation (a non zero value of δ leads to CP violation). The mixing angles can be defined, in the inverse way, via the elements of the neutrino mixing matrix:

$$s_{12}^2 = \frac{|U_{e2}|^2}{1 - |U_{e3}|^2}, \quad c_{12}^2 = \frac{|U_{e1}|^2}{1 - |U_{e3}|^2}, \quad (3.31)$$

$$s_{13}^2 = |U_{e3}|^2, \quad c_{13}^2 = 1 - s_{13}^2, \quad (3.32)$$

$$s_{23}^2 = \frac{|U_{\mu 3}|^2}{1 - |U_{e3}|^2}, \quad c_{23}^2 = \frac{|U_{\tau 3}|^2}{1 - |U_{e3}|^2}. \quad (3.33)$$

3.2.4 Majorana mass and mixing

In the formulation of the SM a massless fermion can be described, in a very simple way, by a single chiral field, i.e. the Dirac equation allows two simple results:

$$(i\gamma^\mu \partial_\mu - m) \psi = 0, \quad (3.34)$$

where ψ is a spinor chiral field, in case of massless fermions we obtain the Weyl equations:

$$i\gamma^\mu \partial_\mu \psi_L = 0, \quad (3.35)$$

$$i\gamma^\mu \partial_\mu \psi_R = 0. \quad (3.36)$$

The possibility of describing a particle using the Weyl spinors ψ_L and ψ_R requires parity violation and it was not considered until its discovery in 1958. Massless neutrinos are the best candidates to be left-handed Weyl spinors, but the discovery of oscillation among flavours complicates the picture. Ettore Majorana in 1937 proposed a different approach, basically considering a dependence between the left and right-handed Weyl spinors, using this trick it is possible to rewrite the Eq.(3.36) for massive particles in such a way:

$$-i\gamma^\mu \partial_\mu \bar{\psi}_R = m\bar{\psi}_L, \quad (3.37)$$

and the charge conjugated related equation:

$$i\gamma^\mu \partial_\mu \psi_L = m\mathcal{C}\bar{\psi}_L^T, \quad (3.38)$$

where \mathcal{C} is the charge conjugation operator. This implies equality of particle and antiparticle or $\psi = \psi^C$. This behaviour is permitted only in the case of neutral particles, carrying out the same calculation for charged states brings to the cancellation of the Noether currents and, thus, destroys the theory.

A proper mass term in the Majorana picture needs a left-handed type term that can replace the right-handed ν_R , the right choice is the charge conjugated field of ν_L :

$$\nu_L^C = \mathcal{C}\bar{\nu}_L^T, \quad (3.39)$$

hence, the Majorana Lagrangian density has the form:

$$\mathcal{L}^M = \frac{1}{2} [\bar{\nu}_L i\not{\partial}\nu_L - m\bar{\nu}_L^C\nu_L] + h.c., \quad (3.40)$$

where the kinetic part is as in the Dirac case, while the mass term has a different form. In the Dirac case the family lepton number is violated by the Lagrangian properties, but the total lepton number is conserved; in the Majorana case, instead, the mass term would produce processes where $\Delta L = \pm 2$. Inside the Majorana framework is not possible to generate a mass with a Higgs triplet, as done for the charged leptons, however, using two Higgs doublets, one can build an interacting Lagrangian [173]:

$$\mathcal{L} = \frac{g}{\mathcal{M}} (L_L^T \sigma_2 \phi) \mathcal{C}^\dagger (\phi^T \sigma_2 L_L) + h.c., \quad (3.41)$$

where σ_i are the Pauli matrices. Since this term is not renormalizable, adding it in the SM translates into a reevaluation of the entire model as a low-energy effective field theory, as the β decay is for the electroweak theory. At high energy $T > \mathcal{M}$ physical particles are real, while at low energy $T < \mathcal{M}$ they contribute only as virtual mediators, such as W^\pm in the *beta* decay at the MeV scale. From Eq.(3.43), spontaneous symmetry breaking implies a mass term:

$$\mathcal{L}_{\text{mass}}^M = \frac{1}{2} \left(\frac{gv^2}{\mathcal{M}} \right) \nu_L^T \mathcal{C}^\dagger \nu_L + h.c., \quad (3.42)$$

the Higgs VEV provides a usual Dirac mass scale (m_D), while the \mathcal{M} can justify the tiny neutrino mass:

$$m_\nu \simeq \frac{m_D^2}{\mathcal{M}}. \quad (3.43)$$

This one family toy model becomes relatively more complicated in a 3 neutrinos mixing, differently from the Dirac case (see [88] for an extended treatment), the U^M matrix

shows 3 phases that cannot be absorbed as in the Dirac case, hence we get:

$$U^M = U^D \times D^M, \quad (3.44)$$

where U^D is defined in Eq.(3.30) and

$$D^M = \text{diag} \left(1, e^{i\lambda_2}, e^{i\lambda_3} \right), \quad (3.45)$$

where λ_2 and λ_3 are the Majorana phases. Discerning between the two pictures is quite hard: in case of massless neutrinos, Dirac and Majorana pictures are indistinguishable, even if they are massive the kinematical effect of the mass and the oscillation pattern are the same in both pictures. The visible effects could be visible in lepton number violation experiments such as $0\nu\beta\beta$, see Sec.(3.3.2).

3.2.5 Dirac-Majorana neutrinos

We have given a brief description of massive neutrinos in the SM both in the Dirac and Majorana case, however it is possible to have a Dirac-Majorana mixed model: in addition to 3 left-handed neutrinos there are N_s sterile right handed neutrinos fields that do not participate to weak interactions. This description, considered the most natural way to explain the tiny mass of neutrinos was presented in 1977 by Minkowsky and later (1979) by Yanagida [176], Gell-Mann [84] and by Schechter and Valle [159]; it provides an smart mass generation mechanism called *Seesaw mechanism*. There are three types of seesaw models:

Type I seesaw The first type requires the introduction of right-handed singlets ν_{sR} (here s -subscript is the number of sterile flavour eigenstates) in order to write the Dirac mass Lagrangian density in the following form:

$$\mathcal{L}_{\text{mass}}^D = -\bar{\nu}_R^s M_{s\alpha}^D \nu_L^\alpha + h.c., \quad (3.46)$$

where $M_{s\alpha}^D$ is a $N_s \times 3$ complex matrix. In this picture we can also consider a Majorana mass term in the Lagrangian density, this is a pure right-hand side term:

$$\mathcal{L}_{\text{mass}}^R = \frac{1}{2} \nu_R^{sT} C^\dagger M_{ss'}^R \nu_R^{s'} + h.c., \quad (3.47)$$

with $M_{ss'}^R$ is a $N_s \times N_s$ complex matrix. If both the terms are present the $D + M$ mass matrix is:

$$M^{D+M} \equiv \begin{pmatrix} 0 & M^{DT} \\ M^D & M^R \end{pmatrix}, \quad (3.48)$$

this matrix can be diagonalized using a procedure similar to Eq.(3.15) , in order to provide a diagonal matrix having the following form:

$$M'^{D+M} = \begin{pmatrix} M'_{\text{light}} & 0 \\ 0 & M'_{\text{heavy}} \end{pmatrix}, \quad (3.49)$$

where $M'_{\text{light}} \sim -M^{D^T} (1/M^R) M^D$ and $M'_{\text{heavy}} \sim M^R$. Passing through another diagonalization via the unitary matrices V'_L and V'_R it is possible to write the light and heavy neutrino masses in a more simple way:

$$m_{\text{light}} \sim \frac{(m^D)^2}{m^R}, \quad m_{\text{heavy}} \sim m^R. \quad (3.50)$$

There are two other type of seesaw mechanism: type II generates neutrino masses via exchange of $SU(2)_L$ -triplet scalar [130, 139, 159, 174] and type III uses a $SU(2)_L$ -triplet fermions [74, 128, 129].

3.2.6 Flavour oscillations in vacuum

Due to the small mass differences, see Tab.(3.2), and to the fact that they are produced in charged currents interactions, basically neutrino mass and flavour eigenstates are not coincident, neutrinos undergo a quantum mechanical phenomenon called *flavour oscillations*. The theory of neutrino oscillations in the plane-wave approximation was developed in 1976 by Eliezer and Swift [68] on the original idea of B. Pontecorvo, it is based on the statement that a flavour state can be written as a linear combination:

$$|\nu_\alpha\rangle = \sum_k U_{\alpha k}^* |\nu_k\rangle. \quad (3.51)$$

The lepton charged current Eq.(3.8) generates a superposition of mass eigenstates if the measurements of the momenta and energies are not accurate enough, the mixing is described by the matrix $U_{\alpha k}^*$. Massive neutrinos states are eigenvalues of the free-particle Hamiltonian,

$$\mathcal{H}|\nu_k\rangle = E_k|\nu_k\rangle, \quad (3.52)$$

and the time evolution of the plane wave is given by the Schroedinger equation,

$$i \frac{d}{dt} |\nu_k(t)\rangle = \mathcal{H}|\nu_k(t)\rangle, \quad (3.53)$$

which implies:

$$|\nu_k(t)\rangle = e^{-iE_k t} |\nu_k\rangle. \quad (3.54)$$

Eqs.(3.51 and 3.54) lead to a pure flavour equation having the following form:

$$|\nu_\alpha(t)\rangle = \sum_{\beta=e,\mu,\tau} \left(\sum_k U_{\alpha k}^* e^{-iE_k t} U_{\beta k} \right) |\nu_\beta\rangle, \quad (3.55)$$

and, thus, the probability of having a $\nu_\alpha \rightarrow \nu_\beta$ oscillation is the squared average of the transition amplitude:

$$P_{\nu_\alpha \rightarrow \nu_\beta}(t) = |\langle \nu_\beta | \nu_\alpha(t) \rangle|^2 = \sum_{kj} U_{\alpha k}^* U_{\beta k} U_{\alpha j} U_{\beta j}^* e^{-i(E_k - E_j)t}. \quad (3.56)$$

Since the difference between the energies of the k and j states can be written in function of the squared mass difference,

$$E_k - E_j = E + \frac{m_k^2}{2E} - E - \frac{m_j^2}{2E} \quad (3.57)$$

$$\simeq \frac{\Delta m_{kj}^2}{2E}, \quad (3.58)$$

it is clear that the probability of oscillations, Eq.(3.56), depends only on the mixing angles and the mass differences and time, however since the time is not measured in a oscillation experiment, we can approximate it with the distance L between the source and the detector (in the ultrarelativistic case neutrinos propagate with the speed of light), leading to:

$$P_{\nu_\alpha \rightarrow \nu_\beta}(E, L) = \sum_{kj} U_{\alpha k}^* U_{\beta k} U_{\alpha j} U_{\beta j}^* e^{-i \frac{\Delta m_{kj}^2}{2|\vec{p}|} L}. \quad (3.59)$$

Notice that the combination of mixing matrices does not change neither in the Dirac nor in the Majorana model, since the phases are destroyed within the quadratic form. Finally, Eq.(3.59) has the same form also in the antineutrino case with the related operation on the complex matrices U due to charge conjugation transformation.

3.2.7 Flavour oscillations in matter

Since the propagation and the distance travelled of are crucial in the oscillation process, the existence of a medium in which neutrinos propagate may change the situation. Let us consider the charged current, Eq.(3.22), it is possible to derive the related Hamiltonian:

$$\mathcal{H}_{\text{eff}}^{CC} = \frac{G_F}{\sqrt{2}} [\bar{\nu}_e \gamma^\mu (1 - \gamma_5) \nu_e] [\bar{e} \gamma_\mu (1 - \gamma_5) e], \quad (3.60)$$

if we, now, consider a gas of electrons and all their properties: density, energy density and energy distribution ($n_e, \rho_e, f(E_e)$), it is possible to find an effective potential

associated to the charged current (see [88, 119] for details),

$$V_{CC} = \sqrt{2}G_F n_e. \quad (3.61)$$

It is possible to perform the same procedure with the neutral current part of the Lagrangian, Eq.(3.22), considering a generic fermion f and the vectorial and axial fermion couplings g_V^f, g_A^f :

$$\mathcal{H}_{\text{eff}}^{CC} = \frac{G_F}{\sqrt{2}} [\bar{\nu}_\alpha \gamma^\mu (1 - \gamma_5) \nu_\alpha] \sum_f \left[\bar{f} \gamma_\mu (g_V^f - g_A^f \gamma_5) f \right], \quad (3.62)$$

obtaining a neutral-current potential:

$$V_{NC} = -\frac{G_F}{\sqrt{2}} n_n, \quad (3.63)$$

where n_n is the number density of neutrons. Putting together the contribution of V_{CC} for electron neutrinos and of V_{NC} for the other kind of neutrinos the potential for a generic α eigenstate is:

$$V_\alpha = V_{CC} \delta_{e\alpha} + V_{NC} = \sqrt{2}G_F \left(n_e \delta_{e\alpha} - \frac{1}{2} n_n \right), \quad (3.64)$$

Hence, the Schroedinger equation becomes:

$$i \frac{d}{dt} |\nu_\alpha(t)\rangle = (\mathcal{H}_0 + \mathcal{H}_1) |\nu_\alpha(t)\rangle, \quad (3.65)$$

where \mathcal{H}_1 is the perturbation due to the potential V_α , while \mathcal{H}_0 is the unperturbed Hamiltonian. In analogy with Eq.(3.56) we can write the Schroedinger equation for the amplitude of the $\nu_\alpha \rightarrow \nu_\beta$ oscillation:

$$i \frac{d}{dx} \langle \nu_\beta | \nu_\alpha(x) \rangle = \sum_\eta \left(\sum_k U_{\beta k} \frac{\Delta m_{k1}^2}{2E} U_{\eta k}^* + \delta_{\beta e} \delta_{\eta e} V_{CC} \right) \langle \nu_\eta | \nu_\alpha(x) \rangle, \quad (3.66)$$

with η is a subscript dummy index running on the flavour eigenstates and x is the distance parameter that approximates time t in analogy to what done for the oscillations in vacuum. The latter equation shows that neutrino oscillations in matter depends on the differences of the squared neutrino masses and on the mixing angles as the vacuum oscillations. Moreover, Eq.(3.66) can be rewritten in a matrix form,

$$i \frac{d}{dx} \Psi_\alpha = \mathbf{H}_F \Psi_\alpha, \quad (3.67)$$

where $\mathbb{H}_F = 1/2E (UM^2U^\dagger + \mathbf{A})$ is the Hamiltonian matrix in the flavour basis and Ψ_α is the wave function matrix, \mathbf{M} is the mass matrix and \mathbf{A} is the charged current contribution:

$$\Psi_\alpha = \begin{pmatrix} \psi_{\alpha e} \\ \psi_{\alpha \mu} \\ \psi_{\alpha \tau} \end{pmatrix}, \quad \mathbf{M}^2 = \begin{pmatrix} 0 & 0 & 0 \\ 0 & \Delta m_{21}^2 & 0 \\ 0 & 0 & \Delta m_{31}^2 \end{pmatrix}, \quad \mathbf{A} = \begin{pmatrix} 2EV_{CC} & 0 & 0 \\ 0 & 0 & 0 \\ 0 & 0 & 0 \end{pmatrix} \quad (3.68)$$

The same observation done in the previous section on the differences between Majorana and Dirac pictures are valid for flavour oscillations in matter, i.e. there is no way to discern between the two natures just looking at oscillation observations.

The MSW effect

We will see some details of neutrino flavour oscillations in matter: lest us consider a two component model $\nu_e - \nu_\mu$ and the corresponding mass eigenstates $\nu_1 - \nu_2$. This case is identical to the $\nu_e - \nu_\tau$ and it can describe accurately also the case of active-sterile neutrino oscillation simply replacing V_{CC} with $V_{CC} + V_{NC}$. The flavour Hamiltonian reduces to a 2×2 matrix:

$$\mathbb{H}_F = \frac{1}{4E} \begin{pmatrix} -\Delta m^2 \cos 2\theta + 2EV_{CC} & \Delta m^2 \sin 2\theta \\ \Delta m^2 \sin 2\theta & \Delta m^2 \cos 2\theta - 2EV_{CC} \end{pmatrix}. \quad (3.69)$$

The flavour mixing follows the rule:

$$|\nu_e\rangle = \cos \theta |\nu_1\rangle + \sin \theta |\nu_2\rangle \quad (3.70)$$

$$|\nu_\mu\rangle = -\sin \theta |\nu_1\rangle + \cos \theta |\nu_2\rangle. \quad (3.71)$$

As a standard procedure, it is possible to diagonalize via an orthonormal transformation $\mathcal{O}(\theta_M)$; at the end of the day the mixing angle in matter results:

$$\tan 2\theta_M = \tan 2\theta \left[1 - \frac{2EV_{CC}}{\Delta m^2 \cos 2\theta} \right]^{-1}. \quad (3.72)$$

The Schroedinger equation, Eq.(3.67) with the Hamiltonian shown in Eq.(3.69) describe a resonance for:

$$\Delta m^2 \cos 2\theta = 2EV_{CC}, \quad (3.73)$$

and considering the expression for the charged current potential in Eq.(3.61) we get:

$$n_e^{res} = \frac{\Delta m^2 \cos 2\theta}{2\sqrt{2}G_F E}. \quad (3.74)$$

This resonance is called Mikheev-Smirnov-Wolfenstein (MSW) effect [134, 175] and it becomes relevant when the free electron density overcomes certain values, such as in stars (it describes the conversion mechanism that solve the solar neutrino problem), supernovae or primordial universe. In matter the value of V_{CC} is positive, thus neutrino flavour oscillations can encounter a resonance only for values of $\theta_M < \pi/4$, the largest transition happens when $\theta_M = \pi/4$, that is different from the behaviour of oscillations in vacuum. In conditions of constant density of the matter medium $d\theta_M/dx = 0$ the transition probability, Eq.(3.56) can be written is the following way:

$$P_{\nu_e \rightarrow \nu_\mu}(L) = \sin^2 2\theta_M \sin^2 \left(\frac{\Delta m_M^2 L}{4E} \right), \quad (3.75)$$

with the oscillation length in matter,

$$L_M^{\text{osc}} = \frac{4\pi E}{\Delta m_M^2} \quad (3.76)$$

3.3 Neutrino experiments

The search of neutrino properties is one of the most florid research field in physics. Before moving to the cosmological aspects, let us present very briefly the current situation for the oscillation and mass parameters.

3.3.1 Oscillation experiments

The main channel for neutrinos oscillations measurements is the observation of a neutrino flux coming from a known source. In case of presence of flavours which are not originated by the source we will notice an *appearance*, the other way around, in case of depletion of neutrinos of a particular flavour we will talk of *disappearance*. As we have shown in the previous sections, the fundamental parameter for the observation of flavour oscillation are the distance that neutrinos cover from the source to the detector and the neutrino energy, assuming a monocromatic neutrino energy distribution (see Eqs.(3.59 and 3.75) for details). Oscillations experiments use three main sources of neutrinos and antineutrinos: nuclear reactors where processes like the β -decay of uranium and thorium generate a neutrino flux peaked at the MeV, solar/atmospheric neutrinos and high energy neutrinos produced in accelerator experiments. In order to classify these experiments the usual parameter used is $\Delta m^2 L/(2E)$, in particular distances of the order of ~ 10 m are called Short Base Line (SBL), moving to distances of ~ 1 km translates into Long Base Line (LBL) experiments and finally Very Long Base Line (VLBL) where the detector is placed at distances $\sim 10^2$ km. In recent years an increasing number of experiments have explored in details the oscillation “parameter

Neutrino experiments

Parameter	Hierarchy	best-fit	3σ
Δm_{21}^2 [10^{-5} eV ²]	/	7.56 ± 0.19	$7.05 \div 8.14$
$ \Delta m^2 $ [10^{-3} eV ²]	NH	2.55 ± 0.04	$2.43 \div 2.67$
	IH	2.49 ± 0.04	$2.37 \div 2.61$
$\sin^2 \theta_{12}$	/	$0.321^{+0.018}_{-0.016}$	$0.273 \div 0.379$
$\sin^2 \theta_{23}$	NH	$0.430^{+0.02}_{-0.018}$	$0.384 \div 0.635$
	IH	$0.596^{+0.017}_{-0.018}$	$0.388 \div 0.638$
$\sin^2 \theta_{13}$	NH	$0.02155^{+0.0090}_{-0.0075}$	$0.0189 \div 0.0239$
	IH	$0.02140^{+0.0082}_{-0.0085}$	$0.0189 \div 0.0239$
δ/π	NH	$1.40^{+0.31}_{-0.20}$	$0.00 \div 2.00$
	IH	$1.44^{+0.26}_{-0.23}$	$0.00 \div 0.17$ & $0.79 \div 2.00$

Table 3.2: In this table we show the best-fit and the 3σ allowed values for the 3-neutrino oscillation model. $\Delta m^2 = m_3^2 - (m_2^2 + m_1^2)/2$ can be positive or negative depending on the hierarchy considered. Normal hierarchy (NH) means that $m_1 < m_2 < m_3$, while inverted hierarchy (IH) corresponds to $m_3 < m_1 < m_2$. For the CP phase δ the 99% CL values are disfavoured, thus we report the 2σ region. [56]

space", LSND experiment [48, 126] reports evidence of $\bar{\nu}_\mu \rightarrow \bar{\nu}_e$ oscillation, the same effect has been searched by the MiniBooNE experiment [15, 149]. SAGE and GALLEX look at radioactive sources suggesting for a ν_e disappearance: the famous "Gallium anomaly". The SNO experiment [38] performed in Canada detects solar neutrinos through charged and neutral current channels $\nu_e + d \rightarrow e^- + p + p$ and $\nu_x + d \rightarrow \nu_x + p + n$ and neutrino electron elastic scattering $\nu_x + e \rightarrow \nu_x + e$ respectively. The KamLAND reactor neutrino experiment [66], located in Kamioka mine in Japan observed the process $\bar{\nu}_e + p \rightarrow e^+ + n$, while Super-Kamikande [76] observes neutrino oscillations looking at the muons and electron produced via neutrino-nucleus scattering. The results of the many observations of neutrino oscillations have produced the knowledge reported in Tab.(3.2) which contains the most recent values for the oscillations parameters both for normal and inverted hierarchy.

Oscillation in the sterile sector The population of experiments that aim to observe the neutrino flavour oscillations is extremely variegated and this is not the right place

for a detailed overview, thus let us focus on a topic useful for the purpose of this thesis. On the most interesting hint of new physics coming from these experiments is the existence of sterile neutrino eigenstates able to explain the appearance and disappearance evidences. As well presented in [112] ν_e and $\bar{\nu}_e$ (ν_μ and $\bar{\nu}_\mu$) disappearance as $\nu_\mu \rightarrow \nu_e$

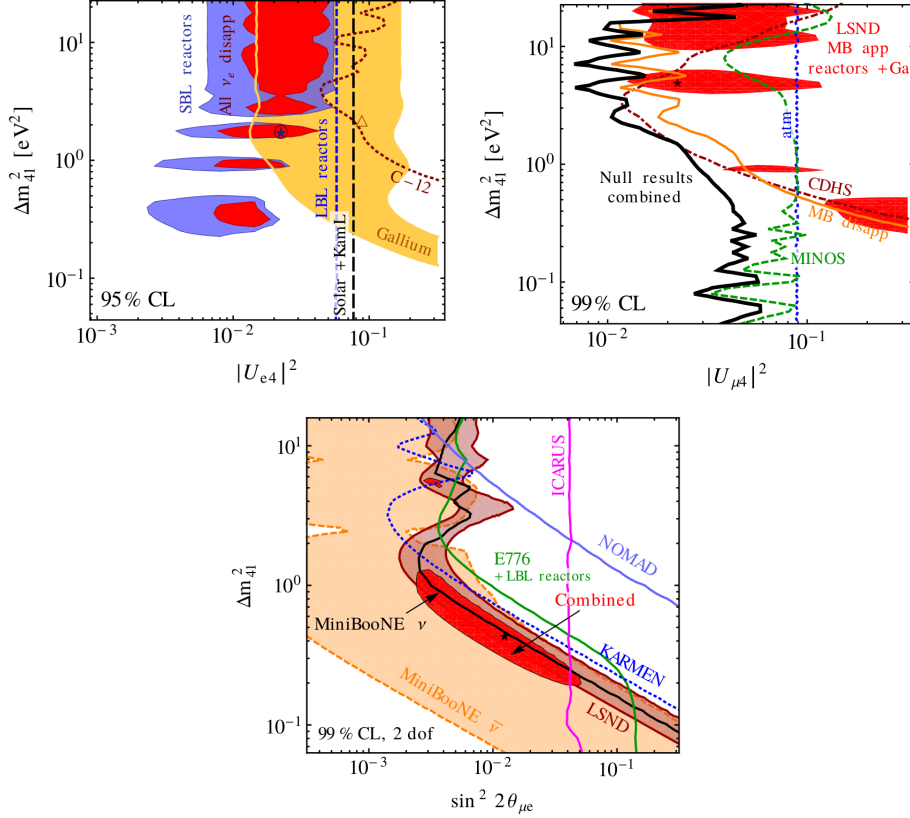


Figure 3.2: Allowed regions of oscillation parameter for the SBL suggested 3 + 1 model, in order of appearance: ν_e ($\bar{\nu}_e$) disappearance, ν_μ ($\bar{\nu}_\mu$) disappearance and $\nu_\mu \rightarrow \nu_e$ ($\bar{\nu}_\mu \rightarrow \bar{\nu}_e$) appearance (See [112] for details).

($\bar{\nu}_\mu \rightarrow \bar{\nu}_e$) appearance can be solved extending the standard neutrino model, which counts 3 neutrino eigenstates, to some 3 + 1 or 3 + 2 model. Let us consider the SBL case, introducing a fourth sterile eigenstate it is possible to write the survival probability

for the channels described in the previous lines in this way:

$$P_{ee}^{\text{SBL}} = 1 - 4 |U_{e4}|^2 \left(1 - |U_{e4}|^2 \right) \sin^2 \frac{\Delta m_{41}^2 L}{4E}, \quad (3.77)$$

$$P_{\mu\mu}^{\text{SBL}} = 1 - 4 |U_{\mu4}|^2 \left(1 - |U_{\mu4}|^2 \right) \sin^2 \frac{\Delta m_{41}^2 L}{4E}, \quad (3.78)$$

$$P_{\nu_e \rightarrow \nu_\mu}^{\text{SBL}} = 4 |U_{e4} U_{\mu4}|^2 \sin^2 \frac{\Delta m_{41}^2 L}{4E}. \quad (3.79)$$

Every channel has its own mixing angle that can be measured:

$$\sin^2 2\theta_{ee} = 4 |U_{e4}|^2 \left(1 - |U_{e4}|^2 \right) \quad (3.80)$$

$$\sin^2 2\theta_{\mu\mu} = 4 |U_{\mu4}|^2 \left(1 - |U_{\mu4}|^2 \right) \quad (3.81)$$

$$\sin^2 2\theta_{\mu e} = 4 |U_{e4} U_{\mu4}|^2 \sin^2. \quad (3.82)$$

In Fig.(3.2) we show the fit obtained in Ref. [112] for the electron end muon neutrino disappearance and appearance. In the same work the authors performed also a dedicated analysis for the 3+2 model, however they do not find considerable differences between the two models. They conclude that, net of some tension in the datasets used, appearance and disappearance rises at the level of 10^{-4} compatible with an additional sterile eigenstate at the $\Delta m_{41}^2 \sim eV^2$ scale.

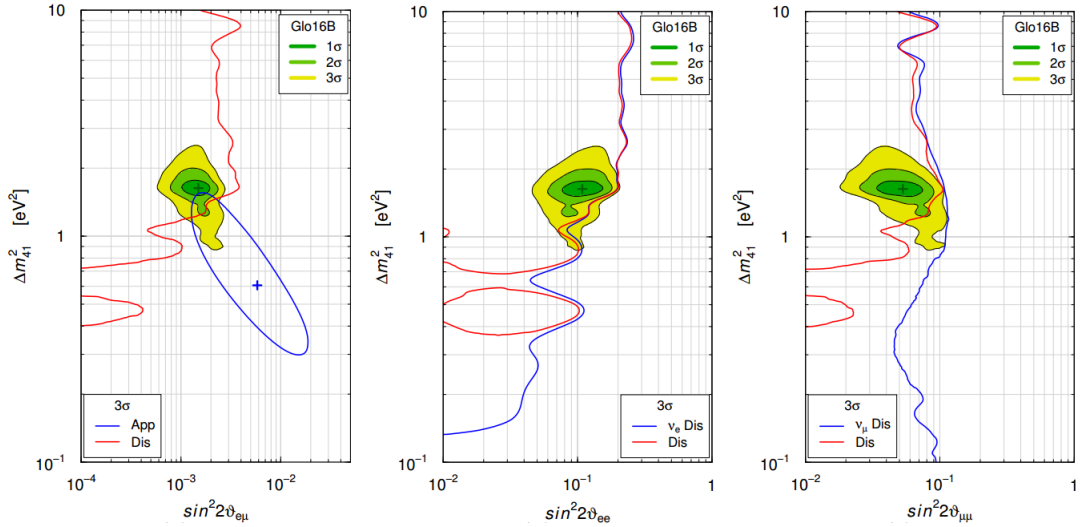


Figure 3.3: Allowed regions in the oscillation parameter space $\sin^2 2\theta_{ee}$, $\sin^2 2\theta_{\mu\mu}$, $\sin^2 2\theta_{e\mu}$ and Δm_{41}^2 . The best fit, is obtained for a 3 + 1 model.

A similar analysis has been performed in [80] where the authors have found similar results, see Fig.(3.3). In this framework one can set that the preferred values for an

additional sterile eigenstate are $\Delta m_{41}^2 \sim 1\text{eV}^2$ and $\sin^2 2\theta_{\alpha\beta} = 0.1 \div 0.001$.

3.3.2 Neutrino mass experiments

Neutrino masses can be measured by direct or indirect methods, the former are experiments that aim to measure the masses of neutrino eigenstates through observations of the single- β decay. Indeed the energy spectrum of β decay electrons provides a model independent channel for the absolute electron neutrino mass. It basically is an extremely precise measurement of the electron energy spectrum, see Fig.(3.4), which takes into account the neutrino mass. Spectral distortions near the endpoint energy of the emitted electron spectrum will be hint of non-zero neutrino mass. The β emitter chosen for this purpose, must have the lower possible Q -value, thus, the most used is the tritium ${}^3\text{H}$. The observable in this type of measurements is the effective mass of the electron neutrino:

$$m_e^2 = \sum_i |U_{ei}|^2 m_i^2, \quad (3.83)$$

where the subscript i runs over the flavour eigenstates. The last experiments have been performed by Mainz and Troitsk groups report the most stringent values for the electron neutrino mass of $m_{\nu_e} \leq 2.1\text{eV}$ (Troitsk) [125] and $m_{\nu_e} \leq 2.1\text{eV}$ (Mainz) [113]. The Karlsruhe Tritium Neutrino experiment (KATRIN) starts to take data in 2017 in order to achieve the impressive sensitivity of $m_e < 0.2\text{eV}$.

Regarding the indirect measurements, the neutrinoless double beta decay ($0\nu\beta\beta$) is the favourite channels for laboratory experiments. The $0\nu\beta\beta$ decay,

$$(Z, A) \rightarrow (Z - 2, A) + 2e^-, \quad (3.84)$$

violates lepton number, thus, it is an extension of the standard electroweak theory presented in Sec.(3.2). This existence of this process requires that neutrinos are Majorana particles. $0\nu\beta\beta$ decay is sensitive to the Majorana mass [159],

$$m_{ee}^2 = \left| \sum_i U_{ei}^2 m_i \right|^2, \quad (3.85)$$

which, is dependent on the Majorana phases, Eq.(3.45)². Fig.(3.5) shows a schematic representation of the spectrum distortion due to the possible presence of $0\nu\beta\beta$ decay. Searches of $0\nu\beta\beta$ spreads over a large variety of different techniques that make use of several isotopes. We report the results of Cuoricino (${}^{130}\text{Te}$) $m_{ee} < [0.2, 0.7], \text{eV}$ [25], IGEX (${}^{100}\text{Mo}$) $m_{ee} < [0.33, 1.35] \text{eV}$ [1]. The future for this kind of laboratory experiments is the sensitivity improvements. It requires progress in background reduction as well as increase the target masses. For example, the GERmanium Detector Array (GERDA) [40]

²Notice that in some references the Majorana mass m_{ee} can be written as $m_{\beta\beta}$

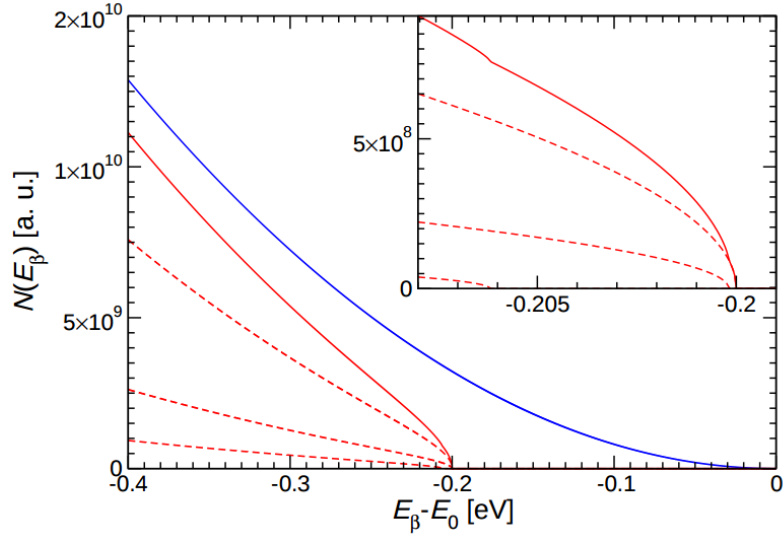


Figure 3.4: Simulated electron spectrum in case of massless neutrinos (blue solid line) and in presence of $m_{\nu e} = 200$ meV. The red dashed curves correspond to the contributions of the three mass states, using the values of mass oscillations in Tab.(3.2). [140]

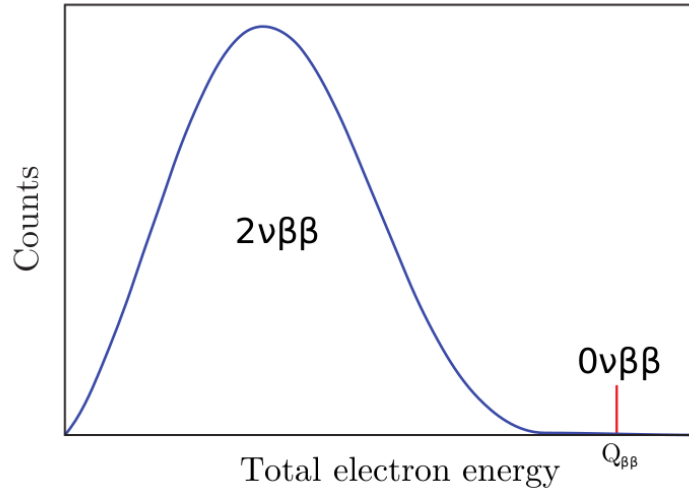


Figure 3.5: Schematic picture of the spectral distortion in emitted electron energy spectrum in case of $0\nu\beta\beta$ decay.

in Phase2 and Phase3 and the Cryogenic Underground Observatory for Rare Events (CUORE) [91] started to take data in 2017. The attended sensitivity is in the meV range, $m_{ee} < [90, 200]$ meV (GERDA) and $m_{ee} < [30]$ meV (CUORE). In order to have

a complete overview of the variety of experiments and a detailed review of the results see Ref. [58].

3.4 Neutrino Cosmology

In the following sections we are going to focus on the implications that neutrinos have on the cosmological evolution. As we have seen in Ch.(1) and in particular in Sec.(1.3), neutrinos impact considerably on the universe evolution: they decoupled from the primordial plasma once $\Gamma_\nu < H$ and this impacts on the light elements abundances due to BBN processes. Including three active neutrino families (as in the standard model of particles) the matter-radiation balance changes leading (we will show it) to contributions on the CMB APS. Let us summarize very briefly the main quantities for standard neutrinos in Tab.(3.3). The main parameters that can be added to the

Cross section	$\sigma_w \sim G_F^2 T^2$	
Decoupling temperature	$T_\nu(z_{\text{dec}}) \sim 0.8 \text{ MeV}$	
Equilibrium distribution	$f(p, t) = (e^{p/T_\nu} + 1)^{-1}$	
Temperature	$T_\nu = \left(\frac{4}{11}\right)^{1/3} T_\gamma$	
Present density parameter	$\Omega_\nu = \frac{\sum m_\nu}{93.14 \text{ eV}}$	
	Relativistic	Non relativistic
Number density	$n_\nu = \frac{3}{4\pi^2} g \zeta(3) T_\nu^3$	$n_\nu = g \left(\frac{m_\nu T_\nu}{2\pi}\right)^{3/2} e^{-\frac{m}{T_\nu}}$
Energy density	$\rho_\nu = \left[\frac{7}{8} \left(\frac{4}{11}\right)^{4/3} N_{\text{eff}}\right] \rho_\gamma$	$\rho_\nu = m_\nu n_\nu$

Table 3.3: Main properties for standard cosmological neutrinos.

standard cosmological model in order to study neutrino properties are the sum of the masses $\sum m_\nu$ and the effective number of neutrino families N_{eff} .³ We can distinguish into two cases, the massless and the massive case in which we take into account also the sum of the neutrino masses.

³Notice that N_{eff} is defined as the effective number of extra relativistic species i.e. relativistic particles that are not photons, however considering the standard particle zoology, the only candidates are neutrinos. This is no longer valid in case of extended pictures that introduces other massless or very light particles to the primordial fluid e.g. axions.)

3.4.1 Massless neutrinos effects

We presented the Boltzmann hierarchy and the whole theory in Sec.(1.4.1), in this case the fluid equations, Eq.(1.126) affect the universe evolution changing directly the Einstein equations through just one parameter N_{eff} . $N_{\text{eff}} = 3.046$ corresponds to the standard model prediction, while increasing it adding some extra contribution ΔN_{eff} translates into deviations from the standard case, such as the introduction of non-standard massless or light components as well as the presence of non-zero chemical potential or low-reheating scenarios which can also lead to negative ΔN_{eff} . In order to study the different effect of including a neutrino contribution we add the effective number of neutrino families to the base six-parameter model i.e. the parameter space will be $(\Omega_b h^2, \Omega_c h^2, \tau_{\text{rei}}, \ln(10^{10} A_s), n_s, 100\theta_{\text{MC}}, N_{\text{eff}})$. We have investigated the effect of cosmological parameters on the power spectra in Ch.(2), however, in that case, we showed a naive approach to the problem. Let us consider $N_{\text{eff}} = 3.046$, this value increases the radiation energy density and, consequently, it has an impact on the redshift of matter-radiation equality:

$$1 + z_{\text{eq}} = \frac{\Omega_m}{\Omega_\gamma \left(1 + \frac{7}{8} \left(\frac{4}{11}\right)^{\frac{4}{3}} N_{\text{eff}}\right)} = \frac{\omega_c + \omega_b}{\omega_\gamma \left(1 + \frac{7}{8} \left(\frac{4}{11}\right)^{\frac{4}{3}} N_{\text{eff}}\right)}, \quad (3.86)$$

where $\omega_i \equiv \Omega_i h^2$. This has a great impact on evolution of the universe and on the cosmological observables: if we increase the number of neutrino families, we are increasing the relativistic content and, thus, we are decreasing the photon mean free path, Eq.(2.69). A smaller λ_{MFP} , in principle, would lead to less damping in the APS, however, at the same time, a larger relativistic energy density moves the last scattering surface away from the observer. This basically changes the ratio between the diffusion scale and the angular-diameter distance to the last scattering surface and, simultaneously, the ratio between the sound horizon and the angular-diameter distance to the last scattering surface. In practice, we have less damping in the APS tail, but all the peaks are shifted to higher multipoles. We can summarize the effects of massless neutrinos on the APS in the following way:

Background level:

- 1) Increase of N_{eff} leads to longer radiation dominated epoch, this leads to more early-integrated ISW and boost of the spectrum due to potential decay.
- 2) Adding energy density implies a greater Hubble expansion rate, this reduces the sound horizon (which is proportional to H^{-1}). Changing H means also a different diffusion length (see Eq.(2.69) for details). As said before the effect is to move the ℓ_{damping} relative to the first peak position enhancing the Silk damping effect.

Perturbation level:

- 3) For free-streaming neutrinos we expect metric fluctuations smaller for wavelengths inside the free-streaming scale, which for relativistic neutrinos is equal to the Hubble radius, due to the fact that neutrinos do not cluster on those scales. In the radiation dominated epoch this is a large effect since neutrinos account for a large part of the total density, this leads to a reduction of the metric fluctuations on that scales and it reduces the boosting of temperature fluctuations in the scales that enter the sound horizon before the recombination. The net effect is a reduction of the power of a factor $(\frac{4R_\nu}{15})^{-1}$ [104], where $R_\nu = \bar{\rho}_\nu / (\bar{\rho}_\gamma + \bar{\rho}_\nu)$.
- 4) Viscosity produce an effect on the phase of the APS producing a shift in the positions of the peaks [29].

Increasing the effective neutrino number enhance the density by a factor:

$$\alpha \equiv (1 + 0.2271N_{\text{eff}}) , \quad (3.87)$$

this leads to the effects described previously. We can compensate the increased amount of relativistic content by increasing the matter density of an equal amount.

$$\Omega'_m h^2 = \Omega_m h^2 \times \alpha . \quad (3.88)$$

Notice that $\Omega_b h^2$ and should be kept constant in order to not effect the APS with additional baryon loading. The reduced Hubble parameter, assuming a flat Universe, is $h = \sqrt{\omega_m / (1 - \Omega_\Lambda)}$, thus, it is affected by a $\sqrt{\alpha}$ factor,

$$h' = h \times \sqrt{\alpha} . \quad (3.89)$$

In Fig.(3.6) we show the temperature APS for two different values of N_{eff} , the purple line represents the standard case with $N_{\text{eff}} = 3.046$ in all the figures. Starting from the top left panel, we show the APS for $N_{\text{eff}} = 5$ in red, in orange the same APS corrected taking into account the additional amount of matter in order to preserve z_{eq} , Eq.(3.88). In the bottom left panel we correct also the impact of the ‘‘additional’’ massless neutrinos on the Hubble parameter H_0 , Eq.(3.89), finally in blue we show the APS corrected for the drop of the scalar amplitude A_s , Eq.(3.90). The residuals between the two cases presented in Fig.(3.6) is due to effects that comes from the perturbations. Since gravitational potentials at a given scale quickly decay once that mode crosses the horizon, the behaviour of the Boltzmann hierarchy is extremely important. In particular, since neutrinos show a viscosity term in the fluid hierarchy, it contributes damping the scales that are smaller than the neutrino free-streaming length. Mapping the effect on the APS the presence of a massless neutrino fluid gives a contribution

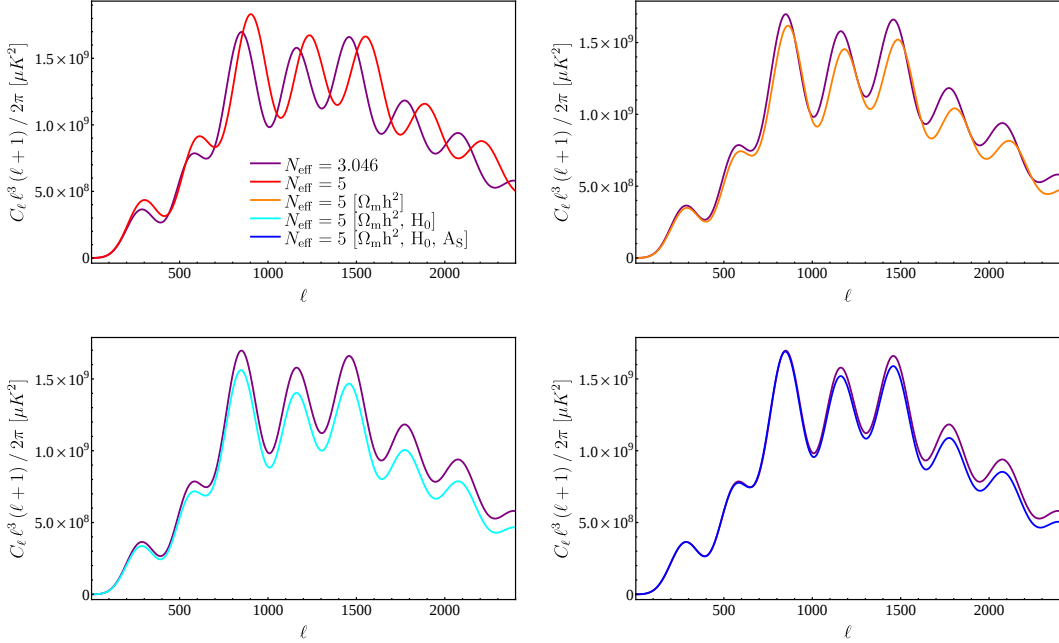


Figure 3.6: Temperature anisotropies power spectrum $\ell^3(\ell+1)C_\ell/2\pi$ for two different values of N_{eff} . Purple solid line correspond, in every panel, to the $N_{\text{eff}} = 3.046$ case, while the other coloured line represents the case with $N_{\text{eff}} = 5$. In each figure starting from the top-left to the bottom-right we add a correction in order to put in evidence the effects of the neutrino fluid on the statistical properties of the temperature anisotropies. In the top-left we are using the same six-base parameters varying only N_{eff} , in the top-right we consider the correction on the matter density. Moving to the bottom panel, in the left figure we correct for the Hubble parameter and in the last plot we rescale the amplitude

reducing the height of the peaks [104]:

$$\frac{\Delta C_\ell}{C_\ell} = \left(1 + \frac{4}{15}R_\nu\right)^{-2} = \left(1 + \frac{4}{15} \times \left(\frac{0.2271N_{\text{eff}}}{1 + 0.2271N_{\text{eff}}}\right)\right)^{-2}, \quad (3.90)$$

This is an analytical approximation of the real effect due to the presence of neutrino viscosity. Moreover the presence of a neutrino fluid, which propagates at the speed of light) tends to pull the photon fluid (which is limited to the sound speed c_s due to coupling with baryons). This impacts on the position of the peaks in the APS shifting the phase oscillation of a quantity,

$$\Delta\ell_{\text{peak}} = -\frac{d_{\text{hor}}(\tau_{\text{LS}})}{d_A(\tau_{\text{LS}})} (0.1912R_\nu + \mathcal{O}(R_\nu^2)). \quad (3.91)$$

Constraints from cosmology

Constraints (1σ CL) on the effective number of neutrino families can be found in Ref. [10] where adding N_{eff} to the six-parameter Λ CDM model space the following values are found:

$$N_{\text{eff}} = 3.13 \pm 0.32 \quad \text{Planck}_{15}\text{TT}, \quad (3.92)$$

$$N_{\text{eff}} = 3.15 \pm 0.23 \quad \text{Planck}_{15}\text{TT} + \text{BAO}, \quad (3.93)$$

$$N_{\text{eff}} = 2.99 \pm 0.20 \quad \text{Planck}_{15}\text{TP}, \quad (3.94)$$

$$N_{\text{eff}} = 3.04 \pm 0.18 \quad \text{Planck}_{15}\text{TP} + \text{BAO}, \quad (3.95)$$

which are all in excellent agreement with the standard value. See Sec.(A) for the detail on the datasets. Note the significantly tighter constraint on N_{eff} using the high- ℓ polarization dataset. In this case a value of $\Delta N_{\text{eff}} \sim 1$ is excluded at 4σ .

3.4.2 Effects of massive neutrinos

Cosmological observations do not provide evidence of neutrino masses, and are therefore consistent with massless neutrinos, however, oscillations arose the picture of massive neutrinos which can be encoded inside the SCM using the sum of the three masses:

$$\sum m_\nu = m_1 + m_2 + m_3, \quad (3.96)$$

In case of massive neutrinos we have to deal, at least, with two parameters in order to describe the behaviour of the fluid: N_{eff} and $\Omega_\nu h^2$ (the total density of neutrinos today). As we have shown in Sec.(1.4.1), it is not possible to reduce the massive picture like we have done for the massless case, i.e. we have to consider the momentum dependence. The simplest approach is to consider 3 standard neutrinos having degenerate mass eigenstates and the same Fermi-Dirac distribution, which is a prediction of the model. In analogy to what we have done for the massless case, we divide the effects into background and perturbation effects.

Background: Knowing the cosmological bounds on the sum of neutrino masses ($\sum m_\nu < 0.22 \text{ eV}$ 95% CL [Planck₁₅TT + lowP + BAO + HST] [10]) we can assume $\sum m_\nu < 1 \text{ eV}$. For these values neutrino behave as relativistic particle well after the z_{eq} , this implies that the considerations made in the previous section in order to keep unchanged the matter radiation equality are still valid. Notice that also a lower value can be inferred from the knowledge of the existence of neutrino oscillations and, thus, difference of squared masses. In the hypothesis of direct hierarchy we can assume that $\sum m_\nu > 0.06 \text{ eV}$. As we have done in the massless case we can divide the impact of the mass into background and perturbation effects. Starting from the background effects, the existence of massive neutrinos introduce a new density parameter ω_ν that has to be

taken into account inside the Friedmann equation:

$$H^2(t) = H_0 \left[(\Omega_c + \Omega_b)(1+z)^3 + \Omega_\gamma(1+z)^4 + \Omega_\Lambda + \frac{\rho_\nu}{\rho_c} \right]. \quad (3.97)$$

Neutrinos behave like radiation until they are relativistic ($z > z_{\text{nr}}$), while contributes to the cold dark matter content when the temperature of the plasma falls down with respect to their mass ($z < z_{\text{nr}}$). Using the temperature relation in Tab.(3.3) it is possible to express the redshift at which neutrinos become non relativistic in function of their mass:

$$1 + z_{\text{nr}} \simeq 1900 \left(\frac{m_\nu}{\text{eV}} \right). \quad (3.98)$$

Let us consider two models: a reference model with three massless neutrino eigenstates (which in terms of the energy density counts $N_{\text{eff}} = 3.046$) and a massive model where we include the $\sum m_\nu$ as additional parameter for the same amount of neutrinos. In the limit of $\sum m_\nu \rightarrow 0$ and assuming a flat geometry, the two models reproduce the same Universe. Eq.(3.98) suggests important considerations: for $z \gg z_{\text{nr}}$ the former and the latter models are comparable, since the energy density in the neutrino sector is the same, see Tab.(3.3), and the changes in $\Omega_\Lambda h^2$ due to the presence of a $\Omega_\nu h^2$ components are negligible at these redshift values. The picture becomes different for $z \leq z_{\text{nr}}$, where the model with a higher value of the mass presents also a larger Hubble expansion and, thus, evolve more rapidly.

At this point the effect of neutrino masses can be seen from different point of views, because dealing with two parameters leads to a complicate scenario where are present several degenerations among the cosmological parameters. For example, taking $\omega_b + \omega_c$ constant on one hand ensures that the equality redshift does not change even in presence of massive neutrinos, on the other hand the angle subtended by the sound horizon at recombination θ_s becomes smaller with the increase of $\sum m_\nu$. This effect is basically due to the fact that increasing $\sum m_\nu$ the last scattering surface is receding from us.

Instead of keeping constant $\omega_c + \omega_b$ one can decide to fix h or Ω_Λ . This changes the expansion history: when neutrinos becomes non relativistic the expansion rate H is kept constant by the changes in the matter density indeed, while at higher redshift, when neutrino are ultrarelativistic and the universe is matter dominated, the matter content results larger with respect the massless reference model, changing $H(t)$. Finally, continuing to go back in time, when the Universe was in the radiation dominated regime, the two models describe again the same expansion history. Hence, modifying $\omega_c + \omega_b$ we are changing the expansion history in the range $z_{\text{nr}} < z < z_{\text{eq}}$, this increases the angular diameter distance to the last scattering at recombination shifting the peaks towards higher angular scales. Obviously, changing the matter content means also to have an impact on z_{eq} , equality happens at higher redshift with the increasing of $\sum m_\nu$. In order to change the matter density, it is possible to act on both ω_c and ω_b , the effect of changing one instead of the other is identical from the point of view of the

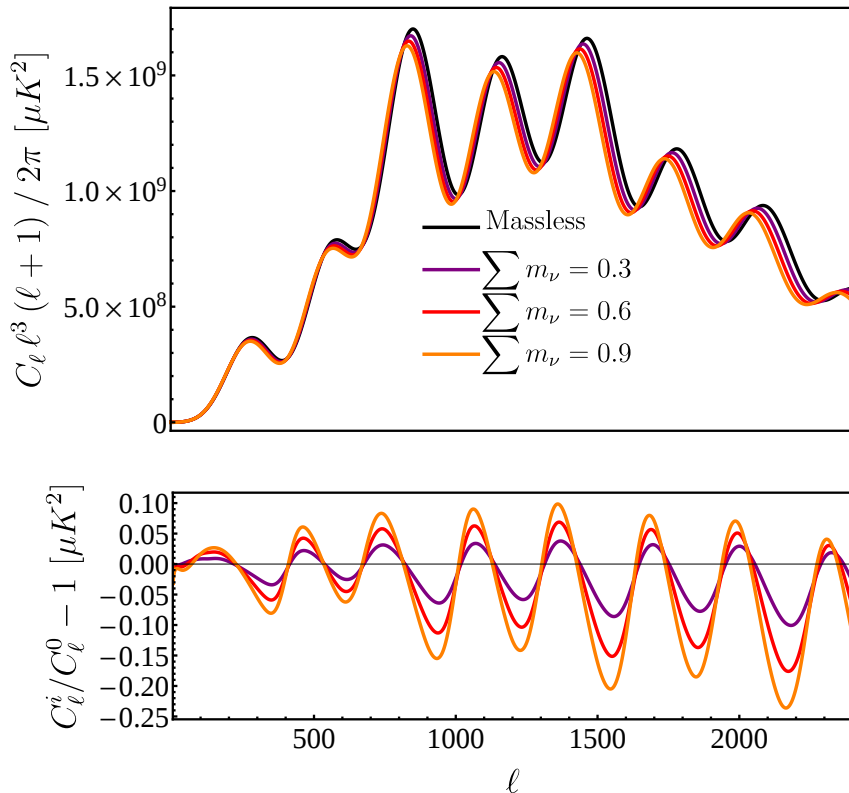


Figure 3.7: Temperature anisotropies power spectrum for the standard Λ CDM model with $N_{\text{eff}} = 3.046$ massless neutrinos (black line) and for the massive neutrino model. We show the power spectrum for three different values of the sum of neutrino masses $\sum m_\nu = 0.3, 0.6$ and 0.9 eV. In the lower panel of the figure we show the normalized ratio between the massive spectra and the standard massless using the same colour.

background evolution, however, as we have said in Sec.(2.2.2) baryons are coupled with photons and even a small changes in its abundance leads to a change in the baryon loading effect. Moreover baryon abundance is well constrained by BBN and observation of light elements. In Fig.(3.7) we show the effect of the mass on the CMB temperature APS. We compare three different mass cases with the correspondent massless model. In every case the effective number of neutrino families has been set at the standard value $N_{\text{eff}} = 3.046$. In order to produce the realization for the massive model we have kept constant the matter density $\omega_c + \omega_b$. In the lower panel it is evident the oscillatory pattern in the middle and high- ℓ region of the spectrum due to the shift of the peaks described above.

Perturbations: The presence of massive neutrino affect also the evolution of perturbations, since the neutrino fluid evolution is described by its own Boltzmann hierarchy, see Sec.(1.4.1). The peculiar effect is related to the characteristic free-stream scale of neutrinos: if neutrinos has a mass, when the transition between the relativistic and nonrelativistic regime happens, the neutrino clustering will be exponentially suppressed. The effect depends on the $\sum m_\nu$ parameter and, thus, on the age at which the transition takes place. In particular if neutrinos become nonrelativistic during the matter dominated era we can write the free-streaming scale as:

$$k_{\text{fs}} = 0.018 \Omega_m^{1/2} \left(\frac{m}{1 \text{ eV}} \right) h \text{Mpc}^{-1}. \quad (3.99)$$

On the other hand, scales larger than the free-streaming scales behaves like ordinary cold dark matter. At the end of the story, increasing the value of the neutrino mass leads to a suppression of the small-scales matter fluctuations.

In addition to this peculiar effect, the neutrino mass term basically changes the gravitational potential, which, in turn, impacts on the photon perturbations leading to modifications on the CMB APS. In particular photon perturbations are sensitive to time-variation of the potential, i.e. the effect is visible in the ISW contribution of the APS. However at the low- ℓ multipoles where the ISW effect is larger, we are limited by the cosmic variance.

Constraints from cosmology

Masses well below 1 eV have no time to change the shape of the CMB power spectra, since they became non-relativistic after recombination. As we said, the effect on the background cosmology can be compensated by changing h or $\omega_c + \omega_b$. However there is sensitivity of the CMB anisotropies to neutrino masses if these are not completely nonrelativistic at the last scattering surface, basically on the ISW effect. In addition to this, several astrophysical observation of "late" effects, such as lensing or baryon acoustic oscillations are suitable source of information. The most recent cosmological constraints (95% CL), expressed in eV, coming from Planck 2015 analysis [10] are:

$$\sum m_\nu < 0.72 \quad \text{Planck}_{15} \text{TT}, \quad (3.100)$$

$$\sum m_\nu < 0.21 \quad \text{Planck}_{15} \text{TT} + \text{BAO}, \quad (3.101)$$

$$\sum m_\nu < 0.68 \quad \text{Planck}_{15} \text{TT} + \text{lensing}, \quad (3.102)$$

$$\sum m_\nu < 0.49 \quad \text{Planck}_{15} \text{TP}, \quad (3.103)$$

$$\sum m_\nu < 0.17 \quad \text{Planck}_{15} \text{TP} + \text{BAO}, \quad (3.104)$$

$$\sum m_\nu < 0.59 \quad \text{Planck}_{15} \text{TP} + \text{lensing}. \quad (3.105)$$

In order to put in evidence the relation between the neutrino mass and the Hubble constant we show in Fig.(3.8) the two-dimensional Bayesian posterior. There is an evident correlation between the two parameters that leads to a reduction of the Hubble constant value with the increase of the sum of the neutrino masses. In addition the figure report also the value of σ_8 which is the matter fluctuation amplitude at $8h^{-1}\text{Mpc}$.

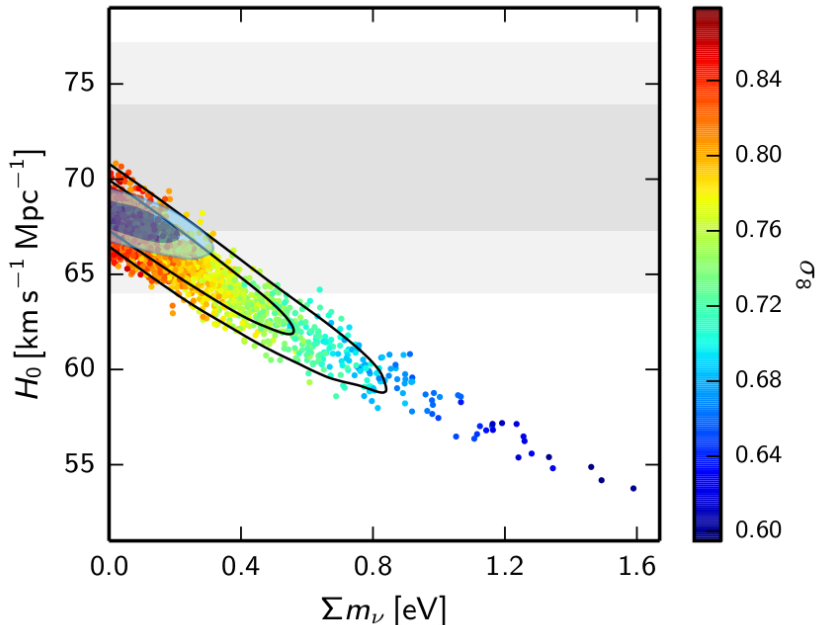


Figure 3.8: Posteriors in the Σm_ν - H_0 plane obtained using Planck₁₅TT data (solid black contours) and Planck₁₅TP (filled blue contours) [10]. The colour scale refers to the parameter σ_8 . The gray bands corresponds to the astrophysical measurements of H_0 from Ref. [65] ($H_0 = 70.6 \pm 3.3$).

3.4.3 Massive sterile neutrinos

Cosmological data, in particular CMB data, can provide constraints on both the number of neutrino families and the neutrino masses also in case of non standard pictures. Here we are going to consider, as we have shown in Sec.(3.3), the possible existence of light sterile neutrino eigenstates suggested by SBL anomalies. The behaviour that we have described for the active massive neutrinos can be applied also in the case of sterile neutrinos, since from a cosmological point of view they behave like radiation when the temperature of the fluid is larger than the mass, while they contribute to the cold dark matter sector when they become nonrelativistic. As explained in Ref. [10], the effective

mass of the sterile neutrino is defined as:

$$m_{\nu,\text{ster}}^{\text{eff}} = (93.14\Omega_{\nu,\text{ster}}h^2) \text{ eV}, \quad (3.106)$$

Aiming to constrain the case of no massive sterile neutrino we can write its mass following two distributions. For thermally distributed sterile neutrinos:

$$m_{\nu,\text{ster}}^{\text{eff}} = \left(\frac{T_s}{T_\nu}\right)^3 m_{\text{ster}}^{\text{ther}} = (\Delta N_{\text{eff}})^{3/4} m_{\text{ster}}^{\text{ther}}, \quad (3.107)$$

or in the Dodelson-Widrow (DW) case:

$$m_{\nu,\text{ster}}^{\text{eff}} = \chi_s m_{\text{ster}}^{\text{DW}} = \Delta N_{\text{eff}} m_{\text{ster}}^{\text{DW}}. \quad (3.108)$$

In Fig.(3.9) we show the results found by the Planck collaboration for the sterile neutrino

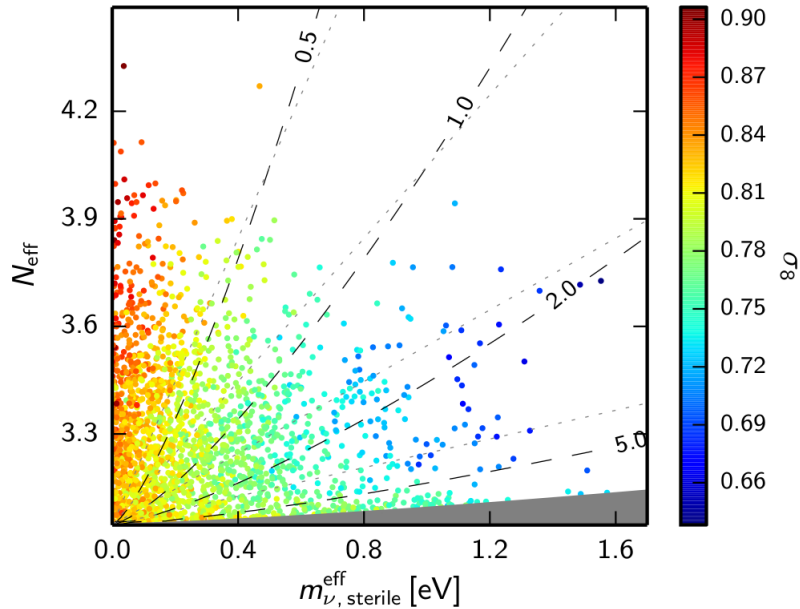


Figure 3.9: Two-dimensional posterior probability for the parameters $m_{\nu,\text{ster}}^{\text{eff}}$ and N_{eff} in the sterile neutrino model obtained using Planck₁₅TT. Gray dashed lines corresponds to the physical mass of the sterile neutrino in the thermal distribution, while the dotted line represent the DW case. Finally the gray region in the lower part of the plot is excluded by the prior used in the analysis. It represents the part of the parameter space in which neutrinos act as cold dark matter [10].

case. Although Planck is perfectly consistent with no massive sterile neutrinos, the

data allow a significant region of the $m_{\nu,\text{ster}}-N_{\text{eff}}$ parameter space. Moreover including a sterile eigenstates leads to a smaller value of σ_8 with respect to the value obtained in the base ΛCMD model. Using a single massive sterile neutrino the constraints are:

$$N_{\text{eff}} < 3.7, \tag{3.109}$$

$$m_{\nu,\text{ster}}^{\text{eff}} < 0.38 \text{ eV}, \tag{3.110}$$

at 95% CL.

4

(Pseudo)scalar interacting neutrinos

Based on [PoS NOW2016 (2017) 084 SISSA
(2017-01-26)] and mainly on [JCAP 1507 (2015)
no.07, 014]

In the previous section we have shown that cosmological observations are a powerful probe of neutrino physics. In the picture described so far, all the expectations are extremely well supported by available cosmological data. In the standard cosmological model (remember that N_{eff} is fixed to 3.046), the only free parameters in the *neutrino sector* of the model are the masses of the three eigenstates, both the absolute scale and the hierarchy of the masses remain unknown. Thanks to the simplicity of this model and to the goodness of data, we are allowed to keep an open mind and test more complicated scenarios for the neutrino sector. In this chapter, we will consider the possibility that neutrinos have interactions beyond the standard model of particle physics, for simplicity we shall call “hidden” or “secret” interactions, and study the constraining power of cosmological observations with respect to such a scenario. We will refer to secret interactions dividing them into two types: scalar or pseudo-scalar (Majoron-like in alternative) and Fermi-like. Argument of this chapter is the (pseudo)scalar interaction that behaves as described in 1.63 turning on again interactions in the neutrino sector at late time with respect to standard neutrino decoupling. As we have seen in Chapter 1, in a cosmological environment it is not possible to provide a unique formalism for massless and massive neutrinos, since in the latter case we have to deal with the momentum integration. However before presenting the work and the constraints we will describe how we treated the interactions.

4.1 (Pseudo)scalar formalism

Let us start from the (pseudo)scalar case. We consider neutrinos interacting with a light boson ϕ through simple scalar h_{ij} and pseudoscalar g_{ij} couplings, as described by the following Lagrangian [42, 85, 160, 161]:

$$\mathcal{L}_{\text{psc}} = h_{ij} \bar{\nu}_i \nu_j \phi + g_{ij} \bar{\nu}_i \gamma_5 \nu_j \phi + h.c., \quad (4.1)$$

where the i and j indices run over the the neutrino eigenstates and γ_5 is the gamma matrix responsible of the parity violation of the pseudoscalar part of the Lagrangian. A pseudoscalar quantity behaves exactly like a scalar one except for the changes in sign under parity transformation, in practice it has different rotation rules. This kind of interaction allows for the binary processes, i.e. neutrino annihilation to bosons ($\nu + \bar{\nu} \leftrightarrow \phi + \phi$), neutrino- ϕ scattering ($\nu + \phi \leftrightarrow \nu + \phi$), neutrino-neutrino scattering mediated by a scalar boson exchange ($\nu + \nu \leftrightarrow \nu + \nu$) and neutrino decay ($\nu \rightarrow \nu + \phi$). In Fig.(4.1) we show the correspondent allowed Feynman diagrams. In general the cross

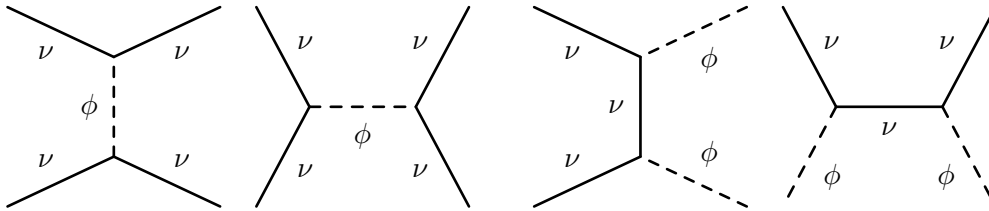


Figure 4.1: Feynman diagrams for the processes allowed by the Lagrangian, Eq.(4.1). In this representation time coordinate is set from left to right. In order of appearance ν - ν scattering (s and t channels), ν - ϕ scattering and $\nu\bar{\nu}$ annihilation to ϕ 's.

section for processes of this type is

$$\sigma^{\text{bin}} \sim g^4/s \quad (4.2)$$

where g is the largest value of the Yukawa coupling or the dimensionless coupling constant and $\sqrt{s} \sim T_\nu^2$ is the center of mass energy. In case of ultra-relativistic particle it can be approximated as we show in Eq.(1.63). In thermal equilibrium this cross-section leads to the following scattering rate:

$$\Gamma^{\text{bin}} = \langle \sigma^{\text{bin}} v \rangle n_{\text{eq}} \propto g^4 T_\nu. \quad (4.3)$$

In analogy to what we described in Ch.(1), considering reaction in thermal equilibrium regime, the fundamental quantity to be kept under control is the ratio between the

scattering rate and the Hubble expansion rate in radiation (H_r) or matter (H_m) dominated epochs:

$$\frac{\Gamma^{\text{bin}}}{H_r} \sim \frac{g^4}{T_\nu}, \quad \frac{\Gamma^{\text{bin}}}{H_m} \sim \frac{g^4}{T_\nu^{1/2}} \quad (4.4)$$

In Fig.(4.2) we show the exact picture for neutrino-neutrino interaction in presence

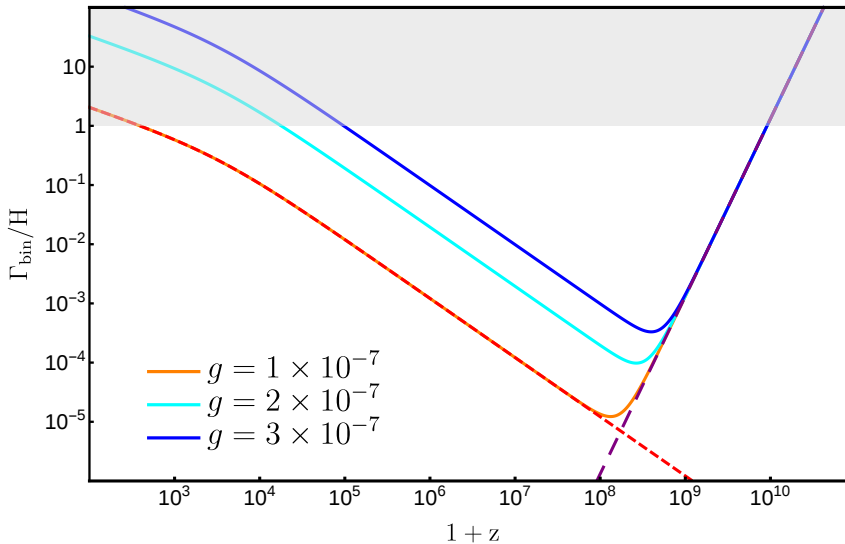


Figure 4.2: Behaviour of (pseudo)scalar interaction in the early universe, we show the ratio between the scattering rate and the Hubble rate in function of the redshift. The gray region is representative of the collisional regime, orange, cyan and blue lines correspond to three different value of Yukawa couplings, purple dashed line is a pure weak Fermi-like interaction and dashed red line represents a pure (pseudo)scalar interaction with $g = 1 \times 10^{-7}$.

of a (pseudo)scalar contribution. We decide to plot the Γ/H ratio in function of the redshift z taking into account both the standard weak (dashed purple line) and the “new” (pseudo)scalar (dashed red line) interactions. The joint behaviour has been shown for three different value of the dimensionless coupling constant g . Notice that the interacting regime is dominant for value of $\Gamma/H > 1$, that is, in the gray upper region, this is perfectly consistent with the standard picture where weak interactions decoupled at $z \sim 10^{10}$, however, the presence of a hidden interaction mediated by a (pseudo)scalar boson increases with time the scattering rate among neutrinos leading to a late recoupling. The exact recoupling redshift depends on the magnitude of the interaction, i.e. increasing the value of g we let us do the recoupling first. Collisional processes induced by the new interaction would affect the evolution of perturbations in the cosmological neutrino fluid in order to describe what we expect let us define the recoupling redshift of neutrinos $z_{\nu rec}$ to be the redshift when the $\Gamma^{\text{bin}}(z_{\nu rec}) = H(z_{\nu rec})$.

At $z \leq z_{\nu rec}$, the neutrino free-streaming length quickly drops below the Hubble length due to scatterings. Thus the neutrino contribution to the cosmic shear becomes negligible. If we consider that recoupling happens close enough to recombination the latter effect should be observable in the CMB anisotropy spectrum. Recoupling implies also a massive production of ϕ 's through neutrino annihilation (last Feynman diagram in Fig.(4.1). The annihilation processes may start when neutrinos are relativistic, this translates into a thermalization of the $\nu - \phi$ fluid through scatterings in this case the total energy stored in relativistic species does not change, so N_{eff} remains constant (at least until chemical equilibrium is maintained). On the other hand, once the temperature fluid falls below the neutrino mass, the annihilation processes allow the production of ϕ , but they can no longer ensure the inverse process, leading to a depletion of the neutrino abundance. The energy stored in the neutrino rest mass would end up increasing N_{eff} [24,95]. As long as we consider massless neutrinos the annihilation process does not change the behaviour of the neutrino fluid since we are dealing with a unique fluid in perfect thermal equilibrium. Moreover considering only diagonal terms in the scattering matrix allow us to neglect also possible decays. The parametrization presented here has some advantages: it allows us to consider a large variety of models. There is a no single theoretical model which provides for the existence of a massless mediator boson, one of the most suitable is represented by Majoron models where the interaction is mediated by the Nambu-Goldstone boson of a hitherto unknown broken $U(1)$ symmetry.

4.1.1 State of the art

Non-standard neutrino interactions of these types have already been considered in a cosmological context in [31], where they argue the possibility that neutrino decay could be induced by new interaction leading to a *neutrinoless* Universe. There are limits on neutrino-neutrino scattering induced by non-standard Majoron-like interactions in Refs. [28, 32] and more recently in Refs. [53, 87, 115]. Allowing scattering processes inside the cosmological framework is not an easy task, in the literature, the neutrino fluid has been modelled in several ways:

- Roughly changing from collisionless to perfectly tightly coupled (or viceversa in the case of Fermi-like interactions) at a given transition redshift, that represents the parameter actually constrained by the data.
- Deriving limits on phenomenological quantities parameterizing the effective sound speed and viscosity of the neutrino fluid [22, 59, 87, 162, 172].
- Solving the entire Boltzmann equation in the collisional case [142, 143].

The first and second approaches, however, as noted by a few authors [53, 142], are not accurate in the detailed description of the interaction. In particular, the first case loses information about the change among tightly coupled, collisional and collisionless

regimes. All the investigations on the subject presented so far assume that the neutrinos remain in tightly coupled regime until the characteristic scale enters the horizon; this treatment fails in all the scenarios where the scattering rate Γ is comparable with the Hubble expansion rate H . While the second approach is accurate in the description of the free streaming case, but does not provide an accurate representation of the collisional regime. It is a phenomenological model inherited from dark matter scenarios where two parameters c_{eff}^2 (the effective sound speed) and c_{vis}^2 (the viscosity parameter) modulate the acoustic oscillations inside the Boltzmann equation,

$$\dot{\delta}_\nu = -\frac{4}{3}\theta_\nu - \frac{2}{3}\dot{h} + H(1 - 3c_{\text{eff}}^2) \left(\delta_\nu + 4H\theta_\nu \frac{\theta_\nu}{k^2} \right), \quad (4.5a)$$

$$\dot{\theta}_\nu = k^2 \left(\frac{1}{4}\delta_\nu - \sigma_\nu \right) - \frac{k^2}{4}(1 - 3c_{\text{eff}}^2) \left(\delta_\nu + 4H\theta_\nu \frac{\theta_\nu}{k^2} \right), \quad (4.5b)$$

$$2\dot{\sigma}_\nu = \frac{8}{15}\theta_\nu - \frac{3}{5}kF_{\nu 3} + \frac{4}{15}\dot{h} + \frac{8}{15}\dot{\eta} - (1 - 3c_{\text{vis}}^2) \left(\frac{8}{15}\theta_\nu + \frac{4}{15}\dot{h} + \frac{8}{15}\dot{\eta} \right). \quad (4.5c)$$

Setting c_{eff}^2 and $c_{\text{vis}}^2 = 1/3$ corresponds to consider the standard free-streaming case, while $c_{\text{vis}}^2 = 0$ should be representative of the tight-coupling regime. Conversely, even starting from a value of $\dot{\sigma}_\nu \neq 0$ (pseudoscalar or scalar case), that in principle would lead to a initial quadrupole moment, the presence of a zero viscosity coefficient does not drive to zero $\ell \geq 2$ moments. The picture is even more incorrect if we start with a Fermi-like interaction which reveal a early tight-coupling regime.

The third approach introduces the collisions inside the Boltzmann equation. Scatterings are described by a complex integral at zero and first order:

$$\begin{aligned} \left(\frac{\partial f}{\partial \tau} \right)_{ij \leftrightarrow kl}^{(0)} &= \frac{g_j g_k g_l}{2|q|(2\pi)^5} \int \frac{d^3 \vec{q}'}{2|\vec{q}'|} \int \frac{d^3 \vec{l}'}{2|\vec{l}'|} \int \frac{d^3 \vec{l}}{2|\vec{l}|} \delta_D^4(q + l - q' - l') \\ &\quad \times |\mathcal{M}_{ij \leftrightarrow kl}|^2 \left(f_k^0(|\vec{q}'|, \tau) f_l^0(|\vec{l}'|, \tau) - f_i^0(|\vec{q}|, \tau) f_j^0(|\vec{l}|, \tau) \right). \end{aligned} \quad (4.6)$$

The zero order represents the background components of the scattering term, while the first order takes into account the perturbed components,

$$\begin{aligned} \left(\frac{\partial f}{\partial \tau} \right)_{ij \leftrightarrow kl}^{(1)} &= \frac{g_j g_k g_l}{2|q|(2\pi)^5} \int \frac{d^3 \vec{q}'}{2|\vec{q}'|} \int \frac{d^3 \vec{l}'}{2|\vec{l}'|} \int \frac{d^3 \vec{l}}{2|\vec{l}|} \delta_D^4(q + l - q' - l') \\ &\quad \times |\mathcal{M}_{ij \leftrightarrow kl}|^2 \left(f_k^0(|\vec{q}'|, \tau) F_l(\vec{k}, \vec{l}', \tau) + f_l^0(|\vec{l}'|, \tau) F_k(\vec{k}, \vec{q}', \tau) \right. \\ &\quad \left. - f_i^0(|\vec{q}|, \tau) F_j(\vec{k}, \vec{l}, \tau) + f_j^0(|\vec{l}|, \tau) F_i(\vec{k}, \vec{q}, \tau) \right), \end{aligned} \quad (4.7)$$

where q , l , q' and l' are the momenta of ingoing and outgoing particles, F_α with $(\alpha = i, j, k, l)$ is the simplified distribution function presented in Eq.(1.122) and f_α^0 is the unperturbed Fermi-Dirac distribution function, in every collisional term quantum

statistical effects have been neglected. The full integration of this formalism has been treated in [143] where the authors presented a very detailed calculation of every component.

Neutrino scalar and pseudoscalar couplings are constrained by laboratory searches for neutrinoless double beta decay ($0\nu\beta\beta$), and by supernovae observations. For example, in addition to the simplest $0\nu\beta\beta$ decay mode, whose existence only requires the neutrino to be a Majorana particle [159], modes in which one or two additional ϕ bosons are emitted:

$$(A, Z) \rightarrow (A, Z + 2) + 2e^- + \phi, \quad (4.8)$$

$$(A, Z) \rightarrow (A, z + 2) + 2e^- + 2\phi, \quad (4.9)$$

are possible if neutrinos possess (pseudo)scalar couplings. $0\nu\beta\beta$ experiments yield constraints on the effective ϕ -neutrino coupling constant $\langle g_{ee} \rangle < (0.8 - 1.6) \times 10^{-5}$, depending on the theoretical model [17, 79]. The quantity g_{ee} is the $e - e$ entry of the coupling matrix in the weak base, related to the couplings g_{ij} in the mass basis through the elements of the neutrino mixing matrix. Neutrino decays $\nu \rightarrow \nu' + \phi$ can also be important in the high-density supernova environment [43, 106, 170]. In the case of Majoron models, limits on Majoron-neutrino couplings from observations of SN 1987A were derived in Ref. [106]. It has been shown there that ϕ emission would shorten too much the observed neutrino signal from SN 1987A if $3 \times 10^{-7} \lesssim g \lesssim 2 \times 10^{-5}$ (here g denotes the largest element of the coupling matrix $g_{\alpha\beta}$ in the weak base), thereby excluding this region. Moreover, the observed $\bar{\nu}_e$ flux from SN1987A can also be used to further constraint $g_{11} \lesssim 10^{-4}$. These limits, together with those from $0\nu\beta\beta$ decay experiments available at that time, were combined and translated into the mass basis in Ref. [170].

4.1.2 Our method

Instead, in this work, we provide a different parametrization in which we derive limits on the strength of neutrino non-standard interactions by directly modifying the Boltzmann equation in order to account for neutrino collisions, without assuming a sudden transition between the two limiting regimes (free-streaming and tight coupling). In this way it is possible to follow the behaviour of the different moments of the Boltzmann hierarchy in order to better understand the physics of the processes involved. Although this approach is less accurate with respect the complete solution of the Boltzmann collisional term (seen in the previous section), it results to be much less numerically demanding. We will introduce the scattering term using the so called *Relaxation Time Approximation* which, on one hand, guarantees an ideal description of the interaction both at fluid equation and power spectra level (see Ref. [143] for details) and, on the other hand, thanks to the numerical advantages, allows us to perform an extended study to massless, massive

and sterile neutrino. The Relaxation time approximation, or BGK approximation, was introduced in 1954 by Bhatnagar, Gross and Krook (as often happens, in the same period, independently, Welander (1954) introduced a similar operator) and provides that the collisional operator at the right-hand side of the Boltzmann equation is replaced by:

$$\left(\frac{\partial f}{\partial \tau}\right)_C \sim \frac{1}{\tau_{\text{col}}}(f_0 - f), \quad (4.10)$$

where τ_{col} is the relaxation factor and $1/\tau_{\text{col}} \equiv \Gamma$ is the collision frequency. Replacing it in Eq.(1.118) and in particular:

$$\frac{1}{f_0} \left(\frac{\partial f}{\partial \tau}\right)_C = \frac{1}{f_0} (\Gamma(f_0 - f)), \quad (4.11a)$$

$$= -\frac{1}{f_0} (\Gamma f_0 \Psi), \quad (4.11b)$$

The latter equation is valid in every case: massless or massive neutrinos, (pseudo)scalar or Fermi-like interaction.

4.2 *Massless neutrinos*

We will start from the massless neutrino case looking at the (pseudo)scalar interaction. Eq.(4.12) in the case of massless neutrinos can be simplified as we did in Sec.(1.122):

$$\frac{1}{f_0} \left(\frac{\partial f}{\partial \tau}\right)_C = -\frac{1}{f_0} (\Gamma f_0 \Psi), \quad (4.12a)$$

$$= -\Gamma \frac{\int dq q^2 q f_0 \Psi}{\int dq q^2 q f_0}, \quad (4.12b)$$

$$= -\Gamma F_\nu. \quad (4.12c)$$

In this formalism we can replace Γ with every scattering rate we want to study. The Boltzmann hierarchy described in Eqs.(1.126) can be rewritten in the following way:

$$\dot{\delta}_\nu = -\frac{4}{3}\theta_\nu - \frac{2}{3}\dot{h}, \quad (4.13a)$$

$$\dot{\theta}_\nu = k^2 \left(\frac{1}{4}\delta_\nu - \sigma_\nu\right) \quad (4.13b)$$

$$\dot{\sigma}_\nu = \frac{4}{15}\theta_\nu - \frac{3}{10}kF_{\nu 3} + \frac{2}{15}\dot{h} + \frac{4}{5}\dot{\eta} - a\Gamma\sigma_\nu, \quad (4.13c)$$

$$\dot{F}_{\nu \ell} = \frac{k}{2\ell + 1} [\ell F_{\nu(\ell-1)} - (\ell + 1) F_{\nu(\ell+1)}] - a\Gamma F_{\nu \ell}. \quad (\ell \geq 3) \quad (4.13d)$$

Of course using the relaxation time approximation we are not obeying the basic conservation laws; if we see the equations Eq.(1.118), the collision term seems to be present in every moment, however, it is natural that $\ell = 0$ and $\ell = 1$ must obey to number density conservation and to momentum conservation respectively. The point is that we cannot think that physical processes, such as the binary scattering that we are considering, can change the number density of a species nor the total momentum distribution. The $2 \leftrightarrow 2$ collisions lead a suppression of the quadrupole ($\ell = 2$), i.e. the anisotropic stress σ_ν , and of all the highest moments of the distribution function, and to a corresponding enhancement of the monopole and dipole ($\ell = 0, 1$), i.e. the density and velocity perturbations δ_ν and θ_ν . This changes propagate to the photon distribution, and thus to the CMB spectrum, through the gravitational potentials. We decided to parametrize the interaction using an effective coupling constant g_{eff} , this choice guarantees the inclusion of many models attributable to a (pseudo)scalar like interaction. Thus we rewrite the scattering rate in the following phenomenological way:

$$\Gamma^{\text{bin}} = 0.183 \times g_{\text{eff}}^4 T_\nu, \quad (4.14)$$

where we have taken into account that $n_\nu = (3/2) \times (\zeta(3)/\pi^2) \times T_\nu^3$ for each neutrino family. This definition of the effective coupling constant encloses such details as the precise Yukawa structure of the theory, the effect of thermal averaging, etc. Given a definite form of the Lagrangian, Eq.(4.1), this can be remapped, to a good approximation, to a collision rate of the form Eq.(4.14), for the purposes of its effect on the evolution of cosmological neutrino perturbations. Seen in another way, the quantity that we are actually constraining is the (temperature-independent in the high-energy limit) combination $\langle \sigma_{\text{bin}} v \rangle T_\nu^2$. In the following, we will not distinguish between scalar and pseudoscalar interactions, and generically speak of scalar-mediated interactions; however, we recall that interactions mediated by a very light (or massless) boson could give rise to long-range forces that are not screened in the strictly scalar case.

4.2.1 Perturbation evolution and APS

As said before the interaction suppress the shear and consequently we have an enhancement of the density perturbation, in Fig.(4.3) we show the evolution of the fluid perturbation comparing the standard model (Λ CDM) with the interacting massless model (Λ CDM + g_{eff}) for three different wave numbers ($k = 0.5, 0.05, 0.005 \text{ Mpc}^{-1}$) and two different interaction strengths. The value of the coupling constant used are $g_{\text{eff}} = 1.8 \times 10^{-7}$ (blue line), which corresponds to a recoupling redshift of $z_{\text{rec}} \sim 1.2 \times 10^3$ and $g_{\text{eff}} = 2.8 \times 10^{-7}$ (red line) that leads to a neutrino recoupling redshift of $z_{\text{rec}} \sim 1.2 \times 10^4$. We take the following benchmark for the cosmological parameters [$\Omega_b h^2 = 0.0226$, $\Omega_c h^2 = 0.12$, $h = 0.68$, $\tau_{\text{rei}} = 0.09$, $n_s = 0.96$, $A_s = 2.1 \times 10^{-9}$, $N_{\text{eff}} = 3.046$].

The top panel refers to a wave number that enters the horizon at $z \sim 5 \times 10^4$, thus well before the recoupling redshift of both the considered cases, the result is that, initially, shear and density are not affected by the interaction, as one should expect. Later, when the scattering rate starts to be non-negligible inside the Boltzmann equation, σ_ν loses power, however the perturbation is already deeply inside the oscillatory regime and, thus, it does not impact much on δ_ν . The middle panel shows a mode ($k = 0.05 \text{ Mpc}^{-1}$) that enter the horizon at $z \sim 3 \times 10^3$; here is evident that the blue line, corresponding to $g_{\text{eff}} = 1.8 \times 10^{-7}$ ($z_{\text{rec}} \sim 1.2 \times 10^3$), is almost unchanged with respect to the standard case. While the red line, that refers to $g_{\text{eff}} = 2.8 \times 10^{-7}$ ($z_{\text{rec}} \sim 1.2 \times 10^4$), shows suppression in the shear component and, consequently, an increase in the oscillatory pattern of density perturbations.

Finally, the lower panels of Fig.(4.3) show perturbation evolution for the largest scale, $k = 5 \times 10^{-3} \text{ Mpc}^{-1}$, entering the horizon well after the time of hydrogen recombination at $z \simeq 50$. For both the values of the coupling constant, when the mode enters the horizon neutrinos are already completely recoupled, and shear oscillations are overdamped.

When we compare perturbation evolution for the three selected cases the behaviour of the interaction becomes clear: density perturbations mirrors the shear: when the dissipation normally associated to neutrino free-streaming is absent, undamped acoustic oscillations set on in the fluid, so that density perturbations are actually boosted by increasing g_{eff} . In the previous chapter we focused on the importance that the parameter in the neutrino sector have on the APS. Thus, in order to understand if cosmology is sensitive to the introduction of scalar secret interactions, we produced a realization of the temperature and temperature-polarization power spectra using the same value of the coupling constant chosen for Fig.(4.3) and adding a further value $g_{\text{eff}} = 3.8 \times 10^{-7}$ in order to test the consequences of an extremely interacting scenario. Looking at Fig.(4.4) the effect of the interaction results into an increase in the power on a large samples of ℓ s and a light shift of peaks towards higher multipoles. These behaviours are caused by the magnified density fluctuations due to the absence of neutrino free streaming. The scattering term makes neutrinos collisional again and, thus, implies the rises of a tight coupled regime where neutrinos can exchange momentum. This, in principle, affects the behaviour of modes that are inside the horizon (or that are becoming sub-horizon). Super-horizon modes remains unchanged while small angular scales are still affected by the Silk damping. In the middle panel of Fig.(4.4) we notice that the TT power spectrum is mostly sensitive in multipoles between $\ell \sim 200$ and $\ell \sim 1500$. Large scales $2 < \ell < 50$ should not be affected since they are always super-horizon and, as said before, the physics of linear perturbations is negligible in such regime. For small scales $\ell > 1500$ the picture is a bit more complicated, we have shown in Fig.(4.3) that in order to evaluate the impact of the interaction we have to identify the wave number that enters the horizon in correspondence to a specific recoupling redshift. For example, considering the values of the interaction strength used

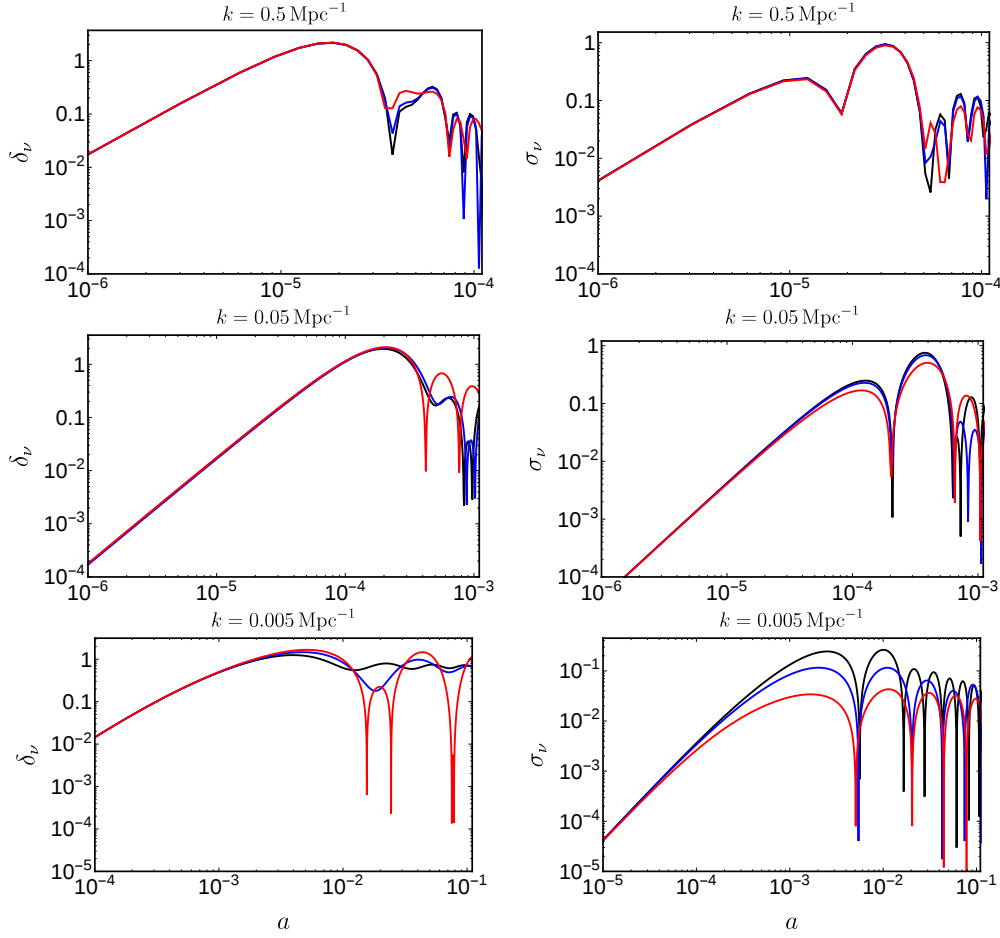


Figure 4.3: Evolution of a massless neutrino eigenstate perturbation, in particular density δ_ν (left column) and shear σ_ν (right column). We show three different modes: first row corresponds to $k = 0.5 \text{ Mpc}^{-1}$, second line is $k = 0.05 \text{ Mpc}^{-1}$ and final one is representative of $k = 0.005 \text{ Mpc}^{-1}$. In black we show the standard evolution in the ΛCDM model, while the blue and red lines show the perturbation evolution for the interacting (pseudo)scalar model ($\Lambda\text{CDM} + g_{\text{eff}}$) with $g_{\text{eff}} = 1.8 \times 10^{-7}$ and $g_{\text{eff}} = 2.8 \times 10^{-7}$ respectively.

in Figs.(4.4, 4.8) and reported in Tab.(4.1), we can examine case by case: in Fig.(4.5) we show an alternative way to see the behaviour of the interaction. The top panel show the evolution of interaction scattering rate (dotted coloured lines) and Hubble rate (black solid line) for the considered value of g_{eff} ; the vertical blue, red and green lines represents the corresponding recoupling redshift. Moreover, in the lower panel we plot the wave number that enters the horizon in correspondence of the redshift values found above. For each value of k we can associate a defined mutipole ℓ in the APS. Through

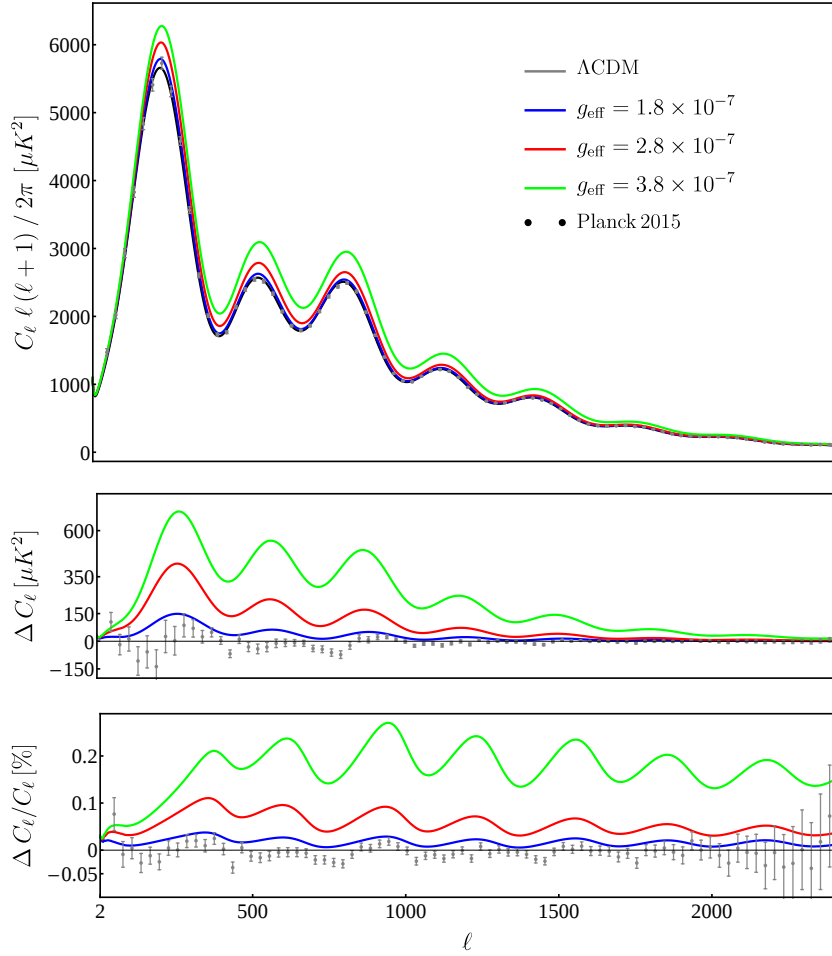


Figure 4.4: Theoretical temperature angular power spectrum for $\Lambda\text{CDM} + g_{\text{eff}}$ model (top panel). We produce three realization for an equal number of values of the coupling constant: 1.8×10^{-7} (blue line), 2.8×10^{-7} (red line), 3.8×10^{-7} (green line) and compare the results with the ΛCDM APS (black line), finally in gray we show Planck 2015 binned data. In the middle panel we plot the residuals of the two interacting models with respect to the ΛCDM one, while in the bottom panel we show the relative residuals weighed by the ΛCDM C_ℓ s.

this procedure we can map in the APS the impact of the interaction on the perturbation evolution. Once we have a recoupling wave number k_{rec} and the correspondent ℓ_{rec} associated to a value of the secret interaction coupling constant, all $k < k_{\text{rec}}$ which are relatively “large” scales imply a time of horizon crossing $t_{\text{hc}}(k) > t_{\text{rec}}$. Vice versa for $k > k_{\text{rec}}$, considered “small scales”, we have $t_{\text{hc}}(k) < t_{\text{rec}}$. We know from Fig.(4.3) that the effect of the interaction is smaller if the wave number is already inside the horizon

Interaction strength	Recoupling redshift	Wave number	multipole
$g_{\text{eff}} = 1.8 \times 10^{-7}$	$z_{\text{rec}} \sim 1.2 \times 10^3$	$k_{\text{rec}} \sim 0.029 \text{ Mpc}^{-1}$	$\ell_{\text{rec}} \sim 420$
$g_{\text{eff}} = 2.8 \times 10^{-7}$	$z_{\text{rec}} \sim 1.2 \times 10^4$	$k_{\text{rec}} \sim 0.153 \text{ Mpc}^{-1}$	$\ell_{\text{rec}} \sim 2150$
$g_{\text{eff}} = 3.8 \times 10^{-7}$	$z_{\text{rec}} \sim 4.5 \times 10^4$	$k_{\text{rec}} \sim 0.495 \text{ Mpc}^{-1}$	$\ell_{\text{rec}} \sim 7000$

Table 4.1: In this table we summarize the main characteristic of the interaction: the left column presents different value of interaction, to every value we associate the recoupling redshift (second column) and the wave number which is entering the horizon at that redshift. The parameters used for deriving these value is $[\Omega_b h^2 = 0.0222, \Omega_c h^2 = 0.119, H_0 = 67.43 \text{ km/s/Mpc}]$.

at the neutrino-neutrino recoupling. This implies that on the high multipoles the effect is smaller; moving towards larger scales, the effect of scatterings induced by the secret interaction becomes larger at least as long as the CMB is sensitive to the interaction, i.e. modes that enter the horizon well after the photon decoupling are screened by SW and ISW effects.

In order to have a better comprehension of the physics involved in these processes we decided to analyse the different components that contribute to the APS. The anisotropy field that we observe is can be decomposed into different parts depending on different variables (see [62] for details):

$$\begin{aligned}
 \Theta_\ell(k) = & \int_0^{\tau_0} d\tau g(\tau) [\Theta_0(k, \tau) + \psi(k, \tau)] j_\ell[k(\tau_0 - \tau)] \\
 & \int_0^{\tau_0} d\tau g(\tau) \frac{iv_b(k, \tau)}{k} \frac{d}{d\tau} j_\ell[k(\tau_0 - \tau)] \\
 & + \int_0^{\tau_0} d\tau e^{-\tau c} [\dot{\psi}(k, \tau) - \dot{\phi}(k, \tau)] \times j_\ell[k(\tau_0 - \tau)].
 \end{aligned} \tag{4.15}$$

The first two integrals are important when $g(\tau)$ that is the visibility function is not zero, i.e. during the photon decoupling, in particular the first takes into account the contribution of the potential $\psi(k, \tau)$ while the second maps the effect of the baryon velocity v_b . The last integral is the contribution along the entire line of sight of the Sachs-Wolfe effect, that is the Integrated Sachs-Wolfe effect. Of course the derivatives of the gravitational potential are important when the universe was radiation dominated and contribute to the early-ISW effect, instead for $z < 30$ the integral is named late-ISW. The contribution of the shear σ_ν enters also in this part of the integral modifying the evolution of the gravitational potential [127]

$$k^2(\phi - \psi) = 12\pi G a^2 \sum_i (\bar{\rho}_i + \bar{P}_i) \sigma_i, \tag{4.16}$$

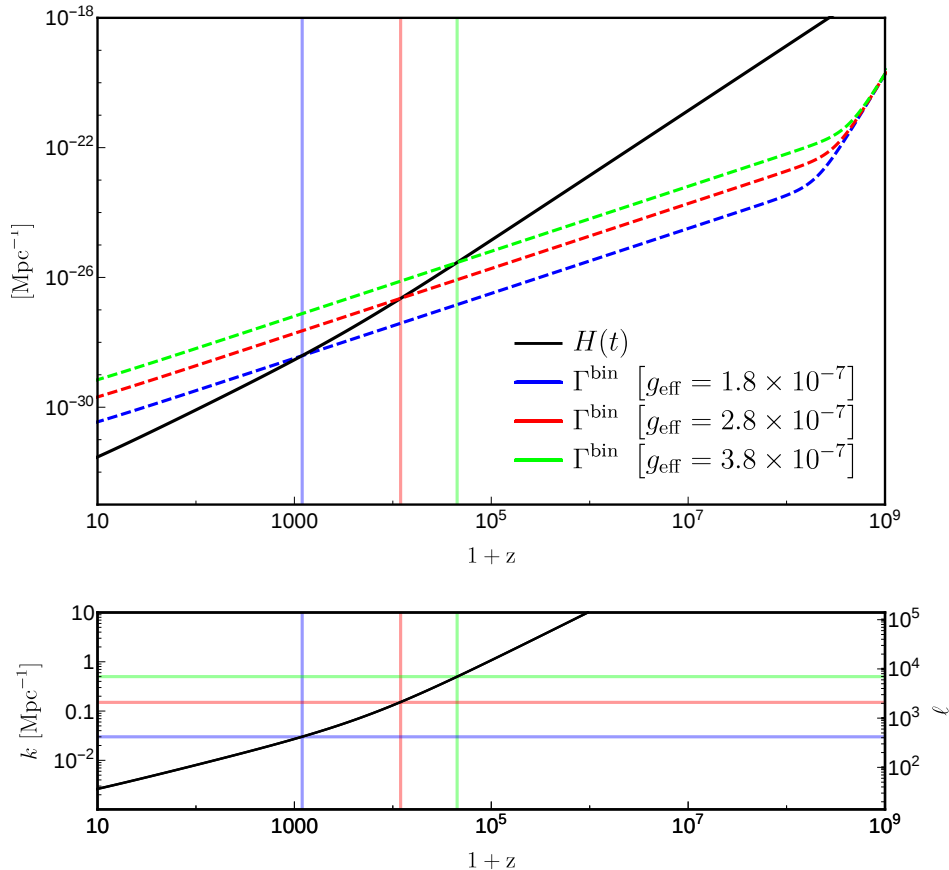


Figure 4.5: In the upper panel we show the scattering rate Γ^{bin} and Hubble rate $H(t)$ evolution in function of the redshift. We show three different value of the interaction strength $g_{\text{eff}} = 1.8 \times 10^{-7}$ (blue dashed line), 2.8×10^{-7} (red dashed line), 3.8×10^{-7} (green dashed line). We put in evidence the corresponding recoupling redshifts with vertical lines having the same colour legend. In the lower panel we present the evolution of the horizon wave number in function of the redshift. The vertical lines have the same purpose explained in the top panel, the horizontal ones, instead, point out the wave number and the correspondent multipole ℓ in the APS associated to the recoupling redshifts.

which is greater when mean neutrino density $\bar{\rho}_\nu$ and average neutrino pressure \bar{P}_ν are large. The low multipole in the APS contain information on the large scales and thus the contribution of the ISW effect is supposed to be the most important. We can separate the contribution in two: early and late-ISW, the first comes from time-varying potentials soon after the recombination when the matter contributions is dominant,

while the latter is due to late time potentials when dark energy becomes important. In Fig. we show the ISW for $z < 30$ (late-ISW) and $z > 30$ (early-ISW) where it is evident that there is an effect, due to secret interactions, in both the components, but the major contribution is hidden in the early-ISW. The reason is that, as shown in

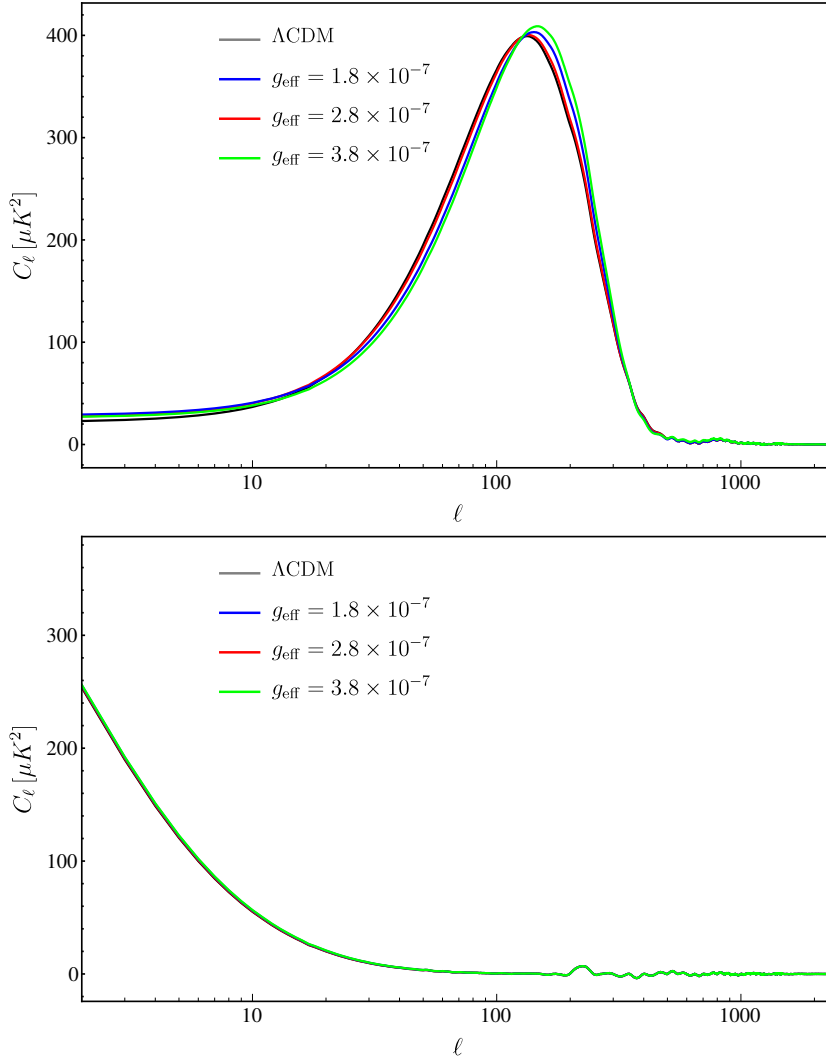


Figure 4.6: Effect of the secret pseudo-scalar interaction on the Early (top panel) and late (bottom panel) ISW. We provide three different cases of the interaction strength (coloured lines) compared with the standard ΛCDM model (black line).

Eq.(4.16) the effect of the interaction on the anisotropic stress is more important when the mean density and pressure of the neutrino fluid is large.

We are also interested in understanding the impact of the secret interaction on the

lensing potential. We know that neutrinos play a role in the large-scale formations: the presence of an extra free-streaming fluid drops the number of structures having dimension smaller than the free-streaming wavelength and this leaves a trace also in the lensing potential measured by Planck. In Fig.(4.7) we can see the proper effect of this type of interaction, also in this case: the middle values of the lensing potential power spectrum are enhanced between $\ell = 10$ and $\ell = 1000$. Moreover, we notice that increasing the magnitude of the interaction the position of the peak moves, as if scatterings were not just raising the potential, but they were also moving it on larger scales. The latter effect generates also the apparent reduction in power of the lensing spectrum for the case $g_{\text{eff}} = 3.8 \times 10^{-7}$ represented by the green line. Thus, what

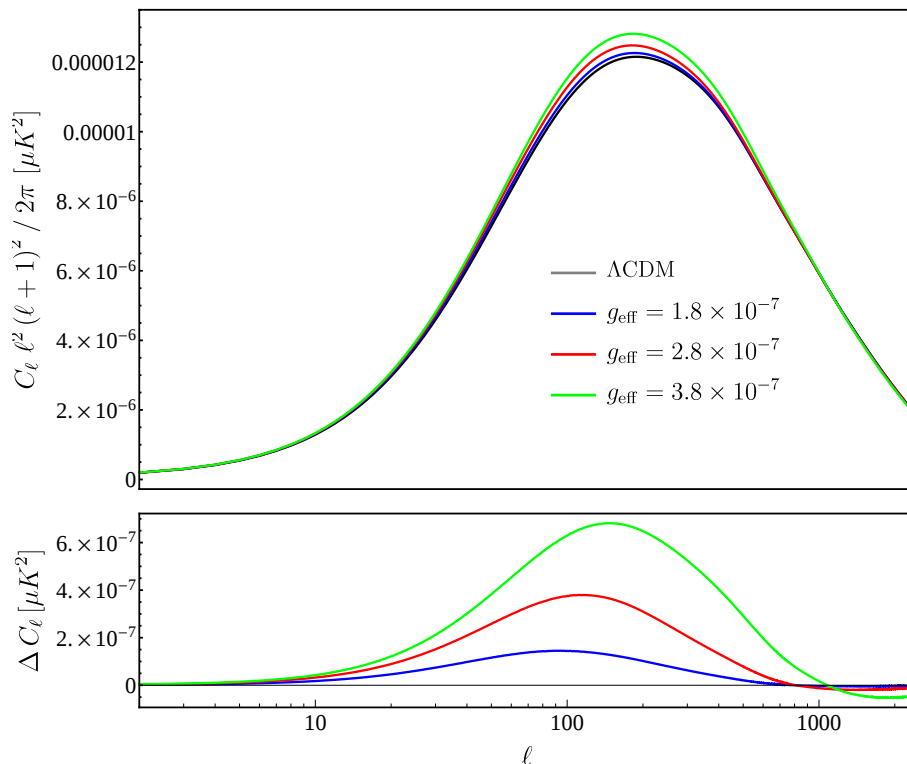


Figure 4.7: Lensing potential for three different values of the secret interaction strength: blue line corresponds to $g_{\text{eff}} = 1.8 \times 10^{-7}$, red line corresponds to $g_{\text{eff}} = 2.8 \times 10^{-7}$, and green line represents $g_{\text{eff}} = 3.8 \times 10^{-7}$. In black we show the standard cosmological best-fit model.

we expect is a greater lensing effect directly on the temperature anisotropies power spectrum.

We want to underline that, even if this is the preliminary part of the study and we can not extract any quantitative information from Fig.(4.4), looking at the residuals for the interacting cases, the strongest one, i.e. $g_{\text{eff}} = 3.8 \times 10^{-7}$, is far farther than the

data compared to $g_{\text{eff}} = 1.8 \times 10^{-7}$. This point towards a predilection of data for a low value of the interaction, in particular we expect that constraints on g_{eff} obtained by a MonteCarlo Markov-Chain study will suggest to bounds compatible with a zero value. In Fig.(4.8) we show the same power spectra presented in Fig.(4.4) but figured with a different ℓ dependence. It is common practice, in order to put in evidence the impact of the interaction, to change the APS from $C_\ell \ell(\ell + 1)/2\pi$ to $C_\ell \ell^3(\ell + 1)/2\pi$, this on one hand allows us to see all the peaks more clearly, but on the other hand can deceive the reader. It is evident that adding a factor ℓ^2 moves power in the APS towards higher

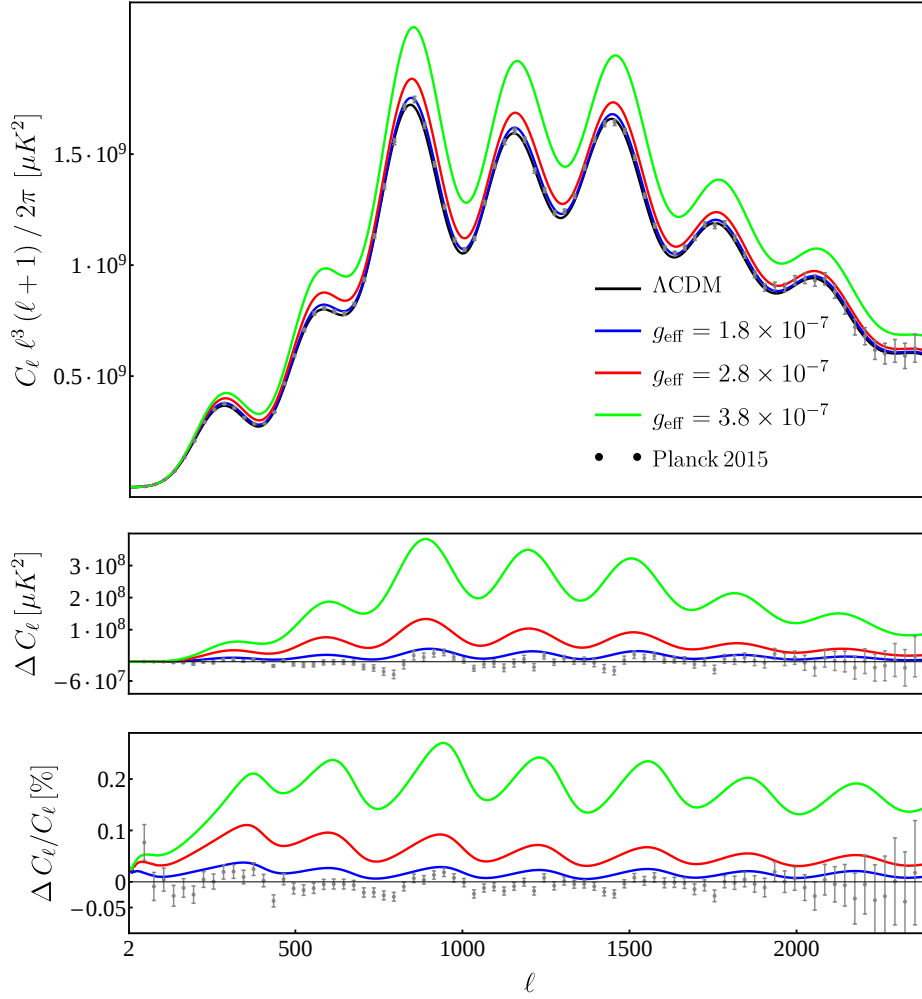


Figure 4.8: Same theoretical temperature angular power spectrum for $\Lambda\text{CDM} + g_{\text{eff}}$ model shown in Fig.(4.4). In this picture we change the representation of the APS that now has the following form $C_\ell \ell^3(\ell + 1)/2\pi$.

multipoles, e.g. considering $\ell = 100$ and $\ell_1 = 1000$ in the latter representation we

are overestimating the APS in ℓ_1 of a factor 100. Hence, in order to be sure that the information in both the representation is the same, we present in the bottom panel of both Fig.(4.4) and Fig.(4.8) the relative residuals, which, by definition, are exactly the same. In order to have a complete overview of the effects of the (pseudo)scalar interaction we performed the same study also on the temperature and polarization anisotropy power spectrum (TE APS). In Fig.(4.9) we show the results using the same formalism of the temperature only analysis. Also in this case we see a greater effect

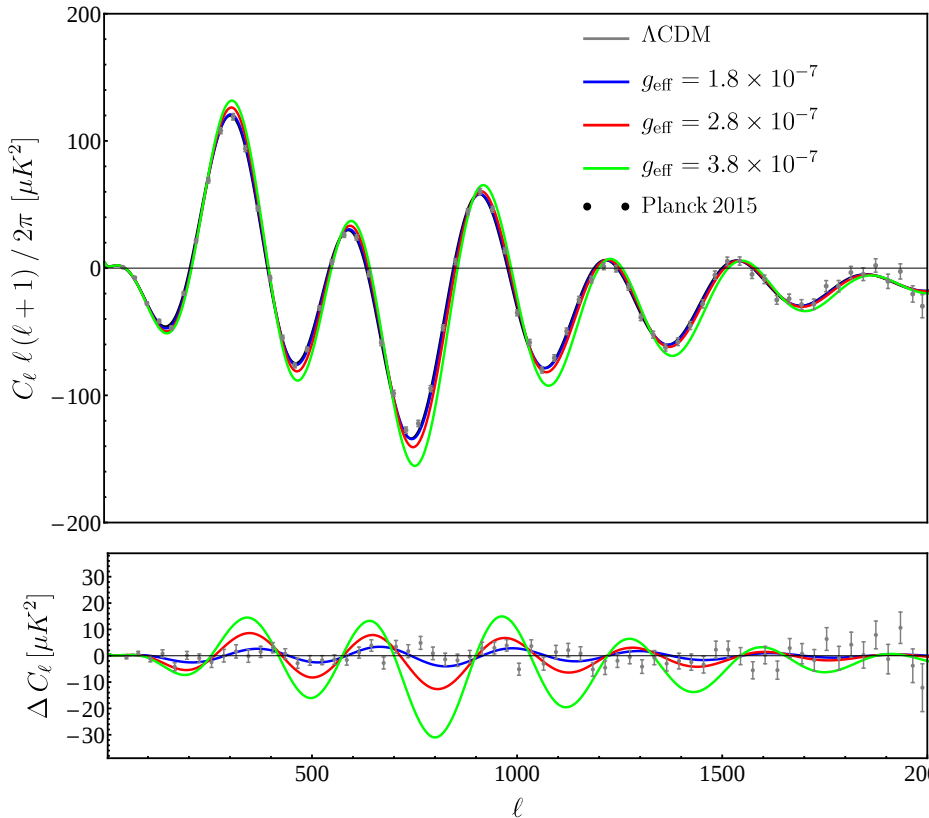


Figure 4.9: Theoretical temperature and polarization power spectrum for the Λ CDM + g_{eff} model with three different values. Blue, red and green solid lines correspond to $g_{\text{eff}} = (1.8, 2.8, 3.8) \times 10^{-7}$ respectively. The black solid line is the theoretical TE APS for the standard Λ CDM model and grey dots show Planck 2015 data and uncertainties. In the lower panel we plot the residuals between the interacting cases and the standard one.

in the middle part of the spectrum that is in agreement with what we infer from the perturbation evolution analysis. Moreover polarization data seem to suggest the same predilection for small values of the interaction coupling constant.

4.3 Constraints from Planck 2013 data

We are now ready to present the constraints that CMB and other astrophysical data provide on the non-standard coupling constant g_{eff} . In the following, we will quote 68% CL uncertainties, unless we are dealing with upper limits, in which case we quote 95% credible intervals. The results shown in the following are summarized in Tabs. 4.4 and 4.6. In this section we show the results obtained using the 2013 Planck data release (Planck₁₃TT), then, in the next section, we will present a similar analysis carried out using the latest 2015 Planck data (Planck₁₅TT, Planck₁₅TP). The 2013 Planck dataset comprehends also the WMAP low- ℓ polarization, see Sec.(1.1) for details.

Let us start by considering the simplest extension of the standard cosmological model, labelled “ Λ CDM+ g_{eff} ” such as the parameter space now is $[\Omega_b h^2, \Omega_c h^2, 100\theta_{MC}, \tau_{\text{rei}}, n_s, \ln(10^{10} A_s), g_{\text{eff}}^4]$. We decided to explore the parameter space constraining directly g_{eff}^4 ¹ in order to have a linear scan. We obtain $g_{\text{eff}}^4 < 4.64 \times 10^{-27}$ which corresponds to $g_{\text{eff}} < 2.61 \times 10^{-7}$ and a neutrino-neutrino recoupling at $z_{\text{rec}} < 8800$. Every time we report the recoupling redshift we calculate it fixing the other parameters to the best estimates. Adding the ACT and SPT datasets, labelled highL, shifts the distribution to larger values of the coupling constant, yielding $g_{\text{eff}}^4 < 5.25 \times 10^{-27}$ or $g_{\text{eff}} < 2.7 \times 10^{-7}$ and $z_{\text{rec}} < 10^4$. We have also constrained the number of relativistic species in conjunction with g_{eff} . In the framework of this “ Λ CDM + g_{eff} + N_{eff} ” model, we find a 95% credible interval $g_{\text{eff}}^4 < 4.10 \times 10^{-27}$ corresponding to $g_{\text{eff}} < 2.53 \times 10^{-7}$ from Planck₁₃TT. This valued provides a $z_{\text{rec}} < 7400$. Adding the contribution of the very high multipoles of ACT and SPT (Planck₁₃TT+highL), also in this case, weakens the constraints on the coupling constant, yielding $g_{\text{eff}}^4 < 5.1 \times 10^{-27}$ ($g_{\text{eff}} < 2.67 \times 10^{-7}$) and a recoupling redshift of $z_{\text{rec}} < 9800$ at 95% CL. The constraint on the effective number of neutrino families is $N_{\text{eff}} = 3.44^{+0.37}_{-0.41}$ (Planck₁₃TT) and $N_{\text{eff}} = 3.27^{+0.33}_{-0.38}$ (Planck₁₃TT+highL), very much consistent with the corresponding values found by the Planck collaboration in the N_{eff} extension of the Λ CDM model for the same datasets [10]. Interestingly enough, there is a weak (at $\sim 1\sigma$ the level) preference for non-zero values of the secret coupling constant at 68% CL when we consider the very high ℓ data coming from ACT and SPT. For the Λ CDM + g_{eff} model we find $g_{\text{eff}}^4 = 2.42^{+0.92}_{-1.97} \times 10^{-27}$ ($g_{\text{eff}} \sim 2.22 \times 10^{-7}$). The 68% lower limit in the latter case corresponds to $z_{\text{rec}} \sim 3500$. Instead, in the Λ CDM + g_{eff} + N_{eff} case the constraint is $g_{\text{eff}}^4 = 2.47^{+0.82}_{-1.27} \times 10^{-27}$ ($g_{\text{eff}} \sim 1.95 \times 10^{-7}$) that translates into $z_{\text{rec}} \sim 2000$.

We performed an additional extension in the parameter space considering the tensor to scalar ratio as a free parameter of the model “ Λ CDM + g_{eff} + r ”. In this case we use the 2013 Planck dataset and the joint analysis made by BICEP2/Keck & Planck (Planck₁₃TT+BKP). In this case we find the same 1σ preference for a non zero value of the coupling constant using both the base Planck₁₃TT data set and the

¹ g_{eff} appears to the fourth power inside the scattering rate Γ^{bin} . See Sec.(4.2) for detail on the interaction parametrization.

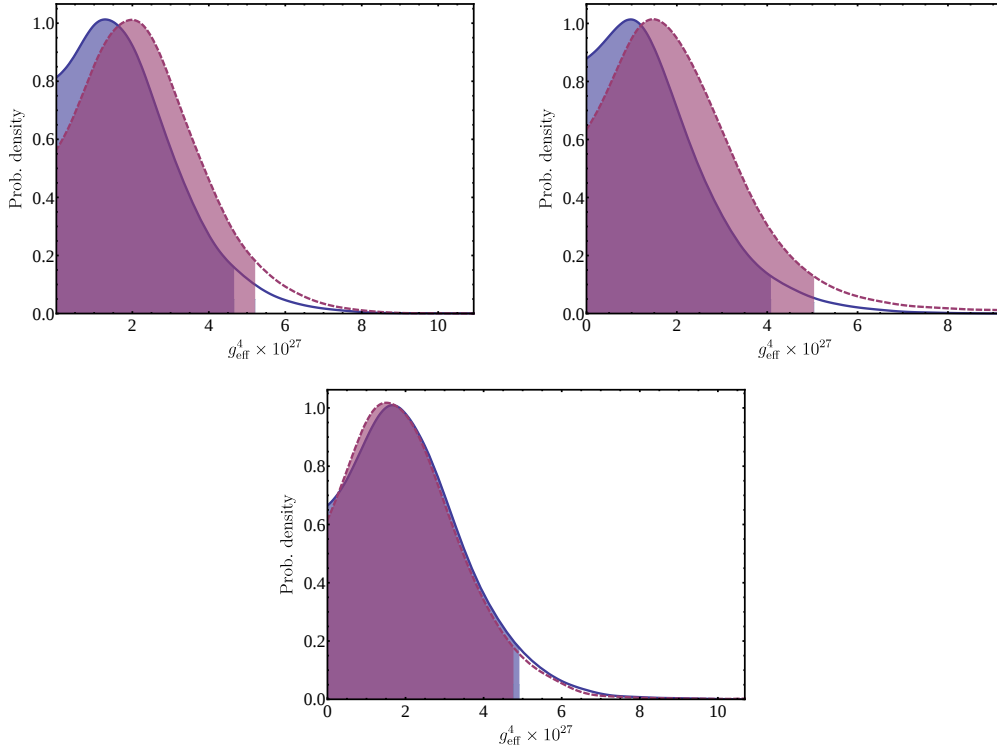


Figure 4.10: One dimensional posterior probability for the interaction strength g_{eff}^4 , in blue we report the constraints obtained using Planck₁₃TT data, red curves in the first row refers to Planck₁₃TT+highL while in the bottom panel is representative of Planck₁₃TT+BKP. From left to right in order of appearance we have $\Lambda\text{CDM} + g_{\text{eff}}$, $\Lambda\text{CDM} + g_{\text{eff}} + N_{\text{eff}}$ and $\Lambda\text{CDM} + g_{\text{eff}} + r$. The shaded areas show the 2σ constraints for the interaction strength.

one extended with BICEP2/Keck & Planck, respectively $g_{\text{eff}}^4 = 2.23^{+0.84}_{-1.83} \times 10^{-27}$ and $g_{\text{eff}}^4 = 2.17^{+0.81}_{-1.79} \times 10^{-27}$. We report also the more conservative 95% CL bounds that are $g_{\text{eff}}^4 < 4.92 \times 10^{-27}$ ($g_{\text{eff}} < 2.65 \times 10^{-7}$) for Planck₁₃TT and $g_{\text{eff}}^4 < 4.75 \times 10^{-27}$ ($g_{\text{eff}} < 2.61 \times 10^{-7}$) for Planck₁₃TT+BKP. For what concerns the tensor to scalar ratio we find $r < 0.14$ and $r < 0.10$ for Planck₁₃TT and Planck₁₃TT+BKP respectively. Both values are consistent with that found by Planck collaboration [10].

In Fig.(4.10) we present the one-dimensional posterior distributions for the interaction strength parameter, the plots in the first row corresponds to $\Lambda\text{CDM} + g_{\text{eff}}$ and $\Lambda\text{CDM} + g_{\text{eff}} + N_{\text{eff}}$ models, blue and red lines represents Planck₁₃TT and Planck₁₃TT+highL dataset. While the bottom panel shows the posterior of the $\Lambda\text{CDM} + g_{\text{eff}} + r$ model for Planck₁₃TT and Planck₁₃TT+BKP (blue and red lines respectively). In Fig.(4.11) we show the most significant correlations between g_{eff} and other parameters, namely $\Omega_c h^2$, $100\theta_{MC}$, $10^9 A_s e^{-2\tau_{\text{rei}}}$ and N_{eff} . The correlations with

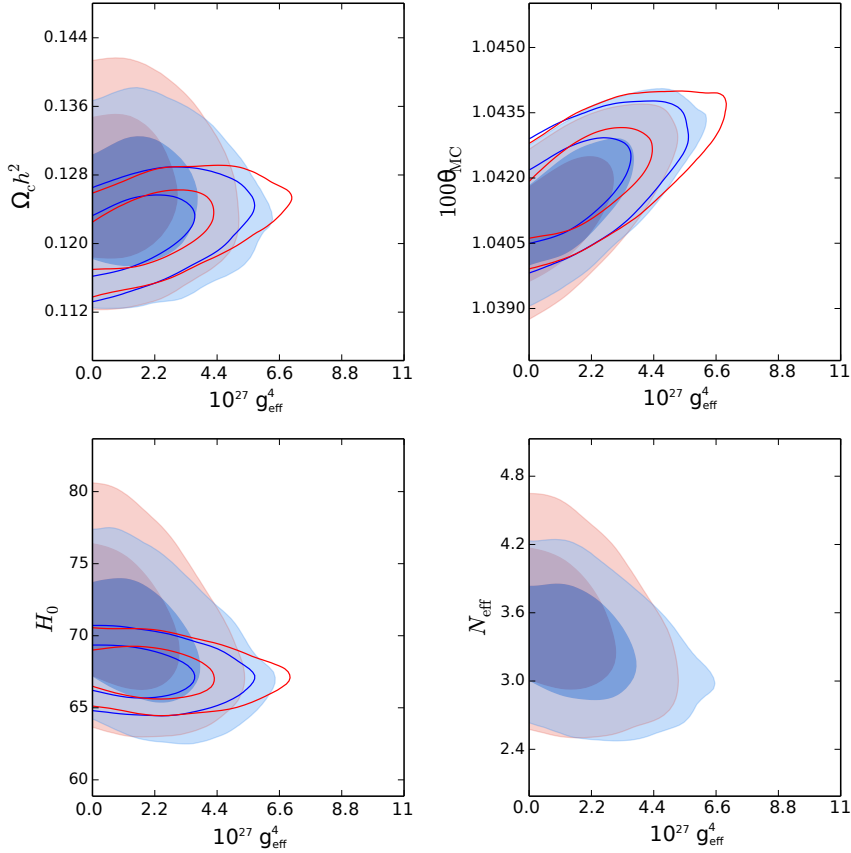


Figure 4.11: 68% and 95% confidence regions for selected parameter pairs involving g_{eff} in the $\Lambda\text{CDM} + g_{\text{eff}}$ (empty contours) and $\Lambda\text{CDM} + g_{\text{eff}} + N_{\text{eff}}$ (filled contours), for Planck₁₃TT (blue) and Planck₁₃TT+highL (red).

the angle $100\theta_{MC}$ subtended by the sound horizon at recombination and with the amplitude $10^9 A_s e^{-2\tau_{\text{rei}}}$ are particularly evident. We argue that the pattern leading to these correlations is the following: the overall amplitude of the spectrum increases for larger values of the coupling constant, while the position of peaks and dips remains unchanged. This can be directly compensated by a lower value of $10^9 A_s e^{-2\tau_{\text{rei}}}$. Alternatively, increasing $\Omega_c h^2$ (or decreasing N_{eff} if the model allows), lowers the height of the first few peaks but shifts their position to lower multipoles; increasing $100\theta_{MC}$ moves the peaks back to their original position. In Tab.(4.2) we show the constraints of the 6 basic parameters of the standard cosmological model plus the additional parameters added in this study for the $\Lambda\text{CDM} + g_{\text{eff}}$ and $\Lambda\text{CDM} + g_{\text{eff}} + N_{\text{eff}}$ models. The results of the $\Lambda\text{CDM} + g_{\text{eff}} + r$, instead, are showed in Tab.(4.3).

The constrains on non-standard neutrino interactions mediated by a (pseudo)scalar massless boson presented in this section, have been obtained using observations of

Constraints from Planck 2013 data

Parameter	$\Lambda\text{CDM} + g_{\text{eff}}$		$\Lambda\text{CDM} + g_{\text{eff}} + N_{\text{eff}}$	
	Planck ₁₃ TT	Planck ₁₃ TT	Planck ₁₃ TT	Planck ₁₃ TT
		+highL		+highL
$\Omega_b h^2$	0.02214 ± 0.00029	0.02219 ± 0.00028	0.02244 ± 0.00041	0.02237 ± 0.00038
$\Omega_c h^2$	0.1217 ± 0.0029	0.1221 ± 0.0029	$0.1265^{+0.0055}_{-0.0059}$	0.1246 ± 0.0050
$100 \theta_{MC}$	$1.04195^{+0.00073}_{-0.00083}$	$1.04210^{+0.00075}_{-0.00087}$	$1.04143^{+0.00084}_{-0.00101}$	$1.04179^{+0.00087}_{-0.00101}$
τ_{rei}	$0.091^{+0.013}_{-0.014}$	0.093 ± 0.013	$0.095^{+0.014}_{-0.016}$	$0.096^{+0.013}_{-0.016}$
n_s	$0.9641^{+0.0073}_{-0.0074}$	0.9627 ± 0.0073	0.979 ± 0.016	0.972 ± 0.015
$\log[10^{10} A_s]$	3.079 ± 0.025	$3.080^{+0.023}_{-0.024}$	$3.100^{+0.034}_{-0.036}$	$3.094^{+0.030}_{-0.033}$
$10^{27} g_{\text{eff}}^4$ [95% CL]	< 4.65	< 5.25	< 4.10	< 5.10
$10^{27} g_{\text{eff}}^4$ [68% CL]	/	$2.42^{+0.92}_{-1.97}$	/	$2.47^{+0.82}_{-1.27}$
N_{eff}	3.046	3.046	$3.45^{+0.39}_{-0.43}$	3.27 ± 0.34
H_0 [km/sec/Mpc]	67.4 ± 1.2	67.4 ± 1.2	$70.5^{+3.1}_{-3.5}$	$69.2^{+2.7}_{-3.0}$
$10^7 g_{\text{eff}}$ [95% CL]	< 2.61	< 2.7	< 2.53	< 2.67
z_{rec} [95% CL]	< 8800	< 10^4	< 7400	< 9800
$10^7 g_{\text{eff}}$ [68% CL]	/	2.22	/	2.3
z_{rec} [68% CL]	/	3500	/	2000

Table 4.2: Constraints on cosmological parameters for the $\Lambda\text{CDM} + g_{\text{eff}}$ and $\Lambda\text{CDM} + g_{\text{eff}} + N_{\text{eff}}$ models from the analysis of the Planck₁₃TT and Planck₁₃TT+highL datasets. We quote 68% C.L., except for upper bounds, which are 95% C.L.

CMB temperature and polarization anisotropies from Planck, WMAP, ACT, SPT and BICEP2/KECK. We have found that, both in a minimal extension of the standard cosmological model ($\Lambda\text{CDM} + g_{\text{eff}}$) and in more complicated scenarios allowing for the presence of extra relativistic degrees of freedom or of primordial tensor perturbations, the strength of non-standard interactions is, quite stable with respect to the models and datasets considered, constrained at 95% C.L to $g_{\text{eff}} < 2.6 \times 10^{-7}$. This, in the most conservative case, corresponds to a recoupling redshift $z_{\text{rec}} \lesssim 9000$ and shows that the possibility of neutrino recoupling happening before recombination is allowed by the data. Moreover, we confirm the preference, also reported in Ref. [23] for non-zero values of the coupling constant, we report a $\sim 1 \sigma$ preference for values of g_{eff} in the range $2.1 \div 2.3 \times 10^{-7}$ corresponding to $z_{\text{rec}} \sim 2000 \div 3500$. In most cases, we find $g_{\text{eff}} \neq 0$ at 68% CL; this tendency is more pronounced when small-scale CMB observations (ACT-SPT), which are sensitive to details of the photon damping regime, are considered, but is alleviated in presence of extra relativistic degrees of freedom if one allows for them. On the other hand, considering a non-vanishing amplitude of tensor modes, still leads to a preference for non-zero coupling at the same level, even for the base

$\Lambda\text{CDM} + g_{\text{eff}} + r$		
	Planck ₁₃ TT	Planck ₁₃ TT +BKP
$\Omega_b h^2$	0.02220 ± 0.00029	0.02216 ± 0.00029
$\Omega_c h^2$	0.1213 ± 0.0029	$0.1218^{+0.0028}_{-0.0031}$
100θ	$1.04211^{+0.00074}_{-0.00083}$	$1.04205^{+0.00075}_{-0.00084}$
τ_{rei}	$0.091^{+0.013}_{-0.015}$	0.091 ± 0.014
n_s	0.9668 ± 0.0079	0.9658 ± 0.076
$\log[10^{10} A_s]$	3.076 ± 0.026	3.077 ± 0.026
$10^{27} g_{\text{eff}}^4$ [95% CL]	< 4.92	< 4.75
$10^{27} g_{\text{eff}}^4$ [68% CL]	$2.23^{+0.84}_{-1.83}$	$2.17^{+0.81}_{-1.79}$
r	< 0.14	< 0.10
H_0 [km/sec/Mpc]	67.7 ± 1.2	67.4 ± 1.2
$10^7 g_{\text{eff}}$ [95% CL]	< 2.65	< 2.61
z_{rec} [95% CL]	< 9400	< 9000
$10^7 g_{\text{eff}}$ [68% CL]	2.17	2.15
z_{rec} [68% CL]	3500	3300
$r_{0.002}$	< 0.13	< 0.09

Table 4.3: Constraints on cosmological parameters for the $\Lambda\text{CDM} + g_{\text{eff}} + r$ model from the analysis of the Planck₁₃TT and Planck₁₃TT+BKP datasets. We quote 68% C.L., except for upper bounds, which are 95% C.L.

Planck₁₃TT dataset.

4.4 Constraints from Planck 2015 data

We decided to develop an updated version of the analysis on massless neutrinos using the latest available Planck data: the 2015 release (see Sec.(1.1) for some details). The theoretical framework is the same used for the 2013 analysis, Sec.(4.1), and also the parametrization is unchanged. In this section we are going to use the Planck₁₅TT, Planck₁₅TP likelihoods with the addition of some astrophysical data, such as Baryon Acoustic Oscillations BAO, Supernovae SN and measurements of H_0 from the Hubble Space Telescope HST (see Sec.(1.1) for details). In analogy to what we have done in

the previous analysis we start from the simplest extension of the standard cosmological model Λ CDM + g_{eff} . In Tab.(4.4) we present the constraints for the main parameters. In particular we obtain $g_{\text{eff}}^4 < 2.9 \times 10^{-27}$ ($g_{\text{eff}} < 2.33 \times 10^{-7}$) using only 2015 Planck temperature data (Planck₁₅TT), $g_{\text{eff}}^4 < 2.78 \times 10^{-27}$ ($g_{\text{eff}} < 2.33 \times 10^{-7}$) adding the additional astrophysical data (Planck₁₅TT+ext) and a more stringent value adding the lensing reconstructed by the Planck team Planck₁₅TT+lensing, i.e. $g_{\text{eff}}^4 < 2.35 \times 10^{-27}$ ($g_{\text{eff}} < 2.20 \times 10^{-7}$). The recoupling redshift are respectively $z_{\text{rec}} < 5050$, 4750, 3800. There is a noticeable improvement with respect to the limit obtained using 2013 Planck

Parameter	Λ CDM + g_{eff}		
	Planck ₁₅ TT	Planck ₁₅ TT + ext	Planck ₁₅ TT + lensing
$\Omega_b h^2$	0.02232 ± 0.00024	0.02237 ± 0.00021	0.02232 ± 0.00023
$\Omega_c h^2$	0.1207 ± 0.0023	0.1200 ± 0.0013	0.1190 ± 0.0020
$100\theta_{MC}$	1.04134 ± 0.00055	$1.04142_{-0.00055}^{+0.00050}$	$1.04143_{-0.00056}^{+0.00051}$
τ_{rei}	0.079 ± 0.020	0.082 ± 0.018	0.062 ± 0.016
n_s	0.9701 ± 0.0066	0.9717 ± 0.0054	0.9719 ± 0.0063
$\ln(10^{10} A_s)$	3.083 ± 0.037	3.088 ± 0.035	3.047 ± 0.030
$10^{27} g_{\text{eff}}^4$ [95% CL]	< 2.9	< 2.78	< 2.35
$10^7 g_{\text{eff}}$ [95% CL]	< 2.33	< 2.3	< 2.20
z_{rec} [95% CL]	< 5050	< 4750	< 3800
H_0 [km/sec/Mpc]	$67.71_{-1.1}^{+0.97}$	68.05 ± 0.56	68.35 ± 0.93
σ_8	0.845 ± 0.015	0.845 ± 0.015	0.825 ± 0.009

Table 4.4: Bayesian credible intervals for the main parameters of the Λ CDM + g_{eff} model obtained using Planck₁₅TT data (first column), Planck₁₅TT+ext (second column) and Planck₁₅TT+lensing (third column).

data, in particular considering that we are comparing the same model using only the temperature data, moreover the results is quite stable also considering the ext dataset. We want to underline that the results improves even further if we decide to introduce the lensing reconstruction which, of course, add information on the small scales. In this analysis we include also σ_8 which is the normalization of the matter power spectrum on scales of $8h^{-1}$ Mpc, for this parameter we find a value $\sigma_8 = 0.845 \pm 0.015$ plenty compatible with the one obtained by the Planck collaboration and still in tension with the astrophysical data e.g. KiDS-450 measures $\sigma_8 = 0.745 \pm 0.039$ [101]. The

“improvement” in the constraints becomes more visible considering the Planck likelihood which includes temperature and polarization data (Planck₁₅TP), results are summarized in Tab.(4.5). In this case we obtain a very stable value for the secret interaction strength: $g_{\text{eff}}^4 < 1.69 \times 10^{-27}$, corresponding to $g_{\text{eff}} < 2.03 \times 10^{-7}$ and $z_{\text{rec}} < 2500$ for Planck₁₅TP and $g_{\text{eff}}^4 < 1.64 \times 10^{-27}$ corresponding to $g_{\text{eff}} < 2 \times 10^{-7}$ and $z_{\text{rec}} < 2300$ for Planck₁₅TP+ext (+lensing). In addition, we report also a predilection for non zero value of the coupling constant, as happened also adding the highL dataset in the 2013 analysis. In particular the best-fit for g_{eff}^4 is fixed to $0.82_{-0.6}^{+0.2} \times 10^{-27}$, which corresponds to $g_{\text{eff}} = 1.7_{-1.4}^{+0.45} \times 10^{-7}$ and to a recoupling redshift of $z_{\text{rec}} = 800$, regardless the data used. The latter result suggests a neutrino-neutrino recoupling happening after the

Parameter	$\Lambda\text{CDM} + g_{\text{eff}}$		
	Planck ₁₅ TP	Planck ₁₅ TP + ext	Planck ₁₅ TP + lensing
$\Omega_b h^2$	0.02230 ± 0.00016	0.02230 ± 0.00014	0.02230 ± 0.00016
$\Omega_c h^2$	0.1194 ± 0.0015	0.1194 ± 0.0010	0.1188 ± 0.0014
$100\theta_{MC}$	1.04127 ± 0.00041	$1.04127_{-0.00038}^{+0.00037}$	$1.04137_{-0.00042}^{+0.00039}$
τ_{rei}	0.082 ± 0.018	0.083 ± 0.017	0.064 ± 0.014
n_s	0.9704 ± 0.0057	0.9705 ± 0.0047	0.9714 ± 0.0054
$\ln(10^{10} A_s)$	3.091 ± 0.034	$3.091_{-0.032}^{+0.033}$	3.052 ± 0.025
$10^{27} g_{\text{eff}}^4$ [95% CL]	< 1.69	< 1.64	< 1.64
$10^{27} g_{\text{eff}}^4$ [68% CL]	$0.82_{-0.6}^{+0.2}$	$0.82_{-0.58}^{+0.18}$	$0.82_{-0.54}^{+0.18}$
$10^7 g_{\text{eff}}$ [95% CL]	< 2.03	< 2.01	< 2.01
$10^7 g_{\text{eff}}$ [68% CL]	$1.7_{-1.4}^{+0.45}$	$1.7_{-1.4}^{+0.45}$	$1.7_{-1.3}^{+0.45}$
z_{rec} [95% CL]	< 2500	< 2300	< 2300
z_{rec} [68% CL]	800	800	800
H_0 [km/sec/Mpc]	68.12 ± 0.69	68.13 ± 0.48	68.38 ± 0.67
σ_8	0.844 ± 0.013	0.845 ± 0.014	0.8262 ± 0.0090

Table 4.5: Bayesian credible intervals for the main parameters of the $\Lambda\text{CDM} + g_{\text{eff}}$ model obtained using Planck₁₅TP data.

photon decoupling, this is the perfect situation in which our method show its power: modifying and evolving directly the Boltzmann equation, instead of roughly switch on and off the tight coupling regime, ensures that even the smallest effects are taken into account. Looking at Figs.(4.2 and 4.3) we know that the (pseudo)scalar interaction

scattering rate grows slowly with time, this leads to a contribution of the scattering term also in modes that are not completely inside the horizon. Let us spend a couple of words on the robustness of the constraints obtained adding other astrophysical data ext and lensing to the standard Planck 2015. Both the 95% and the 68% Bayesian CLs are equal and this means that the most of the information useful to constrain the secret interaction strength is contained in CMB observations, in particular inside the additional contribution given by the polarization data introduced in the 2015 Planck release. In Fig.(4.12) we show the one-dimensional posteriors of the secret dimensionless

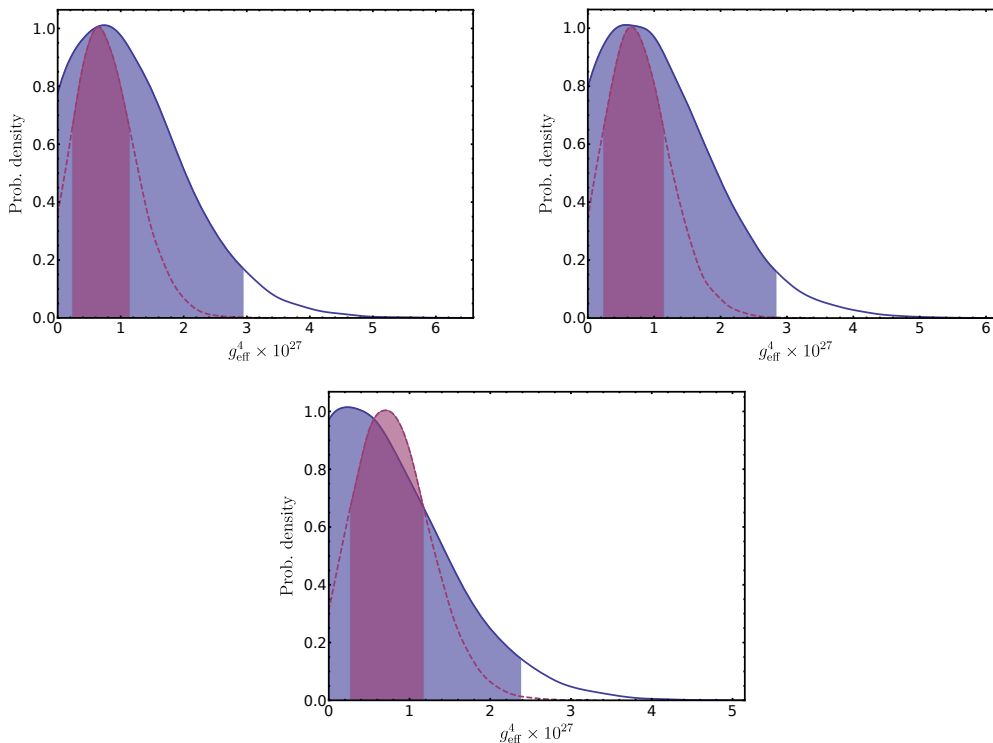


Figure 4.12: One dimensional posterior probability for the interaction strength g_{eff}^4 in the $\Lambda\text{CDM} + g_{\text{eff}}$ model, blue curves always corresponds to Planck₁₅TT and red ones to Planck₁₅TP. In the top left panel we use only 2015 Planck data, the top right picture is representative of Planck₁₅TT+ext and the bottom panel shows posteriors for the Planck₁₅TT+lensing dataset. The shaded areas show the 2σ constraints for the interaction strength (blue lines) and 1σ Bayesian CL (red lines).

coupling constant g_{eff} . In all the plots we presents the Bayesian posterior for the same model $\Lambda\text{CDM} + g_{\text{eff}}$ with all the used datasets (Planck₁₅TT and Planck₁₅TP) in the first figure from the left, we add the ext data in the second figure and lensing in the last one. In this case we present the 1σ level of confidence for the results obtained with temperature and polarization data. Looking at Tab.(4.5) we notice an interesting

shift of some parameters (H_0 , n_s , σ_8) in presence of the secret interaction. Fig.(4.13) shows the one dimensional posterior and the associated correlations for H_0 , n_s and σ_8 parameters between the standard case Λ CDM and our model Λ CDM + g_{eff} . We report a light ($0.4 - 0.5 \sigma$) shift towards larger values for all the considered parameters. It

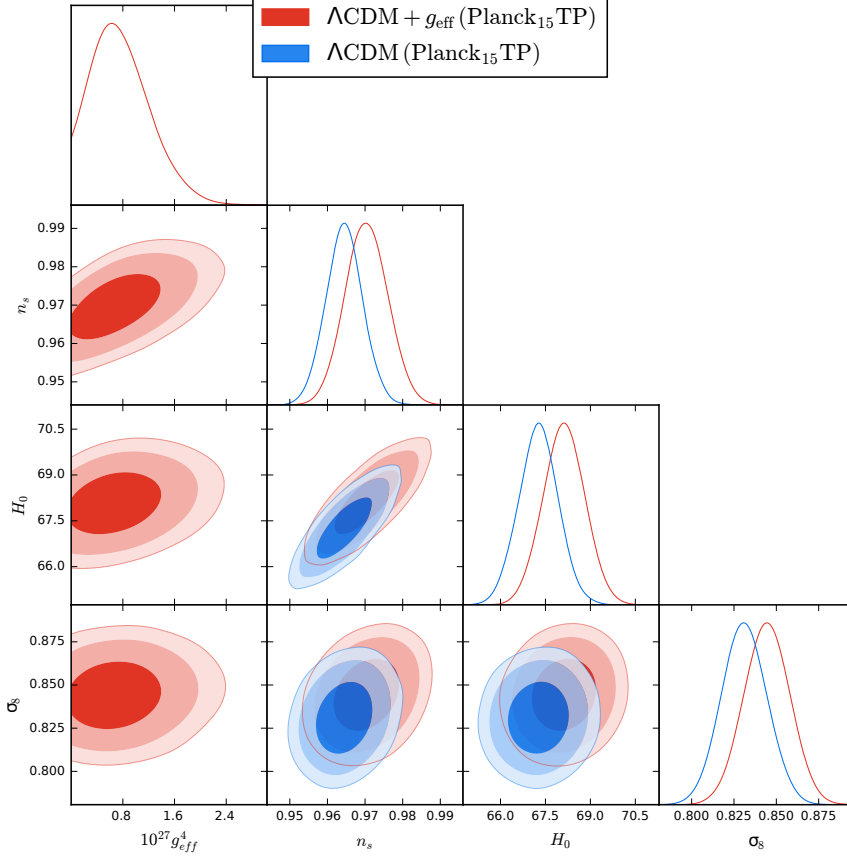


Figure 4.13: One-dimensional and two-dimensional posteriors for Λ CDM (blue) and Λ CDM + g_{eff} (red) models obtained using Planck₁₅TP dataset. We show the credible intervals for the following parameters: $10^{27}g_{\text{eff}}^4$, n_s , H_0 and σ_8 . Shaded areas corresponds to 68%, 95% and 99% CL.

is known that there are tensions between Planck constraints and other astrophysical bounds on H_0 and σ_8 [101, 152], whose origin is still unknown. The constraints obtained in this analysis, on one hand, goes in the direction of alleviate the H_0 tension, but, on the other, increase the discrepancies for σ_8 .

As done in the 2013 analysis, we further extend the parameter space adding one by one the effective number of neutrino families N_{eff} and the tensor to scalar ratio r . Results are summarized in Tab.(4.6). Extending the parameter space including N_{eff} we obtain a constraint on the secret coupling constant $g_{\text{eff}}^4 < 3.1 \times 10^{-27}$ corresponding

to $g_{\text{eff}} < 2.35 \times 10^{-7}$ and $z_{\text{rec}} < 5300$ using the Planck₁₅TT dataset. We found the associated value of $N_{\text{eff}} = 3.09_{-0.33}^{+0.31}$ which is consistent with the constraint obtained by the Planck collaboration [9]. Using the Planck₁₅TP likelihood the constraints becomes: $g_{\text{eff}}^4 < 1.7 \times 10^{-27}$ which corresponds to $g_{\text{eff}} < 2.0 \times 10^{-7}$ and $z_{\text{rec}} < 2400$, while the bound on $N_{\text{eff}} = 3.09_{-0.33}^{+0.31}$ does not change. Passing to the $\Lambda\text{CDM} + g_{\text{eff}} + r$ model we get very similar constraints: using Planck₁₅TT data we report a value for the interaction strength of $g_{\text{eff}}^4 < 2.95 \times 10^{-27}$ corresponding to $g_{\text{eff}} < 2.33 \times 10^{-7}$ and $z_{\text{rec}} < 5000$. Also in this case the tensor to scalar ration is comparable to the value provided by Planck [9]. Let us highlight that every time we use Planck₁₅TP data we recover exactly the same constraints for the coupling constant, regardless the model used, moreover, the value found is always fixed to $g_{\text{eff}}^4 < 1.7 \times 10^{-27}$ at 95% CL with a best-fit value of $g_{\text{eff}}^4 \simeq 2 \times 10^{-27}$. The extremely stable constraints for g_{eff} found in this analysis suggests

Parameter	$\Lambda\text{CDM} + g_{\text{eff}} + N_{\text{eff}}$		$\Lambda\text{CDM} + g_{\text{eff}} + r$	
	Planck ₁₅ TT	Planck ₁₅ TP	Planck ₁₅ TT	Planck ₁₅ TP
$\Omega_b h^2$	$0.02236_{-0.00040}^{+0.00036}$	0.02234 ± 0.00026	0.02233 ± 0.00023	0.02230 ± 0.00016
$\Omega_c h^2$	0.1212 ± 0.0040	0.1200 ± 0.0032	0.1206 ± 0.0023	0.1193 ± 0.0015
$100\theta_{MC}$	$1.04132_{-0.00069}^{+0.00062}$	1.04125 ± 0.00049	$1.04140_{-0.00059}^{+0.00054}$	1.04132 ± 0.00042
τ_{rei}	$0.081_{-0.024}^{+0.021}$	0.084 ± 0.019	0.078 ± 0.019	0.081 ± 0.018
n_s	0.972 ± 0.016	0.972 ± 0.011	0.972 ± 0.007	0.972 ± 0.006
$\ln(10^{10} A_s)$	$3.088_{-0.051}^{+0.047}$	$3.095_{-0.040}^{+0.039}$	3.080 ± 0.037	3.088 ± 0.034
$10^{27} g_{\text{eff}}^4$ [95% CL]	< 3.1	< 1.7	< 2.95	< 1.7
$10^{27} g_{\text{eff}}^4$ [68% CL]	/	$0.82_{-0.6}^{+0.2}$	/	$0.82_{-0.6}^{+0.2}$
N_{eff}	$3.09_{-0.33}^{+0.31}$	3.09 ± 0.21	/	/
r	/	/	< 0.13	< 0.12
H_0 [km/sec/Mpc]	$68.1_{-3.0}^{+2.7}$	68.5 ± 1.8	67.80 ± 0.98	68.20 ± 0.69
$10^7 g_{\text{eff}}$ [95% CL]	< 2.35	< 2.0	2.33	< 2.0
z_{rec} [95% CL]	< 5300	< 2400	< 5000	< 2400
$10^7 g_{\text{eff}}$ [68% CL]	/	$1.7_{-1.4}^{+0.4}$	/	$1.7_{-1.4}^{+0.4}$
z_{rec} [68% CL]	/	800	/	800
σ_8	$0.848_{-0.024}^{+0.021}$	0.847 ± 0.019	0.844 ± 0.015	0.843 ± 0.014

Table 4.6: Constraints on cosmological parameters for the $\Lambda\text{CDM} + g_{\text{eff}} + N_{\text{eff}}$ and $\Lambda\text{CDM} + g_{\text{eff}} + r$ models from the analysis of the Planck₁₅TT and Planck₁₅TP datasets. We quote 68% C.L., except for upper bounds, which are 95% C.L.

that Planck 2015 polarization data are, at the moment, the main source of information for a cosmological study regarding secret neutrino interactions.

A simple way to evaluate how the model under investigation fits the data is to perform a χ^2 test in order to evaluate the goodness of fit. We present the best-fit values of the χ^2 distributions comparing the value our model $\Lambda\text{CDM} + g_{\text{eff}}$ with the standard cosmological model ΛCDM . In Tab.(4.7) lists the separate values of χ^2 divided in independent contributions: χ_{plik}^2 is the value associated to high- ℓ likelihood contribution, while χ_{lowTEB}^2 and χ_{prior}^2 refer to the low- ℓ temperature and polarization and to the priors imposed to the parameters. The secret interacting model under investigation has to be considered nested, that is the ΛCDM can be thought as a special case of $\Lambda\text{CDM} + g_{\text{eff}}$, roughly speaking, if we set the interaction coupling constant to zero, we recover the standard cosmological results. Interestingly enough, using the Planck₁₅TP we notice

	Planck ₁₅ TP		Planck ₁₅ TT	
	ΛCDM	$\Lambda\text{CDM} + g_{\text{eff}}$	ΛCDM	$\Lambda\text{CDM} + g_{\text{eff}}$
χ_{plik}^2	2435.7	2431.6	766.4	765.7
χ_{lowTEB}^2	10496.6	10496.6	10496	10496.6
χ_{prior}^2	12.3	11.8	2.7	1.9
χ_{CMB}^2	12932.3	12929.1	11262.4	11261.3
$-\log(\text{Like})$	12944.7	12941.4	11265.1	11264.3
$\Delta\chi_{\text{min}}^2$		-3.3		-0.8
$-\ln(\text{mean Like})$	12953.1	12950.5	11275.9	11275.7
$\Delta\chi^2$		-2.6		-0.2

Table 4.7: Mean values of the χ^2 distributions for the ΛCDM and the $\Lambda\text{CDM} + g_{\text{eff}}$ models for the Planck₁₅TP dataset (left table) and Planck₁₅TT dataset (right table).

and improvement in the goodness of fit of $\Delta\chi^2 = -2.6$ and $\Delta\chi_{\text{min}}^2 = -3.3$. Putting together this information and the non-zero preference of g_{eff} states that (pseudo)scalar interacting neutrinos not only are not rejected by cosmological data, but they provide a better fit.

Fermi-like interacting neutrinos

Based on [J.Phys.Conf.Ser. 841 (2017) no.1, 012002]
and mainly on [JCAP 1707 (2017) no.07, 038]

In this chapter we are going to introduce a second type of interaction which we had to deal with. The Fermi-like interaction follows what we presented in Sec.(3.2.2), it basically extend the standard weak interaction regime, only in the neutrino sector, in function of the magnitude of the secret coupling constant. The existence of a vector mediator with a mass $m_X < m_{W^\pm}(m_{Z^0})$ allows stronger interactions and this will leave imprints on the anisotropies power spectrum.

5.1 Fermi-like formalism

Fermi-like interaction behaves exactly in the opposite way; we have already presented the physics in Sec.(3.2.2) and roughly the behaviour in Sec.(1.3.2) (in particular Eq.(1.67)), however the case of weak interaction can be generalized assuming the existence of a different mediator M_X having different mass and different couplings \mathfrak{g}_X or G_X^{bin} . The Lagrangian describing this type of interaction has the following form:

$$\mathcal{L}_{\text{F-L}} = \mathfrak{g}_X \bar{\nu}_s \gamma_\mu \frac{1}{2} (1 - \gamma_5) \nu_s X^\mu . \quad (5.1)$$

As we did in the (pseudo)scalar case, we can derive the scattering-to-Hubble rate ratio in matter and radiation dominated epochs: the cross section for such a binary process is:

$$\sigma_X^{\text{bin}} = \left(G_X^{\text{bin}} \right)^2 T_\nu^2 , \quad (5.2)$$

where

$$G_X^{\text{bin}} = \frac{\sqrt{2}}{8} \frac{\mathbf{g}_X^2}{M_X^2}. \quad (5.3)$$

Hence, it is easy to write the scattering rate as:

$$\Gamma_X^{\text{bin}} = \langle \sigma_X^{\text{bin}, \nu} \rangle n_{\text{eq}} \propto \left(G_X^{\text{bin}} \right)^2 T_\nu^5, \quad (5.4)$$

and the ratio with respect the Hubble expansion,

$$\frac{\Gamma_X^{\text{bin}}}{H_r} \sim \left(G_X^{\text{bin}} \right)^2 T_\nu^3, \quad \frac{\Gamma_X^{\text{bin}}}{H_m} \sim \left(G_X^{\text{bin}} \right)^2 (T_\nu)^{\frac{7}{2}}. \quad (5.5)$$

In Fig.(5.2) we show the evolution of the Γ/H ratio for four different values of the couplings G_X^{bin} , the demeanour for the generalized interactions is comparable with standard weak interaction behaviour, what change is, basically, the strength of the cross section. This translates into a late decoupling in the neutrino sector, i.e. the secret interaction remains in equilibrium for longer time. Moreover, a larger value of the coupling constant implies an extremely tight coupling regime in the early universe. The latter aspect, in particular during the evolution of Boltzmann perturbation, must be treated with care. Considering such an interaction in the neutrino sector requires taking into account constraints coming from laboratory experiments [36]. If strong Fermi-like neutrino interactions exist, four-neutrino decays

$$Z^0 \rightarrow \nu\bar{\nu}\nu\bar{\nu}, \quad (5.6)$$

have to contribute to the width of the Z^0 boson. In Fig.(5.1) we can see the two

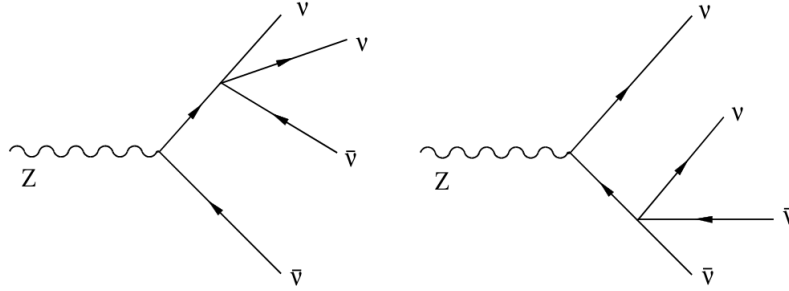


Figure 5.1: Feynman diagrams allowed by the presence of non-standard interaction in the neutrino sector.

possible configurations of Z boson decay into a neutrino-antineutrino pair, one of the products, in turn, can give rise to a “secret” process possible only if non-standard Fermi-like interactions have been introduced in the picture. This allows strong constraints for the interaction coupling constant G_X^{bin} : using the Large Electron-Positron collider

(LEP) data on the invisible decay width $\Gamma_{\text{inv}} = 3\Gamma(Z^0 \rightarrow \nu_\ell \bar{\nu}_\ell)^{\text{SM}} + \Delta\Gamma_{\text{inv}}$ where $\Delta\Gamma_{\text{inv}} = \Gamma(Z^0 \rightarrow \nu \bar{\nu} \nu \bar{\nu})$ in [36] authors found an upper limit for the interaction strength that can be roughly translated into $G_X^{\text{bin}} \lesssim \text{few} \times 10^2 G_F$ (we are not taking into account numerical coefficients). Every cosmological study that pretends to be credible must hold the comparison with laboratory experiments especially if we think that any limit obtained, for example, using CMB data or BBN abundances is not a direct measurement of the physical properties of relic neutrinos. In Fig.(5.2) we show the limit coming from LEP measurements: the green area represents the excluded region, i.e. every value of the coupling G_X^{bin} obtained from cosmological data which lies in that region is excluded a priori.

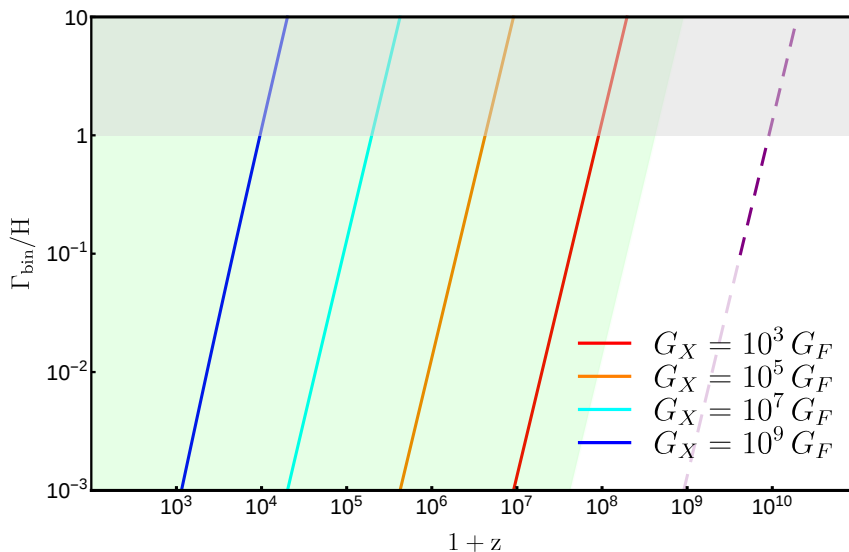


Figure 5.2: Behaviour of Fermi-like interaction in the early universe, we show the ratio between the scattering rate and the Hubble rate in function of the redshift. Red, orange, cyan and blue lines correspond to four different values of G_X couplings, while purple dashed line is always the weak interaction (G_F). The gray shaded zone corresponds to the region where $\Gamma/H > 1$, while the green region represents the part excluded by constraints coming from laboratory experiments [36].

5.2 Massive sterile neutrinos

In light to laboratories observations and constraints [36] we decided to investigate a scenario that should not be completely ruled out. Considering non standard Fermi-like

interaction in the massless neutrino sector has been studied in some works [23, 53, 115] where the authors found upper limits for the interaction strength G_X several orders of magnitude above the limits coming from LEP. Hence we decided to investigate this type of interaction inside the sterile neutrino sector. In recent years there has been a renewed interest towards light sterile neutrinos, suggested by different anomalies observed in short-baseline (SBL) neutrino experiments (see [3, 80, 81, 112] for recent reviews).

The existence of an extra neutrino eigenstate is hinted in short-baseline neutrino experiments [3, 81], in particular laboratory data suggest a sterile neutrino mass of the order of 1 eV and active-sterile mixing angle $\theta_{as} \simeq 0.1$. The production of this new state in the primordial universe would lead to an increase in the extra-relativistic energy content $\Delta N_{\text{eff}} \simeq 1$ in tension with the actual bounds coming from the Planck experiment and with other cosmological bounds [93, 97, 136]. In order to avoid this behaviour several mechanisms have been proposed in the literature, e.g. scenarios with large primordial neutrino asymmetries [136, 157].

An alternative approach introduces a Fermi-like non-standard interaction between active and sterile eigenstates mediated by a massive gauge boson X , with $M_X \ll M_W$ [39, 54, 96]. The strength of the non-standard secret interaction G_X drives the collisional rate and as long as the universe expands the matter potential generated by the secret coupling declines leading to a resonance in the sterile neutrino sector. This translates into a sterile production due to the combination of the resonant Mikheyev-Smirnov-Wolfenstein effect (see Sec.(3.2.7) and non-resonant Dodelson-Widrow production [164]. Considering a coupling constant $g_X \leq 10^{-2}$ and for masses of the mediator larger or of the order of 10 eV, the sterile production would have a considerable effect on the light elements production during the Big Bang Nucleosynthesis (BBN). Assuming smaller values of the mediator mass, sterile neutrinos would still be produced at $T \ll 0.1$ MeV [158]. Mirizzi et al. in [136] have shown that in a certain region of the parameter space (g_X - M_X) where the mass of the mediator is smaller enough to allow the sterile production after the neutrino decoupling, the process of flavour equilibration is fast and produces a sizeable ν_s abundance. In addition this mechanism reduces the effective number of neutrinos to $N_{\text{eff}} \simeq 2.7$ at matter radiation equality (see Sec.(5.2.1) for further details) [136, 158].

The existence of a possible window for this secret interaction which allows the presence of a sterile eigenstate without adding a tension in the extra-relativistic energy content is tempting. Aim of this paper is to investigate a secret Fermi-like interaction considering a scenario with 3 active massive neutrinos, having $\sum_i m_{\nu_i} = 0.06$ eV and one light $m_{\nu_s} \sim 1$ eV sterile neutrino.

5.2.1 Sterile neutrino production in the primordial Universe

The existence of a fourth sterile neutrino eigenstate requires the extension of the standard 3 neutrino families scenario to a 3 + 1 active-sterile neutrino mixing scenario. Describing the neutrino system in terms of 4×4 density matrices $\rho = \rho(p)$, the active-sterile flavour evolution is ruled by the kinetic equations [63]

$$i \frac{d\rho}{dt} = [\Omega, \rho] + C[\rho], \quad (5.7)$$

see [137] for a detailed treatment. The first term on the right-hand side of Eq.(5.7) describes the flavour oscillations Hamiltonian, given by

$$\begin{aligned} \Omega = & \frac{M^2}{2p} + \sqrt{2} G_F \left[-\frac{8p}{3} \left(\frac{E_\ell}{M_W^2} + \frac{E_\nu}{M_Z^2} \right) \right] \\ & + \sqrt{2} G_X \left[-\frac{8pE_s}{3M_X^2} \right], \end{aligned} \quad (5.8)$$

where $M^2 = \mathcal{U}^\dagger \mathcal{M}^2 \mathcal{U}$ is the neutrino mass matrix in flavour basis, with \mathcal{U} the active-sterile vacuum mixing matrix (see Ch.(3) for details). The terms proportional to the Fermi constant G_F in Eq.(5.8) are the standard matter effects in active neutrino oscillations, while the term proportional to G_X represents the new matter secret potential. Inter alia, E_ℓ is related to the energy density of e^- and e^+ , while E_ν corresponds to the ν - ν interaction term proportional to a primordial neutrino asymmetry (that it is assumed to be negligible). Finally E_s is the energy density associated with ν_s . The last term is the collisional integral given by the sum of the standard ($\propto G_F^2$) and the secret one ($\propto G_X^2$).

As said before, the strong collisional effects produce a damping of the resonant transitions and would bring the system towards the flavour equilibrium among the different neutrino species with a production rate given by [107, 135]

$$\Gamma_t \simeq \langle P(\nu_\alpha \rightarrow \nu_s) \rangle_{\text{coll}} \Gamma_X, \quad (5.9)$$

where $\langle P(\nu_\alpha \rightarrow \nu_s) \rangle_{\text{coll}}$ is the average probability of conversions among an active ν_α and a sterile neutrino ν_s in a scattering time scale $(\Gamma_X)^{-1}$, where the scattering rate is given by a slightly different version of the Eq.(5.4) weighed by the sterile and active neutrino abundance n_s and n_a :

$$\Gamma_X \simeq G_X^2 T_\nu^5 \frac{p}{\langle p \rangle} \frac{n_s}{n_a}. \quad (5.10)$$

In the latter equation $\langle p \rangle \simeq 3.15 T_\nu$ is the average-momentum for a thermal Fermi-Dirac distribution.

It is possible to constrain the secret interaction using different cosmological observ-

ables. In [158] the authors perform a study on deuterium primordial abundances ${}^2H/H$ for a coupling constant $g_X \gtrsim 10^{-2}$ and masses of the mediator $M_X \gtrsim 10$ MeV, thus excluding a large part of the parameter space. Alteration in the production of light elements during BBN is due to a larger value of N_{eff} and to the spectral distortion of electron neutrinos when active-sterile oscillations occur close to the neutrino decoupling. Taking smaller values of the mediator mass the sterile production is suppressed before the neutrino decoupling and this choice leaves unchanged the BBN dynamics, but at temperatures less than 1 MeV sterile neutrinos are still in a collisional regime, due to their secret self-interactions. Neglecting the contribution of the resonance and considering only a pure collisional production, the average probability of conversion takes the form:

$$\langle P(\nu_a \rightarrow \nu_s) \rangle \simeq \frac{1}{2} \sin^2 \theta_{as}. \quad (5.11)$$

In this framework even a small population of sterile neutrinos can generate a large scattering rate at relatively low temperatures for sufficiently large values of the coupling constant G_X . In particular if $G_X > 10^8 G_F$. The decoupling of the non-standard interaction would take place at redshift $z \sim 5 \times 10^4$. This implies the following energy density equilibration, going from an initial energy density to a final one [135]:

$$\rho_\nu^{\text{in}} = 3 \cdot \frac{7}{8} \left(\frac{4}{11} \right)^{\frac{4}{3}} \rho_\gamma \rightarrow \rho_\nu^{\text{fin}} = 4 \left(\frac{3}{4} \right)^{\frac{4}{3}} \cdot \frac{7}{8} \left(\frac{4}{11} \right)^{\frac{4}{3}} \rho_\gamma. \quad (5.12)$$

The consequence of this behaviour is a reduction in the energy density of the neutrino sector which translates into a slightly lower value for the effective number of neutrino families with respect to the standard value:

$$N_{\text{eff}} = 4 \cdot \left(\frac{3}{4} \right)^{\frac{4}{3}} = 2.7. \quad (5.13)$$

The latter basically means that neutrinos encounter a fast flavour equilibration between the three active and the sterile species, leading from an initial abundance

$$(n_e, n_\mu, n_\tau, n_s)_{\text{initial}} = (1, 1, 1, 0), \quad (5.14)$$

to a final one:

$$(n_e, n_\mu, n_\tau, n_s)_{\text{final}} = \left(\frac{3}{4}, \frac{3}{4}, \frac{3}{4}, \frac{3}{4} \right), \quad (5.15)$$

for all the parameters associated with eV sterile neutrino anomalies. Soon after ν_s are produced via oscillation, active and sterile neutrinos have a shared grey-body distribution, namely a Fermi-Dirac function weighted by a factor $3/4$ for each species. However, in the presence of strong secret interactions, these grey-body distributions will fastly evolve towards a Fermi-Dirac equilibrium function. The constant number density (or entropy) constraint implies that the temperature of this final spectrum is

reduced by a factor $(3/4)^{1/3}$ with respect to the initial active neutrino temperature $T_\nu = (4/11)^{1/3}T_\gamma$. As a consequence of this effect, the total energy density stored in active and sterile neutrinos is reduced and the value of the effective number of neutrino species decreases down to $N_{\text{eff}} \sim 2.7$ for relativistic neutrinos. A further slight reduction would occur at the matter radiation equality, i.e. for $T_\gamma \sim 0.7$ eV since eV sterile neutrinos would not be fully relativistic.

Secret interactions also affect the evolution of perturbations in the sterile neutrino fluid. In fact, if sterile states scatter via secret interactions, the free streaming regime is delayed until the scattering rate becomes smaller than the Hubble parameter. It means that if G_X is large enough so that this condition holds at the non relativistic transition, sterile neutrinos would never have a free streaming phase, but always diffuse [135]. One can obtain the smaller value of G_X for which this occurs comparing the scattering rate with the Hubble rate H at a temperature $3.15T_\nu \sim \langle p \rangle \sim m_s$

$$G_X^2 T_\nu^5 \sim H(T_\gamma) . \quad (5.16)$$

Writing the Hubble rate for $T_\gamma \sim$ eV and using that $T_\nu = (4/11)^{1/3}(3/4)^{1/3}T_\gamma$ one obtains:

$$G_X \sim 10^{10} G_F , \quad (5.17)$$

which corresponds to $M_X \sim 10^{-1}$ MeV for $g_X \simeq 10^{-1}$.

5.2.2 Sterile massive interacting neutrinos

As we have done for the (pseudo)scalar massless case, we act directly introducing a scattering term in the right-hand side of on the Boltzmann equation, however, in this work we have to deal with massive neutrinos and thus it requires a modification of the massive version Eq.(1.128):

$$\frac{\partial \Psi_i}{\partial \tau} + i \frac{q(\vec{k} \cdot \hat{n})}{\epsilon} \Psi_i + \frac{d \ln f_0}{d \ln q} \left[\dot{\eta} - \frac{\dot{h} + 6\dot{\eta}}{2} (\hat{k} \cdot \hat{n})^2 \right] = -\Gamma_{ij} \Psi_j , \quad (5.18)$$

where the indices i and j label neutrino mass eigenstates, and summation over repeated indices should be understood. Considering massive neutrinos introduces several issues to take into account, first of all we have to derive the interacting hierarchy, From a computational point of view it is necessary to pass through a series of approximations. Basically when the CAMB Boltzmann code follows the massive neutrino fluid evolution it evolves three set of equation: one for the massless regime, one for the massive regime and a final set of perturbations (let us call them *quasi-massive* regime) that would be added to the massless regime in order to recover gradually the massive one. The purpose of studying a secret interaction in the neutrino fluid requires the proper addition of the scattering term in every step of the approximation.

Massless and quasi-massless approximations

Let us start considering the complete derivation of the whole set of equations for the massless and quasi-massive regimes, the basic elements are:

$$\nu'_\ell = \frac{kv}{(2\ell+1)} \left[\ell \nu_{(\ell-1)} - (\ell+1) \nu_{(\ell+1)} \right] + \frac{8}{15} k \sigma \delta_{\ell 2} - \frac{4}{3} k Z \delta_{\ell 0} \quad (5.19)$$

$$- a \Gamma \nu_\ell (1 - \delta_{\ell 0}) (1 - \delta_{\ell 1}) ,$$

$$\nu_\ell = J_\ell + \epsilon_v \Delta J_\ell , \quad (5.20)$$

where, mirroring the notation of Ref. [121], $\nu_\ell = -4F_{\nu\ell} / \left(\frac{d \ln F}{d \ln q} \right)$, while the metric (its derivatives) are hidden inside $Z = \frac{\dot{h}}{2k}$ and $\sigma = \frac{\dot{h} + 6\dot{\eta}}{k}$. Finally J_ℓ and ΔJ_ℓ are the massless unperturbed part of the neutrino fluid term and the correspondent perturbation. The perturbed part of the neutrino distribution function is weighted by the term $\epsilon_v = \frac{m^2}{2q^2}$ that appears also in the time dependent velocity $v = q/\epsilon \sim 1 - a^2 \epsilon_v$. Thus by definition a perturbed approximation is valid when the $\epsilon_v < 1$. Thus replacing Eq.(5.20) inside Eq.(5.19) we get:

$$J'_\ell + \epsilon_v \Delta J'_\ell = \frac{k(1 - a^2 \epsilon_v)}{(2\ell+1)} \left[\ell (J_{(\ell-1)} + \epsilon_v \Delta J_{(\ell-1)}) - (\ell+1) (J_{(\ell+1)} + \epsilon_v \Delta J_{(\ell+1)}) \right] + \frac{8}{15} k \sigma \delta_{\ell 2} - \frac{4}{3} k Z \delta_{\ell 0} - a \Gamma (J_\ell + \epsilon_v \Delta J_\ell) (1 - \delta_{\ell 0}) (1 - \delta_{\ell 1}) . \quad (5.21)$$

The zero-th order, of the latter equation can be written in the following way:

$$J'_\ell = \frac{k}{2\ell+1} \left[\ell J_{(\ell-1)} - (\ell+1) J_{(\ell+1)} \right] + \frac{8}{15} k \sigma \delta_{\ell 2} - \frac{4}{3} k Z \delta_{\ell 0} - a \Gamma J_\ell \tilde{\delta}_{\ell 0} \tilde{\delta}_{\ell 1} , \quad (5.22)$$

where $\tilde{\delta}_{\ell i} = (1 - \delta_{\ell i})$. Expanding in the harmonic space the latter equation leads to the interacting hierarchy:

$$J'_0 = -k J_1 - \frac{4}{3} k Z , \quad (5.23a)$$

$$J'_1 = \frac{k}{3} (J_0 - 2J_2) , \quad (5.23b)$$

$$J'_2 = \frac{k}{5} (2J_1 - 3J_3) - \frac{8}{15} k \sigma - a \Gamma J_2 , \quad (5.23c)$$

$$J'_\ell = \frac{k}{(2\ell+1)} \left[\ell J_{(\ell-1)} - (\ell+1) J_{(\ell+1)} \right] - a \Gamma J_\ell \quad (\ell \geq 3) . \quad (5.23d)$$

Which is exactly what we have presented in Eq.(4.13), i.e. the massless case. Instead the first-order perturbative part of Eq.(5.19) can be written as:

$$\begin{aligned} \epsilon_v \Delta J'_\ell &= \frac{k}{2\ell+1} [\ell \epsilon_v \Delta J_{(\ell-1)} - (\ell+1) \epsilon_v \Delta J_{(\ell+1)}] \\ &\quad - \frac{ka^2 \epsilon_v}{2\ell+1} [\ell J_{(\ell-1)} - (\ell+1) J_{(\ell+1)}] - a\Gamma \epsilon_v \Delta J_\ell \tilde{\delta}_{\ell 0} \tilde{\delta}_{\ell 1}, \end{aligned} \quad (5.24)$$

Once again, performing an expansion in the harmonic space we can find an infinite hierarchy,

$$\Delta J'_0 = -k \Delta J_1 + ka^2 J_1, \quad (5.25a)$$

$$\Delta J'_1 = \frac{k}{3} (\Delta J_0 - 2\Delta J_2) - \frac{ka^2}{3} (J_0 - 2J_2), \quad (5.25b)$$

$$\begin{aligned} \Delta J'_\ell &= \frac{k}{2\ell+1} (\ell \Delta J_{(\ell-1)} - (\ell+1) \Delta J_{(\ell+1)}) \\ &\quad - \frac{ka^2}{2\ell+1} (\ell J_{(\ell-1)} - (\ell+1) J_{(\ell+1)}) - a\Gamma \Delta J_\ell \quad (1 \geq 2). \end{aligned} \quad (5.25c)$$

In order to truncate the series we need to derive the correspondent approximation, thus, one again, we start from the general form,

$$\begin{aligned} J'_\ell + \Delta J'_\ell &= k (1 - a^2 \epsilon_v) (J_{(\ell_{\max}-1)} + \epsilon_v \Delta J_{(\ell_{\max}-1)}) \\ &\quad - (\ell_{\max} + 1) \frac{1}{\tau} (J_{\ell_{\max}} - \epsilon_v \Delta J_{\ell_{\max}}) - a\Gamma (J_{\ell_{\max}} + \epsilon_v \Delta J_{\ell_{\max}}), \end{aligned} \quad (5.26)$$

where the zero-th order, which again represent the pure massless part, is:

$$J'_{\ell_{\max}} = k J_{(\ell_{\max}-1)} - (\ell_{\max} + 1) \frac{1}{\tau} J_{\ell_{\max}} - a\Gamma J_{\ell_{\max}}, \quad (5.27)$$

and at the perturbation level, we get:

$$\Delta J'_{\ell_{\max}} = k \Delta J_{(\ell_{\max}-1)} + (\ell_{\max} + 1) \frac{1}{\tau} \Delta J_{\ell_{\max}} - ka^2 J_{(\ell_{\max}-1)} - a\Gamma J_{\ell_{\max}}. \quad (5.28)$$

Tight coupling regime Dealing with a Fermi-like interaction and ignoring, a priori, the magnitude of the coupling requires the developing of a tight coupling approximation valid in the $\Gamma \gg H$ regime. Allowing large values of G_X in the scattering part of the Boltzmann hierarchy will change dramatically the derivative of the shear (it would be also negative) and thus will introduce discontinuities in the shear, velocity and density. This is a big issue in the numerical solution of Boltzmann equations. We act on the massless, massive and quasi-massive approximation, basically setting to zero the derivative of the shear $\dot{\sigma}_\nu$ (J'_2) for the massless case, $\dot{\Psi}_2$ for massive neutrinos and $\Delta J'_2$ for the quasi-massive hierarchy. In this way we obtain an expression for the shear, in

every case, that takes into account the presence of the secret interaction:

$$J_2 = -\Gamma^{-1} \left[\frac{2}{5} k J_1 + \frac{8}{15} k \sigma \right], \quad (5.29)$$

$$\Delta J_2 = -\Gamma^{-1} \frac{2}{5} \Delta J_1. \quad (5.30)$$

Massive approximation

It is possible to make the same calculation also for the massive Boltzmann equation, starting from Eq.(5.18) rewriting the latter as infinite hierarchy of multipoles:

$$\dot{\Psi}_{i,0} = -\frac{qk}{\epsilon} \Psi_{i,1} + \frac{1}{6} \dot{h} \frac{d \ln f_0}{d \ln q}, \quad (5.31a)$$

$$\dot{\Psi}_{i,1} = \frac{qk}{3\epsilon} (\Psi_{i,0} - 2\Psi_{i,2}), \quad (5.31b)$$

$$\dot{\Psi}_{i,2} = \frac{qk}{5\epsilon} (2\Psi_{i,1} - 3\Psi_{i,3}) - \left(\frac{1}{15} \dot{h} + \frac{2}{5} \dot{\eta} \right) \frac{d \ln f_0}{d \ln q} - \Gamma_{ij} \Psi_{j,2}, \quad (5.31c)$$

$$\dot{\Psi}_{i,\ell} = \frac{qk}{(2\ell+1)\epsilon} \left[\ell \Psi_{i,(\ell-1)} - (\ell+1) \Psi_{i,(\ell+1)} \right] - \Gamma_{ij} \Psi_{j,\ell} \quad (\ell \geq 3), \quad (5.31d)$$

The associated tight coupling approximation can be written in the following way:

$$\Psi_2 = -\Gamma^{-1} \left[\frac{2}{5} k v \Psi_1 \right]. \quad (5.32)$$

5.2.3 Effects on the cosmological perturbations

As said before, Boltzmann codes like `camb` [120] evolve the perturbations in the distribution functions of the mass eigenstates. In order to obtain the scattering rates between mass eigenstates, those should be projected from the flavour basis through the mixing matrix. We shall assume that the sterile state is the superposition of the 1 and 4 mass eigenstates through the vacuum mixing angle θ_s as

$$\nu_s \simeq \sin \theta_s \nu_1 + \cos \theta_s \nu_4, \quad (5.33)$$

so that we are in the situation in which the mass eigenstates ν_1 and ν_4 interact with relative rates $\sin^2 \theta_s$ and $\cos^2 \theta_s$, while ν_2 and ν_3 are essentially free-streaming [44], and

the scattering rate term becomes:

$$\Gamma_{ij} = \begin{bmatrix} \sin^2 \theta_s & 0 & 0 & \sin \theta_s \cos \theta_s \\ 0 & 0 & 0 & 0 \\ 0 & 0 & 0 & 0 \\ \sin \theta_s \cos \theta_s & 0 & 0 & \cos^2 \theta_s \end{bmatrix} (3/2)(\zeta(3)/\pi^2) aG_X^2 T_\nu^5. \quad (5.34)$$

where we considered the mass basis in order to evolve the perturbations inside the public code `camb`, basically considering the sterile state as a superposition of neutrino mass eigenstates ν_1 and ν_4 . The latter equation will be the scattering ration we will use inside the hierarchy equations presented in the previous section. Looking at the Eq.(5.34) it is evident that the interaction will act on the first and fourth massive eigenstates while ν_2 and ν_3 remains unchanged, in particular we expect to see the greater contribution on the sterile eigenstate, which is weighted with a $\cos^2 \theta_s$ while the first eigenstate is affected by the interaction by a smaller $\sin \theta_s \cos \theta_s$ factor. In Fig.(5.3) it is possible to appreciate the effects of the interaction on the density perturbations $\delta_\nu = \delta\rho_\nu/\rho_\nu$ (the first order of Boltzmann hierarchy) for different perturbation wave numbers. Out of the horizon the physics is unchanged and the evolution is dominated by the metric perturbation. As the mode enters the horizon it starts to oscillate and from this moment on the dynamic is influenced by micro-physics, thus the larger the magnitude of the interaction the larger the effects on the oscillations of the density perturbations. Considering the interacting cases, the blue dashed line refers to the mode $k = 0.5 \text{ Mpc}^{-1}$ which crosses the horizon at approximately $z \sim \text{few} \times 10^5$, the mode $k = 0.05 \text{ Mpc}^{-1}$ (red dashed line) enters the horizon at a redshift an order of magnitude lower, this translates into a greater effect. The impact of the interaction is larger, as we have predicted, on the ν_4 and ν_1 density perturbations, however we notice that, even if the ν_2 and ν_3 , in principle, should not be affected by the interaction, the associated density perturbations are slightly affected by the metric. Looking at the the middle-right panel, the $k = 0.5 \text{ Mpc}^{-1}$ mode for the interacting case, it is possible to appreciate a small increase in the amplitude of the oscillations where the effect of the interaction is supposed to be stronger.

Let us move to the CMB APS, the net effect of the interaction is that, at scales that are within the horizon during the interacting regime, density and pressure perturbations are enhanced with respect to the non-interacting case. This enhancement propagates to the photon fluid, and thus to CMB anisotropies, through the metric perturbations, as it can be clearly seen in Fig.(5.4), where we plot the temperature angular power spectrum (APS) (multiplied by an additional factor of ℓ^2) for three models with an interacting sterile neutrino with $m_s = 1 \text{ eV}$ and different values of the coupling strength G_X . In all cases we take $N_{\text{eff}} = 2.7$, consistently with the expectation of flavour equilibration.

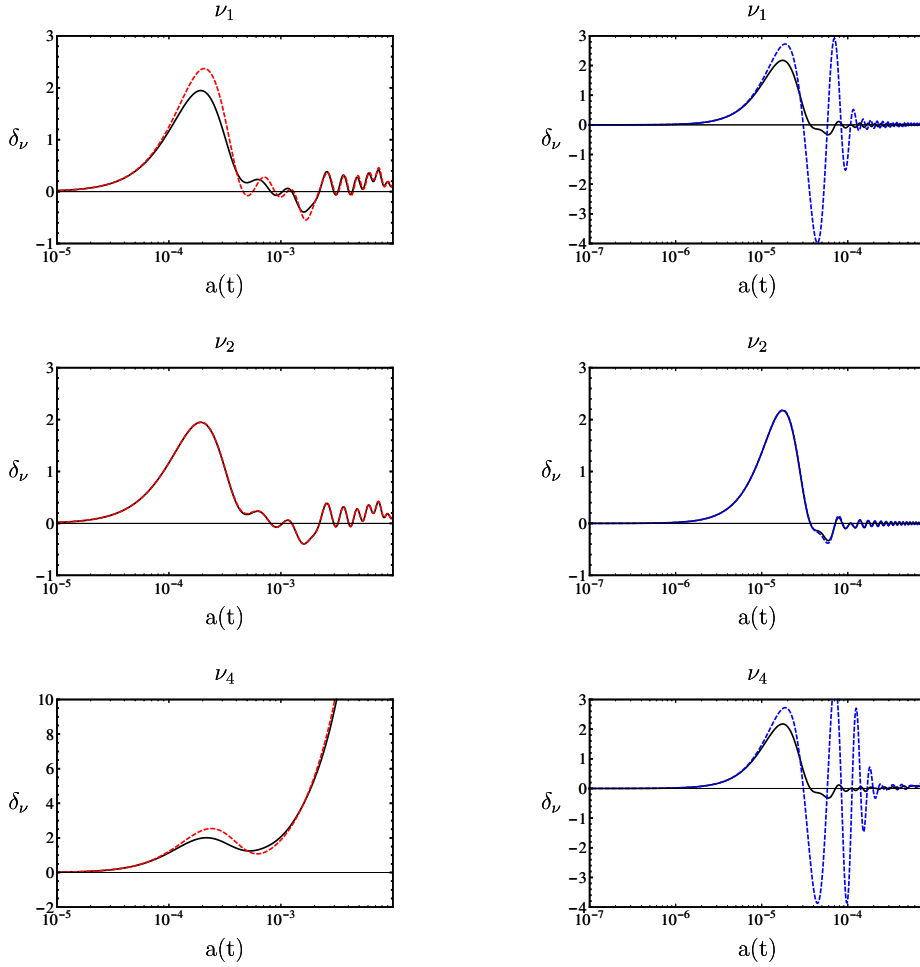


Figure 5.3: Density perturbations as function of the universe scale factor $a(t)$ for 3 light massive active neutrinos with $\sum m_\nu = 0.06 \text{ eV}$ and 1 massive sterile with $m_s = 1 \text{ eV}$ models. We performed the analysis for two different wave numbers, left column $k = 0.05 \text{ Mpc}^{-1}$, right column $k = 0.5 \text{ Mpc}^{-1}$, in case of no interaction (black solid line) and in case of interaction mediated by a coupling constant $G_X = 10^5 G_F$ (coloured dashed line)

The prediction for the case with $G_X \sim 10^8 G_F \simeq 10^3 \text{ GeV}^{-2}$ is practically identical to that of a ΛCDM extension with one non-interacting sterile neutrino and $N_{\text{eff}} = 2.7$. This means that there is a range of values around $G_X \sim 10^8 G_F$ in which we still have a copious production of sterile neutrinos and flavour equilibration, but no direct effects of the interaction are visible on the APS (still, the effective number of relativistic degrees of freedom is $N_{\text{eff}} = 2.7$). Larger values of G_X change the spectrum by increasing the

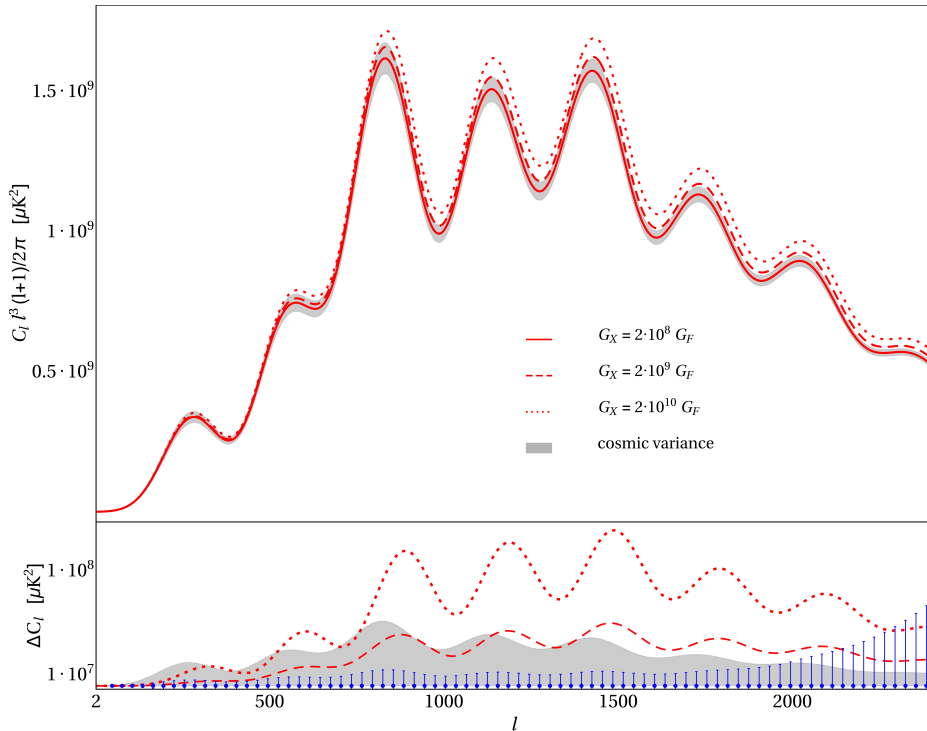


Figure 5.4: CMB temperature anisotropies power spectrum. In the upper panel, we show spectra for three different values of the coupling constant $G_X = 2 \times \{10^8, 10^9, 10^{10}\} G_F$ (red solid, dashed, dotted lines, respectively). The non-interacting case is undistinguishable from the $G_X = 2 \times 10^8 G_F$ case. The APS is obtained assuming 3 active neutrinos having $\sum m_i = 0.06$ eV and a sterile neutrino species with $m_s = 1$ eV. In the lower panel, we show residuals with respect to the non-interacting case. The error bars represent the uncertainties of the Planck 2015 data.

power below a critical scale, related to the size of the horizon at the time at which neutrinos enter the free-streaming regime. For the parameter values used in the plot, we have that the comoving scale that enters the horizon at this time is $k \simeq 0.01 \text{ Mpc}^{-1}$ ($k \simeq 0.03 \text{ Mpc}^{-1}$), mapped to $\ell \simeq 130$ ($\ell \simeq 400$) for $G_X = 10^9 G_F$ ($G_X = 10^{10} G_F$).

5.3 Cosmological analysis

In this section we discuss our analysis of available cosmological data to constrain the coupling of the secret interaction. We first describe the method and data used, and

then we present our results.

5.3.1 Method and data

We use the Boltzmann code `camb`, modified as described in the previous section, to follow the evolution of cosmological perturbations and compute the CMB anisotropy power spectra for given values of the cosmological parameters, including the secret coupling G_X and the mass $m_s \equiv m_4$ of the (mostly) sterile neutrino. In order to derive Bayesian credible intervals for the parameters, we use the Markov Chain Monte Carlo (MCMC) engine `CosmoMC` [122] (interfaced with the modified `camb`). Our parameter space consists of the six parameters of the Λ CDM model, augmented by the parameters describing the sterile neutrino sector. As we show in the previous section, the neutrino sector is described by the secret coupling G_X and the sterile neutrino mass m_s . As explained in the previous section, we fix $N_{\text{eff}} = 2.7$, consistently with the assumption that all neutrino states (both active and sterile) have a common temperature $T_\nu = (3/11)^{1/3}T_\gamma$. This amounts to the assumption that $G_X \gtrsim 10^8 G_F$. We also fix the active-sterile mixing angle to $\theta_s = 0.1$ and the sum of the masses of the (mostly) active neutrinos to 0.06 eV, equally shared among three mass eigenstates, see Sec.(5.2). We further assume flat spatial geometry and adiabatic initial conditions.

In our analysis, we always take flat, wide (in the sense that they are much larger than the expected posterior widths) priors for the six Λ CDM parameters. We also consider priors on G_X and m_s in order to model limiting cases of the scenario under consideration, to include additional pieces of experimental information, or simply to explore different regions of the parameter space. We start by performing a set of exploratory MCMC runs in which we assume a flat prior distributions in $\log_{10} [G_X]$ and m_s . The advantage of a logarithmic prior in G_X is that it allows to explore several orders of magnitude in the parameter with equal probability per decade and thus to assess when the effect of secret interactions on the CMB APS becomes “large”, at least in comparison with the experimental sensitivity. However, a logarithmic prior gives more weight to small values of the parameter with respect to a flat prior, resulting in tighter bounds on the parameter itself. Moreover, it is an improper prior, since it does not integrate to a finite value if $G_X \geq 0$, and in order to give meaningful credible intervals an arbitrary, non-zero, lower bound on G_X has to be assumed. For these reasons, we only use the results from this analysis to estimate the sensitivity of the data to G_X and to gauge the initial step of the subsequent MCMC runs, that always use a flat prior on G_X .

The full model, in which the Λ CDM parameters as well as G_X and m_s are varied, is dubbed $\text{S}\Lambda\text{CDM}$ (standing for “ Λ CDM with secret interactions”). In this case, and unless otherwise stated, we take flat and wide priors also on G_X and m_s . Note that, as explained above, we always have $N_{\text{eff}} = 2.7$. A limiting scenario is obtained by fixing G_X to a very small value in our modified `camb` while keeping $N_{\text{eff}} = 2.7$, in order to

reproduce the case in which G_X is large enough for the flavour equilibration to happen, while still being small enough not to affect the evolution of cosmological perturbations. As we have mentioned, this approximately corresponds to $G_X \sim 10^8 G_F$. Since, as noted in the previous section, this case is practically indistinguishable, as long as the evolution of cosmological perturbations is concerned, from a Λ CDM scenario with $N_{\text{eff}} = 2.7$ and $G_X = 0$, we shall refer to this model as “SACDM_GX0”. Finally, we also consider prior on m_s to model information from short baseline experiments. We refer to Ref. [81] in which the allowed 3σ (i.e., 99.73% CL) range for the squared mass difference $\Delta m_{41}^2 = m_4^2 - m_1^2$ that explains the SBL anomalies is $0.87 \text{ eV}^2 \leq \Delta m_{41}^2 \leq 2.04 \text{ eV}^2$. Not knowing the full shape of the probability density distribution for m_s , we decided to model it considering two “extreme” cases: in the first (“narrow m_s prior”) we impose a gaussian prior $m_s = 1.27 \pm 0.03 \text{ eV}$ (the width of the prior is chosen to match the 1σ confidence interval for Δm_{41}^2 [81], assuming $m_4 \gg m_1$), while in the second (“broad m_s prior”) we impose a flat prior $0.93 \text{ eV} \leq m_s \leq 1.43 \text{ eV}$, corresponding to the 3σ interval reported above. Finally, we will often compare our results to those obtained in the framework of the standard Λ CDM model; for these, we refer to the values reported in the Planck 2015 parameters paper [10], and in this case it should be understood that $N_{\text{eff}} = 3.046$ [55, 132]. A list of the abbreviations used for the models considered in this paper, including a short description, can be found in Tab.(5.1).

Our data consists of the baseline Planck 2015 dataset (dubbed **Planck₁₅TT**), see Appendix.(A) for detail on the datasets. We also consider geometrical information coming from baryon acoustic oscillations; in particular we make use of the BAO results. The extended dataset combining the Planck 2015 data with the BAO information will be denoted **Planck₁₅TT + BAO**). Once again we refer to Appendix.(A) for details on the used datasets.

Description	
Λ CDM	Standard six-parameter Λ CDM, $N_{\text{eff}} = 3.046$.
SACDM_GX0	Sterile neutrino extension, $N_{\text{eff}} = 2.7$, m_s free, “small” G_X ($\sim 10^8 G_F$).
SACDM	Sterile neutrino extension, $N_{\text{eff}} = 2.7$, m_s and G_X free.
SACDM_Narrow	Sterile neutrino extension, $N_{\text{eff}} = 2.7$, G_X free, $m_s = 1.27 \pm 0.03 \text{ eV}$ (gaussian prior).
SACDM_Broad	Sterile neutrino extension, $N_{\text{eff}} = 2.7$, G_X free, $0.93 \text{ eV} \leq m_s \leq 1.43 \text{ eV}$ (flat prior).

Table 5.1: Description of the models considered in this work.

5.4 Constraints from Planck 2105 data

We are now ready to present our results, summarized in Tabs.(5.2 and 5.3), where we show the Bayesian credible intervals for the parameters, for the various models and dataset combinations under consideration. As seen above, the presence of an interacting sterile neutrino impacts the cosmological observables in three ways:

- smaller N_{eff} due to flavour equilibration;
- larger density of (possibly) free-streaming species;
- reduced shear in the neutrino component of the cosmological fluid.

We start by considering the limit of small G_X ($\sim 10^8 G_F$), in which the third effect listed above is negligible, in order to disentangle the first two effects. Comparing the columns for ΛCDM and $\text{S}\Lambda\text{CDM_GX0}$, we note that there are considerable shifts in some parameters, in particular H_0 and n_s . The direction of the shifts is consistent with what we would expect given the well-known degeneracies of these parameters with both N_{eff} and the total density in light species. Looking at the χ^2 values for the best-fit models, reported in Tab.(5.4), we find that $\text{S}\Lambda\text{CDM_GX0}$ performs worse in terms of goodness-of-fit, with a $\Delta\chi^2 = 7.7$ with respect to ΛCDM . This is due to the low value of N_{eff} imposed by the flavour equilibration, while Planck data prefer a value closer to the standard expectation $N_{\text{eff}} = 3.046$. We also note that the mass of the sterile is constrained to be $m_s < 0.82$ eV at 95% CL, thus being in strong tension with the values suggested by the SBL anomalies.

Parameter	ΛCDM	$\text{S}\Lambda\text{CDM_GX0}$	$\text{S}\Lambda\text{CDM}$	$\text{S}\Lambda\text{CDM_Broad}$	$\text{S}\Lambda\text{CDM_Narrow}$
$\Omega_b h^2$	0.02222 ± 0.00023	0.02177 ± 0.00024	0.02172 ± 0.00025	0.02167 ± 0.00025	$0.02166^{+0.00024}_{-0.00024}$
$\Omega_c h^2$	0.1197 ± 0.0021	0.1167 ± 0.0022	0.1171 ± 0.0023	0.1165 ± 0.0022	0.1160 ± 0.0021
$100\theta_{MC}$	1.04085 ± 0.00047	1.04103 ± 0.00050	$1.04323^{+0.00091}_{-0.00073}$	1.04319 ± 0.00074	$1.04307^{+0.0010}_{-0.00077}$
τ	0.078 ± 0.019	0.070 ± 0.018	0.065 ± 0.018	0.067 ± 0.018	0.066 ± 0.018
n_s	0.9655 ± 0.0061	0.9448 ± 0.0070	0.9284 ± 0.0088	$0.9191^{+0.0076}_{-0.0078}$	$0.9161^{+0.0081}_{-0.0072}$
$\ln(10^{10} A_s)$	3.089 ± 0.036	3.063 ± 0.035	3.023 ± 0.038	3.027 ± 0.037	3.028 ± 0.036
G_X/G_F	–	10^8	$< 2.8 \times 10^{10}$	$< 2.9 \times 10^{10}$	$< 4.0 \times 10^{10}$
m_s	–	< 0.82	< 0.82	$[0.93, 1.30]$	1.27 ± 0.028
H_0	67.31 ± 0.95	$62.2^{+2.0}_{-1.7}$	$62.6^{+1.8}_{-1.8}$	59.56 ± 0.88	$58.91^{+0.82}_{-0.79}$

Table 5.2: Parameter constraints for the models under consideration, from the Planck₁₅TT dataset. We either quote constraints in the form “mean \pm 68% uncertainty”, or as 95% credible intervals (when not indicated, the lower limit should be understood to be zero). Units of m_s and H_0 are eV and $\text{km s}^{-1} \text{Mpc}^{-1}$, respectively.

The impact of secret interactions can be assessed by varying the coupling strength as a free parameter of the model. To this purpose we compare $\text{S}\Lambda\text{CDM_GX0}$ to $\text{S}\Lambda\text{CDM}$,

shown in columns 2 and 3 of Tab.(5.2). There are several points worth noticing: first of all, the constraints on the mass of the fourth eigenstate do not change with respect to the case of small G_X , thus remaining in tension with the preferred SBL solution. Secondly, secret interactions stronger than $G_X = 2.8 \times 10^{10} G_F$ are disfavoured, precluding the possibility of the collisional regime lasting after $z \sim \text{few} \times 10^3$. Thus the scenario in the sterile neutrino starts to free stream only after recombination, is disfavoured. This is consistent with the fact that the bound on m_s that we get is of the same order of magnitude as the ones obtained by the Planck collaboration in a minimal extension of the Λ CDM model. In that analysis, the effective mass $m_s^{\text{eff}} \equiv 94.1 \Omega_\nu h^2$ is used to parametrize the contribution of the sterile neutrino to the cosmological energy density. It is straightforward to see that, in our model, $m_s^{\text{eff}} = (3/4) m_s$, so that in terms of the effective parameter the 95% upper bound for SACDM reads $m_s^{\text{eff}} < 0.61$ eV. This should be compared with the result from the Planck collaboration for the same dataset, $m_s^{\text{eff}} < 0.88$ eV at 95% CL. The two values cannot be directly compared, since the

Parameter	SACDM
$\Omega_b h^2$	0.02197 ± 0.00021
$\Omega_c h^2$	$0.1144^{+0.0016}_{-0.0015}$
$100\theta_{MC}$	$1.04332^{+0.00090}_{-0.00063}$
τ	0.074 ± 0.018
n_s	0.9392 ± 0.0063
$\ln(10^{10} A_s)$	3.038 ± 0.036
G_X/G_F	$< 1.97 \times 10^{10}$
m_s	< 0.29
H_0	65.26 ± 0.68

Table 5.3: *Parameter constraints for the models under consideration, from the PlanckTT+lowP+BAO dataset. We either quote constraints in the form “mean \pm 68% uncertainty”, or as 95% credible intervals (when not indicated, the lower limit should be understood to be zero). Units of m_s and H_0 are eV and $\text{km s}^{-1} \text{Mpc}^{-1}$, respectively.*

Planck analysis considers N_{eff} as a free parameter, with a prior $N_{\text{eff}} \geq 3.046$, while in our analysis it is fixed to $N_{\text{eff}} = 2.7$. However, the tighter limit we find for m_s^{eff} is consistent with the lower value of N_{eff} , given the direct correlation between the two parameters. In any case, the best-fit χ^2 for SACDM is still worse than Λ CDM ($\Delta\chi^2 = 3.9$) but yet better than SACDM_GX0. When we also include information from BAO, we get tighter limits on G_X and, especially, m_s , with 95% upper bounds of

$1.97 \times 10^{10} G_F$ and 0.29 eV , respectively (see Tab.(5.3) for details). In Fig.(5.5), we show the joint constraints and the marginalized one-dimensional posterior distributions for G_X and m_s . For comparison, in the two-dimensional plot, we also indicate with a red star a model with $G_X = 1.5 \times 10^{10} G_F$ and $m_s = 1 \text{ eV}$, representative of the strong self-interacting scenario of Refs. [44, 54], that was argued to reconcile cosmological measurements and sterile neutrino interpretation of SBL anomalies (note that the other scenario considered in Ref. [44], with weak self-interactions, is not mapped by our analysis). In particular, a value $G_X \sim 10^{10} G_F$ roughly corresponds to the white band in the upper left part of Fig. 4 of Ref. [44] (at least down to the point where the 4-point approximation is valid, namely $M_X \sim 10^{-2} \text{ MeV}$ and $g_X \sim 10^{-3}$) and the red star in that figure corresponds to a model with $G_X = 1.5 \times 10^{10} G_F$. We stress that, even if from this figure the scenario considered in Refs. [44, 54] seems to be excluded at the $\sim 3\sigma$ level for our most conservative choice of the dataset, i.e. Planck₁₅TT, and even more strongly for Planck₁₅TT + BAO, the actual statistical significance of the exclusion is somehow larger in both cases. A proper assessment should take into account that models with sterile secret interactions with $G_X > 10^8 G_F$ have $N_{\text{eff}} = 2.7$, a value that is itself mildly disfavoured with respect to the Λ CDM prediction of $N_{\text{eff}} = 3.046$. In the following paragraph, we will better quantify this statement, for the PlanckTT+lowP dataset, by comparing χ^2 values between the best-fit models for Λ CDM and SACDM.

In order to better assess the (dis)agreement between Planck CMB observations and the SBL anomalies, also in the presence of secret interactions, we look at the fourth and fifth columns of Tab.(5.2), where we show the results for the cases in which we impose priors on m_s that mimic the preferred SBL solution. For the SACDM_Broad model, column 4 of Tab.(5.2), we obtain almost the same constraint on the strength of the secret interaction we have obtained for the SACDM scenario, in spite of the larger value of m_s imposed by the prior. We notice however that the posterior distribution for m_s is peaked in the lower edge of the prior, $m_s = 0.93 \text{ eV}$. In the SACDM_Narrow analysis, on the other hand, the larger *a priori* value of the sterile neutrino mass, $m_s \simeq 1.27 \text{ eV}$, yields a looser constraint $G_X < 4 \times 10^{10} G_F$. For these two models, we see that the best-fit χ^2 (computed on the Planck₁₅TT dataset) is much worse than Λ CDM: $\Delta\chi^2 = 11.1$ and 12.5 for the “broad” and “narrow” priors, respectively. We argue that

Parameter	Λ CDM	SACDM_GX0	SACDM	SACDM_Broad	SACDM_Narrow
χ^2_{min}	11265.1	11272.8	11269.0	11275.2	11277.6

Table 5.4: Best-fit χ^2 values for the models under consideration, for the Planck₁₅TT dataset.

the inclusion of BAO information would make the tension even stronger, given the preference of that dataset for small values of the sterile neutrino mass. Finally, we notice how all models with non-standard interactions show a preference for values of H_0

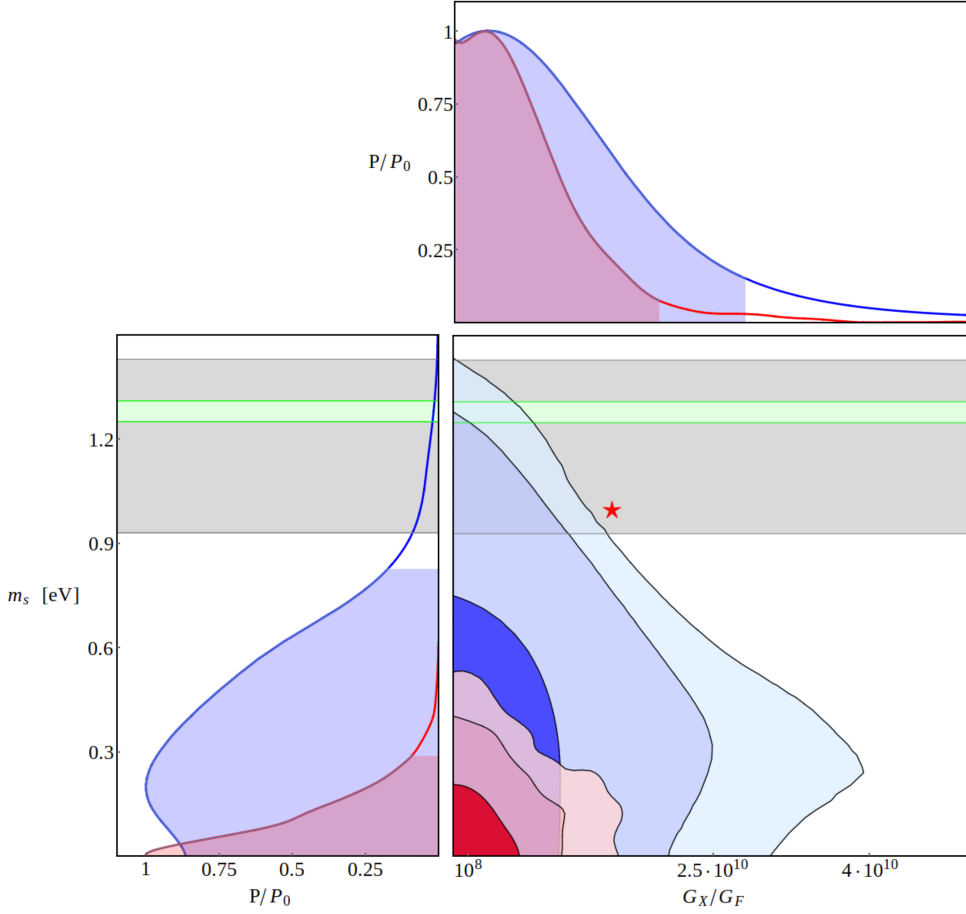


Figure 5.5: Two-dimensional (bottom right) and corresponding one-dimensional posteriors for the effective strength of the interaction $G_X = \sqrt{2}g_X^2/8M_X^2$ in units of the Fermi constant (top) and the sterile neutrino mass m_s (bottom left). Blue constraints are obtained using Planck₁₅TT data, while the red ones come from Planck₁₅TT + BAO, both for the S Λ CDM scenario (that assumes $G_X \geq 10^8 G_F$ and thus $N_{\text{eff}} = 2.7$). The filled regions in the contour plot, from darker to lighter, show the 68, 95 and 99% credible intervals. The shaded regions in the one-dimensional plots correspond to the 95% credible interval. The grey and green horizontal regions are representative of the 68% and 99.73% priors on m_s suggested by SBL anomalies. The red star at $G_X = 1.5 \times 10^{10} G_F$ and $m_s = 1$ eV is representative of the strongly self-interacting scenario described in Refs. [44, 54].

even smaller than the one obtained in the framework of Λ CDM see corresponding row of Tab.(5.2), further increasing the tension between CMB and direct estimates of the Hubble constant [152]; this is not captured by the χ^2 figures reported above, that are computed on CMB data only. The increased tension is due in part to the low value of

N_{eff} , and, in the models with the SBL priors, by the large value of m_s ; both effects, as per known degeneracies, push towards a smaller H_0 . Finally, we summarize our findings

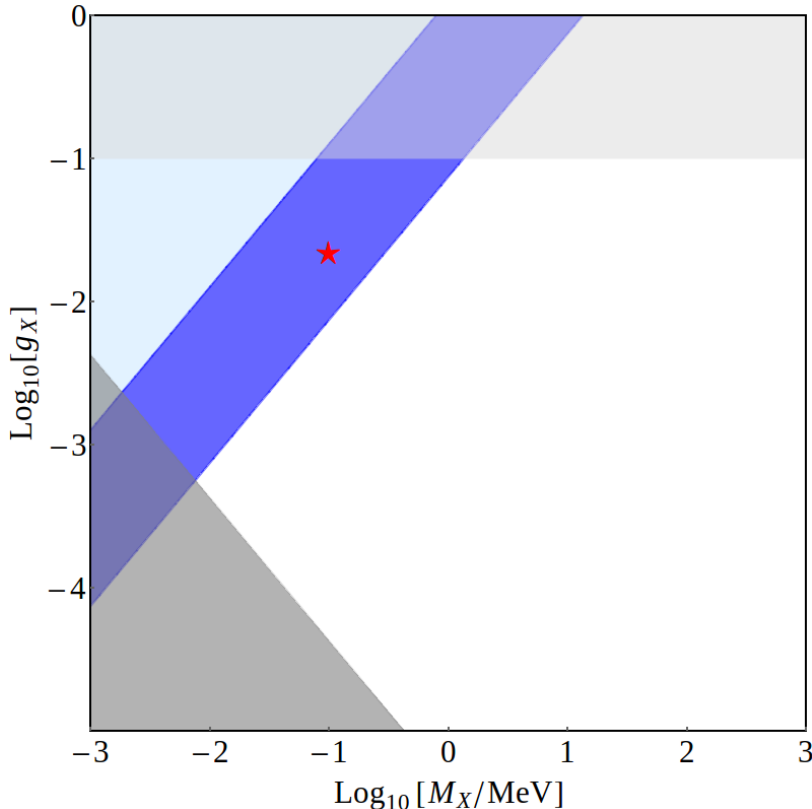


Figure 5.6: Two-dimensional allowed parameter space for the dimensionless coupling constant g_X and the mediator mass M_X . The light and dark blue areas show the region excluded by this study. The light blue region corresponds to values of the interaction strength $G_X > 2.9 \times 10^{10} \text{ GeV}^{-2}$, thus larger than the 95% upper limit on this parameter from Planck. In the dark blue region $10^8 \text{ GeV}^{-2} < G_X < 2.9 \times 10^{10} \text{ GeV}^{-2}$, but is still disfavoured as it does not allow to circumvent the neutrino mass bound. The regions where the approximations used in our study become to break down are colored in gray: the light gray band on top indicates the non-perturbative regime ($g_X \gtrsim 0.1$) while the dark gray triangle on the bottom-left is where the interaction cannot be described as four-point. The red star is representative of the strongly self-interacting scenario described in Refs. [44, 54].

in Fig.(5.6), where we show the parameter space excluded by our analysis in terms of the dimensionless coupling constant g_X and the mediator mass M_X . The excluded region coincides with the whole region in which our assumptions hold and the approximations used are valid. The light and dark blue areas show the region excluded by our work.

In particular, the light blue region corresponds to values of the interaction strength $G_X > 2.9 \times 10^{10} \text{ GeV}^{-2}$, thus larger than the 95% upper limit on this parameter from Planck. In the dark blue region the range $10^8 \text{ GeV}^{-2} < G_X < 2.9 \times 10^{10} \text{ GeV}^{-2}$ is still disfavoured by the neutrino mass bound. The red star is representative of the strong self-interacting scenario described in Refs. [44, 54]. The regions where the approximations used in our study become to break down are colored in gray. The horizontal band in light gray band on top indicates the non-perturbative regime ($g_X \gtrsim 0.1$) while the dark gray triangle on the bottom-left is where the interaction cannot be described as four-point interaction. This is obtained when the temperature at which ν_s are produced (approximated with Eq.(12) of [158]) is comparable or larger than the mediator mass M_X .

Conclusions and Outlook

In this thesis we have studied the impact of neutrino properties, in particular of non-standard interactions on the cosmological observables. We have provided constraints on these non-standard interactions using cosmological data and in particular the CMB data coming from the Planck experiment.

We start providing a description of the standard cosmological model in Ch.(1), with a particular attention for the physics that describe the evolution of cosmological perturbations. In Ch.(2) we focus our attention on the main cosmological observable: the cosmic microwave background radiation. We gave a detailed description of the processes that lead to the anisotropies formation and we explain the physics encoded inside the anisotropies power spectra. Before to present the original part of the work, in Ch.(3) we move our attention on the neutrino sector. A detailed description of its properties has been provided both from particle and cosmological point of view.

Chapters 4 and 5 are reserved for the original work of this thesis. In the former we consider the possibility that neutrinos possess secret scalar or pseudoscalar interactions mediated by the Nambu-Goldstone boson of a still unknown spontaneously broken global U(1) symmetry, as in, e.g., Majoron models. In such scenarios, neutrinos still decouple at $T \sim 1$ MeV, but become tightly coupled again (“recouple”) at later stages of the cosmological evolution. The magnitude of the interaction is parametrized through the effective coupling constant g_{eff} . We add the collisional term, corresponding to an interaction rate of $\Gamma = 0.183 \times g_{\text{eff}}^4 T_\nu$, proper of the (pseudo)scalar interaction, directly inside the Boltzmann equation. In order to do this we use the *relaxation time* approximation which provides a simpler expression for the scattering term avoiding the whole integration procedure. This method guarantees to follow the neutrino perturbation evolution in all the fundamental steps, leading to the understanding of the mechanism involved during the recoupling process. In Fig.(4.3) we show how the presence of (pseudo)scalar interaction among active massless neutrinos modifies the shear σ_ν , basically decreasing the amplitude of the oscillations, this translates into larger density perturbations and pressure leading to more power in the anisotropies

power spectrum, see Fig.(4.4). To derive constraints on g_{eff} we consider both a minimal extension of the standard ΛCDM model (we refer to it as $\Lambda\text{CMD} + g_{\text{eff}}$ model), and more complicated scenarios with extra relativistic degrees of freedom $\Lambda\text{CMD} + g_{\text{eff}} + N_{\text{eff}}$ or non-vanishing tensor amplitude $\Lambda\text{CMD} + g_{\text{eff}} + r$. More over we perform the analysis using the Planck 2013 ($\text{Planck}_{13}\text{TT}$) and 2015 ($\text{Planck}_{15}\text{TT}$) datasets. Starting from the analysis conducted using the Planck 2013 dataset, for a wide range of dataset and model combinations, we find a typical constraint of $g_{\text{eff}}^4 < 4.5 \div 5.2 \times 10^{-27}$ ($g_{\text{eff}} < 2.6 \div 2.7 \times 10^{-7}$), this corresponds to a largest redshift of neutrino recoupling of $z_{\text{rec}} \sim 8800 \div 10^4$ larger than the value $z_{\text{rec}} < 1887$ found in Ref. [23]. This shows that the possibility of secret interaction among neutrinos, leading to a recoupling happening before recombination, is allowed by the data. On the other hand, adding to the standard $\text{Planck}_{13}\text{TT}$ data the observations coming from ACT and SPT ground telescopes (we label this joint analysis with $\text{Planck}_{13}\text{TT} + \text{highL}$), we confirm the preference, also reported in Ref. [23], for non-zero values of the coupling constant. We find best-fit values of $g_{\text{eff}}^4 = 2.2 \div 3 \times 10^{-27}$ ($g_{\text{eff}} < 2.2 \div 2.3 \times 10^{-7}$) corresponding to z_{rec} in the range $2000 \div 3500$. In most cases, we find $g_{\text{eff}} \neq 0$ at 68% CL; this tendency, as said before, is more pronounced when small-scale CMB observations, which are sensitive to details of the photon damping regime, are considered, but is alleviated in presence of extra relativistic degrees of freedom if one allows for them. On the other hand, if we consider a non-vanishing amplitude of tensor modes r , we find a preference for non-zero value of the coupling constant also using the baseline Planck dataset. We report a 68% CL constraints for the interaction strength of $g_{\text{eff}} = 2.17 \times 10^{-7}$, corresponding to a recoupling redshift of $z_{\text{eff}} = 3500$, this results seems to be very stable also adding the joins analysis of Planck and Bicep collaborations (BKP).

We performed a similar analysis using the Planck 2015 temperature ($\text{Planck}_{15}\text{TT}$) and temperature-polarization ($\text{Planck}_{15}\text{TP}$) likelihoods. This time we considered also other astrophysical data, such as, Supernovae (SN), BAO and measurements of H_0 from the Hubble space telescope HST, all these datasets are labelled as *ext*. For the standard analysis, based on the base Planck temperature dataset, we find results comparable with what we obtained with the $\text{Planck}_{13}\text{TT}$. Instead the picture changes when we use the polarization data, we find much tighter constraints at the 95 % CL and stronger hints of a non-zero preferred value for g_{eff} . With all the dataset considered and considering also the lensing of the CMB reconstructed by Planck (*lensing*) we obtain a very stable result: $g_{\text{eff}}^4 < 1.7 \times 10^{-27}$ ($g_{\text{eff}} < 2 \times 10^{-7}$) at 95 % CL, which corresponds to a recoupling redshift of $z_{\text{rec}} < 2500$. However $g_{\text{eff}} = 0$ lies outside the 68 % confidence region, with the probability distribution peaking in $g_{\text{eff}} = 0.82 \times 10^{-7}$ or $g_{\text{eff}} = 1.7 \times 10^{-7}$. The recoupling redshift in this case is $z_{\text{rec}} = 800$. The result is extremely solid also if we extend the model under consideration. For example, adding as a free parameter the effective number of neutrino families N_{eff} or the tensor to scalar ration r , we obtain very similar constraints. Interestingly enough we analyse the goodness of fit, with a χ^2 test, for the $\Lambda\text{CDM} + g_{\text{eff}}$ model comparing it with the standard ΛCMD one. We

obtain an improvement of $\Delta\chi^2 = -3.3$ for one additional parameter. In this analysis we report also a mild shift (at 0.5σ level) of some cosmological parameters that are correlated with the interaction strength. In particular n_s and H_0 move to larger values in correspondence of a larger value of g_{eff} .

The exact relationship between our parameter g_{eff} and the elements of the Yukawa matrix g_{ij} depends on the details of the underlying particle physics model. As an example, we have considered the class of models in which neutrinos acquire mass through violation of ungauged lepton number. In this case the neutrino mass eigenstates couple diagonally, to lowest order approximation, to the Nambu-Goldstone boson of the broken global symmetry, the Majoron. Neutrino masses are proportional to the diagonal couplings: $m_i \propto g_{ii}$. Neglecting the small off-diagonal couplings, $g_{ij} = \delta_{ij}g_i$, and further assuming that the diagonal ones are of the same order of magnitude, $g_i \sim g$, We can translate our limits on g_{eff} to limits on g . Considering the latest results obtained using Planck₁₅TP data, we are at the margins of the region excluded by the observation of the SN1987A [106], i.e. $3 \times 10^{-7} < g < 2 \times 10^{-5}$.

We then move to the Fermi-like interactions conducting a detailed study on the feasibility of cosmological models with sterile neutrinos, in addition to the three active states of the standard model of particle physics, with new, secret self-interactions mediated by a massive vector boson and confined in the sterile sector. This model has been proposed in order to alleviate the tension between the preferred solution of the SBL neutrino anomalies and cosmological observations, that disfavour a fourth fully thermalized neutrino species. Notably the effect of the new interactions would be to effectively dilute the density of both the active and sterile states (leading to an effective number of relativistic species $N_{\text{eff}} = 2.7$, more compatible with the Planck data than $N_{\text{eff}} = 4$). However, the mass of the sterile neutrino required to explain the SBL anomalies still appears to be too large with respect to the corresponding cosmological bounds. It was not clear a priori if and to what extent such bounds could be evaded thanks to the secret interactions that, if very strong, could significantly delay the onset of sterile neutrino free streaming. Secret interactions also leave an imprint on the CMB spectra, by extending the collisional regime for the neutrino fluid. Using this effect, we have constrained the effective ‘‘Fermi constant’’ G_X of the new interaction to be smaller than $2.8 \times 10^{10} G_F$ at 95% CL from the Planck 2015 temperature and large-scale polarization data. This limit is improved to $2.0 \times 10^{10} G_F$ at 95% CL when information from BAO are included. These results disfavour the range, corresponding to $G_X \gtrsim 10^{10} G_F$, in which the onset of sterile neutrino free streaming is delayed until after recombination, and cosmological mass bounds could be possibly evaded. In fact, our self-consistent analysis yields, at 95% CL, $m_s < 0.82$ eV and $m_s < 0.29$ eV from the Planck 2015 data alone and in combination with BAO, respectively, smaller than the value required to explain SBL anomalies, allowing to conclude that the tension between the SBL oscillation experiments and CMB observations still holds even in extended models with secret sterile neutrino interactions. Even disregarding BAO data,

secret interactions with $G_X \gtrsim 10^8 G_F$ are disfavoured with respect to standard Λ CDM, by CMB data, due to their prediction of a low N_{eff} . Moreover, CMB estimates of the Hubble constant H_0 in the secret interactions framework are smaller than their Λ CDM counterparts, thus increasing the tension with astrophysical measurements of the same quantity. Summarizing, our analysis has excluded the possibility of a single sterile neutrino with ~ 1 eV mass and ~ 0.1 mixing (as preferred by the SBL anomalies) with active neutrinos, having strong, four-fermion pointlike self-interactions. This is because it is not possible to hide the cosmological effects of such a large neutrino mass by means of a reduced free-streaming, without at the same time injecting too much extra power in the CMB angular power spectra. As it can be seen by comparing our Fig.(5.6) with Fig. 4 of Ref. [54], where the quantities reported on the vertical axes of the two figures are related by $\alpha_s = g_X^2/4\pi$, the present analysis excludes the thin white band in the upper left part of Fig. 4 of Ref. [54] (dubbed there “strong self-interactions” region). That region was regarded as being of particular interest as it could help explain the problems that arise at small scales in cold dark matter models of structure formation. We have not considered the case of two or more species of sterile neutrinos, although we argue that, in the case of complete thermalisation, they would be even more in tension with observations due to i) an even lower value of N_{eff} , and ii) a larger density of interacting species, presumably resulting in a stronger bound on G_X .

Appendices



Tools and data

1.1 Tools and data

In this section we will describe the tools and data used. We are going to describe very briefly codes and data addressing the reader's curiosity towards the articles of the respective collaborations which are, of course, much more complete and exhaustive.

Numerical codes used in this work are `CosmoMC` [122] and `CAMB` [103,122], the first is the MCMC while the second is a Boltzmann solver. The Code for Anisotropies in the Microwave Background (`CAMB`) is a Boltzmann code, written in FORTRAN90, which works with the linear perturbation theory, explained into the previous chapters, and solve the perturbation equations in order to compute the matter and power spectra. The code allows to change the parameters of the model, starting from the six parameters of the simple Λ CDM model described in Ch. 1, [$\Omega_b h^2$, $\Omega_c h^2$, τ , A_s , n_s and θ]. However it is also possible to consider extended models, such as adding neutrino masses, increasing the number of neutrino families, changing of the equation of state parameter, changing the geometry of the universe (close, open, flat) and so on. The Cosmological Monte Carlo (`CosmoMC`) is a Markov Chain Monte Carlo engine which use the Metropolis-Hastings algorithm to explore the cosmological parameter space and derive posteriors for the parameters of the model. It is completely integrated with `CAMB`: once it generates some values in the parameter space it passes these numbers to the Boltzmann solver which produces the power spectra; these theoretical spectra are then compared with the data to obtain their likelihood. One of the most useful characteristic of `CosmoMC` is the simplicity in the selection of the likelihood, we can choose from different public datasets easily available.

As far as the data are concerned, here there is a list of data and likelihoods used for the aim of this thesis.

- WMAP the Wilkinson Microwave Anisotropy Probe was a NASA Explorer mission that launched June 2001 to make fundamental measurements of cosmology [33,102]

- Planck₁₃TT Planck 2013 data [8]
- Planck₁₅TT and Planck₁₅TP data [13]
- BKP BICEP2/Keck are a series of cosmic microwave background experiments. They aim to measure the polarization of the CMB, in 2015 they produced a joint analysis with the Planck collaboration. [7]
 - highL {
 - ACT the Atacama Cosmology Telescope has measured the angular power spectra of microwave fluctuations to arcminute scales at frequencies of 148 and 218 GHz [64]
 - SPT the South Pole Telescope is a 10 meter diameter telescope operating at the NSF South Pole research station. The telescope is designed for conducting large-area millimeter and sub-millimeter wave surveys of faint, low contrast emission, as required to map primary and secondary anisotropies in the cosmic microwave background. [150]
 - ext {
 - HST Hubble space telescope.
 - SN
 - BAO data coming from the 6dF Galaxy Survey [35], from the BOSS DR11 LOWZ and CMASS samples and from the Main Galaxy Sample of the Sloan Digital Sky Survey [21].

Since cosmic microwave background radiation is the most important source of information used in this thesis, we mainly work with the Planck (2013 and 2015) dataset, in particular:

Planck 2013 release [46]

- Planck₁₃TT for the temperature only data. The spectrum covers the wide range of multipoles $\ell = 2 \div 2479$. Over the multipole range $\ell = 2 \div 49$, the power spectrum is derived from the “Commander” component-separation algorithm applied to the combination of Planck temperature data between 30 and 353 GHz over 91% of the sky. For multipoles greater than $\ell = 50$, instead, the spectrum is derived from the CAMspec [8] likelihood by optimally combining the spectra in the frequency range $100 \div 217$ GHz, and correcting them for unresolved foregrounds.

The likelihood code (and the data that comes with it) used to compute the likelihood of a model that predicts the CMB power spectra, lensing power spectrum, together with some foreground and some instrumental parameters. The data files are built primarily from the Planck mission results, but include also some results from the WMAP-9 data release. The data files are written in a specific format that can only be read by the code. The code consists in a *c/f90* library, along with

some optional tools in python. The code is used to read the data files, and given model power spectra and nuisance parameters it computes the log likelihood of that model. The CMB full likelihood has been divided into four parts to allow using selectively different ranges of multipoles. It also reflects the fact that the mathematical approximations used for those different parts are very different, as is the underlying data [8]. In detail:

- low- ℓ temperature only likelihood (commander) covering $\ell = 2 \div 49$.
- low- ℓ temperature and polarization likelihood (lowlike) from $\ell = 2$ to $\ell = 32$ the polarization used comes from WMAP9.
- high- ℓ temperature (CAMspec) that covers $\ell = 50 \div 2479$.

In 2013, together with Planck data, was released also the very high- ℓ ACT-SPT likelihood that covers the multipoles 1500 to 10000 for temperature. Finally the lensing likelihood covers the multipoles 40 to 400 using the result of the lensing reconstruction [8].

Planck 2015 release [47]

- **Planck₁₅TT** The Planck best-fit CMB temperature power spectrum (shown in 2.4) covers the wide range of multipoles $\ell = 2 \div 2508$. Over the multipole range $\ell = 2 \div 29$, the power spectrum is derived from the “Commander” component-separation algorithm applied to the combination of Planck 2015 temperature data between 30 and 857 GHz, the 9-year WMAP sky maps, and the 408 – MHz [98] survey, including 93% of the sky [6]. For multipoles equal or greater than $\ell = 30$, instead, the spectrum is derived from the “Plik” likelihood [13] by optimally combining the spectra in the frequency range 100 \div 217 GHz, and correcting them for unresolved foregrounds using the best-fit foreground solution from a PlanckTT Λ CDM run.
- **Planck₁₅TP** The Planck best-fit CMB polarization and temperature-polarization cross-correlation power spectra, shown in the figure 2.9, cover the multipole range $\ell = 2 \div 1996$. The data points relative to the multipole range $\ell = 2 \div 29$ are estimated from foreground-cleaned Planck 70 GHz Q and U Stokes parameter maps using 46% of the sky, the same maps that are used in the “lowP” likelihood [13].

The 2015 baseline likelihood release consists of a code package and a single data package. Four extended data packages are also available enabling exploration of alternatives to the baseline results. The code compiles to a library allowing for the computation of log likelihoods for a given data set. Each data package contains multiple data sets. A data set permits the computation of a single likelihood among:

- the high- ℓ temperature and polarization CMB (jointly or separately),

- the low- ℓ temperature and polarization CMB (jointly or separately),
- the CMB lensing reconstruction.

Differences between Planck 2013 and 2015 datasets. It is quite important to underline the differences that lie between 2013 and 2015 Planck releases, as described in details in Ref. [51]. Here we want to put in evidence that the greatest contributions comes from the development of the polarization likelihood and the correspondent power spectra. For example, as the authors of Ref. [77] proved, polarization data can be an extremely good source of information, they show that, for a cosmic variance limited experiment, polarization (EE) data can constrain parameters better than temperature only data up to a factor 2.8 considering a multipole range of $\ell = 30 \div 2500$. In order to give the flavour of the improvement we show in Fig.A.1 the 2015 temperature map obtained with the Commander routine (top panel), where the gray line represents the mask applied which covers the 7% of the sky. In the middle panel it is possible to see the differences between the 2015 and 2013 temperature maps where the masked region is the 2013 mask. Finally in the bottom panel we report the 2013 (gray) and 2015 (black) masks. Of course it is not possible to do the same exercise with the polarization maps since they are not available in the 2013 release.

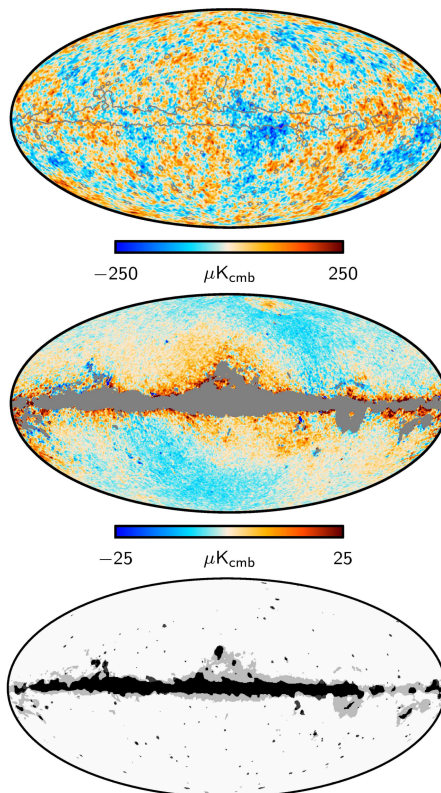


Figure A.1: Top panel: Commander CMB temperature map derived from the Planck 2015, 9-year WMAP and 408 MHz Haslam et al. observations [13]. The gray boundary indicates the 2015 temperature mask that covers the 7% of the sky. In the middle panel we show the difference between the 2015 and 2013 temperature maps. The masked region indicates the 2013 likelihood mask, removing 13% of the sky. The bottom panel shows a comparison of the 2013 (gray) and 2015 (black) temperature masks. [51]

B

Bayesian inference

Cosmologists which study CMB anisotropies use the Bayesian inference [171] instead of the frequentist statistics; the main difference between these two frameworks lies in the definition of probability:

- Bayesian: probability is a measure of the confidence of belief about a proposition.
- Frequency: probability is the number of times the event occurs over the total number of trials, in the limit of an infinite series of equiprobable repetitions.

This second definition of probability is unsatisfactory in many cases, first of all the definition is circular, i.e. it assumes that the of having an event is based on the evidence of the outcomes which is the hypothesis of the probability, secondly, it has no meaning in case of singular cases or unrepeatable situations and finally the probability is exact, by definitions, only in case of an infinite sequence of repetitions.

The intrinsic limitations in cosmology make this type of probability hard to be used.

The Bayesian definition, instead, opens to us a greater possibility of action, it is immediately clear that the circular problem that afflicts the frequency probability vanishes, another great advantage is that there is no difference between statistical and systematic uncertainty and finally we have no problems with a limited data set, i.e. we do not need an infinite sequence of repetitions.

The Bayesian statistics is based on Bayes' theorem, which is the natural consequence of the definition of probability given previously, and gives us the rules by which the probability should be manipulated. So let us consider a set of data \mathcal{D} and the hypothesis made on these data \mathcal{H} , assuming that we have true informations \mathcal{I} , Bayes theorem says:

$$p(\mathcal{H}|\mathcal{D}, \mathcal{I}) = \frac{p(\mathcal{D}|\mathcal{H}, \mathcal{I}) p(\mathcal{H}|\mathcal{I})}{p(\mathcal{D}|\mathcal{I})}. \quad (\text{B.1})$$

On the left we have the so called **posterior probability** of the hypothesis, while in

the right-hand side, at the numerator we have the **sampling distribution of data**, $p(\mathcal{D}|\mathcal{H}, \mathcal{I})$, assuming the hypothesis true and the $(p(\mathcal{H}|\mathcal{I}))$ is the **prior probability** for the hypothesis, which represents the knowledge before to see the data. At the denominator there is the **marginal Likelihood**, often called "Bayesian evidence" ($p(\mathcal{D}|\mathcal{I})$) which is the crucial term for the model comparison. The posterior probability is the relevant part of the theorem and it represents our current state of belief about the hypothesis after we have considered the information hidden in the data, from this point of view we can consider the Bayesian statistics a running statistics which change with the changing of data and priors.

As we can see here there is no temporal sequence in the Bayesian definition but only a logical consequence going from priors to posteriors.

All these statements allow us to define in a better way the concepts of sampling distribution, prior, sampling distribution, posteriors, marginal Likelihood and their importance in the definition of Bayes' theorem.

I Priors: the guiding principle of Bayesian probability theory is that there are no inference without assumptions or, using the right terms, there is no posteriors without priors. Thus prior must reflect the assumption and the state of the knowledge about the problem before the collection of the data. There is a vast literature about priors, here we can distinguish three different situations: **priors** which reflects the state of indifference with respect the symmetries of the problem, **reference priors** which consist in the idea of using the expectations about the experiment as priors and **flat priors**, which are usually the standard choice, where priors are taken to be constant within the minimum and the maximum value of the parameters. Considering this last choice, we have to take a look at the linearity of the flat prior, that is if we are considering a flat prior over the hypothesis \mathcal{H} this does not correspond to a flat prior over a non linear function of the parameter \mathcal{G} . The two priors are related by

$$p(\mathcal{G}) = p(\mathcal{H}) \left| \frac{d\mathcal{H}}{d\mathcal{G}} \right|, \quad (\text{B.2})$$

(in a multi-dimensional case the derivative is replaced by the Jacobian). So for a non-linear dependence $\mathcal{G}(\mathcal{H})$ the derivative represent how much the flat prior on \mathcal{H} knows about \mathcal{G} .

II Sampling distribution of the data shows us how the truth of the hypothesis changes with the acquisition of the data. Usually the name that is used for this parameter is Likelihood, and we can use the more convenient notation:

$$L(\mathcal{H}) = (p(\mathcal{H}|\mathcal{I})). \quad (\text{B.3})$$

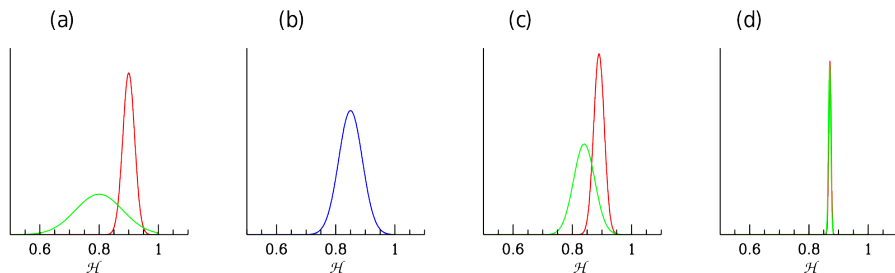


Figure B.1: Simple example of two different priors (figure a) which, after the application of the Likelihood $L(\mathcal{H})$, (figure b) infer posteriors (figure c). Finally the same posteriors after 100 data point are indistinguishable

Notice that the Likelihood is not a probability distribution on the parameters, but a value that helps the convergence of priors into posteriors. Let us see how priors and Likelihood are related with a simple example: take two scientists who have different priors and, for simplicity, assume that all the distribution that they consider are Gaussian. If the Likelihood is enough good, priors will converge to a common posterior, usually we consider a good Likelihood the one which carries more informations than the prior itself. All the possible criticism that should be raised to this method of inference, especially those regarding priors, vanish when the Likelihood is good; as we can see in Fig.B.1 the final posterior is completely independent from the selected priors, and different priors can converge into common posteriors.

III Bayesian evidence or marginal Likelihood: the evaluation of a model in the light of the data is based on this parameter which, essentially, represent the normalization of the Bayes theorem (or the normalization integral). Considering a model M the marginal Likelihood takes the form:

$$p(\mathcal{D}|M) = \int p(\mathcal{D}|\mathcal{H}, M)p(\mathcal{H}|M)d\mathcal{H}, \quad (\text{B.4})$$

thus it is the average of the Likelihood under the prior for a specific model M . Using the Bayes theorem over this definition comes out that:

$$p(M|\mathcal{D}) \propto p(M)p(\mathcal{D}|M). \quad (\text{B.5})$$

Now is easy understand why the Bayesian evidence is so crucial for model comparison, if we consider two different models M_0 and M_1 , the relation between these samples will be:

$$\frac{p(M_0|\mathcal{D})}{p(M_1|\mathcal{D})} = \frac{p(\mathcal{D}|M_0) p(M_0)}{p(\mathcal{D}|M_1) p(M_1)}. \quad (\text{B.6})$$

Here we can define the Bayes factor $B_{01} = \frac{p(\mathcal{D}|M_0)}{p(\mathcal{D}|M_1)}$ which represent the decrease or the increase of the support in favour of one of the two models.

There are several types of Bayesian evidences which are useful in different sector of statistical analysis, but, here, we have the necessity of study the possible cosmological applications.

One of the most important aspects consist of constraining the cosmological parameters, we can classify them into four categories:

- Parameters describing the background evolution such as matter or energy densities, expansion rate, redshift and curvature.
- Parameters describing the initial conditions for the fluctuations such as adiabatic conditions or isocurvature. In the most general case, the initial condition can be represented into a correlation matrix containing six degrees of freedom each one representing the excitation amplitude of scalar, vectorial and tensorial perturbations.
- Nuisance parameters such as bias factor in galaxies, weak lensing and so on.
- Parameters describing new physics such as new possible interactions, massive neutrinos, the behaviour of time-variable structure 'constants', time dependence of the properties of Dark matter and Dark energy...

The general problem of Bayesian parameter inference consists on the estimation of the posterior through the construction of the Likelihood function from the measurement; this usually reflects the way the data has been obtained. If we have a set of parameters describing any aspect of a model and a set priors, it is not so trivial to obtain posteriors. Applying the standard Bayes' theorem in the case of a set of physical interesting parameters \mathcal{H}' and a set of nuisance parameters \mathcal{G} , the joint posterior for θ is:

$$p(\theta|\mathcal{D}, M) = L(\theta) \frac{p(\theta|M)}{p(\mathcal{D}|M)}. \quad (\text{B.7})$$

In some cases, we can approximate the real result integrating on the nuisance:

$$p(\mathcal{H}'|\mathcal{D}, M) \propto \int L(\mathcal{H}', \mathcal{G}) p(\mathcal{H}', \mathcal{G}|M) d\mathcal{G}, \quad (\text{B.8})$$

Bibliography

- [1] CE Aalseth, FT Avignone III, RL Brodzinski, S Cebrian, E Garcia, D Gonzalez, WK Hensley, IG Irastorza, IV Kirpichnikov, AA Klimenko, et al. Igex 76 ge neutrinoless double-beta decay experiment: prospects for next generation experiments. *Physical Review D*, 65(9):092007, 2002.
- [2] P Aarnio, P Abreu, W Adam, P Adrianos, T Adye, G Akopdzhanov, G Alekseev, J Allaby, P Allen, P Allport, et al. Measurement of the mass and width of the z^0 -particle from multihadronic final states produced in $e^+ e^-$ annihilations. *Physics Letters B*, 231(4):539–547, 1989.
- [3] Kevork N Abazajian, MA Acero, SK Agarwalla, AA Aguilar-Arevalo, CH Albright, S Antusch, CA Argüelles, AB Balantekin, G Barenboim, V Barger, et al. Light sterile neutrinos: a white paper. *arXiv preprint arXiv:1204.5379*, 2012.
- [4] JN Abdurashitov, EP Veretenkin, VM Vermul, VN Gavrin, SV Girin, VV Gorbachev, PP Gurkina, GT Zatsepin, TV Ibragimova, AV Kalikhov, et al. Solar neutrino flux measurements by the soviet-american gallium experiment (sage) for half the 22-year solar cycle. *Journal of Experimental and Theoretical Physics*, 95(2):181–193, 2002.
- [5] R Acquafredda, T Adam, N Agafonova, P Alvarez Sanchez, M Ambrosio, A Anokhina, S Aoki, A Ariga, T Ariga, L Arrabito, et al. The opera experiment in the cern to gran sasso neutrino beam. *Journal of Instrumentation*, 4(04):P04018, 2009.
- [6] R Adam, PAR Ade, N Aghanim, MIR Alves, M Arnaud, M Ashdown, J Aumont, C Baccigalupi, AJ Banday, RB Barreiro, et al. Planck 2015 results-x. diffuse component separation: Foreground maps. *Astronomy & Astrophysics*, 594:A10, 2016.

BIBLIOGRAPHY

- [7] Peter AR Ade, N Aghanim, Z Ahmed, RW Aikin, Kate Denham Alexander, M Arnaud, J Aumont, C Baccigalupi, Anthony J Banday, D Barkats, et al. Joint analysis of bicep2/keck array and planck data. *Physical Review Letters*, 114(10):101301, 2015.
- [8] Peter AR Ade, N Aghanim, C Armitage-Caplan, M Arnaud, M Ashdown, F Atrio-Barandela, J Aumont, C Baccigalupi, Anthony J Banday, RB Barreiro, et al. Planck 2013 results. xv. cmb power spectra and likelihood. *Astronomy & Astrophysics*, 571:A15, 2014.
- [9] Peter AR Ade, N Aghanim, M Arnaud, M Ashdown, J Aumont, C Baccigalupi, AJ Banday, RB Barreiro, JG Bartlett, N Bartolo, et al. Planck 2015 results-xiii. cosmological parameters. *Astronomy & Astrophysics*, 594:A13, 2016.
- [10] Peter AR Ade, N Aghanim, M Arnaud, M Ashdown, J Aumont, C Baccigalupi, AJ Banday, RB Barreiro, JG Bartlett, N Bartolo, et al. Planck 2015 results-xiii. cosmological parameters. *Astronomy & Astrophysics*, 594:A13, 2016.
- [11] N Aghanim, C Armitage-Caplan, M Arnaud, M Ashdown, F Atrio-Barandela, J Aumont, C Baccigalupi, AJ Banday, RB Barreiro, E Battaner, et al. Planck 2013 results. v. lfi calibration. *Astronomy & Astrophysics*, 571:A5, 2014.
- [12] N Aghanim, C Armitage-Caplan, M Arnaud, M Ashdown, F Atrio-Barandela, J Aumont, C Baccigalupi, Anthony J Banday, RB Barreiro, E Battaner, et al. Planck 2013 results. iii. lfi systematic uncertainties. *Astronomy & Astrophysics*, 571:A3, 2014.
- [13] N Aghanim, M Arnaud, M Ashdown, J Aumont, C Baccigalupi, AJ Banday, RB Barreiro, JG Bartlett, N Bartolo, E Battaner, et al. Planck 2015 results-xi. cmb power spectra, likelihoods, and robustness of parameters. *Astronomy & Astrophysics*, 594:A11, 2016.
- [14] M Agostini, M Allardt, E Andreotti, AM Bakalyarov, M Balata, I Barabanov, M Barnabé Heider, N Barros, L Baudis, C Bauer, et al. Results on neutrinoless double- β decay of ge 76 from phase i of the gerda experiment. *Physical Review Letters*, 111(12):122503, 2013.
- [15] AA Aguilar-Arevalo, BC Brown, L Bugel, G Cheng, ED Church, JM Conrad, R Dharmapalan, Z Djurcic, DA Finley, R Ford, et al. Improved search for neutrinos oscillations in the minibooone experiment. *Physical Review Letters*, 110(16):161801, 2013.
- [16] MZ Akrawy, G Alexander, J Allison, PP Allport, KJ Anderson, JC Armitage, GTJ Arnison, P Ashton, G Azuelos, JTM Baines, et al. Measurement of the z_0

BIBLIOGRAPHY

- mass and width with the opal detector at lep. *Physics Letters B*, 231(4):530–538, 1989.
- [17] JB Albert, DJ Auty, PS Barbeau, E Beauchamp, D Beck, V Belov, C Benitez-Medina, M Breidenbach, T Brunner, A Burenkov, et al. Search for majoron-emitting modes of double-beta decay of xe 136 with exo-200. *Physical Review D*, 90(9):092004, 2014.
- [18] Andreas Albrecht, Paul J Steinhardt, Michael S Turner, and Frank Wilczek. Reheating an inflationary universe. *Physical Review Letters*, 48(20):1437, 1982.
- [19] Ralph A Alpher, Hans Bethe, and George Gamow. The origin of chemical elements. *Physical Review*, 73(7):803, 1948.
- [20] Fengpeng An, Guangpeng An, Qi An, Vito Antonelli, Eric Baussan, John Beacom, Leonid Bezrukov, Simon Blyth, Riccardo Brugnera, Margherita Buizza Avanzini, et al. Neutrino physics with junos. *Journal of Physics G: Nuclear and Particle Physics*, 43(3):030401, 2016.
- [21] Lauren Anderson, Éric Aubourg, Stephen Bailey, Florian Beutler, Vaishali Bhargava, Michael Blanton, Adam S Bolton, Jon Brinkmann, Joel R Brownstein, Angela Burden, et al. The clustering of galaxies in the sdss-iii baryon oscillation spectroscopic survey: baryon acoustic oscillations in the data releases 10 and 11 galaxy samples. *Monthly Notices of the Royal Astronomical Society*, 441(1):24–62, 2014.
- [22] Maria Archidiacono, Elena Giusarma, Alessandro Melchiorri, and Olga Mena. Dark radiation in extended cosmological scenarios. *Physical Review D*, 86(4):043509, 2012.
- [23] Maria Archidiacono and Steen Hannestad. Updated constraints on non-standard neutrino interactions from planck. *Journal of Cosmology and Astroparticle Physics*, 2014(07):046, 2014.
- [24] Maria Archidiacono, Steen Hannestad, Rasmus Sloth Hansen, and Thomas Tram. Cosmology with self-interacting sterile neutrinos and dark matter: A pseudoscalar model. *Physical Review D*, 91(6):065021, 2015.
- [25] C Arnaboldi, DR Artusa, FT Avignone, M Balata, I Bandac, M Barucci, JW Beeman, C Brofferio, C Bucci, S Capelli, et al. First results on neutrinoless double beta decay of 130 te with the calorimetric cuoricino experiment. *Physics Letters B*, 584(3):260–268, 2004.
- [26] M. Aschbacher. *Finite Group Theory*. Cambridge Studies in Advanced Mathematics. Cambridge University Press, 2000.

BIBLIOGRAPHY

- [27] Erik Aver, Keith A Olive, and Evan D Skillman. The effects of he i $\lambda 10830$ on helium abundance determinations. *Journal of Cosmology and Astroparticle Physics*, 2015(07):011, 2015.
- [28] Anders Basbøll and Steen Hannestad. Decay of heavy majorana neutrinos studied using the full boltzmann equation, including its implications for leptogenesis. *Journal of Cosmology and Astroparticle Physics*, 2007(01):003, 2007.
- [29] Sergei Bashinsky and Uroš Seljak. Signatures of relativistic neutrinos in cmb anisotropy and matter clustering. *Physical Review D*, 69(8):083002, 2004.
- [30] Daniel Baumann. Tasi lectures on inflation. *arXiv preprint arXiv:0907.5424*, 2009.
- [31] John F Beacom, Nicole F Bell, and Scott Dodelson. Neutrinoless universe. *Physical Review Letters*, 93(12):121302, 2004.
- [32] Nicole F Bell, Elena Pierpaoli, and Kris Sigurdson. Cosmological signatures of interacting neutrinos. *Physical Review D*, 73(6):063523, 2006.
- [33] CL Bennett, D Larson, JL Weiland, N Jarosik, G Hinshaw, N Odegard, KM Smith, RS Hill, B Gold, M Halpern, et al. Nine-year wilkinson microwave anisotropy probe (wmap) observations: final maps and results. *The Astrophysical Journal Supplement Series*, 208(2):20, 2013.
- [34] Edmund Bertschinger. Cosmic structure formation. *Physica D: Nonlinear Phenomena*, 77(1-3):354–379, 1994.
- [35] Florian Beutler, Chris Blake, Matthew Colless, D Heath Jones, Lister Staveley-Smith, Lachlan Campbell, Quentin Parker, Will Saunders, and Fred Watson. The 6df galaxy survey: baryon acoustic oscillations and the local hubble constant. *Monthly Notices of the Royal Astronomical Society*, 416(4):3017–3032, 2011.
- [36] Mikhail Bilenky and Arcadi Santamaria. " secret " neutrino interactions. *arXiv preprint hep-ph/9908272*, 1999.
- [37] Samoil M Bilenky and B Pontecorvo. Lepton mixing and neutrino oscillations. *Physics Reports*, 41(4):225–261, 1978.
- [38] J Boger, RL Hahn, JK Rowley, AL Carter, B Hollebhone, D Kessler, I Blevis, F Dalnoki-Veress, A DeKok, J Farine, et al. The sudbury neutrino observatory. *Nuclear Instruments and Methods in Physics Research Section A: Accelerators, Spectrometers, Detectors and Associated Equipment*, 449(1):172–207, 2000.
- [39] Torsten Bringmann, Jasper Hasenkamp, and Jörn Kersten. Tight bonds between sterile neutrinos and dark matter. *Journal of Cosmology and Astroparticle Physics*, 2014(07):042, 2014.

BIBLIOGRAPHY

- [40] R Brugnera and A Garfagnini. Status of the gerda experiment at the laboratori nazionali del gran sasso. *Advances in High Energy Physics*, 2013, 2013.
- [41] Sean M Carroll. Lecture notes on general relativity. *arXiv preprint gr-qc/9712019*, 1997.
- [42] Y Chikashige, Rabindra N Mohapatra, and Roberto D Peccei. Are there real goldstone bosons associated with broken lepton number? *Physics Letters B*, 98(4):265–268, 1981.
- [43] Kiwoon Choi and Arcadi Santamaria. Majorons and supernova cooling. *Physical Review D*, 42(2):293, 1990.
- [44] Xiaoyong Chu, Basudeb Dasgupta, and Joachim Kopp. Sterile neutrinos with secret interactions—lasting friendship with cosmology. *Journal of Cosmology and Astroparticle Physics*, 2015(10):011, 2015.
- [45] C. Cohen-Tannoudji, B. Diu, and F. Laloe. *Quantum Mechanics*. Number v. 1 in Quantum Mechanics. Wiley, 1991.
- [46] Planck collaboration. Cmb spectrum and likelihood code. https://wiki.cosmos.esa.int/planckpla/index.php/Main_Page, 2014. Online; 23 July 2014.
- [47] Planck collaboration. Cmb spectrum and likelihood code. https://wiki.cosmos.esa.int/planckpla2015/index.php/CMB_spectrum_%26_Likelihood_Code, 2014. Online; 23 July 2014.
- [48] Janet M Conrad, William C Louis, and Michael H Shaevitz. The lsnd and miniboone oscillation searches at high δm^2 . *Annual Review of Nuclear and Particle Science*, 63:45–67, 2013.
- [49] W Noel Cottingham and Derek A Greenwood. *An introduction to the standard model of particle physics*. Cambridge university press, 2007.
- [50] Oliviero Cremonesi and Maura Pavan. Challenges in double beta decay. *Advances in High Energy Physics*, 2014, 2014.
- [51] B Crill, L Colombo, L Danese, J Bock, A Catalano, A Bonaldi, L Bonavera, J Dunkley, A Coulais, A Benoit-Lévy, et al. Planck 2015 results: Xi. cmb power spectra, likelihoods, and robustness of parameters. 2016.
- [52] Richard H Cyburt, Brian D Fields, Keith A Olive, and Tsung-Han Yeh. Big bang nucleosynthesis: Present status. *Reviews of Modern Physics*, 88(1):015004, 2016.
- [53] Francis-Yan Cyr-Racine and Kris Sigurdson. Limits on neutrino-neutrino scattering in the early universe. *Physical Review D*, 90(12):123533, 2014.

BIBLIOGRAPHY

- [54] Basudeb Dasgupta and Joachim Kopp. Cosmologically safe ev-scale sterile neutrinos and improved dark matter structure. *Physical Review Letters*, 112(3):031803, 2014.
- [55] Pablo F de Salas and Sergio Pastor. Relic neutrino decoupling with flavour oscillations revisited. *Journal of Cosmology and Astroparticle Physics*, 2016(07):051, 2016.
- [56] PF de Salas, DV Forero, CA Ternes, M Tortola, and JWF Valle. Status of neutrino oscillations 2017. *arXiv preprint arXiv:1708.01186*, 2017.
- [57] D Decamp, B Deschizeaux, J-P Lees, M-N Minard, JM Crespo, M Delfino, E Fernandez, M Martinez, R Miquel, ML Mir, et al. Determination of the number of light neutrino species. *Physics Letters B*, 231(4):519–529, 1989.
- [58] Stefano Dell’Oro, Simone Marcocci, Matteo Viel, and Francesco Vissani. Neutrinoless double beta decay: 2015 review. *Advances in High Energy Physics*, 2016, 2016.
- [59] Roberta Diamanti, Elena Giusarma, Olga Mena, Maria Archidiacono, and Alessandro Melchiorri. Dark radiation and interacting scenarios. *Physical Review D*, 87(6):063509, 2013.
- [60] Robert H Dicke, P James E Peebles, Peter G Roll, and David T Wilkinson. Cosmic black-body radiation. *The Astrophysical Journal*, 142:414–419, 1965.
- [61] Paul AM Dirac. The quantum theory of the electron. In *Proceedings of the Royal Society of London A: Mathematical, Physical and Engineering Sciences*, volume 117, pages 610–624. The Royal Society, 1928.
- [62] Scott Dodelson. *Modern cosmology*. Academic press, 2003.
- [63] AD Dolgov, Steen H Hansen, Sergio Pastor, Serguey T Petcov, Georg G Raffelt, and DV Semikoz. Cosmological bounds on neutrino degeneracy improved by flavor oscillations. *Nuclear Physics B*, 632(1):363–382, 2002.
- [64] J Dunkley, E Calabrese, J Sievers, GE Addison, N Battaglia, ES Battistelli, JR Bond, S Das, MJ Devlin, R Dünner, et al. The atacama cosmology telescope: likelihood for small-scale cmb data. *Journal of Cosmology and Astroparticle Physics*, 2013(07):025, 2013.
- [65] G Efstathiou. H0 revisited. 2014. *MNRAS*, 440:1138.
- [66] K Eguchi, S Enomoto, K Furuno, J Goldman, H Hanada, H Ikeda, K Ikeda, K Inoue, K Ishihara, W Itoh, et al. First results from kamland: evidence for reactor antineutrino disappearance. *Physical Review Letters*, 90(2):021802, 2003.

BIBLIOGRAPHY

- [67] KamLAND& Eguchi, S Enomoto, K Furuno, H Ikeda, K Ikeda, K Inoue, K Ishihara, T Iwamoto, T Kawashima, Y Kishimoto, et al. High sensitivity search for ν e's from the sun and other sources at kamland. *Physical Review Letters*, 92(7):071301, 2004.
- [68] Shalom Eliezer and Arthur R Swift. Experimental consequences of νe - $\nu\mu$ mixing in neutrino beams. *Nuclear Physics B*, 105(1):45–51, 1976.
- [69] Enrico Fermi. Attempt at a theory of beta-rays. *Il Nuovo Cimento*, 11(1), 1934.
- [70] Richard P Feynman and Murray Gell-Mann. Theory of the fermi interaction. *Physical Review*, 109(1):193, 1958.
- [71] Brian D Fields and Keith A Olive. The evolution of ${}^6\text{Li}$ in standard cosmic-ray nucleosynthesis. *New Astronomy*, 4(4):255–263, 1999.
- [72] DJ Fixsen, ES Cheng, DA Cottingham, RE Eplee Jr, RB Isaacman, JC Mather, SS Meyer, PD Noerdlinger, RA Shafer, R Weiss, et al. Cosmic microwave background dipole spectrum measured by the coBE FIRS instrument. *The Astrophysical Journal*, 420:445–449, 1994.
- [73] DJ Fixsen, ES Cheng, JM Gales, John C Mather, RA Shafer, and EL Wright. The cosmic microwave background spectrum from the full coBE* FIRS data set. *The Astrophysical Journal*, 473(2):576, 1996.
- [74] Robert Foot, H Lew, X-G He, and Girish C Joshi. See-saw neutrino masses induced by a triplet of leptons. *Zeitschrift für Physik C Particles and Fields*, 44(3):441–444, 1989.
- [75] S Fukuda, Y Fukuda, T Hayakawa, E Ichihara, M Ishitsuka, Y Itow, T Kajita, J Kameda, K Kaneyuki, S Kasuga, et al. The super-kamiokande detector. *Nuclear Instruments and Methods in Physics Research Section A: Accelerators, Spectrometers, Detectors and Associated Equipment*, 501(2):418–462, 2003.
- [76] Y Fukuda, T Hayakawa, E Ichihara, K Inoue, K Ishihara, H Ishino, Y Itow, T Kajita, J Kameda, S Kasuga, et al. Evidence for oscillation of atmospheric neutrinos. *Physical Review Letters*, 81(8):1562, 1998.
- [77] Silvia Galli, Karim Benabed, François Bouchet, Jean-François Cardoso, Franz Elsner, Eric Hivon, Anna Mangilli, Simon Prunet, and Benjamin Wandelt. CMB polarization can constrain cosmology better than CMB temperature. *Physical Review D*, 90(6):063504, 2014.
- [78] George Gamow. Expanding universe and the origin of elements. *Physical Review*, 70(7-8):572, 1946.

BIBLIOGRAPHY

- [79] A Gando, H Watanabe, MP Decowski, M Koga, I Shimizu, W Tornow, A Suzuki, Y Gando, JA Detwiler, H Ikeda, et al. Limits on majoron-emitting double-beta decays of xe-136 in kamland-zen. Technical report, 2012.
- [80] S Gariazzo, C Giunti, M Laveder, and YF Li. Updated global $3+1$ analysis of short-baseline neutrino oscillations. *arXiv preprint arXiv:1703.00860*, 2017.
- [81] S Gariazzo, C Giunti, M Laveder, YF Li, and EM Zavanin. Light sterile neutrinos. *Journal of Physics G: Nuclear and Particle Physics*, 43(3):033001, 2016.
- [82] Maurizio Gasperini. *Lezioni di cosmologia teorica*. Springer Science & Business Media, 2012.
- [83] Murray Gell-Mann and Abraham Pais. Behavior of neutral particles under charge conjugation. *Physical Review*, 97(5):1387, 1955.
- [84] Murray Gell-Mann, Pierre Ramond, and Richard Slansky. Complex spinors and unified theories. *arXiv preprint arXiv:1306.4669*, 2013.
- [85] Graciela B Gelmini and Marco Roncadelli. Left-handed neutrino mass scale and spontaneously broken lepton number. *Physics Letters B*, 99(5):411–415, 1981.
- [86] H. Georgi. *Lie Algebras In Particle Physics: from Isospin To Unified Theories*. Frontiers in Physics. Avalon Publishing, 1999.
- [87] Martina Gerbino, Eleonora Di Valentino, and Najla Said. Neutrino anisotropies after planck. *Physical Review D*, 88(6):063538, 2013.
- [88] Carlo Giunti and Chung W. Kim. *Fundamentals of Neutrino Physics and Astrophysics*. 2007.
- [89] Sheldon L Glashow. Partial-symmetries of weak interactions. *Nuclear Physics*, 22(4):579–588, 1961.
- [90] H. Goldstein, C.P. Poole, and J.L. Safko. *Classical Mechanics*. Addison Wesley, 2002.
- [91] Paolo Gorla et al. The cuore experiment: Status and prospects. In *Journal of Physics: Conference Series*, volume 375, page 042013. IOP Publishing, 2012.
- [92] Alan H Guth. Inflationary universe: A possible solution to the horizon and flatness problems. *Physical Review D*, 23(2):347, 1981.
- [93] Jan Hamann, Steen Hannestad, Georg G Raffelt, and Yvonne YY Wong. Sterile neutrinos with ev masses in cosmology—how disfavoured exactly? *Journal of Cosmology and Astroparticle Physics*, 2011(09):034, 2011.

BIBLIOGRAPHY

- [94] Wolfgang Hampel, J Handt, G Heusser, J Kiko, T Kirsten, M Laubenstein, E Pernicka, W Rau, M Wojcik, Yu Zakharov, et al. Gallex solar neutrino observations: Results for gallex iv. *Physics Letters B*, 447(1):127–133, 1999.
- [95] Steen Hannestad. Structure formation with strongly interacting neutrinos—implications for the cosmological neutrino mass bound. *Journal of Cosmology and Astroparticle Physics*, 2005(02):011, 2005.
- [96] Steen Hannestad, Rasmus Sloth Hansen, and Thomas Tram. How self-interactions can reconcile sterile neutrinos with cosmology. *Physical Review Letters*, 112(3):031802, 2014.
- [97] Steen Hannestad, Irene Tamborra, and Thomas Tram. Thermalisation of light sterile neutrinos in the early universe. *Journal of Cosmology and Astroparticle Physics*, 2012(07):025, 2012.
- [98] CGT Haslam, CJ Salter, H Stoffel, and WEz Wilson. A 408 mhz all-sky continuum survey. ii-the atlas of contour maps. *Astronomy and Astrophysics Supplement Series*, 47:1, 1982.
- [99] Peter W. Higgs. Broken symmetries and the masses of gauge bosons. *Phys. Rev. Lett.*, 13:508–509, Oct 1964.
- [100] Peter W Higgs. Broken symmetries and the masses of gauge bosons. *Physical Review Letters*, 13(16):508, 1964.
- [101] H Hildebrandt, M Viola, C Heymans, S Joudaki, K Kuijken, C Blake, T Erben, B Joachimi, D Klaes, L Miller, et al. KIDS-450: Cosmological parameter constraints from tomographic weak gravitational lensing. *Monthly Notices of the Royal Astronomical Society*, 2017.
- [102] Gary Hinshaw, D Larson, Eiichiro Komatsu, DN Spergel, CL Bennett, J Dunkley, MR Nolta, M Halpern, RS Hill, N Odegard, et al. Nine-year wilkinson microwave anisotropy probe (wmap) observations: cosmological parameter results. *The Astrophysical Journal Supplement Series*, 208(2):19, 2013.
- [103] Cullan Howlett, Antony Lewis, Alex Hall, and Anthony Challinor. Cmb power spectrum parameter degeneracies in the era of precision cosmology. *Journal of Cosmology and Astroparticle Physics*, 2012(04):027, 2012.
- [104] Wayne Hu and Naoshi Sugiyama. Small-scale cosmological perturbations: an analytic approach. *The Astrophysical Journal*, 471(2):542, 1996.
- [105] E. Hubble. A Relation between Distance and Radial Velocity among Extra-Galactic Nebulae. *Proceedings of the National Academy of Science*, 15:168–173, March 1929.

BIBLIOGRAPHY

- [106] Michael Kachelriess, Ricard Tomàs, and JWF Valle. Supernova bounds on majoron-emitting decays of light neutrinos. *Physical Review D*, 62(2):023004, 2000.
- [107] Kimmo Kainulainen. Light singlet neutrinos and the primordial nucleosynthesis. *Physics Letters B*, 244(2):191–195, 1990.
- [108] Demosthenes Kazanas. Dynamics of the universe and spontaneous symmetry breaking. *The Astrophysical Journal*, 241:L59–L63, 1980.
- [109] William H Kinney. Tasi lectures on inflation. *arXiv preprint arXiv:0902.1529*, 2009.
- [110] Robert P Kirshner. Hubble’s diagram and cosmic expansion. *Proceedings of the National Academy of Sciences*, 101(1):8–13, 2004.
- [111] Edward Kolb and Michael Turner. *The early universe*. Westview press, 1994.
- [112] Joachim Kopp, Pedro AN Machado, Michele Maltoni, and Thomas Schwetz. Sterile neutrino oscillations: the global picture. *Journal of High Energy Physics*, 2013(5):50, 2013.
- [113] Ch Kraus, B Bornschein, L Bornschein, J Bonn, B Flatt, A Kovalik, B Ostrick, EW Otten, JP Schall, Th Thümmel, et al. Final results from phase ii of the mainz neutrino mass search in tritium decay. *The European Physical Journal C-Particles and Fields*, 40(4):447–468, 2005.
- [114] Christine Kraus and Simon JM Peeters. The rich neutrino programme of the sno+ experiment. *Progress in Particle and Nuclear Physics*, 64(2):273–277, 2010.
- [115] Lachlan Lancaster, Francis-Yan Cyr-Racine, Lloyd Knox, and Zhen Pan. A tale of two modes: Neutrino free-streaming in the early universe. *arXiv preprint arXiv:1704.06657*, 2017.
- [116] L Landau. On the conservation laws for weak interactions. *Nuclear Physics*, 3(1):127–131, 1957.
- [117] Lev Davidovich Landau. *The classical theory of fields, Volume 2*. Elsevier, 2013.
- [118] Tsung-Dao Lee and Chen-Ning Yang. Question of parity conservation in weak interactions. *Physical Review*, 104(1):254, 1956.
- [119] Julien Lesgourgues, Gianpiero Mangano, Gennaro Miele, and Sergio Pastor. *Neutrino cosmology*. Cambridge University Press, 2013.
- [120] A Lewis, A Challinor, and A Lasenby. Efficient computation of cmb anisotropies in closed frw models, 2000. *Astrophys. J*, 538:473.

BIBLIOGRAPHY

- [121] Antony Lewis. Camb notes, 2011.
- [122] Antony Lewis and Sarah Bridle. Cosmological parameters from cmb and other data: A monte carlo approach. *Physical Review D*, 66(10):103511, 2002.
- [123] Andrei Linde. Particle physics and inflationary cosmology. *arXiv preprint hep-th/0503203*, 2005.
- [124] Andrei D Linde. Chaotic inflation. *Physics Letters B*, 129(3-4):177–181, 1983.
- [125] VM Lobashev, VN Aseev, AI Belesev, AI Berlev, EV Geraskin, AA Golubev, OV Kazachenko, Yu E Kuznetsov, RP Ostroumov, LA Rivkis, et al. Direct search for mass of neutrino and anomaly in the tritium beta-spectrum. *Physics Letters B*, 460(1):227–235, 1999.
- [126] WC Louis. Searches for muon-to-electron (anti) neutrino flavor change. *Progress in Particle and Nuclear Physics*, 63(1):51–73, 2009.
- [127] Chung-Pei Ma and Edmund Bertschinger. Cosmological perturbation theory in the synchronous and conformal newtonian gauges. *arXiv preprint astro-ph/9506072*, 1995.
- [128] Ernest Ma. Pathways to naturally small neutrino masses. *Physical Review Letters*, 81(6):1171, 1998.
- [129] Ernest Ma and DP Roy. Heavy triplet leptons and new gauge boson. *Nuclear Physics B*, 644(1):290–302, 2002.
- [130] M Magg and Ch Wetterich. Neutrino mass problem and gauge hierarchy. *Physics Letters B*, 94(1):61–64, 1980.
- [131] F. Mandl and G. Shaw. *Quantum Field Theory*. Wiley, 2013.
- [132] Gianpiero Mangano, Gennaro Miele, Sergio Pastor, Teguyco Pinto, Ofelia Pisanti, and Pasquale D Serpico. Relic neutrino decoupling including flavour oscillations. *Nuclear Physics B*, 729(1):221–234, 2005.
- [133] A Marrone, F Capozzi, E Lisi, D Montanino, and A Palazzo. Three-neutrino mixing: status and prospects. In *Journal of Physics: Conference Series*, volume 718, pages 62042–62046. IOP Publishing, 2016.
- [134] SP Mikheev and A Yu Smirnov. Resonance amplification of oscillations in matter and spectroscopy of solar neutrinos. *Yadernaya Fizika*, 42(6):1441–1448, 1985.
- [135] Alessandro Mirizzi, Gianpiero Mangano, Ofelia Pisanti, and Ninetta Saviano. Collisional production of sterile neutrinos via secret interactions and cosmological implications. *Physical Review D*, 91(2):025019, 2015.

BIBLIOGRAPHY

- [136] Alessandro Mirizzi, Gianpiero Mangano, Ninetta Saviano, Enrico Borriello, Carlo Giunti, Gennaro Miele, and Ofelia Pisanti. The strongest bounds on active-sterile neutrino mixing after planck data. *Physics Letters B*, 726(1):8–14, 2013.
- [137] Alessandro Mirizzi, Ninetta Saviano, Gennaro Miele, and Pasquale Dario Serpico. Light sterile neutrino production in the early universe with dynamical neutrino asymmetries. *Physical Review D*, 86(5):053009, 2012.
- [138] Charles W Misner, Kip S Thorne, and John Archibald Wheeler. *Gravitation*. Macmillan, 1973.
- [139] Rabindra N Mohapatra and Goran Senjanović. Neutrino masses and mixings in gauge models with spontaneous parity violation. *Physical Review D*, 23(1):165, 1981.
- [140] Angelo Nucciotti. The use of low temperature detectors for direct measurements of the mass of the electron neutrino. *Advances in High Energy Physics*, 2016, 2016.
- [141] Takemi Okamoto and Wayne Hu. Cosmic microwave background lensing reconstruction on the full sky. *Physical Review D*, 67(8):083002, 2003.
- [142] Isabel M Oldengott, Cornelius Rampf, and Yvonne YY Wong. Boltzmann hierarchy for interacting neutrinos i: formalism. *Journal of Cosmology and Astroparticle Physics*, 2015(04):016, 2015.
- [143] Isabel M Oldengott, Thomas Tram, Cornelius Rampf, and Yvonne YY Wong. Interacting neutrinos in cosmology: exact description and constraints. *arXiv preprint arXiv:1706.02123*, 2017.
- [144] Keith A Olive, Particle Data Group, et al. Review of particle physics. *Chinese physics C*, 38(9):090001, 2014.
- [145] S Perlmutter et al. Measurements of omega and lambda from 42 high-redshift supernovae, 1999 astrophys. *J*, 517:565, 1998.
- [146] M.E. Peskin and D.V. Schroeder. *An Introduction To Quantum Field Theory*. Frontiers in Physics. Avalon Publishing, 1995.
- [147] Bruno Pontecorvo. Nuclear capture of mesons and the meson decay. *Physical Review*, 72(3):246, 1947.
- [148] Bruno Pontecorvo. Mesonium and antimesonium. *Soviet Journal of Experimental and Theoretical Physics*, 6:429, 1958.
- [149] H Ray. The miniboone experiment: An overview. *arXiv preprint hep-ex/0701040*, 2007.

BIBLIOGRAPHY

- [150] CL Reichardt, L Shaw, O Zahn, KA Aird, BA Benson, LE Bleem, JE Carlstrom, CL Chang, HM Cho, TM Crawford, et al. A measurement of secondary cosmic microwave background anisotropies with two years of south pole telescope observations. *The Astrophysical Journal*, 755(1):70, 2012.
- [151] Adam G Riess, Alexei V Filippenko, Peter Challis, Alejandro Clocchiatti, Diercks, et al. Observational evidence from supernovae for an accelerating universe and a cosmological constant. *The Astronomical Journal*, 116(3):1009, 1998.
- [152] Adam G Riess, Lucas M Macri, Samantha L Hoffmann, Dan Scolnic, Stefano Casertano, Alexei V Filippenko, Brad E Tucker, Mark J Reid, David O Jones, Jeffrey M Silverman, et al. A 2.4% determination of the local value of the hubble constant based on observations with the nasa/esa hubble space telescope, obtained at the space telescope science institute, which is operated by auras, inc., under nasa contract nas 5-26555. *The Astrophysical Journal*, 826(1):56, 2016.
- [153] Barbara Ryden. *Introduction to cosmology*. Cambridge University Press, 2016.
- [154] J.J. Sakurai and J.J. Napolitano. *Modern Quantum Mechanics*. Pearson Education, 2014.
- [155] Abdus Salam. On parity conservation and neutrino mass. *Il Nuovo Cimento (1955-1965)*, 5(1):299–301, 1957.
- [156] Laura Salvati, Luca Pagano, Massimiliano Lattanzi, Martina Gerbino, and Alessandro Melchiorri. Breaking be: a sterile neutrino solution to the cosmological lithium problem. *Journal of Cosmology and Astroparticle Physics*, 2016(08):022, 2016.
- [157] Ninetta Saviano, Alessandro Mirizzi, Ofelia Pisanti, Pasquale Dario Serpico, Gianpiero Mangano, and Gennaro Miele. Multimomentum and multiflavor active-sterile neutrino oscillations in the early universe: Role of neutrino asymmetries and effects on nucleosynthesis. *Physical Review D*, 87(7):073006, 2013.
- [158] Ninetta Saviano, Ofelia Pisanti, Gianpiero Mangano, and Alessandro Mirizzi. Unveiling secret interactions among sterile neutrinos with big-bang nucleosynthesis. *Physical Review D*, 90(11):113009, 2014.
- [159] J Schechter and José WF Valle. Neutrino masses in $su(2) \times u(1)$ theories. *Physical Review D*, 22(9):2227, 1980.
- [160] J Schechter and José WF Valle. Neutrino decay and spontaneous violation of lepton number. *Physical Review D*, 25(3):774, 1982.
- [161] Joseph Schechter and José WF Valle. Neutrinoless double- β decay in $su(2) \times u(1)$ theories. *Physical Review D*, 25(11):2951, 1982.

BIBLIOGRAPHY

- [162] Tristan L Smith, Sudeep Das, and Oliver Zahn. Constraints on neutrino and dark radiation interactions using cosmological observations. *Physical Review D*, 85(2):023001, 2012.
- [163] George Fitzgerald Smoot, Charles L Bennett, A Kogut, J Aymon, C Backus, G De Amici, K Galuk, Peter D Jackson, P Keegstra, L Rokke, et al. Preliminary results from the coBE differential microwave radiometers-large angular scale isotropy of the cosmic microwave background. *The Astrophysical Journal*, 371:L1–L5, 1991.
- [164] Leo Stodolsky. Treatment of neutrino oscillations in a thermal environment. *Physical Review D*, 36(8):2273, 1987.
- [165] GW Sullivan, IceCube Collaboration, et al. Results from the icecube experiment. *Nuclear Physics B-Proceedings Supplements*, 235:346–351, 2013.
- [166] Yoichiro Suzuki. Kamiokande solar neutrino results. *Nuclear Physics B-Proceedings Supplements*, 38(1-3):54–59, 1995.
- [167] Jan Tauber, Peter AR Ade, N Aghanim, MIR Alves, C Armitage-Caplan, M Arnaud, M Ashdown, F Atrio-Barandela, J Aumont, H Aussel, et al. Planck 2013 results. i. overview of products and scientific results. *Astronomy and Astrophysics*, 571, 2014.
- [168] Rex Tayloe, MiniBooNE Collaboration, et al. The miniboone experiment: Status and plans. *Nuclear Physics B-Proceedings Supplements*, 118:157–163, 2003.
- [169] J.R. Taylor. *Classical Mechanics*. University Science Books, 2005.
- [170] Ricard Tomàs, Heinrich Päs, and JWF Valle. Generalized bounds on majoron-neutrino couplings. *Physical Review D*, 64(9):095005, 2001.
- [171] Roberto Trotta. Bayes in the sky: Bayesian inference and model selection in cosmology. *Contemporary Physics*, 49(2):71–104, 2008.
- [172] Roberto Trotta and Alessandro Melchiorri. Indication for primordial anisotropies in the neutrino background from the wilkinson microwave anisotropy probe and the sloan digital sky survey. *Physical Review Letters*, 95(1):011305, 2005.
- [173] Steven Weinberg. *Gravitation and cosmology: principles and applications of the general theory of relativity*. Wiley New York, 1972.
- [174] Ch Wetterich. Neutrino masses and the scale of bl violation. *Nuclear Physics B*, 187(2):343–375, 1981.
- [175] Lincoln Wolfenstein. Neutrino oscillations in matter. *Physical Review D*, 17(9):2369, 1978.

- [176] Tsutomu Yanagida. Horizontal symmetry and masses of neutrinos. *Progress of Theoretical Physics*, 64(3):1103–1105, 1980.
- [177] Matias Zaldarriaga and Uroš Seljak. Gravitational lensing effect on cosmic microwave background polarization. *Physical Review D*, 58(2):023003, 1998.

Thanks

I would like to thank my family, in particular my mother, for the support and constant encouragement. In addition I want to thank all the people who shared with me beautiful and less beautiful moments during these years.

I would like to thank my advisor Paolo Natoli and my co-advisor Massimiliano Lattanzi for guiding and supporting me over the years.

A very special thank goes to Linda who is my pillar, Diggy and Benry. They know how much I am grateful to them and how fundamental they are. Nevertheless I want to to thank Erica, Carda, Bea, Manu, Giulia, Elena, Gambero,

Finally, thanks to Alessandro for the commitment devolved to the realization of the remarkable succession of defeats inflicted to Cama.